LASER ELECTROSPRAY MASS SPECTROMETRY: INSTRUMENTATION AND APPLICATION FOR DIRECT ANALYSIS AND MOLECULAR IMAGING OF BIOLOGICAL TISSUE

A Dissertation
Submitted to
the Temple University Graduate Board

In Partial Fulfillment
of the Requirements for the Degree
DOCTOR OF PHILOSOPHY

---

by
Fengjian Shi
May 2017

Examining Committee Members:

Robert J. Levis, Advisory Chair, Department of Chemistry, Temple University
Ann M. Valentine, Department of Chemistry, Temple University
Daniel R. Strongin, Department of Chemistry, Temple University
Charles N. McEwen, External Member, Department of Chemistry and Biochemistry, University of the Sciences

ABSTRACT

This dissertation elucidates the instrumentation and application of a hybrid ambient ionization source, laser electrospray mass spectrometry (LEMS), for the direct analysis and molecular imaging of biological tissue without matrix deposition. In LEMS, laser pulses from a Ti:Sapphire laser amplifier (60 fs, 800 nm, and 1 mJ) interact with surface analytes and transfer them from the condensed phase into the gas phase without the requirement of either exogenous matrix or endogenous water in the sample. The laser vaporized analytes are captured and ionized by an electrospray source, and finally detected by a mass analyzer. It was found that a turn-key, robust femtosecond fiber laser with longer wavelength, longer duration, and lower pulse energy at 1042 nm, 425 fs, and 50 μJ, respectively, provided comparable results with the Ti:Sapphire laser. Vaporization of intact, dried or aqueous cytochrome c and lysozyme samples was demonstrated by the fiber laser. A charge states distribution at lower charge states indicating folded conformation of proteins and the hemoglobin α subunit-heme complex from whole blood was observed. Endogenous anthocyanins, sugars, and other metabolites were detected and revealed the anticipated metabolite profile for the flower petal and leaf samples by the fiber laser. Phospholipids, especially phosphatidylcholine, were identified from a fresh mouse brain section sample. These lipid features were suppressed in both the fiber laser and Ti:Sapphire LEMS measurement in the presence of optimal cutting temperature compounds which are commonly used in animal tissue cryosectioning.

This dissertation also details the design of an automated mass spectrometry imaging source based on the Ti:Sapphire LEMS. The laser, translation stage, and mass analyzer are

synchronized and controlled using a customized user interface to enable step-by-step scanning of the area of interest on a given tissue sample. The imaging source is coupled with a high resolution accurate mass quadrupole time-of-flight (QTOF) mass analyzer with tandem mass analysis capability. A lateral resolution of 60 μm was demonstrated on a patterned ink film by LEMS imaging. Plant metabolites including sugar and anthocyanins were directly imaged from a leaf sample. Small metabolites, lipids and proteins were simultaneously imaged from a single tissue section of a pig liver sample. Biomarkers of blood-brain barrier damage and traumatic brain injury (TBI) that occurred during the injury were detected and imaged from a TBI mouse brain. The loading values from principal component analysis (PCA) were shown to be useful for identification of features of interest from the large LEMS imaging dataset.

DEDICATION

To my family, friends, and colleagues

for all their support

ACKNOWLEDGMENTS

First, I would like to thank my research advisor, Robert Levis, for his support throughout my graduate research. By providing the funding, resources, and general direction of the project, Dr. Levis has enriched my understanding of scientific research and allowed me to grow as an independent researcher. In addition to my advisor, I want to thank my committee members Dr. Ann Valentine, Dr. Daniel Strongin and Dr. Charles McEwen.

I would like to thank previous group member, Paul Flanigan, for mass spectrometry instrumentation instruction and assistance when I first joined into the group. I would like to thank Johanan Odhner for help in troubleshooting the femtosecond laser system. I would like to thank the members of the Levis group, in particular Santosh Karki, Jieutonne Archer, Habib Sistani, Johnny Perez, and Rachel Parise. Finally, I would like to thank my wife Weiqi Yang and all the family members for their support and encouragement throughout this endeavor.

TABLE OF CONTENTS

Page

LIST OF TABLES

LIST OF FIGURES

CHAPTER 1

INTRODUCTION

1.1 Ionization Methods for Mass Spectrometry

Mass spectrometry (MS) has the advantage of detecting multiple analytes in parallel qualitatively or quantitatively without any labeling [1]. Because of these advantages, mass spectrometry has been an attractive tool for bioanalysis applications, such as structural elucidation of pharmaceuticals and their metabolites, discovery of endogenous biomarkers, and quantitation of compounds in biological matrices. A critical step in mass spectrometry is conversion of the samples into gas phase ions, or ionization. Before the 1980s, the mass analysis of biomolecules was mostly limited to compounds with masses less than 1 kDa. The detection of nonvolatile macromolecules, such as polymers and proteins, was revolutionized with the invention of electrospray ionization (ESI) [2] and matrix-assisted laser desorption ionization (MALDI) [3, 4]. Recently ambient ionization techniques have enabled the *in situ*, real time analysis of both small and large molecules from a surface with minimal sample preparation [5, 6].

1.1.1 Electrospray Ionization

In the electrospray ionization (ESI) source, a sample typically needs to be homogenized and dissolved in solvent, and is then infused through a tip with a diameter of ~100 μm where a high pressure nebulizing gas (10–50 psi) and high tip voltage (4–5 kV) are applied. As a result, the solvent breaks into small, charged droplets, and these droplets undergo solvent evaporation and Coulomb fission to generate smaller progeny droplets.

These progeny droplets will undergo further desolvation and become gas phase ions. In the case of a miniaturized version of ESI, nanoelectrospray (nano-ESI), a stable electrospray is obtained using smaller tip diameter (< 50 μm) and lower flow rate (nL/min) without the requirement of nebulizing gas [7]. Nano-ESI has lower sample consumption and higher salt tolerance in comparison with conventional ESI [7, 8].

ESI is well suited for ionizing intact molecules, including small organic and inorganic molecules, drugs, lipids, peptides, nucleotides, polymers, and proteins [1]. Large molecules, e.g., a protein, are likely to be multiply charged and thus can be detected in a lower mass range. When a nondenaturing solvent is used, noncovalent protein-protein and protein-ligand complexes and tertiary protein conformation are preserved during the ESI process [9]. Analytes as large as a tobacco mosaic virus (40 MDa) consisting of a 6395 nucleotide strand RNA surrounded by approximately 2140 protein subunits has been successfully electrosprayed intact and detected by mass spectrometry [10]. The power of ESI-MS is leveraged when coupled with a separation technique such as capillary electrophoresis (CE) [11] or liquid chromatography (LC) [12]. The addition of a separation step can separate chemical species from a mixture and acquire ESI-MS spectra while the species are eluting, allowing for increased sensitivity and compound coverage for complex sample analysis. Despite the aforementioned advantages of ESI, major shortcomings include the requirement of extensive sample preparation and loss of spatial information during the analysis. As a result, ESI is not suitable for mass spectrometry imaging analysis where the spatial distribution of molecules will be mapped on the sample surface.

1.1.2 Matrix-Assisted Laser Desorption Ionization

Laser desorption ionization (LDI) was used for mass analysis of solid materials shortly after the invention of Ruby laser [13]. LDI was limited to small molecule analysis because large molecules tend to fragment in the presence of high energy, nanosecond duration laser irradiation. Hence, different research groups started exploring the possibility of adding a matrix for intact macromolecule analysis, also known as matrix-assisted laser desorption ionization (MALDI) [3, 4, 14]. The matrix serves as an absorbing media to resonantly absorb the energy from the laser to induce desorption. The matrix then carries the sample mixture into the gas phase to minimize sample fragmentation. The focused nanosecond UV laser beam desorbs and ionizes analytes allowing detection.

MALDI is particularly suitable for large molecule analysis, including synthetic polymers and proteins. The detection of low abundance small molecules with low resolution mass analyzer can be difficult because of the interference from the abundant matrix ions in the low mass range. One way to circumvent this problem is to monitor the fragment ions instead of the parent ion from the species of interest by coupling the MALDI source with tandem mass spectrometry (MS/MS) analysis; high specificity can be achieved in this manner for small molecule analysis [15]. A critical step in MALDI analysis is matrix deposition. First, matrix must be deposited homogenously on the sample to avoid "hot spots" and assure reproducibility using either acoustic spotting [16], sublimation [17], or electrospray deposition [18]. Secondly, the choice of matrix depends on the compounds of interest. For example, α-cyano-4-hydroxycinnamic acid nitrobenzoic acid (CHCA) is used for low molecular weight peptides while sinapinic acid (SA) is more suitable for high molecular weight proteins. For phospholipids, 2,5-dihydroxybenzoic acid (DHB) is

recommended [19]. Although MALDI at atmospheric pressure (AP MALDI) has been developed [20, 21], the MALDI source is typically placed in the vacuum chamber to couple to the mass spectrometer, which is not suitable for *in situ*, real time analysis.

1.1.3 Ambient Ionization

The concept of ambient ionization emerged with the introduction of desorption electrospray ionization (DESI) [22]. Ambient ionization allows direct analysis of the sample under atmospheric pressure without extensive sample pretreatment. Ambient ionization techniques have been reviewed in detail [5, 6, 23]. In spatially-resolved ambient ionization MS, a solvent spray [22], liquid extraction probe [24, 25], plasma stream [26, 27], or laser beam [28, 29] is typically scanned over the sample to sample molecules from a given region of the surface. An additional postionization step, such as ESI [29, 30], chemical ionization (CI) [31], or photoionization (PI) [32], may be required depending on the ionization efficiency of the desorption probe. The goal of direct analysis and molecular imaging of complex biological systems, ranging from whole body [33, 34] to tissue section, body fluid [35, 36], and single cell [37, 38], has been one driving force for the development of ambient ionization.

Here, ambient ionization sources used for molecular imaging under atmospheric pressure with minimal sample preparation will be reviewed. Figure 1.1 summarizes the number of publications searched in Web of Science for ambient ionization mass spectrometry imaging since 2006 using keywords ambient mass spectrometry imaging or atmospheric pressure mass spectrometry imaging [39]. Reviews, book chapters, protocols

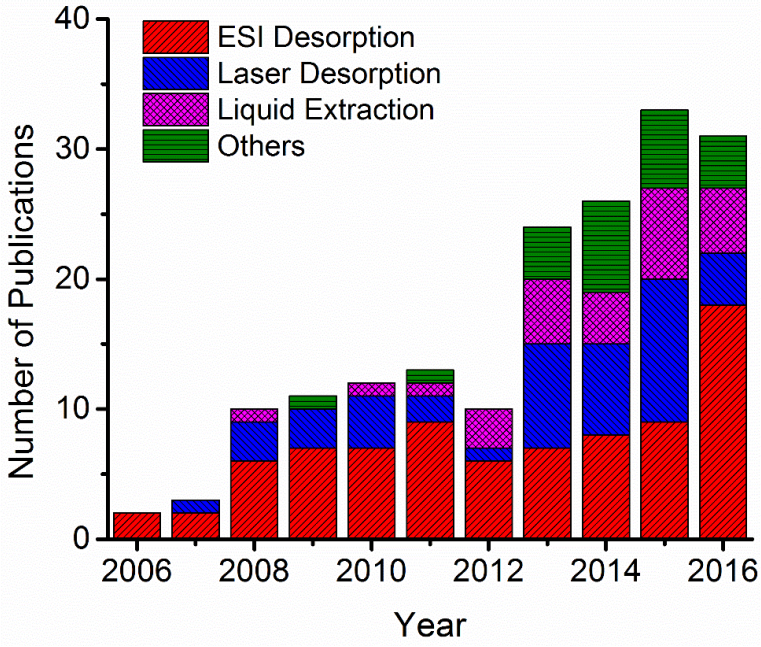

Figure 1.1. Number of publications of ambient ionization mass spectrometry imaging.

and conference papers are excluded. The most widely used ambient or atmospheric pressure imaging ion sources are composed of electrospray, liquid extraction, or laser probe based methods.

1.1.3.1 Desorption Electrospray Ionization

In desorption electrospray ionization (DESI), charged droplets from a pneumatically assisted electrospray emitter impinge the sample surface, and secondary droplets with analytes contained are desorbed from the surface, as seen in the schematic of DESI in Figure 1.2 [40]. A droplet pickup model where condensed phase analytes are solvated by the impinging droplets is suggested as the primary desorption mechanism in the analysis of biomolecules by DESI [41]. The secondary droplets will undergo solvent evaporation, become gas phase ions and transfer to the MS inlet in a similar manner as ESI.

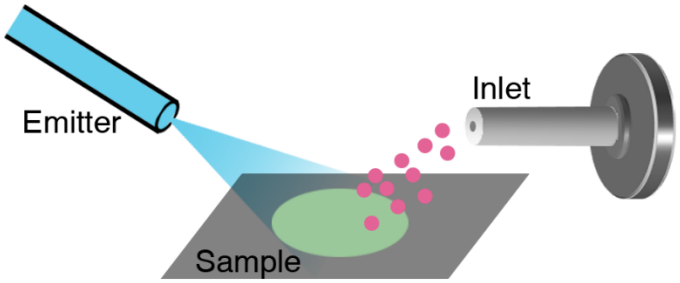

Figure 1.2. Schematic of desorption electrospray ionization (DESI).

1.1.3.2 Direct Liquid Extraction

In direct liquid extraction techniques, a confined liquid microjunction is formed between a solvent flow probe and sample surface to extract and desorb analytes from the surface for mass analysis [42]. There have been several different designs of direct liquid extraction techniques, including liquid microjunction surface sampling probe (LMJ-SSP) [24], liquid extraction surface analysis (LESA) [43], nanospray desorption electrospray ionization (nano-DESI) [25], and the Single probe [38]. A schematic of nano-DESI is shown in Figure 1.3. A liquid microjunction is formed by two capillaries: the primary capillary supplies solvent to the microjunction, while the nanospray capillary removes the solvent containing the dissolved analytes and generates charged droplets at the MS inlet.

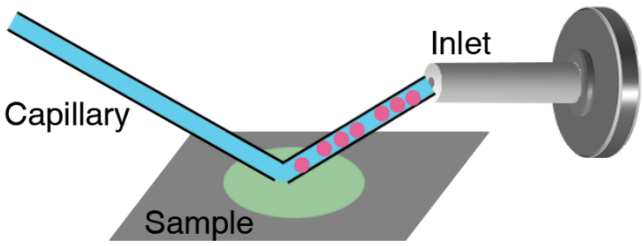

Figure 1.3. Schematic of nanospray desorption electrospray ionization (nano-DESI).

1.1.3.3 Laser Desorption and Postionization

Comparing with laser desorption ionization (LDI) under vacuum condition, the mass analysis by LDI at atmospheric pressure is very difficult because of the collisional loss of ions with ambient background gas molecules [20]. The addition of an atmospheric pressure ionization method, e.g., ESI, following laser desorption greatly increases the ion yield as the number of neutrals desorbed by the laser beam far exceeds the number of ions [44]. In 2005, Shiea's group demonstrated direct analysis of synthetic organic compounds and proteins at atmospheric pressure by coupling UV laser desorption with electrospray ionization, known as electrospray-assisted laser desorption/ionization (ELDI) [29]. A schematic setup of laser desorption followed by electrospray postionization is shown in Figure 1.4. The laser vaporized analytes from the sample are captured and ionized by the charged droplets from electrospray [45]. Several laser-electrospray hybrid ambient ionization sources using different wavelength (UV, IR, and near-IR) and pulse duration (nanosecond, picosecond, and femtosecond) will be discussed in detail in Section 1.2.4.

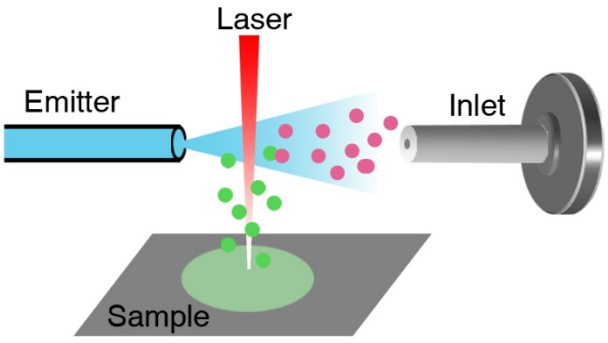

Figure 1.4. Schematic of laser desorption coupled with electrospray ionization.

1.2 Ambient Ionization Mass Spectrometry Imaging

1.2.1 Introduction to Mass Spectrometry Imaging (MSI)

Imaging techniques for characterizing biological samples include magnetic resonance imaging (MRI) [46], white light microscopy, infrared microscopy [47], Raman microscopy [48], fluorescence microscopy [49], and mass spectrometry imaging [50, 51]. Label-assisted fluorescence microscopy offers exquisite spatial resolution (< μm), *in vivo* or *ex vivo*, but relies on labeling/staining probes. Label-free techniques such as infrared and Raman microscopy can interrogate the sample with submicron lateral resolution in a noninvasive manner. However, optical signal from vibrational modes provides a limited amount of chemical information. Mass spectrometry imaging (MSI) provides excellent chemical specificity, and multiple compounds can be measured in parallel without any labeling. MSI is, however, destructive to biological sample.

In mass spectrometry imaging (MSI), sample material is desorbed from the surface, ionized, and detected by a mass analyzer as a function of spatial location, providing the distribution of molecules on a sample surface. Given the high sensitivity and molecular specificity, MSI demonstrates significant potential for application in areas such as imaging drugs, lipids, proteins and metabolites in tissues [52, 53], mapping chemical residues in latent fingerprints [54, 55], and discovering biomarkers for tumor detection [56, 57].

Table 1.1 summarizes the parameters, including sample requirement, spatial resolution, pixel time, and type of analytes, for different MSI techniques used for biological tissue imaging. Spatial resolution is a key parameter for any MSI method, and it is mainly determined by the size of the probe. For example, DESI is routinely operated at 200 μm spatial resolution, which is directly affected by the erosion diameter of the DESI spray jet

Table 1.1. Comparison of typical parameters of different mass spectrometry imaging techniques for tissue imaging.

	Ionization Source	Sample Requirement	Spatial Resolution	Pixel Time	Type of Analytes	Ref
MALDI	UV laser	Matrix deposition and vacuum condition	10–100 µm (typically), 1–2 µm (best reported)	0.03 s	Lipids, peptides, proteins	[57-59]
DESI	Solvent spray	None	200 µm (typically), 35 µm (best reported)	1.16 s	Small molecules, lipids, peptides	[60, 61]
nano-DESI	Liquid probe	Ideally flat sample, non-flat sample is possible with height tracking	100–150 µm (typically), 12 µm (best reported)	2 s	Small molecules, lipids, peptides, proteins	[42, 62, 63]
LEMS	Laser desorption electrospray ionization	None	100 µm (typically), 65 µm (best reported)	2 s	Small molecules, lipids, peptides, proteins	[64]

on the sample surface [65]. Spatial features of approximately 35 μm on a mouse brain cerebellum tissue section were resolved by DESI-MS using a combination of smaller step size, slower step scan rates, shorter MS scan, plus the use of morphologically friendly solvent (DMF/EtOH 1:2) and relatively low solvent flow rate [61]. For direct liquid extract techniques, like LMJ-SSP and LESA, the size of the liquid microjunction limits the spatial resolution to >500 μm. The size of the liquid junction can be significantly reduced to 8 μm by optimizing the microjunction-surface distance using a non-coaxial configuration with pulled capillaries in nano-DESI, enabling MSI with a resolution of 12 μm on a dye film [66]. In laser-based MSI ion sources, the size of the laser probe is relatively easy to control by laser focusing optics in comparison with electrospray and liquid extraction based approaches. However, there is also a trade-off between the size of the probe and the sensitivity. Smaller diameter laser spots desorb less material for subsequent ionization.

1.2.2 Desorption Electrospray Ionization MSI

The potential of DESI for spatially-resolved analysis was first introduced in the Cooks group by scanning the electrospray probe over a cross section of a plant stem, and the signal of coniceine was observed to change over the stem [22]. Later, a DESI source coupled with an automated stage scanning system was introduced and applied for imaging of Rhodamine dyes separated on thin-layer chromatography (TLC) plates [67]. Wiseman et al. [68] demonstrated the first example of tissue imaging by DESI-MS where lipids were observed from a coronal rat brain tissue section at negative mode using methanol/water as spray solvent. Since then, DESI imaging of small metabolites and lipids has been applied to tissues including dog bladder [69], human plaque [70], human kidney [71], human lens

[72], rat spinal cord [73], and porcine and rabbit adrenal glands [74]. Three-dimensional visualization of lipids in a mouse brain model was constructed from a set of 2D ion images by analyzing consecutive sections of the brain [75]. The spatial resolution of DESI is routinely operated at 200 μm, although 35 μm was reported on one study in which spatial features as small as 35 μm was observed on a mouse brain cerebellum tissue section by systematic optimization of the experimental condition [61].

Imaging lipids using DESI has been shown to be useful for tumor detection and classification [76]. In one study, distinctive lipid profiles associated with sulfatides and galactoceramides were observed from human brain astrocytomas tumors with different degree of malignancy [77], and from human brain tumors from different histology types, including oligodendroglioma, astrocytoma and meningioma [78]. Clozapine and its main active metabolites *N*-desmethylclozapine and clozapine-*N*-oxide were imaged in brain, lung, kidney, and testis of orally dosed rats [52]. Comparison of DESI imaging with whole-body autoradiography (WBA) for whole-body tissue sections of mice intravenously dosed with drug propranolol was made [34]. Nominal agreement for the relative distributions of propranolol in the brain, lung, and liver was observed between the ion signal from DESI and the radioactivity from WBA. Ion images of natural products from leaf samples by DESI show the distribution of plant metabolites and secondary metabolites after pre-treatment, including physical stripping [79], solvent extraction [80], and surface imprinting [81].

DESI is not effective for mass spectrometry imaging of large molecules from tissue samples. In one study, MALDI-MS was combined with DESI-MS for the imaging of small analytes and large proteins from a single mouse brain section [82]. Pre-washing tissue section with organic solvent and coupling DESI ion source with an ion filtering device,

high-field asymmetric ion mobility spectrometer (FAIMS), were adopted to remove the interference from small analytes, and DESI was able to image cardiolipins (<2 kDa) and failed to detect large proteins from the tissue [83].

1.2.3 Nanospray Desorption Electrospray Ionization MSI

Nanospray desorption electrospray ionization (nano-DESI) has been used for imaging of small metabolites and lipids from rat brain [66, 84], mouse spinal cord [85], human kidney [66], and bacterial colony [62, 86]. Three-dimensional imaging of a mouse uterine sample was enabled by imaging ~20 successive 12 μm thick sections with a spatial resolution of 150 μm [87]. Proteins, including ubiquitin, β-thymosin, myelin basic protein, and hemoglobin, were spatially mapped by nano-DESI from a mice brain section after rinsing the section with chloroform to remove small analytes [88]. The spatial resolution of nano-DESI for tissue imaging is about 100–150 μm, although 12 μm was reported for dye film imaging using pulled capillaries [66]. A critical parameter for nano-DESI imaging is to keep the distance between the probe and the sample constant to prevent the probe from crashing or losing contact with the sample. Biological samples with complex topography such as bacterial colony have been imaged by integrating nano-DESI with shear-force probe to constantly control the distance between the sample and nano-DESI probe [87].

1.2.4 Laser Desorption and Electrospray Ionization MSI

1.2.4.1 Electrospray-Assisted Laser Desorption/Ionization

Electrospray-assisted laser desorption/ionization (ELDI) uses a nanosecond UV laser (337 nm, 4 ns) to ablate sample material from the tissue for ESI postionization. Even

though ELDI was introduced in 2005, the first example of tissue imaging was not demonstrated until 2012 [89]. Two types of fungus, *Ganoderma lucidum* and *Antrodia camphorate*, were imaged by ELDI with a spot size of approximately 100 × 150 μm^2 [89]. Several ions distributed on the skin compared to the interior of the *G. lucidum* section.

Continuous liquid flow probe has also been demonstrated as an efficient source to capture UV nanosecond laser vaporized material and infuse the analytes to ESI ionization by the Van Berkel group at Oak Ridge National Laboratory [90-92]. In one study, a continuous flow surface sampling probe was placed in close proximity to the surface to collect the plume produced by laser ablation using a 337 nm laser with 11 ns pulse width. A spatial resolution of approximately 100 μm was obtained for chemical imaging of blue ink film [90]. In another study, a chemical image of a selected lipid was obtained with an estimated imaging resolution of about 50 μm from a mouse brain section, based on the smallest feature distinguished in the image [91]. Using a 'cut and drop' method, tissue microdissections as small as 20 × 20 μm^2 were cut on a commercial laser microscope and dropped into the flowing solvent of a liquid capture probe. Absolute quantitation of a drug, propranolol and its metabolite, was achieved from mouse brain, kidney, and liver tissues [92].

1.2.4.2 Laser Ablation Electrospray Ionization

IR lasers have seen increased use for laser ablation taking advantage of the abundant water content in the sample since the application of IR lasers in MALDI [93] and AP MALDI [28] for biological sample analysis. Direct LDI using an infrared laser (2940 nm) was used for the imaging of plant tissue under atmospheric pressure without

application of an external matrix [28]. The endogenous water in the plant serves as the matrix because the strong O-H vibrational mode absorbs the IR laser pulse. Similar to ELDI, laser ablation electrospray ionization (LAESI) couples IR laser ablation with electrospray ionization [35]. The LAESI signal increased by one or two orders of magnitude compared to AP IR-LDI without electrospray ionization [94].

LAESI has been predominantly applied for plant tissue imaging. Two-dimensional imaging of zebra plant leaves resulted in ion images corresponding to the green and yellow regions of the leaf with a lateral resolution of ~350 μm [95]. Three-dimensional imaging of metabolites of in the plant was demonstrated by continuously scanning the leaf layer-by-layer with lateral and depth resolution of 300 and 30 μm, respectively [96]. In situ cell-by-cell imaging of *Allium cepa* epidermal cells was enabled by focusing the laser pulses to 30 to 40 μm ablation spot diameter through the etched tip of a GeO_2-based glass fiber [37, 97]. In addition, imaging of small metabolites and lipids in rat brain tissues was studied by LAESI [98]. However, a peltier cooling stage was required to maintain the water content of the tissue during the analysis time of 3 hours. Coupling the LAESI-MS ion source with ion mobility separation allows the detection of isobaric ions and enhances the coverage of small metabolites from *Pelargonium peltatum* leaf and mouse brain [99]. In a recent study, metabolites and lipids in *E. coli* and *B. subtilis* bacterial colonies were imaged by LAESI-MS to study the antibiotic inhibition of bacterial growth [100].

1.2.4.3 Matrix-Assisted Laser Desorption Electrospray Ionization

Like MALDI, matrix-assisted laser desorption electrospray ionization (MALDESI) uses a MALDI matrix to improve the desorption of analytes by a UV nanosecond laser

[101]. The desorbed analyte plume is then ionized by electrospray under atmospheric pressure. Multiply charged peptides and proteins were detected by MALDESI using a UV laser when the analytes were mixed with MALDI matrices [101]. But the concept of MALDESI using an organic matrix was never applied in chemical imaging. Later, the UV laser was replaced by an IR laser in IR-MALDESI and endogenous water in biological tissue was used as a matrix, just like LAESI. Spatial images of lipids were demonstrated from mouse heart and lung samples at a spatial resolution of 200 μm by IR-MALDESI, and spatial features as small as 45 μm were resolved by oversampling methods where 30 μm laser spot spacing was used in mouse brain tissue samples [102]. The distribution of drug lapatinib and its metabolites in the liver tissue of a dosed dog was studied by IR-MALDESI and demonstrated comparable results with UV-MALDI [103]. Pharmaceutical drugs and endogenous lipids in whole-body sections of neonate mouse was also shown by IR-MALDESI [104]. In one study, lipids corresponding to the mesocarp and exocarp regions of a cucumber fermented and stored in 1 M sodium chloride brine were imaged by IR-MALDESI without the need of any desalting process [105].

1.2.4.4 Picosecond Infrared Laser Ablation Electrospray Ionization

One of the drawbacks of using nanosecond lasers to ablate biological tissue samples, e.g., in ELDI, LAESI and MALDESI, is the extensive thermal tissue damage outside the ablated zone in comparison with picosecond or femtosecond lasers [106-108]. Picosecond infrared laser ablation electrospray ionization (PIR-LAESI) combines a picosecond IR laser (2880 nm wavelength and 80 ps pulse duration) ablation with electrospray ionization for biological tissue analysis [109]. In this study, the distribution of

endogenous metabolites in zebra plant leaves was imaged with a lateral resolution of 100 μm. A chemical reagent, gadoteridol, was found to be predominantly distributed in the medulla region compared to cortex region in a mouse kidney injected with gadoteridol by PIR-LAESI.

1.2.4.5 Laser Electrospray Mass Spectrometry

Laser electrospray mass spectrometry (LEMS), proposed in the Levis group in 2009, integrates femtosecond duration laser pulses from a Ti:Sapphire laser (50 fs and 800 nm) for vaporization with electrospray ionization [110]. In LEMS, the femtosecond laser pulses will interact directly with the analytes via a nonlinear, multiphoton excitation mechanism because of the high laser intensity provided (10^{12}–10^{13} W/cm^2). This intensity is 6 to 7 orders of magnitude higher than methods that use nanosecond lasers. Direct analysis of a variety of biomolecules was successfully demonstrated by LEMS without any matrices, including pharmaceuticals [111], lipids [112], proteins [113, 114], whole blood [112, 113], milk [112], plant [115, 116], and animal tissue samples [64]. Recently, a commercial turn-key femtosecond fiber laser with longer duration (435 fs) and lower energy (50 μJ) was compared with Ti:Sapphire laser for direct analysis of lipids, proteins, flower and mouse brain samples, and showed comparable laser desorption capability [117, 118].

The spatial imaging capability of LEMS was first shown by scanning an oxycodone film deposited on a stainless steel sample slide with 250 μm spatial step size [111]. Mass spectra from selected green and white regions of a single leaf were detected with distinct molecular profiles, suggesting the potential of LEMS for biological tissue imaging [115].

Femtosecond laser desorption, an automated XY position sampling stage, and a high resolution accurate mass mass spectrometer were synchronized using a custom user interface. The source provided a spatial resolution of ~60 μm measuring an ink pattern [64]. Features corresponding to the vein and non-vein area of a plant leaf were also successfully resolved by LEMS imaging, and will be discussed in Chapter 4. Statistical analysis, principal component analysis and nonnegative matrix factorization, can be applied to the LEMS imaging dataset (>1 GB) for automated feature extraction within minutes. Chemical imaging of animal tissue sample, including pig liver and mouse brain, by LEMS will be discussed in Chapter 5.

1.3 Scope of this Dissertation

In Chapter 2, a turn-key femtosecond fiber laser with a pulse duration of 435 fs and a wavelength of 1042 nm was used to investigate the vaporization of biological macromolecules from the condensed phase into the gas phase for nanospray ionization and mass analysis. The mass spectra from cytochrome c and lysozyme samples with the low-energy, longer-duration fiber laser were compared with results from high energy (500 μJ), 45 fs, 800 nm Ti:Sapphire-based femtosecond laser. The effect of sample substrate, sample volume, and pulse energy was investigated in the laser vaporization step of aqueous protein samples. Direct analysis of hemoglobin subunit-heme complex from whole blood was enabled by the fiber laser.

Ambient molecular analysis of biological tissue using the lower-energy, longer-duration femtosecond fiber laser is highlighted in Chapter 3. LEMS mass spectra of flower petal and leaf samples were compared between the fiber laser and high energy Ti:Sapphire

laser. Anthocyanins, sugars and other metabolites were detected and revealed the anticipated metabolite profile. Phospholipids were identified from a mouse brain sampling using Ti:Sapphire LEMS without matrix deposition. The effect of optimal cutting temperature compounds on ion suppression were studied in the analysis of brain species.

Chapter 4 details the design of a high spatial and mass resolution LEMS source, including instrumental design, software development and data analysis. The Ti:Sapphire laser, translation stage, and mass analyzer are synchronized to enable step-by-step scanning of tissue sample for mass analysis. Measurement of a patterned ink film was shown with a lateral resolution of ~60 μm by LEMS. Metabolites including sugar, anthocyanins and other small metabolites were successfully mapped from plant samples without oversampling using a spot size of 60 × 70 μm^2.

Animal tissue imaging using the LEMS imaging source is highlighted in Chapter 5. Small metabolites, lipids and proteins are simultaneously vaporized directly from the tissue into the gas phase by a single femtosecond laser pulse (800 nm, 1.5 mJ, 50 fs) and ionized by electrospray droplets. Lipids, including glycerophosphocholine (GPC), lysophosphatidylcholine (LysoPC), phosphatidylcholine (PC) and bile acid, were detected from pig liver samples without application of matrix. Pig hemoglobin α subunit (~15 kDa) and its mono- and di-glycosylated derivatives were spatially imaged in the liver sample. Grey and white matter regions of a mouse brain section were spatially resolved in the LEMS imaging measurement. Molecular signatures, including free heme, hemoglobin α, and β subunits, accompanied by LysoPC(16:0), were mapped in the mouse brain with mild traumatic brain injury (TBI), indicating that blood-brain barrier disruption occurred during the injury. Potential biomarkers of TBI were also detected from the brain injury region.

1.4 References

1. J.H. Gross. *Mass spectrometry: A textbook.* Springer, Berlin Heidelberg (2011).

2. J.B. Fenn, M. Mann, C.K. Meng, S.F. Wong, C.M. Whitehouse. Electrospray ionization for mass spectrometry of large biomolecules. *Science* **246**, 64 (1989).

3. K. Tanaka, H. Waki, Y. Ido, S. Akita, Y. Yoshida, T. Yoshida, T. Matsuo. Protein and polymer analyses up to m/z 100 000 by laser ionization time-of-flight mass spectrometry. *Rapid Commun. Mass Spectrom.* **2**, 151 (1988).

4. M. Karas, F. Hillenkamp. Laser desorption ionization of proteins with molecular masses exceeding 10,000 daltons. *Anal. Chem.* **60**, 2299 (1988).

5. M.-Z. Huang, S.-C. Cheng, Y.-T. Cho, J. Shiea. Ambient ionization mass spectrometry: A tutorial. *Anal. Chim. Acta* **702**, 1 (2011).

6. M.E. Monge, G.A. Harris, P. Dwivedi, F.M. Fernández. Mass spectrometry: Recent advances in direct open air surface sampling/ionization. *Chem. Rev.* **113**, 2269 (2013).

7. M. Wilm, M. Mann. Analytical properties of the nanoelectrospray ion source. *Anal. Chem.* **68**, 1 (1996).

8. R. Juraschek, T. Dülcks, M. Karas. Nanoelectrospray—more than just a minimized-flow electrospray ionization source. *J. Am. Soc. Mass Spectrom.* **10**, 300 (1999).

9. A.C. Leney, A.J.R. Heck. Native mass spectrometry: What is in the name? *J. Am. Soc. Mass Spectrom.* **28**, 5 (2017).

10. S.D. Fuerstenau, W.H. Benner, J.J. Thomas, C. Brugidou, B. Bothner, G. Siuzdak. Mass spectrometry of an intact virus. *Angew. Chem. Int. Ed.* **40**, 541 (2001).

11. S.S. Zhao, X. Zhong, C. Tie, D.D.Y. Chen. Capillary electrophoresis-mass spectrometry for analysis of complex samples. *Proteomics* **12**, 2991 (2012).

12. W. Li, J. Zhang, F.L.S. Tse. *Handbook of LC-MS bioanalysis: Best practices, experimental protocols, and regulations.* John Wiley & Sons Inc., Hoboken, NJ (2013).

13. F. Hillenkamp, E. UnsoLd, R. Kaufmann, R. Nitsche. Laser microprobe mass analysis of organic materials. *Nature* **256**, 119 (1975).

14. M. Karas, D. Bachmann, U. Bahr, F. Hillenkamp. Matrix-assisted ultraviolet laser desorption of non-volatile compounds. *Int. J. Mass Spectrom. Ion Processes* **78**, 53 (1987).

15. N.V. Gogichaeva, T. Williams, M.A. Alterman. MALDI TOF/TOF tandem mass spectrometry as a new tool for amino acid analysis. *J. Am. Soc. Mass Spectrom.* **18**, 279 (2007).

16. H.-R. Aerni, D.S. Cornett, R.M. Caprioli. Automated acoustic matrix deposition for MALDI sample preparation. *Anal. Chem.* **78**, 827 (2006).

17. J.A. Hankin, R.M. Barkley, R.C. Murphy. Sublimation as a method of matrix application for mass spectrometric imaging. *J. Am. Soc. Mass Spectrom.* **18**, 1646 (2007).

18. S. Li, Y. Zhang, J.a. Liu, J. Han, M. Guan, H. Yang, Y. Lin, S. Xiong, Z. Zhao. Electrospray deposition device used to precisely control the matrix crystal to improve the performance of MALDI MSI. *Sci. Rep.* **6**, 37903 (2016).

19. B.K. Kaletaş, I.M. van der Wiel, J. Stauber, J.D. Lennard, C. Güzel, J.M. Kros, T.M. Luider, R.M.A. Heeren. Sample preparation issues for tissue imaging by imaging MS. *Proteomics* **9**, 2622 (2009).

20. V.V. Laiko, M.A. Baldwin, A.L. Burlingame. Atmospheric pressure matrix-assisted laser desorption/ionization mass spectrometry. *Anal. Chem.* **72**, 652 (2000).

21. V.V. Laiko, A.L. Burlingame. *Atmospheric pressure matrix assisted laser desorption.* U.S. Patent 5965884 (1999).

22. Z. Takáts, J.M. Wiseman, B. Gologan, R.G. Cooks. Mass spectrometry sampling under ambient conditions with desorption electrospray ionization. *Science* **306**, 471 (2004).

23. G.A. Harris, A.S. Galhena, F.M. Fernández. Ambient sampling/ionization mass spectrometry: Applications and current trends. *Anal. Chem.* **83**, 4508 (2011).

24. G.J. Van Berkel, V. Kertesz, K.A. Koeplinger, M. Vavrek, A.-N.T. Kong. Liquid microjunction surface sampling probe electrospray mass spectrometry for detection of drugs and metabolites in thin tissue sections. *J. Mass Spectrom.* **43**, 500 (2008).

25. P.J. Roach, J. Laskin, A. Laskin. Nanospray desorption electrospray ionization: An ambient method for liquid-extraction surface sampling in mass spectrometry. *Analyst* **135**, 2233 (2010).

26. R.B. Cody, J.A. Laramée, H.D. Durst. Versatile new ion source for the analysis of materials in open air under ambient conditions. *Anal. Chem.* **77**, 2297 (2005).

27. J.D. Harper, N.A. Charipar, C.C. Mulligan, X. Zhang, R.G. Cooks, Z. Ouyang. Low-temperature plasma probe for ambient desorption ionization. *Anal. Chem.* **80**, 9097 (2008).

28. Y. Li, B. Shrestha, A. Vertes. Atmospheric pressure molecular imaging by infrared MALDI mass spectrometry. *Anal. Chem.* **79**, 523 (2007).

29. J. Shiea, M.-Z. Huang, H.-J. Hsu, C.-Y. Lee, C.-H. Yuan, I. Beech, J. Sunner. Electrospray-assisted laser desorption/ionization mass spectrometry for direct ambient analysis of solids. *Rapid Commun. Mass Spectrom.* **19**, 3701 (2005).

30. H. Chen, A. Venter, R.G. Cooks. Extractive electrospray ionization for direct analysis of undiluted urine, milk and other complex mixtures without sample preparation. *Chem. Commun.* 2042 (2006).

31. J.J. Coon, K.J. McHale, W.W. Harrison. Atmospheric pressure laser desorption/chemical ionization mass spectrometry: A new ionization method based on existing themes. *Rapid Commun. Mass Spectrom.* **16**, 681 (2002).

32. M. Haapala, J. Pól, V. Saarela, V. Arvola, T. Kotiaho, R.A. Ketola, S. Franssila, T.J. Kauppila, R. Kostiainen. Desorption atmospheric pressure photoionization. *Anal. Chem.* **79**, 7867 (2007).

33. J.Y. Yew, R.B. Cody, E.A. Kravitz. Cuticular hydrocarbon analysis of an awake behaving fly using direct analysis in real-time time-of-flight mass spectrometry. *Proc. Natl. Acad. Sci. U.S.A.* **105**, 7135 (2008).

34. V. Kertesz, G.J. Van Berkel, M. Vavrek, K.A. Koeplinger, B.B. Schneider, T.R. Covey. Comparison of drug distribution images from whole-body thin tissue sections obtained using desorption electrospray ionization tandem mass spectrometry and autoradiography. *Anal. Chem.* **80**, 5168 (2008).

35. P. Nemes, A. Vertes. Laser ablation electrospray ionization for atmospheric pressure, in vivo, and imaging mass spectrometry. *Anal. Chem.* **79**, 8098 (2007).

36. N.E. Manicke, Q. Yang, H. Wang, S. Oradu, Z. Ouyang, R.G. Cooks. Assessment of paper spray ionization for quantitation of pharmaceuticals in blood spots. *Int. J. Mass Spectrom.* **300**, 123 (2011).

37. B. Shrestha, A. Vertes. In situ metabolic profiling of single cells by laser ablation electrospray ionization mass spectrometry. *Anal. Chem.* **81**, 8265 (2009).

38. N. Pan, W. Rao, N.R. Kothapalli, R. Liu, A.W.G. Burgett, Z. Yang. The Single-probe: A miniaturized multifunctional device for single cell mass spectrometry analysis. *Anal. Chem.* **86**, 9376 (2014).

39. Web of Science. www.webofknowledge.com/. accessed Feburay 23 2017.

40. Z. Takáts, J.M. Wiseman, R.G. Cooks. Ambient mass spectrometry using desorption electrospray ionization (DESI): Instrumentation, mechanisms and

applications in forensics, chemistry, and biology. *J. Mass Spectrom.* **40**, 1261 (2005).

41. A. Venter, P.E. Sojka, R.G. Cooks. Droplet dynamics and ionization mechanisms in desorption electrospray ionization mass spectrometry. *Anal. Chem.* **78**, 8549 (2006).

42. J. Laskin, I. Lanekoff. Ambient mass spectrometry imaging using direct liquid extraction techniques. *Anal. Chem.* **88**, 52 (2016).

43. V. Kertesz, G.J. Van Berkel. Fully automated liquid extraction-based surface sampling and ionization using a chip-based robotic nanoelectrospray platform. *J. Mass Spectrom.* **45**, 252 (2010).

44. R.B. Van Breemen, M. Snow, R.J. Cotter. Time-resolved laser desorption mass spectrometry. I. Desorption of preformed ions. *Int. J. Mass Spectrom. Ion Phys* **49**, 35 (1983).

45. P.M. Flanigan, R.J. Levis. Ambient femtosecond laser vaporization and nanosecond laser desorption electrospray ionization mass spectrometry. *Annu. Rev. Anal. Chem.* **7**, 229 (2014).

46. E. Terreno, D.D. Castelli, A. Viale, S. Aime. Challenges for molecular magnetic resonance imaging. *Chem. Rev.* **110**, 3019 (2010).

47. M.J. Baker, J. Trevisan, P. Bassan, R. Bhargava, H.J. Butler, K.M. Dorling, P.R. Fielden, S.W. Fogarty, N.J. Fullwood, K.A. Heys, C. Hughes, P. Lasch, P.L. Martin-Hirsch, B. Obinaju, G.D. Sockalingum, J. Sulé-Suso, R.J. Strong, M.J. Walsh, B.R. Wood, P. Gardner, F.L. Martin. Using Fourier Transform IR spectroscopy to analyze biological materials. *Nat. Protoc.* **9**, 1771 (2014).

48. L. Opilik, T. Schmid, R. Zenobi. Modern Raman imaging: Vibrational spectroscopy on the micrometer and nanometer scales. *Annu. Rev. Anal. Chem.* **6**, 379 (2013).

49. J.W. Lichtman, J.-A. Conchello. Fluorescence microscopy. *Nat. Methods* **2**, 910 (2005).

50. L.A. McDonnell, R.M.A. Heeren. Imaging mass spectrometry. *Mass Spectrom. Rev.* **26**, 606 (2007).

51. C. Wu, A.L. Dill, L.S. Eberlin, R.G. Cooks, D.R. Ifa. Mass spectrometry imaging under ambient conditions. *Mass Spectrom. Rev.* **32**, 218 (2013).

52. J.M. Wiseman, D.R. Ifa, Y. Zhu, C.B. Kissinger, N.E. Manicke, P.T. Kissinger, R.G. Cooks. Desorption electrospray ionization mass spectrometry: Imaging drugs and metabolites in tissues. *Proc. Natl. Acad. Sci. U.S.A.* **105**, 18120 (2008).

53. E.H. Seeley, R.M. Caprioli. Molecular imaging of proteins in tissues by mass spectrometry. *Proc. Natl. Acad. Sci. U.S.A.* **105**, 18126 (2008).

54. M.J. Bailey, N.J. Bright, R.S. Croxton, S. Francese, L.S. Ferguson, S. Hinder, S. Jickells, B.J. Jones, B.N. Jones, S.G. Kazarian, J.J. Ojeda, R.P. Webb, R. Wolstenholme, S. Bleay. Chemical characterization of latent fingerprints by matrix-assisted laser desorption ionization, time-of-flight secondary ion mass spectrometry, mega electron volt secondary mass spectrometry, gas chromatography/mass spectrometry, X-ray photoelectron spectroscopy, and attenuated total reflection Fourier Transform infrared spectroscopic imaging: An intercomparison. *Anal. Chem.* **84**, 8514 (2012).

55. D.R. Ifa, N.E. Manicke, A.L. Dill, R.G. Cooks. Latent fingerprint chemical imaging by mass spectrometry. *Science* **321**, 805 (2008).

56. H. Meistermann, J.L. Norris, H.-R. Aerni, D.S. Cornett, A. Friedlein, A.R. Erskine, A. Augustin, M.C. De Vera Mudry, S. Ruepp, L. Suter, H. Langen, R.M. Caprioli, A. Ducret. Biomarker discovery by imaging mass spectrometry: Transthyretin is a biomarker for gentamicin-induced nephrotoxicity in rat. *Mol. Cell. Proteomics* **5**, 1876 (2006).

57. J.L. Norris, R.M. Caprioli. Analysis of tissue specimens by matrix-assisted laser desorption/ionization imaging mass spectrometry in biological and clinical research. *Chem. Rev.* **113**, 2309 (2013).

58. A. Zavalin, E.M. Todd, P.D. Rawhouser, J. Yang, J.L. Norris, R.M. Caprioli. Direct imaging of single cells and tissue at sub-cellular spatial resolution using transmission geometry MALDI MS. *J. Mass Spectrom.* **47**, 1473 (2012).

59. A. Zavalin, J. Yang, K. Hayden, M. Vestal, R.M. Caprioli. Tissue protein imaging at 1 μm laser spot diameter for high spatial resolution and high imaging speed using transmission geometry MALDI TOF MS. *Anal. Bioanal. Chem.* **407**, 2337 (2015).

60. J.M. Wiseman, D.R. Ifa, A. Venter, R.G. Cooks. Ambient molecular imaging by desorption electrospray ionization mass spectrometry. *Nat. Protoc.* **3**, 517 (2008).

61. D. Campbell, C. Ferreira, L. Eberlin, R.G. Cooks. Improved spatial resolution in the imaging of biological tissue using desorption electrospray ionization. *Anal. Bioanal. Chem.* **404**, 389 (2012).

62. S.N. Nguyen, A.V. Liyu, R.K. Chu, C.R. Anderton, J. Laskin. Constant-distance mode nanospray desorption electrospray ionization mass spectrometry imaging of biological samples with complex topography. *Anal. Chem.* **89**, 1131 (2017).

63. S.E. Dautel, J.E. Kyle, G. Clair, R.L. Sontag, K.K. Weitz, A.K. Shukla, S.N. Nguyen, Y.-M. Kim, E.M. Zink, T. Luders, C.W. Frevert, S.A. Gharib, J. Laskin,

J.P. Carson, T.O. Metz, R.A. Corley, C. Ansong. Lipidomics reveals dramatic lipid compositional changes in the maturing postnatal lung. *Sci. Rep.* **7**, 40555 (2017).

64. F. Shi, J.J. Archer, R.J. Levis. Nonresonant, femtosecond laser vaporization and electrospray post-ionization mass spectrometry as a tool for biological tissue imaging. *Methods* **104**, 79 (2016).

65. F.M. Green, T.L. Salter, I.S. Gilmore, P. Stokes, G. O'Connor. The effect of electrospray solvent composition on desorption electrospray ionisation (DESI) efficiency and spatial resolution. *Analyst* **135**, 731 (2010).

66. J. Laskin, B.S. Heath, P.J. Roach, L. Cazares, O.J. Semmes. Tissue imaging using nanospray desorption electrospray ionization mass spectrometry. *Anal. Chem.* **84**, 141 (2012).

67. G.J. Van Berkel, V. Kertesz. Automated sampling and imaging of analytes separated on thin-layer chromatography plates using desorption electrospray ionization mass spectrometry. *Anal. Chem.* **78**, 4938 (2006).

68. J.M. Wiseman, D.R. Ifa, Q. Song, R.G. Cooks. Tissue imaging at atmospheric pressure using desorption electrospray ionization (DESI) mass spectrometry. *Angew. Chem. Int. Ed.* **45**, 7188 (2006).

69. A.L. Dill, D.R. Ifa, N.E. Manicke, A.B. Costa, J.A. Ramos-Vara, D.W. Knapp, R.G. Cooks. Lipid profiles of canine invasive transitional cell carcinoma of the urinary bladder and adjacent normal tissue by desorption electrospray ionization imaging mass spectrometry. *Anal. Chem.* **81**, 8758 (2009).

70. N.E. Manicke, M. Nefliu, C. Wu, J.W. Woods, V. Reiser, R.C. Hendrickson, R.G. Cooks. Imaging of lipids in atheroma by desorption eectrospray ionization mass spectrometry. *Anal. Chem.* **81**, 8702 (2009).

71. A.L. Dill, L.S. Eberlin, C. Zheng, A.B. Costa, D.R. Ifa, L. Cheng, T.A. Masterson, M.O. Koch, O. Vitek, R.G. Cooks. Multivariate statistical differentiation of renal cell carcinomas based on lipidomic analysis by ambient ionization imaging mass spectrometry. *Anal. Bioanal. Chem.* **398**, 2969 (2010).

72. S.R. Ellis, C. Wu, J.M. Deeley, X. Zhu, R.J.W. Truscott, M.i.h. Panhuis, R.G. Cooks, T.W. Mitchell, S.J. Blanksby. Imaging of human lens lipids by desorption electrospray ionization mass spectrometry. *J. Am. Soc. Mass Spectrom.* **21**, 2095 (2010).

73. M. Girod, Y. Shi, J.-X. Cheng, R.G. Cooks. Desorption electrospray ionization imaging mass spectrometry of lipids in rat spinal cord. *J. Am. Soc. Mass Spectrom.* **21**, 1177 (2010).

74. C. Wu, D.R. Ifa, N.E. Manicke, R.G. Cooks. Molecular imaging of adrenal gland by desorption electrospray ionization mass spectrometry. *Analyst* **135**, 28 (2010).

75. L.S. Eberlin, D.R. Ifa, C. Wu, R.G. Cooks. Three-dimensional vizualization of mouse brain by lipid analysis using ambient ionization mass spectrometry. *Angew. Chem. Int. Ed.* **49**, 873 (2010).

76. L.S. Eberlin, I. Norton, A.L. Dill, A.J. Golby, K.L. Ligon, S. Santagata, R.G. Cooks, N.Y.R. Agar. Classifying human brain tumors by lipid imaging with mass spectrometry. *Cancer Res.* **72**, 645 (2012).

77. L.S. Eberlin, A.L. Dill, A.J. Golby, K.L. Ligon, J.M. Wiseman, R.G. Cooks, N.Y.R. Agar. Discrimination of human astrocytoma subtypes by lipid analysis using desorption electrospray ionization imaging mass spectrometry. *Angew. Chem. Int. Ed.* **49**, 5953 (2010).

78. L.S. Eberlin, I. Norton, D. Orringer, I.F. Dunn, X. Liu, J.L. Ide, A.K. Jarmusch, K.L. Ligon, F.A. Jolesz, A.J. Golby, S. Santagata, N.Y.R. Agar, R.G. Cooks. Ambient mass spectrometry for the intraoperative molecular diagnosis of human brain tumors. *Proc. Natl. Acad. Sci. U.S.A.* **110**, 1611 (2013).

79. B. Li, N. Bjarnholt, S.H. Hansen, C. Janfelt. Characterization of barley leaf tissue using direct and indirect desorption electrospray ionization imaging mass spectrometry. *J. Mass Spectrom.* **46**, 1241 (2011).

80. B. Li, S.H. Hansen, C. Janfelt. Direct imaging of plant metabolites in leaves and petals by desorption electrospray ionization mass spectrometry. *Int. J. Mass Spectrom.* **348**, 15 (2013).

81. T. Müller, S. Oradu, D.R. Ifa, R.G. Cooks, B. Kräutler. Direct plant tissue analysis and imprint imaging by desorption electrospray ionization mass spectrometry. *Anal. Chem.* **83**, 5754 (2011).

82. L.S. Eberlin, X. Liu, C.R. Ferreira, S. Santagata, N.Y.R. Agar, R.G. Cooks. Desorption electrospray ionization then MALDI mass spectrometry imaging of lipid and protein distributions in single tissue sections. *Anal. Chem.* **83**, 8366 (2011).

83. C.L. Feider, N. Elizondo, L.S. Eberlin. Ambient ionization and FAIMS mass spectrometry for enhanced imaging of multiply charged molecular ions in biological tissues. *Anal. Chem.* **88**, 11533 (2016).

84. I. Lanekoff, B.S. Heath, A. Liyu, M. Thomas, J.P. Carson, J. Laskin. Automated platform for high-resolution tissue imaging using nanospray desorption electrospray ionization mass spectrometry. *Anal. Chem.* **84**, 8351 (2012).

85. C.-C. Hsu, N.M. White, M. Hayashi, E.C. Lin, T. Poon, I. Banerjee, J. Chen, S.L. Pfaff, E.R. Macagno, P.C. Dorrestein. Microscopy ambient ionization top-down mass spectrometry reveals developmental patterning. *Proc. Natl. Acad. Sci. U.S.A.* **110**, 14855 (2013).

86. I. Lanekoff, O. Geydebrekht, G.E. Pinchuk, A.E. Konopka, J. Laskin. Spatially resolved analysis of glycolipids and metabolites in living Synechococcus sp. PCC 7002 using nanospray desorption electrospray ionization. *Analyst* **138**, 1971 (2013).

87. I. Lanekoff, K. Burnum-Johnson, M. Thomas, J. Cha, S.K. Dey, P. Yang, M.C. Prieto Conaway, J. Laskin. Three-dimensional imaging of lipids and metabolites in tissues by nanospray desorption electrospray ionization mass spectrometry. *Anal. Bioanal. Chem.* **407**, 2063 (2015).

88. C.-C. Hsu, P.-T. Chou, R.N. Zare. Imaging of proteins in tissue samples using nanospray desorption electrospray ionization mass spectrometry. *Anal. Chem.* **87**, 11171 (2015).

89. M.-Z. Huang, S.-C. Cheng, S.-S. Jhang, C.-C. Chou, C.-N. Cheng, J. Shiea, I.A. Popov, E.N. Nikolaev. Ambient molecular imaging of dry fungus surface by electrospray laser desorption ionization mass spectrometry. *Int. J. Mass Spectrom.* **325–327**, 172 (2012).

90. O.S. Ovchinnikova, V. Kertesz, G.J. Van Berkel. Combining transmission geometry laser ablation and a non-contact continuous flow surface sampling probe/electrospray emitter for mass spectrometry based chemical imaging. *Rapid Commun. Mass Spectrom.* **25**, 3735 (2011).

91. O.S. Ovchinnikova, D. Bhandari, M. Lorenz, G.J. Van Berkel. Transmission geometry laser ablation into a non-contact liquid vortex capture probe for mass spectrometry imaging. *Rapid Commun. Mass Spectrom.* **28**, 1665 (2014).

92. J.F. Cahill, V. Kertesz, T.M. Weiskittel, M. Vavrek, C. Freddo, G.J. Van Berkel. Online, absolute quantitation of propranolol from spatially distinct 20- and 40-µm dissections of brain, liver, and kidney thin tissue sections by laser microdissection–liquid vortex capture–mass spectrometry. *Anal. Chem.* **88**, 6026 (2016).

93. S. Berkenkamp, M. Karas, F. Hillenkamp. Ice as a matrix for IR-matrix-assisted laser desorption/ionization: Mass spectra from a protein single crystal. *Proc. Natl. Acad. Sci. U.S.A.* **93**, 7003 (1996).

94. A. Vertes, P. Nemes, B. Shrestha, A.A. Barton, Z. Chen, Y. Li. Molecular imaging by Mid-IR laser ablation mass spectrometry. *Appl. Phys. A* **93**, 885 (2008).

95. P. Nemes, A.A. Barton, Y. Li, A. Vertes. Ambient molecular imaging and depth profiling of live tissue by infrared laser ablation electrospray ionization mass spectrometry. *Anal. Chem.* **80**, 4575 (2008).

96. P. Nemes, A.A. Barton, A. Vertes. Three-dimensional imaging of metabolites in tissues under ambient conditions by laser ablation electrospray ionization mass spectrometry. *Anal. Chem.* **81**, 6668 (2009).

97. B. Shrestha, J.M. Patt, A. Vertes. In situ cell-by-cell imaging and analysis of small cell populations by mass spectrometry. *Anal. Chem.* **83**, 2947 (2011).

98. P. Nemes, A.S. Woods, A. Vertes. Simultaneous imaging of small metabolites and lipids in rat brain tissues at atmospheric pressure by laser ablation electrospray ionization mass spectrometry. *Anal. Chem.* **82**, 982 (2010).

99. H. Li, B.K. Smith, L. Márk, P. Nemes, J. Nazarian, A. Vertes. Ambient molecular imaging by laser ablation electrospray ionization mass spectrometry with ion mobility separation. *Int. J. Mass Spectrom.* **377**, 681 (2015).

100. H. Li, P. Balan, A. Vertes. Molecular imaging of growth, metabolism, and antibiotic inhibition in bacterial colonies by laser ablation electrospray ionization mass spectrometry. *Angew. Chem. Int. Ed.* **55**, 15035 (2016).

101. J.S. Sampson, A.M. Hawkridge, D.C. Muddiman. Generation and detection of multiply-charged peptides and proteins by matrix-assisted laser desorption electrospray ionization (MALDESI) Fourier Transform ion cyclotron resonance mass spectrometry. *J. Am. Soc. Mass Spectrom.* **17**, 1712 (2006).

102. G. Robichaud, J.A. Barry, K.P. Garrard, D.C. Muddiman. Infrared matrix-assisted laser desorption electrospray ionization (IR-MALDESI) imaging source coupled to a FT-ICR mass spectrometer. *J. Am. Soc. Mass Spectrom.* **24**, 92 (2013).

103. J.A. Barry, M.R. Groseclose, G. Robichaud, S. Castellino, D.C. Muddiman. Assessing drug and metabolite detection in liver tissue by UV-MALDI and IR-MALDESI mass spectrometry imaging coupled to FT-ICR MS. *Int. J. Mass Spectrom.* **377**, 448 (2015).

104. E.P. Rosen, M.T. Bokhart, H.T. Ghashghaei, D.C. Muddiman. Influence of desorption conditions on analyte sensitivity and internal energy in discrete tissue or whole body imaging by IR-MALDESI. *J. Am. Soc. Mass Spectrom.* **26**, 899 (2015).

105. M. Ekelöf, E.K. McMurtrie, M. Nazari, S.D. Johanningsmeier, D.C. Muddiman. Direct analysis of triterpenes from high-salt fermented cucumbers using infrared matrix-assisted laser desorption electrospray ionization (IR-MALDESI). *J. Am. Soc. Mass Spectrom.* **28**, 370 (2017).

106. S. Amini-Nik, D. Kraemer, M.L. Cowan, K. Gunaratne, P. Nadesan, B.A. Alman, R.J.D. Miller. Ultrafast mid-IR laser scalpel: Protein signals of the fundamental limits to minimally invasive surgery. *PLoS ONE* **5**, e13053 (2010).

107. N. Jowett, W. Wöllmer, A.M. Mlynarek, et al. Heat generation during ablation of porcine skin with erbium:yAg laser vs a novel picosecond infrared laser. *JAMA Otolaryngol. Head Neck Surg.* **139**, 828 (2013).

108. A.A. Oraevsky, L.B. Da Silva, A.M. Rubenchik, M.D. Feit, M.E. Glinsky, M.D. Perry, B.M. Mammini, W. Small, B.C. Stuart. Plasma mediated ablation of biological tissues with nanosecond-to-femtosecond laser pulses: Relative role of linear and nonlinear absorption. *IEEE J. Sel. Topics Quantum Electron.* **2**, 801 (1996).

109. J. Zou, F. Talbot, A. Tata, L. Ermini, K. Franjic, M. Ventura, J. Zheng, H. Ginsberg, M. Post, D.R. Ifa, D. Jaffray, R.J.D. Miller, A. Zarrine-Afsar. Ambient mass spectrometry imaging with picosecond infrared laser ablation electrospray ionization (PIR-LAESI). *Anal. Chem.* **87**, 12071 (2015).

110. J.J. Brady, E.J. Judge, R.J. Levis. Mass spectrometry of intact neutral macromolecules using intense non-resonant femtosecond laser vaporization with electrospray post-ionization. *Rapid Commun. Mass Spectrom.* **23**, 3151 (2009).

111. E.J. Judge, J.J. Brady, D. Dalton, R.J. Levis. Analysis of pharmaceutical compounds from glass, fabric, steel, and wood surfaces at atmospheric pressure using spatially resolved, nonresonant femtosecond laser vaporization electrospray mass spectrometry. *Anal. Chem.* **82**, 3231 (2010).

112. J.J. Brady, E.J. Judge, R.J. Levis. Analysis of amphiphilic lipids and hydrophobic proteins using nonresonant femtosecond laser vaporization with electrospray post-Ionization. *J. Am. Soc. Mass Spectrom.* **22**, 762 (2011).

113. E.J. Judge, J.J. Brady, R.J. Levis. Mass analysis of biological macromolecules at atmospheric pressure using nonresonant femtosecond laser vaporization and electrospray ionization. *Anal. Chem.* **82**, 10203 (2010).

114. J.J. Brady, E.J. Judge, R.J. Levis. Nonresonant femtosecond laser vaporization of aqueous protein preserves folded structure. *Proc. Natl. Acad. Sci. U.S.A.* **108**, 12217 (2011).

115. E.J. Judge, J.J. Brady, P.E. Barbano, R.J. Levis. Nonresonant femtosecond laser vaporization with electrospray postionization for ex vivo plant tissue typing using compressive linear classification. *Anal. Chem.* **83**, 2145 (2011).

116. P.M. Flanigan, L.L. Radell, J.J. Brady, R.J. Levis. Differentiation of eight phenotypes and discovery of potential biomarkers for a single plant organ class using laser electrospray mass spectrometry and multivariate statistical analysis. *Anal. Chem.* **84**, 6225 (2012).

117. F. Shi, P.M. Flanigan, J.J. Archer, R.J. Levis. Direct analysis of intact biological macromolecules by low-energy, fiber-based femtosecond laser vaporization at

1042 nm wavelength with nanospray postionization mass spectrometry. *Anal. Chem.* **87**, 3187 (2015).

118. F. Shi, P.M. Flanigan, J.J. Archer, R.J. Levis. Ambient molecular analysis of biological tissue using low-energy, femtosecond laser vaporization and nanospray postionization mass spectrometry. *J. Am. Soc. Mass Spectrom.* **27**, 542 (2016).

CHAPTER 2

DIRECT ANALYSIS OF INTACT BIOLOGICAL MACROMOLECULES BY LOW-ENERGY, FIBER-BASED LASER ELECTROSPRAY MASS SPECTROMETRY

2.1 Overview

In this chapter, a fiber-based laser with a pulse duration of 435 fs and a wavelength of 1042 nm was used to vaporize biological macromolecules intact from the condensed phase into the gas phase for nanospray postionization and mass analysis. Laser vaporization of dried standard protein samples from a glass substrate by 10 Hz bursts of 20 pulses having 10 μs pulse separation and < 50 μJ pulse energy resulted in comparable signal as a metal substrate. The protein signal observed from an aqueous droplet on a glass substrate was negligible compared to either a droplet on metal or a thin aqueous film on glass. The mass spectra generated from dried and aqueous protein samples by the low-energy, fiber laser were similar to the results from high energy (500 μJ), 45 fs, 800mnm Ti:Sapphire-based femtosecond laser electrospray mass spectrometry (LEMS) experiments, suggesting that the fiber-based femtosecond laser desorption mechanism involves a nonresonant, multiphoton process, rather than thermal- or photoacoustic-induced desorption. Direct analysis of whole blood performed without any pretreatment resulted in features corresponding to hemoglobin subunit-heme complex ions.

2.2 Introduction

With the advent of electrospray ionization (ESI) [1] and matrix-assisted laser desorption ionization (MALDI) [2, 3], mass spectrometry (MS) has become a powerful tool for analyzing macromolecules including synthetic polymers [4], nucleic acids [5], and proteins [6-8]. One of the limitations of ESI and MALDI is that extensive sample preparation (*e.g.,* solvent extraction, chromatographic separation, or matrix deposition) is required to remove analytes from their native environment and enable analysis [9, 10]. For example, a given sample typically needs to be homogenized and dissolved in a moderately polar organic and aqueous solvent mixture for ESI analysis. However, this solvation process will modify the chemical composition or structural conformation of the analytes of interest (*i.e.,* protein or protein-substrate complex) unless great care is taken [11]. MALDI requires the application of a matrix that cocrystalizes with analyte(s), and this process may also interfere with the sample [12]. Ambient ionization methods emerged with the introduction of desorption electrospray ionization (DESI) allowing direct sampling from the surface under ambient conditions with little sample preparation [13]. Ambient ionization has the advantages of short analysis time, little or no sample preparation, and the ability to interface with most mass analyzers [9, 10, 14]. Ambient MS techniques have been applied for forensics [15, 16], explosives [17-19], food [20, 21], pharmaceuticals [17, 22], environmental [20, 23], and biomolecule [24-27] analysis, as well as molecular imaging [22, 26, 28].

The characterization of biological macromolecules under ambient conditions is used for proteomics research [29]. Dried lysozyme was directly analyzed from a PTFE substrate by DESI and produced mass spectra similar to conventional ESI-MS [13]. Hybrid

laser-based ambient MS techniques can directly transfer protein analytes to an electrospray source for postionization. Two such techniques, laser ablation electrospray ionization (LAESI) [26] and infrared matrix-assisted laser desorption electrospray ionization (IR-MALDESI) [30], desorb analytes from water-rich biological samples through a phase explosion wherein a 2.94 μm nanosecond laser resonantly excites the vibrational O-H stretching mode of water molecules. Similarly, laser-induced acoustic desorption/electrospray ionization (LIAD/ESI) desorbs neutral molecules for ESI postionization, including large biomolecules, off a surface through a shockwave resulting from the ablation at the rear side of an aluminum foil substrate by a focused laser beam [31].

Laser electrospray mass spectrometry (LEMS) employs a 1 mJ, 800 nm laser pulse with a pulse duration as short as 70 fs for vaporization and an electrospray ion source for capture and postionization of vaporized analytes at atmospheric pressure with little sample preparation. Nonresonant, multiphoton vaporization occurs without the aid of a matrix because of the high laser intensity (~10^{12}–10^{13} W/cm^2) applied. This intensity is 6–7 orders of magnitude higher than the intensity by nanosecond laser, for example, in MALDI (~10^6 W/cm^2) [32]. LEMS has been applied to analyze a variety of samples including peptides [32], lipids [33], proteins [24], pharmaceuticals [22], explosives [18, 19], smokeless powders [34], plant tissues [35, 36], milk, and whole blood [33]. Quantitative measurements of multicomponent mixtures of small molecules [37] and proteins [38] using LEMS showed similar dynamic range as conventional ESI while having minimized ion suppression due to a higher limit of detection.

However, wider application of LEMS is hampered by the cost and robustness of the femtosecond laser amplifier in comparison with more common nanosecond UV and IR lasers. Laser pulses centered at 800 nm with high pulse energy (μJ to mJ) and controllable repetition rate (1–1000 Hz) are created by a commercial Ti:Sapphire (Ti:S) amplifier using chirped pulse amplification (CPA) technique [39]. With the development of femtosecond fiber lasers, generating high-energy pulses using rare-earth doped fiber as the gain medium offers a robust design at a fraction of the cost and space of a Ti:S laser amplifier [40].

Here, the mass analysis of biological macromolecules using an ytterbium-doped fiber-based femtosecond laser for vaporization and a nanospray source for postionization were explored. Vaporization of cytochrome c and lysozyme was performed from both stainless steel and glass sample slides with proteins in the dried or aqueous state. The measurements were compared to 800 nm experiments to determine whether nonresonant vaporization can be used to vaporize large biomolecules using longer wavelength, longer duration laser pulses with lower pulse energy. The possibility of photoacoustic-induced desorption was studied. Finally, laser vaporization of whole blood was investigated.

2.3 Experimental Section

2.3.1 Sample Preparation

Stock solutions of horse heart cytochrome c (Sigma-Aldrich, St. Louis, MO) and chicken egg white lysozyme (USB Corporation, Cleveland, OH) were prepared in HPLC-grade water (Fisher Scientific, Fair Lawn, NJ) at concentrations of 1 mM and then diluted to 250 μM with water for laser vaporization experiments. For vaporization of dried samples, 15 μL of the 250 μM protein solutions were spotted on either a stainless steel or

glass sample slide (7×7 mm^2) and air dried to be a circular spot of ~5 mm in diameter. For vaporization of aqueous samples, 15 or 4 μL of 250 μM protein were pipetted onto the stainless steel and glass sample slides, respectively, and directly subjected to laser irradiation. For analysis of thin aqueous films, 4 μL of aqueous protein solution was deposited on the glass substrate by slowly translating the pipette tip over the substrate while dispensing the sample. The 4 μL aliquot of aqueous cytochrome c droplet and film deposited on the glass substrate were estimated to be 900 and 50 μm in height by measuring the height difference between the solid-liquid and the top of liquid-air interface with a confocal microscope (LabRAM HR800 Evolution, HORIBA Scientific, Edison, NJ). Undiluted human blood was taken from a healthy volunteer and printed (~5 μL) directly on both stainless steel and glass slides by the finger and then analyzed before the film dried without any pretreatment. No further sample preparation was necessary other than transfer of the sample slides to the sample stage for all the experiments.

2.3.2 Laser Vaporization

A laser vaporization and ionization region (see Figure 2.1) similar to our previous design [32] was constructed by interfacing a fiber-based femtosecond laser (μJewel DE series, IMRA America Inc., Ann Arbor, MI) with a micrOTOF-Q II mass spectrometer (Bruker Daltonik GmbH, Bremen, Germany). The ytterbium-doped fiber laser with fiber chirped pulse amplification (FCPA) technology delivers 50 μJ, 435 fs laser pulses at 1042 nm as the radiation source [40]. The repetition rate of the laser was reduced from 100 kHz to be 10 Hz pulse-bursts by two optical choppers that had all but one slot of each chopper covered by non-transparent paper. The first chopper (MC1000A, Thorlabs, Newton, NJ)

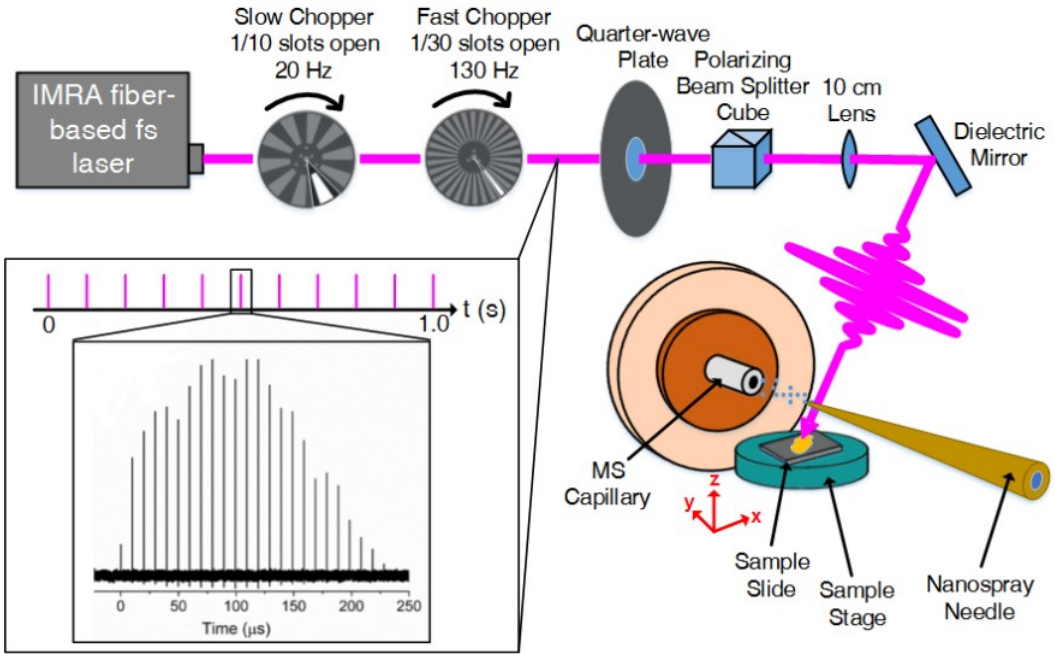

Figure 2.1. A schematic representation of the fiber laser-based laser nanospray mass spectrometry (F-LEMS) system. The surface analytes from a sample slide placed on a three-dimensional translation stage were vaporized by the attenuated fiber laser pulse-bursts, postionized by the nanospray source, and finally mass-analyzed by the time-of-flight mass spectrometer. The inset shows the oscilloscope trace of the pulse-burst measured by a photodiode.

ran at 20 Hz to set the overall frequency of pulse-bursts and the second chopper (SR540, Stanford Research Systems, Sunnyvale, CA) ran at 130 Hz to set the number of pulses in each burst to be ~20. An oscilloscope trace of the pulse-burst focused onto a photodiode is shown in the inset of Figure 2.1. The pulse energy of each laser pulse in the pulse burst was varied from 20 μJ to 46.5 μJ by a quarter-wave plate and a polarizing beam splitter cube. The maximum pulse energy of 46.5 μJ was used for all the experiments unless otherwise stated.

The laser beam was directed to the vaporization and ionization region by dielectric mirrors and focused to a spot size around 75 μm in diameter at a ~45° incident angle with a 10 cm focusing lens. The intensity for a single laser pulse spot was estimated to be 2.39×10^{12} W/cm^2 when using 46.5 μJ pulse energy. A copper sample stage was placed below the axis from the nanospray needle to the mass spectrometer capillary inlet. Sample slides were placed on the sample stage attached to a mini Z-axis linear stage (UMR5.16, Newport, Irvine, CA), which was mounted on a motorized XY microscopy stage (MLS203-1, Thorlabs, Newton, NJ), to enable XYZ translation of the sample slides. The sample surface was rastered with respect to the stationary nanospray stream by moving the XY motorized stage at a speed of 1 mm/s to ensure sampling of a fresh spot for each laser shot.

Laser vaporization using high-energy, Ti:Sapphire laser vaporization (Ti:S-LEMS) was also performed to compare with the low-energy, fiber-based laser electrospray mass spectrometry (F-LEMS) under the same experimental condition except a different laser. Briefly, a Ti:S regenerative amplifier seeded by a Ti:S oscillator (Legend Elite HE series, Coherent Inc., Santa Clara, CA) generates 5 mJ, 45 fs pulses centered at 800 nm in 10 Hz. The energy of the pulse was reduced to 75, 160, 280, and 505 μJ by neutral density filters

(Thorlabs, Newton, NJ) for laser vaporization in Ti:S-LEMS. The intensity of the laser (505 μJ) at the substrate was approximately 2.54×10^{14} W/cm^2 after being focused to a spot size of 75 μm by a 10 cm focal length lens.

2.3.3 Ionization and Mass Spectrometry

The fiber and Ti:Sapphire laser vaporized neutral analytes were captured and ionized by a nanospray stream produced from a silicon tapered nanospray needle with 360 μm OD, 20 μm ID and 10 μm tip ID (New Objective, Woburn, MA). A syringe pump (Model 100, KD Scientific, Holliston, MA) infused the nanospray solvent at a flow rate of 200 nL/min. The nanospray solvent was composed of 1:1 (v:v) water:methanol (Honeywell Burdick & Jackson, Muskegon, MI) with 20 mM ammonium acetate (EMD Chemicals, Gibbstown, NJ) for all the experiments except for the experiments where Teflon was used to prevent shockwaves, where 1:1 (v:v) water:methanol with 1% glacial acetic acid (EMD Chemicals, Gibbstown, NJ) was used.

Typical parameters of the nanospray source are listed as follows. The nanospray needle and MS inlet, separated by 8.25 mm, were kept at a voltage of 0 and −2 to −2.5 kV, respectively. A stable solvent spray was obtained with the help of countercurrent, hot N_2 gas (flow rate 3 L/min, temperature 180 ºC) for desolvation. The sample stage was set to a bias of −1.3 kV to correct for the distortion of the field lines between the nanospray needle and capillary inlet caused by the stage. The motorized stage was insulated from the sample stage by a 3 mm thick PMMA plate. The vertical distance between the sample slides and the nanospray needle was kept at 4.75 mm and the focused laser was positioned about 1 mm in front of the needle tip. The optimal spot was found by vaporizing Rhodamine 6G

from stainless steel slides (data not shown). The spectrometer was calibrated with a 99:1 (v:v) acetonitrile:ESI calibrant solution (#63606-10ML, Fluka Analytical/Sigma Aldrich, Buchs, Switzerland) over a mass range of *m/z* 50–3000. The in-source collision region (ISCID) and collision cell (CID) voltages were set to be 0 and 10 eV, respectively, to ensure minimal fragmentation and denaturation induced from the spectrometer. The vaporized and postionized analytes were mass analyzed by the mass spectrometer with a spectral resolution of 10000 at *m/z* 922. Raw spectra were recorded at a spectral rate of 1 Hz with a summation of 5000 scans in each spectra when the motorized stage was scanned during each sample run. The mass spectra are presented after signal averaging and background subtraction by the nanospray-only spectra taken before each sample run. Each analysis lasted about 30 s and was repeated at least 2 times for a total of at least 60 mass spectra.

2.3.4 Control Experiments

The first control experiment was the irradiation of blank stainless steel and glass slides without any sample deposited using the maximum pulse energy for fiber laser. A second control was the analysis of cytochrome c deposited as a dried and aqueous droplet on the stainless steel slides for fiber laser vaporization with no nanospray postionization present. No protein related signals except solvent peaks were observed in the acquired mass spectra of the control experiments (see Figure 2.2).

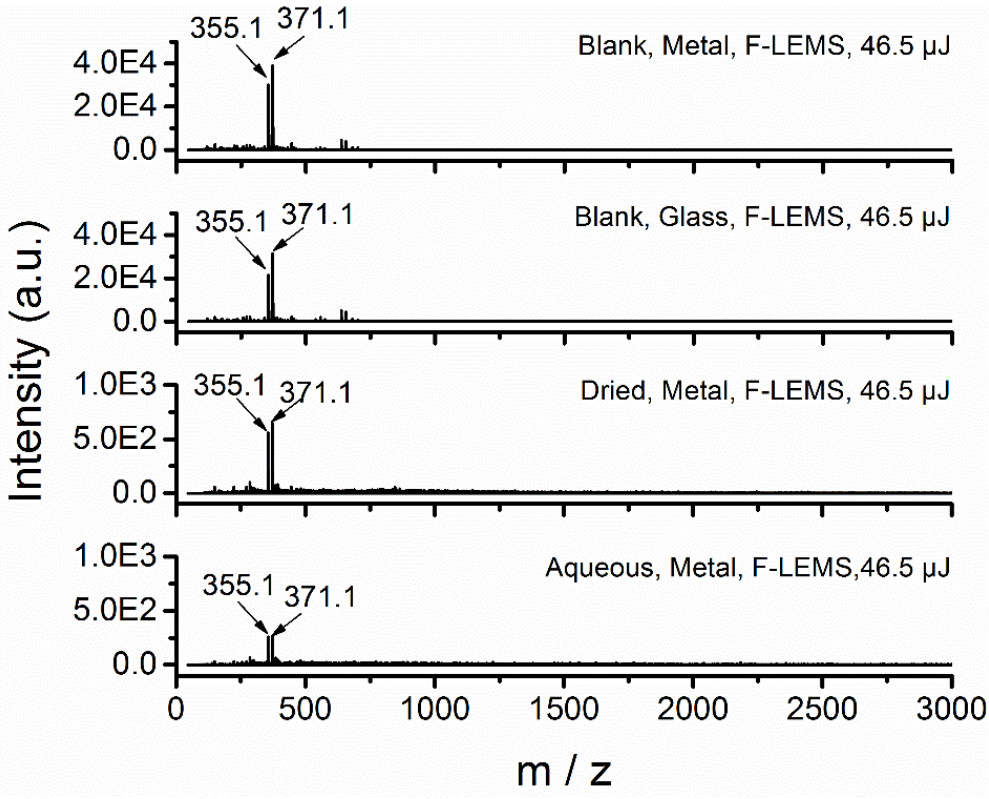

Figure 2.2. Background-subtracted F-LEMS mass spectra of the control experiments. Blank stainless steel and glass sample slides without any protein sample were placed on the sample stage and analyzed. Cytochrome c was deposited on stainless steel sample slides and analyzed as dried and aqueous droplets.

2.3.5 Safety Considerations

All lab personnel were required to wear appropriate laser eye protection during the experiments. Insulating and opaque shields protected lab personnel from any exposed invisible laser irradiation and high voltage supplies. The blood analysis procedure followed an exposure control plan approved by the University (No. 13314).

2.4 Results and Discussion

2.4.1 Vaporization of Dried Cytochrome c from Stainless Steel and Glass Slides

Dried cytochrome c absorbed on a stainless steel slide was investigated to determine whether a 1042 nm femtosecond laser pulse is capable of vaporizing macromolecules. Cytochrome c is a ~12 kDa protein consisting of a peptide chain 104 residues long and a single heme group, which is covalently bonded to the cysteine residues in positions 14 and 17 [41]. Cytochrome c has been well-studied by mass spectrometry not only for chemical analysis in proteomics [30, 31, 42, 43] but also for protein conformation studies in structural biology [44-47]. ESI-MS of a given protein usually results in a charge state distribution (CSD) corresponding to multiply charged ions and the CSD shifts to higher charge states (low *m/z*) when the protein unfolds under extreme conditions such as an acidic or heated solution [48]. While there has been some debate concerning the use of charge states to determine the conformation of protein molecules in mass spectrometry [45, 49, 50], evidence from both computational and experimental results reveals that charge states observed are strongly related to the degree of folding of the proteins, with the most compact conformations corresponding to the lowest charge states [51].

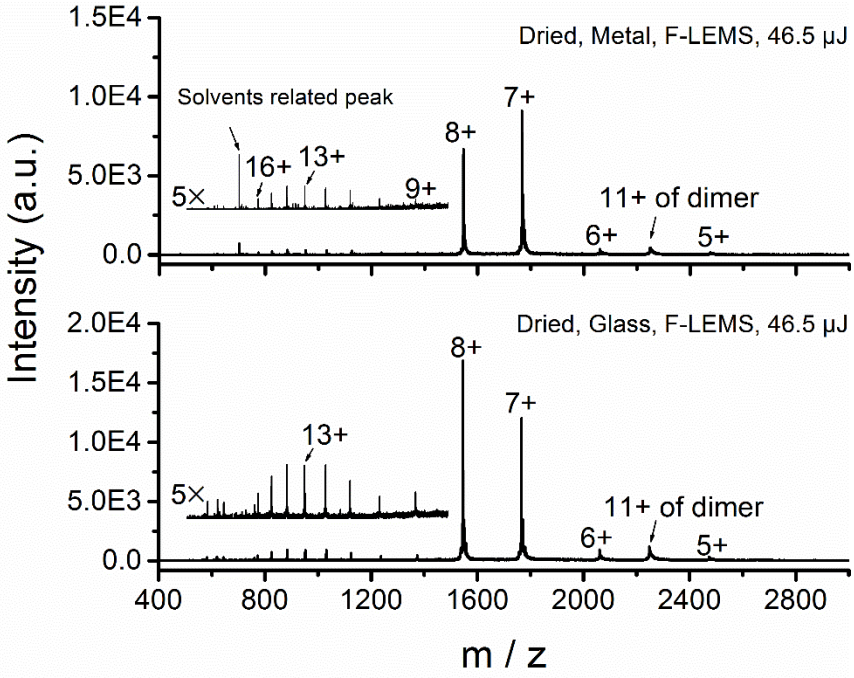

Figure 2.3. Background-subtracted F-LEMS mass spectra of an air-dried droplet of 15 µL of 250 µM cytochrome c aqueous sample deposited on stainless steel and glass sample slides, respectively. A magnified view of the *m/z* 500–1500 region is shown in the inset.

The F-LEMS mass spectrum acquired for dried cytochrome c from a stainless steel sample slide is shown in Figure 2.3. The high *m/z* region reveals two major peaks at *m/z* 1545.9 and 1766.6 and two minor ones at *m/z* 2060.8 and 2473.1. These features correspond to the 8+, 7+, 6+, and 5+ charge states of protonated cytochrome c, respectively. The peak at *m/z* 2248.2 is the 11+ charge state of a cytochrome c dimer. In addition, a magnified view of *m/z* 500–1500 (see the inset of Figure 2.3) shows a bell-shaped CSD centered around the 13+ charge state. The 8+ and 7+ charge states of cytochrome c correspond to the folded conformation whereas charge states around 13+ correspond to the unfolded conformation as shown in a nano-ESI experiment [48]. The vaporization of dried cytochrome c using the fiber laser mainly resulted in folded conformations with detection of a small amount of unfolded protein. Partial unfolding occurred in Ti:S-LEMS [24] as well as in LIAD/ESI [31] experiments when cytochrome c was analyzed from the dried state. Protein partially unfolds when adsorbed on a substrate due to the protein-substrate interactions [52].

To determine whether absorption of the laser by the substrate is required for vaporization, direct analysis of dried cytochrome c was investigated on the glass substrate. Glass is transparent at 1042 nm so no significant absorption of the laser is expected that might induce thermal desorption. The corresponding mass spectrum (Figure 2.3) reveals molecular features similar to the stainless steel substrate experiment with the dominant 8+ and 7+ charge state peaks accompanied by the minor high charge state features. Femtosecond laser pulses presumably couple directly with the dried protein molecules via a multiphoton mechanism under laser intensity of 10^{12} W/cm^2. The laser wavelength employed for vaporization is not expected to be important because of the high-order

multiphoton excitation mechanism. This experiment demonstrates that linear (one photon resonant) absorption of the laser radiation by the analyte at 1042 nm is not required for vaporization and is consistent with the nonresonant excitation mechanism reported in the previous 800 nm fs laser vaporization experiment [24]. This is different from the desorption mechanism using nanosecond laser pulses where a resonance must occur and hence a specific matrix must be present.

2.4.2 Vaporization of Aqueous Cytochrome c Droplet from Stainless Steel and Glass Slides

Previous studies indicated that various proteins vaporized from the aqueous phase into the gas phase by 800 nm femtosecond laser pulses displayed charge states corresponding to the solution phase conformations, whether folded or unfolded, depending on the pH of the sample solution [45, 49, 50]. Here, cytochrome c was directly vaporized from aqueous solution deposited on either a stainless steel or glass substrate using the 435 fs, 1042 nm laser pulses. Endogenous water within a sample is usually used as the laser absorbing matrix for LAESI [26] and IR-MALDESI [30] experiments in which a 2.94 μm nanosecond laser is employed. Laser pulses from the fiber laser do not couple linearly with the water molecules as water has no appreciable absorbance feature at 1042 nm. Mass spectra acquired for 15 μL of cytochrome c solution deposited as a droplet on the stainless steel and glass substrates are shown in Figure 2.4. The 8+ and 7+ charge state peaks corresponding to the native-like conformation of cytochrome c without any other high charge state peaks were observed for the stainless steel substrate, analogous to 800 nm femtosecond laser vaporization experiments [45]. However, the laser vaporization of a 15

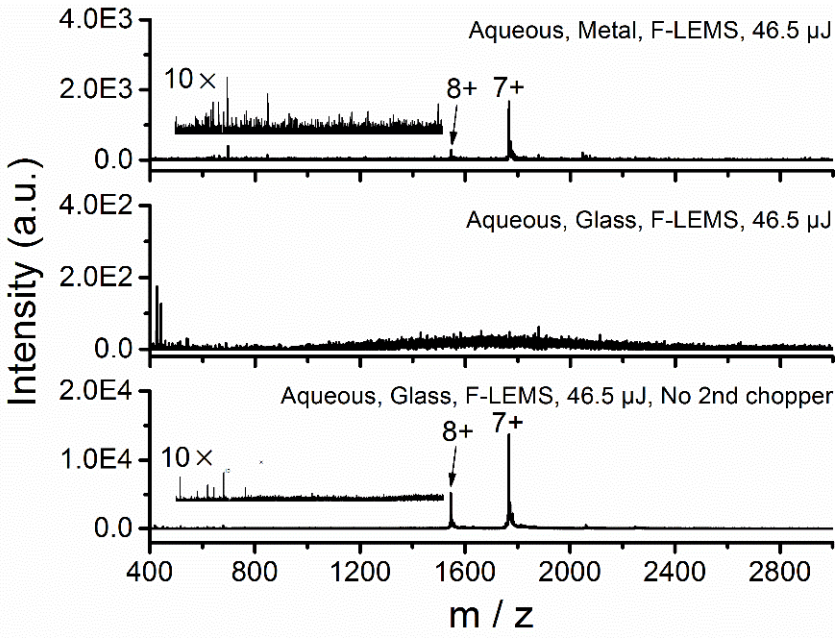

Figure 2.4. Background-subtracted F-LEMS mass spectra of 15 µL of 250 µM cytochrome c aqueous droplets from stainless steel and glass with the second chopper, and glass with the second chopper removed. A magnified view of *m/z* 500–1500 region is shown in the inset of the spectrum.

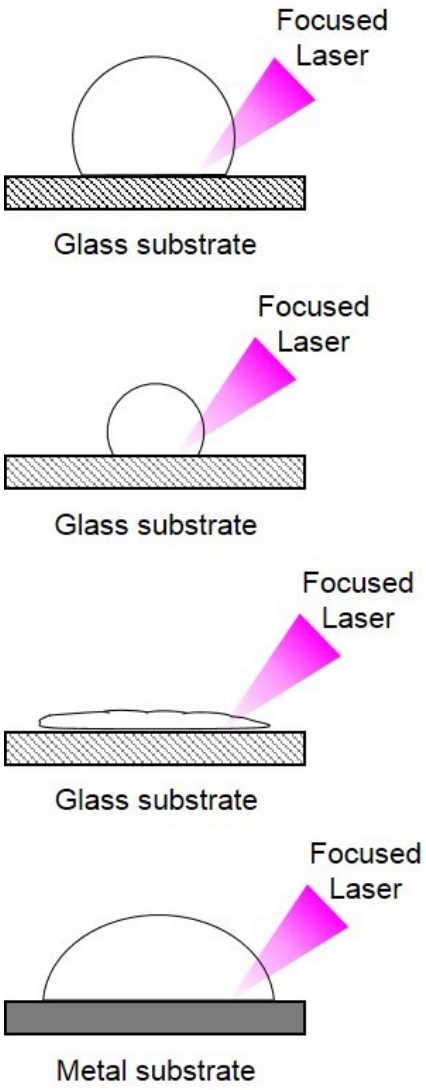

Figure 2.5. Diagram of a static 15 µL aqueous droplet, 4 µL aqueous droplet, 4 µL aqueous film on a glass substrate and 15 µL aqueous droplet on a stainless steel substrate.

μL of aqueous cytochrome c droplet on the glass substrate did not result in any analyte-related mass spectral features. One possible reason for the lack of signal is that the droplet on the stainless steel tends to spread itself more over the surface due to the enhanced wettability in comparison with glass (see Figure 2.5). The wettability of the surface is related to the hydrophobicity/hydrophilicity [53], roughness [54], and conductivity [55] properties of the substrate. The energy density of the focused laser pulses can apparently overcome the analyte-containing solvent-cages at the liquid-air interface, which ensures a sufficient amount of analyte being vaporized, overcoming the limit of detection for F-LEMS, if the droplet spreads on the surface to form a thin film on metal rather than remaining as an intact droplet on glass.

2.4.3 Vaporization of Aqueous Cytochrome c Film from Glass Slides

Several methods were investigated to enable the analysis of aqueous cytochrome c from the glass substrate. Focusing 20 consecutive laser pulses onto the aqueous sample droplet at 10 Hz using the maximum pulse energy resulted in no observable protein ion signal. The number of consecutive pulses was then increased by removing the second high frequency chopper, producing 10 Hz bursts with ~2600 pulses per burst. The mass spectrum of a 15 μL droplet on a glass substrate without the second chopper, as shown in Figure 2.4, resulted in substantial ion signal corresponding to the 7+ and 8+ charge states of cytochrome c. This configuration provided sufficient energy deposition into the droplet that the amount of material vaporized was above the limit of detection of F-LEMS.

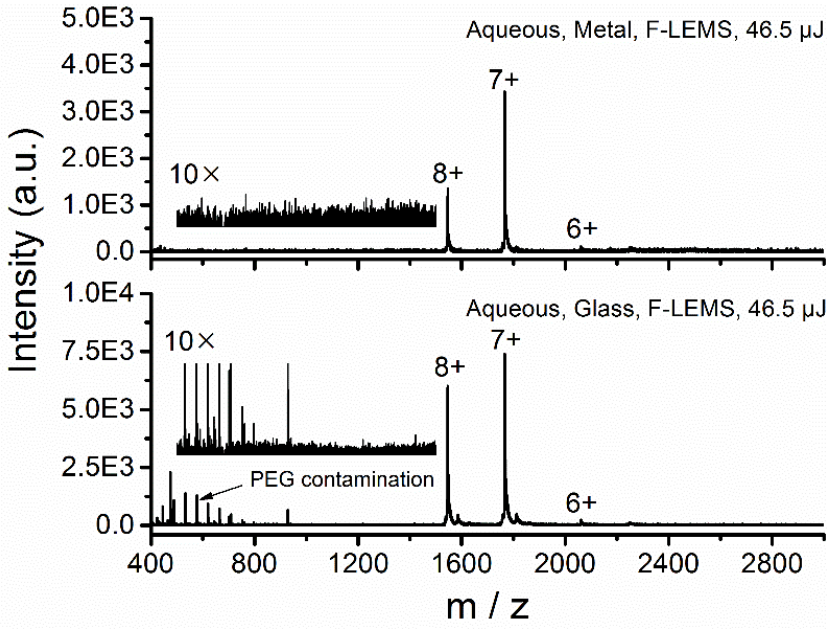

Figure 2.6. Background-subtracted F-LEMS mass spectra of 4 µL of 250 µM cytochrome c from an aqueous droplet on stainless steel and an aqueous film on glass sample slides. A magnified view of the *m/z* 500–1500 region is shown in the inset for each spectrum.

The effect of the volume of the droplet was studied using the 20 consecutive pulses when the second chopper was present. A 4 μL aliquot of cytochrome c was deposited onto stainless steel and glass slides to compare with the 15 μL measurements. The ion intensity of the 7+ charge state for the 4 μL deposition on the stainless steel substrate (see Figure 2.6) increased by a factor of 2 compared with the 15 μL deposition. However, the analyte was not observed from the glass substrate for the 4 μL sample deposition. Decreasing the volume only caused a small change in the signal intensity for the stainless steel substrate and no increase for the glass substrate.

The signal resulting from the aqueous droplet was compared with an aqueous film produced by spreading the protein solution on the glass substrate. To produce the aqueous film, a pipette with 4 μL of cytochrome c solution was slowly rastered across the glass while dispensing the sample solution. The mass spectrum of the aqueous film on the glass (see Figure 2.6) displayed features corresponding to the 8+ and 7+ charge states of cytochrome c and no other features corresponding to higher charge states indicative of unfolded protein. Analysis of an aqueous film from a glass substrate revealed higher signal intensity than the analysis of an aqueous droplet on a stainless steel substrate, suggesting that the absorption of the laser light by the sample substrate is not required for femtosecond laser vaporization. A liquid film (see Figure 2.5) spread on the surface via the raster method resulted in vaporization presumably because there was sufficient energy density at the liquid-air interface to induce vaporization. This was different from the analysis of an intact droplet (see Figure 2.5) where the energy density was insufficient to overcome the cage effect of the remaining water in the droplet. As a result, raster deposition of aqueous films was adopted as the standard method for analysis of liquid samples from a glass substrate.

The question arises as to why only the 8+ and 7+ charge states, corresponding to the folded conformation, were detected during femtosecond laser vaporization of aqueous cytochrome c using either stainless steel or glass substrates. The detection of the native, folded conformation using femtosecond laser vaporization may be due to the short time scale of energy deposition in comparison with nanosecond laser. Collisional cooling of the protein molecules with neighboring gas molecules upon laser vaporization may also contribute to preservation of the structure of the protein [56, 57]. A liquid droplet of para-substituted benzylpyridinium thermometer ions vaporized using high-energy, 800 nm femtosecond laser revealed a lower extent of fragmentation in comparison with analysis performed using the dried samples [58]. Internal energy measurements of dried and liquid thermometer ions using the 1042 nm fiber laser show that F-LEMS is as soft as nanospray with little fragmentation and equivalent mean internal energy distributions [59]. This again suggests that fiber-based femtosecond laser vaporization is a "soft" process even with a burst of 20 successive pulses with a pulse intensity of 10^{12} W/cm^2.

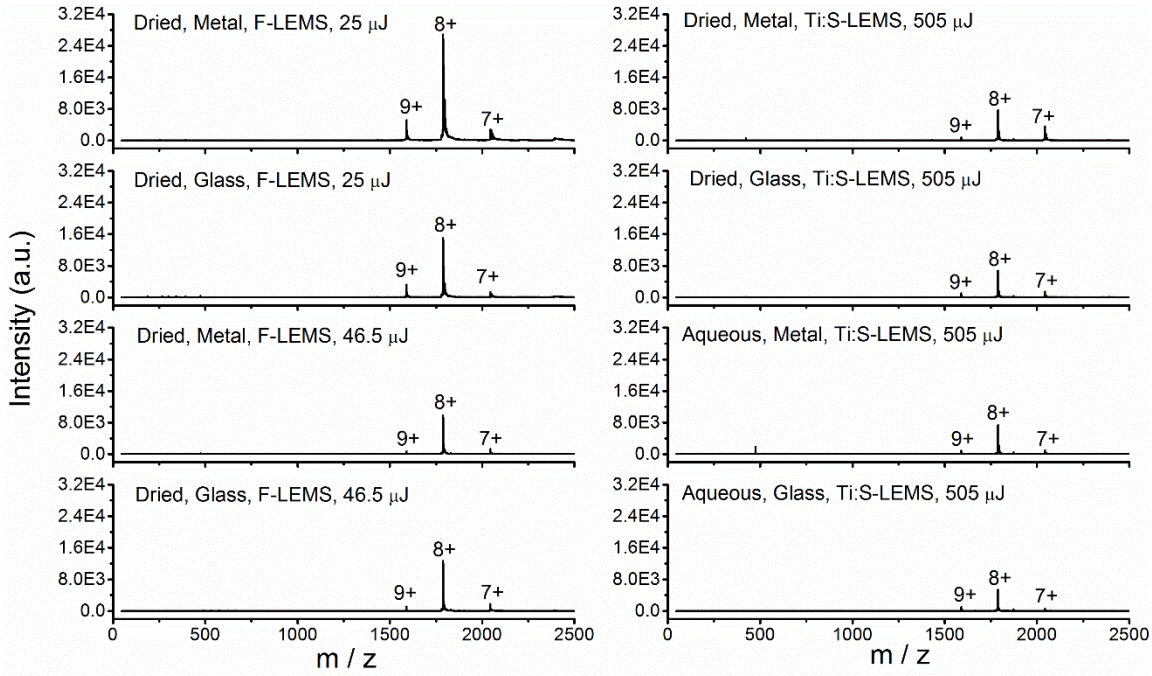

Figure 2.7. Comparison of background-subtracted F-LEMS and Ti:S-LEMS mass spectra of lysozyme using 1042 nm fiber laser and 800 nm Ti:S laser, respectively.

2.4.4 Comparison of F-LEMS and Ti:S-LEMS for Vaporization of Dried and Aqueous Lysozyme from Stainless Steel and Glass Slides

To test whether other proteins could be desorbed from surfaces using fiber laser vaporization, additional experiments were performed on lysozyme. Lysozyme is a 14.3 kDa single chain protein with four disulfide bonds. Lysozyme was analyzed under the same experimental conditions described for cytochrome c, including as a dried sample on stainless steel and glass, an aqueous droplet on stainless steel, and an aqueous film on glass. Laser vaporization was also performed using high energy (500 μJ), 800 nm pulses from a Ti:S laser to compare with F-LEMS. All of the lysozyme F-LEMS mass spectra (resulted in similar features as Ti:S-LEMS (see Figure 2.7), with three peaks at *m/z* 1590.5, 1789.1 and 2044.6 corresponding to the 9+, 8+ and 7+ charge states of lysozyme, respectively. These features indicate that lysozyme was transferred from the condensed phase to the gas phase intact and in a folded conformation. Measurements of dried lysozyme using a low laser pulse energy (25 μJ) for F-LEMS displayed signal from both stainless steel and glass substrates, as seen in Figure 2.7. In the Ti:S-LEMS experiment, single pulses with high energy were required to couple with the dried lysozyme analytes on the substrates (see Figure 2.7) while lower energy pulses at 75 μJ resulted in less signal from metal and negligible signal from glass (see Figure 2.8). Analysis of dried lysozyme revealed no high charge state features corresponding to unfolded protein that were observed for dried cytochrome c. This is attributed to the presence of disulfide bonds that stabilize the three-dimensional conformation structure of lysozyme.

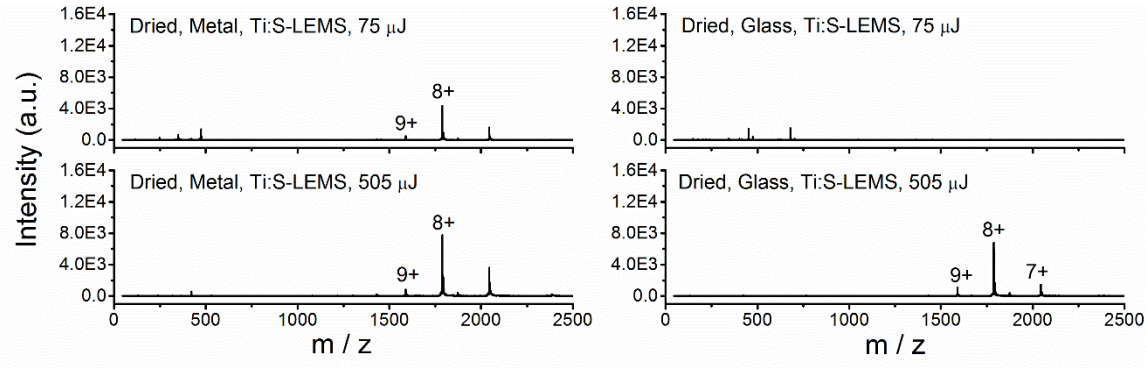

Figure 2.8. Background-subtracted Ti:S-LEMS mass spectra of an air-dried droplet of 15 μL of 250 μM lysozyme deposited on stainless steel and glass slides.

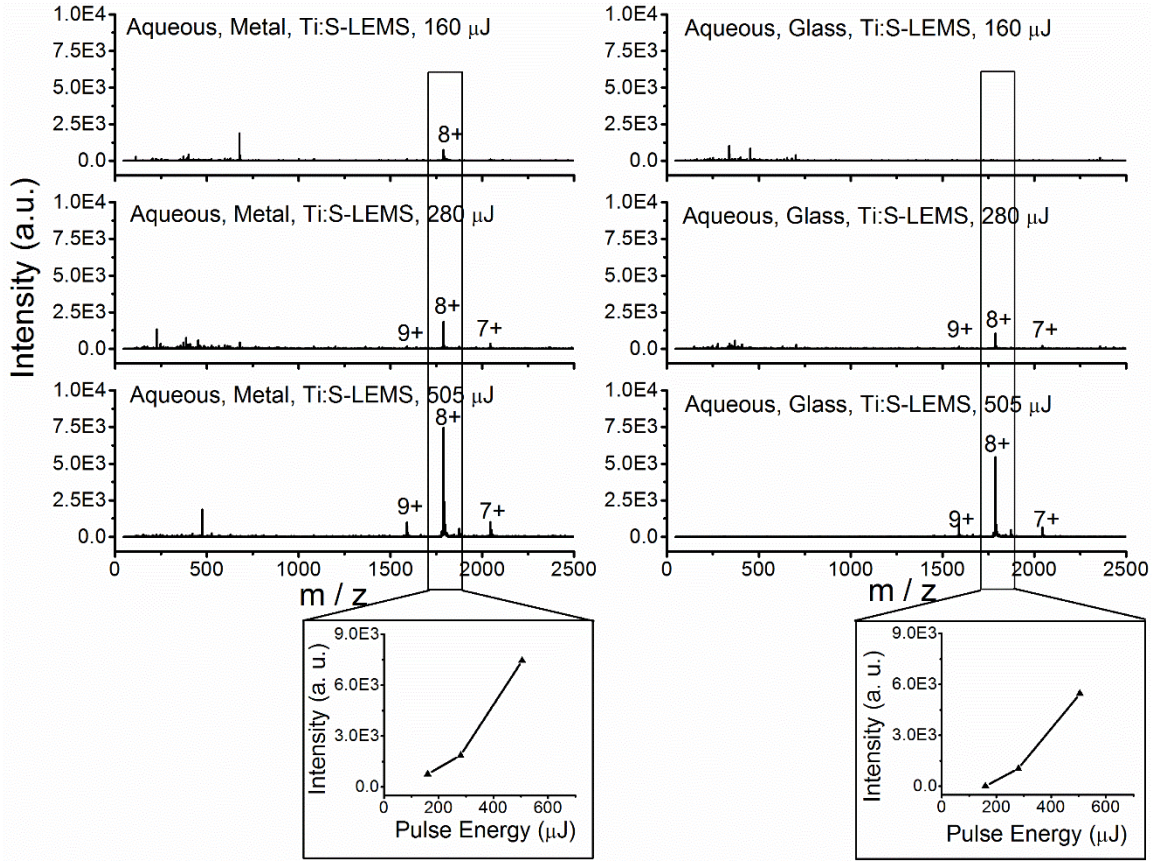

Figure 2.9. Background-subtracted Ti:S-LEMS mass spectra of a 4 µL aliquot of 250 µM lysozyme was analyzed as a droplet on stainless steel and an aqueous film on glass slides. The insets show the plot of the 8+ charge state peak (*m/z* 1789.1) intensity as a function of laser pulse energy on metal and glass slides.

The maximum pulse energy of the fiber laser (46.5 μJ) was required to analyze aqueous lysozyme (see Figure 2.7) to overcome the solvent cage in liquid analysis, which is in agreement with the results of Ti:S-LEMS (see Figure 2.9) that sufficient energy (~500 μJ) is essential to excite the lysozyme from the liquid and gain appreciable signal. Analysis of an aqueous film of lysozyme on a glass substrate by F-LEMS and Ti:S-LEMS with sufficient pulse energy showed comparable intensity to the analysis of a droplet from a stainless steel substrate, further proving that linear absorption by the substrate is not necessary for femtosecond laser vaporization. Note that no low mass fragments were observed in the analysis of dried and aqueous cytochrome c and lysozyme protein standard samples using fiber laser vaporization.

2.4.5 Is the Vaporization Mechanism Shockwave-Related in F-LEMS?: Use of Teflon Spacers

In the experiments using glass substrates, significant ablation was observed on the side of the glass adjacent to the copper sample stage. One possible mechanism for vaporization, then, could be an acoustic shockwave created by the ablation of the metal stage that travels through the glass and desorbs the analytes off the surface in a manner similar to the LIAD experiments [31]. To test the shockwave vaporization mechanism, protein sample was vaporized from a glass substrate placed on top of a four-layer thick glass stack with a Teflon tape spacer in between each layer, as depicted in Figure 2.10. In this experiment, aqueous films of cytochrome c and lysozyme were laser vaporized and postionized using a nanospray solvent of 1:1 (v:v) water:methanol with 1% glacial acetic acid. The mass spectra shown in Figure 2.11 display comparable ion intensities with the

spectra from experiments without any Teflon spacers or stacked glass layers, suggesting that the vaporization mechanism is not shockwave-dependent. The use of the Teflon spacer to separate the glass layers decoupled the glass sample substrates from the metal sample stage and reduced the effect of a potential acoustic shockwave from the ablation of metal. A shift to higher charge states was also observed because an acidified nanospray was used for postionization in this measurement rather than the buffered nanospray. The analysis of an aqueous film of cytochrome c using the acidified nanospray postionization revealed a significant shift of the CSD centroid from 7+ (Figure 2.6) to 17+ (Figure 2.11) while lysozyme revealed a similar trend with the centroid increasing from 8+ (Figure 2.7) to 9+ (Figure 2.11). This shift of the CSD to higher charge states is expected and indicates a change of vaporized proteins to the denatured conformation, similar to the trend observed in previous 800 nm experiments when an acidified ESI postionization solvent is used [45].

Figure 2.10. Picture of a four-layer glass substrate stack with Teflon tape put in between each glass layer as a spacer. The sample slides were placed at the center of the glass stack where the Teflon was cut to avoid laser damage.

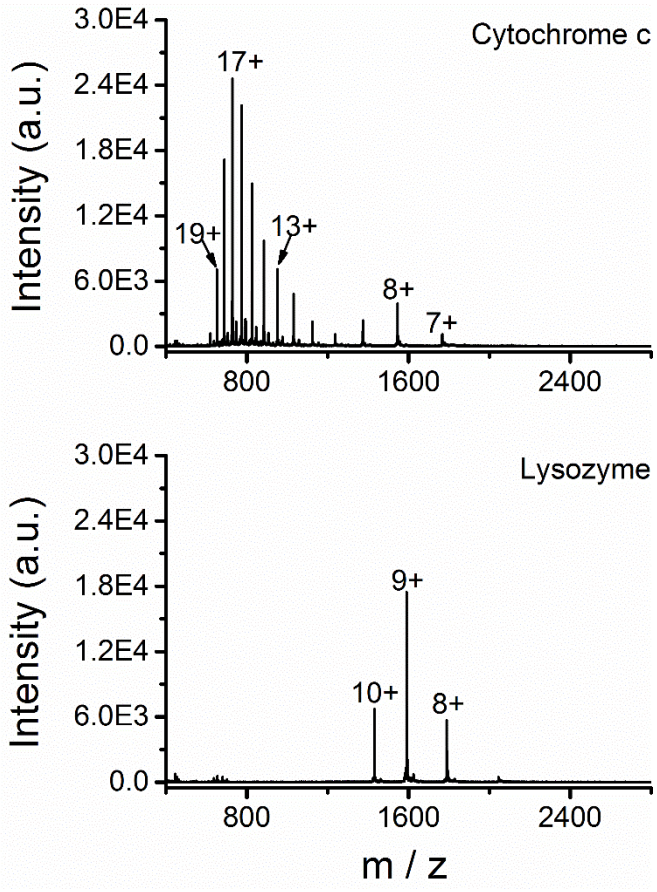

Figure 2.11. Background-subtracted F-LEMS mass spectra of 4 μL aqueous films of 250 μM cytochrome c and lysozyme from glass slides.

2.4.6 Vaporization of Whole Blood without Pretreatment from Stainless Steel and Glass Slides

Chemical analysis of biological fluids, like whole blood and human serum, is a challenging task for mass spectrometry because of the interference from the high concentrations of salt present in the sample. Direct sampling of whole blood without sample preparation is promising and has been performed successfully by electrospray-assisted laser desorption/ionization (ELDI) [60], infrared laser-assisted desorption electrospray ionization (IR LADESI or IR-MALDESI) [61, 62], DESI [63], LAESI [26], as well as 800 nm LEMS [24]. In this experiment, whole blood was deposited on the sample slides and directly analyzed by the fiber laser coupled with buffered nanospray postionization. The raw spectra of whole blood analyzed on stainless steel and glass substrates are presented in Figure 2.12. The solvent background subtracted F-LEMS mass spectra from *m/z* 50 to 2500 are also shown in Figure 2.13. The F-LEMS mass spectra revealed two peaks at *m/z* 1968.7 and 1750.2 in the high mass region. The deconvolution of the two high mass peaks corresponded to the 8+ and 9+ charge states of a protonated protein with a molecular mass of 15742 Da, which is equal to the total mass of one α hemoglobin subunit (15126 Da) and a heme group (616 Da). The small peak at *m/z* 1575.2, assigned to the 10+ charge state of this protein complex, was observed from the stainless steel substrate but not observed from the glass substrate (see Figure 2.12). The hemoglobin features detected using buffered solvent are different from previous 800 nm LEMS studies that employed an acidified solvent and resulted in higher charge states for the α and β subunits, as well as free heme molecular ions [24]. The low signal-to-noise ratio (S/N) measured in the F-LEMS experiment is likely caused by the larger sample deposition area

(49 mm^2 *vs* 19.6 mm^2) for the whole blood sample in comparison with the protein standard samples, which led the amount of analytes vaporized to be at the limit of detection of the technique. The low ionization efficiency of buffered nanospray may also have limited the postionization efficiency of vaporized protein analytes from the blood in comparison with the acidified electrospray measurements as observed for protein standard measurements (Figure 2.6 *vs* Figure 2.11, Figure 2.7 *vs* Figure 2.11). Note that the tuning of the mass spectrometer, *i.e.,* extraction lens and collision cell voltages, is optimized to achieve the least possible unfolding of the protein structure and thus may not correspond to the optimal signal intensity. The analytes observed at *m/z* 393.1, 717.5, and 943.7 (see Figure 2.13) are most likely lipids or metabolites in the blood. This experiment further demonstrates that the fiber laser system results in soft desorption of protein complexes without fragmentation for mass analysis.

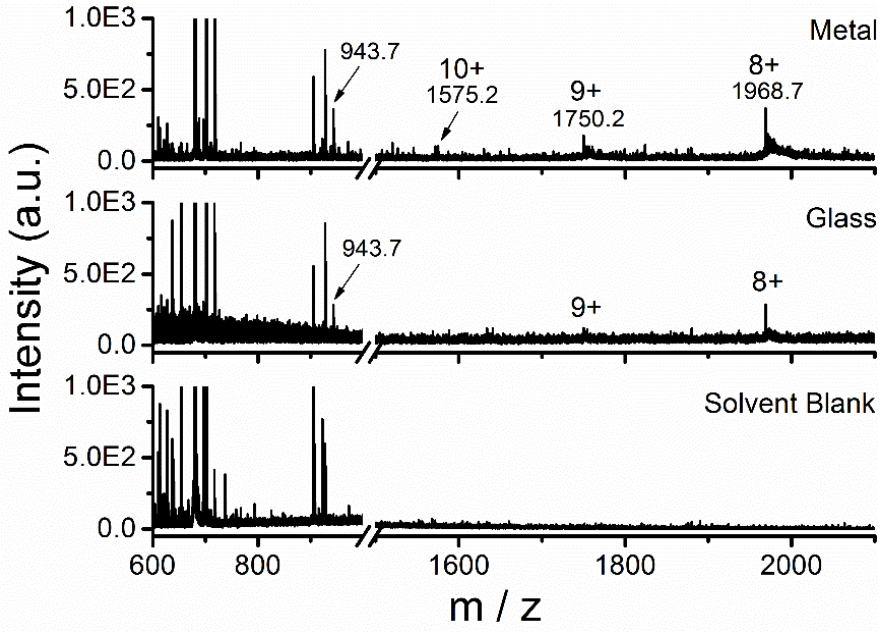

Figure 2.12. Raw F-LEMS mass spectra of whole blood analyzed from metal and glass slides. The nanospray solvent blank mass spectrum is also shown.

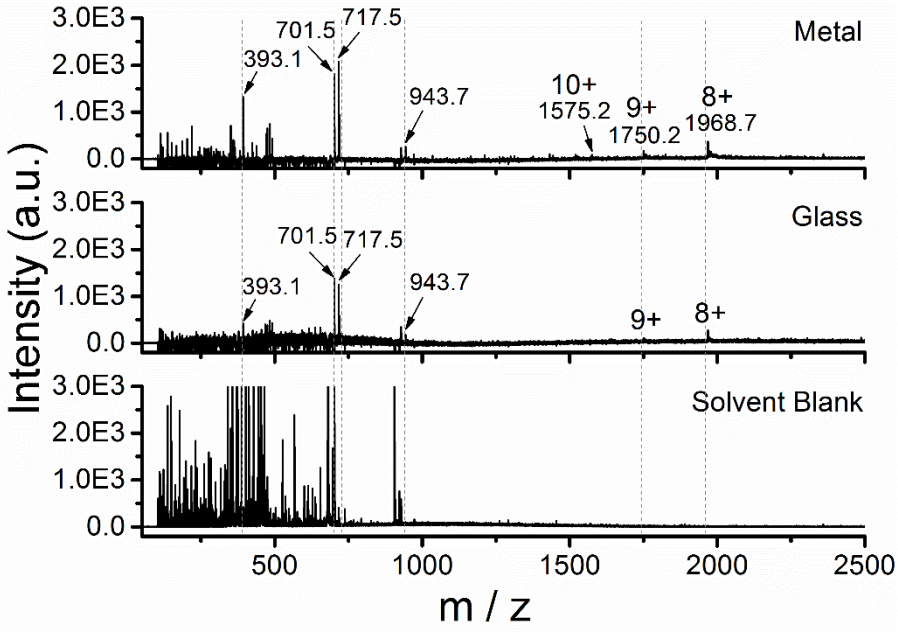

Figure 2.13. Background-subtracted F-LEMS mass spectra of whole blood analyzed from metal and glass slides. The nanospray solvent blank mass spectrum is also shown.

2.5 Conclusions

Mass analysis has been performed using longer duration femtosecond laser vaporization at 1042 nm wavelength when coupled with nanospray postionization for the analysis of pure proteins and whole blood. Vaporization of dried or aqueous protein samples was demonstrated from metal and dielectric substrates. The wettability of the substrate may play a role in the ablation of liquid samples, differing from the vaporization of dried samples. The observation of the folded conformation of proteins and the hemoglobin α subunit-heme complex indicates that fiber-based femtosecond laser vaporization at 1042 nm is a "soft" method for transferring protein molecules from the condensed phase to the gas phase. The mechanism is shown to be neither thermal- nor acoustic wave-induced, therefore, a multiphoton, nonresonant process is proposed for matrix-free femtosecond laser vaporization.

Finally, note that the limit of detection of this fiber laser-based LEMS technique is higher than conventional ESI-MS presumably due to the low capture and ionization efficiency of the ESI plume. A recent report demonstrated that the sample transfer efficiency of LAESI was increased from 2% to 50% by using a continuous flow solvent probe as the plume capture source in comparison to direct ESI where significant sample losses and low ionization efficiency occur [64]. The limit of detection of LEMS could benefit from the use of related technologies such as the design of novel neutral material transfer devices [65], neutral/liquid interfaces [66], or continuous flow solvent probes [64], that are able to increase the neutral capture and ionization efficiency for mass spectrometric techniques using ESI as a postionization source. Presently, the experimental configuration only enables successful analysis when performed with a focal spot diameter of 75 μm. The

femtosecond fiber laser is a turnkey, robust system that is amenable to nonspecialist laboratories. The fact that LEMS is viable by using the longer wavelength, longer duration, and lower energy laser pulses is advantageous for the implementation of an affordable femtosecond laser.

2.6 References

1. J.B. Fenn, M. Mann, C.K. Meng, S.F. Wong, C.M. Whitehouse. Electrospray ionization for mass spectrometry of large biomolecules. *Science* **246**, 64 (1989).

2. K. Tanaka, H. Waki, Y. Ido, S. Akita, Y. Yoshida, T. Yoshida, T. Matsuo. Protein and polymer analyses up to m/z 100 000 by laser ionization time-of-flight mass spectrometry. *Rapid Commun. Mass Spectrom.* **2**, 151 (1988).

3. M. Karas, F. Hillenkamp. Laser desorption ionization of proteins with molecular masses exceeding 10,000 daltons. *Anal. Chem.* **60**, 2299 (1988).

4. M.W.F. Nielen. Maldi time-of-flight mass spectrometry of synthetic polymers. *Mass Spectrom. Rev.* **18**, 309 (1999).

5. E. Nordhoff, F. Kirpekar, P. Roepstorff. Mass spectrometry of nucleic acids. *Mass Spectrom. Rev.* **15**, 67 (1996).

6. J.A. Loo. Studying noncovalent protein complexes by electrospray ionization mass spectrometry. *Mass Spectrom. Rev.* **16**, 1 (1997).

7. P. Chaurand, M. Stoeckli, R.M. Caprioli. Direct profiling of proteins in biological tissue sections by MALDI mass spectrometry. *Anal. Chem.* **71**, 5263 (1999).

8. J.J. Nicklay, G.A. Harris, K.L. Schey, R.M. Caprioli. MALDI imaging and in situ identification of integral membrane proteins from rat brain tissue sections. *Anal. Chem.* **85**, 7191 (2013).

9. G.A. Harris, A.S. Galhena, F.M. Fernández. Ambient sampling/ionization mass spectrometry: Applications and current trends. *Anal. Chem.* **83**, 4508 (2011).

10. M.-Z. Huang, S.-C. Cheng, Y.-T. Cho, J. Shiea. Ambient ionization mass spectrometry: A tutorial. *Anal. Chim. Acta* **702**, 1 (2011).

11. A.J.R. Heck. Native mass spectrometry: A bridge between interactomics and structural biology. *Nat. Methods* **5**, 927 (2008).

12. B.K. Kaletaş, I.M. van der Wiel, J. Stauber, J.D. Lennard, C. Güzel, J.M. Kros, T.M. Luider, R.M.A. Heeren. Sample preparation issues for tissue imaging by imaging MS. *Proteomics* **9**, 2622 (2009).

13. Z. Takáts, J.M. Wiseman, B. Gologan, R.G. Cooks. Mass spectrometry sampling under ambient conditions with desorption electrospray ionization. *Science* **306**, 471 (2004).

14. M.E. Monge, G.A. Harris, P. Dwivedi, F.M. Fernández. Mass spectrometry: Recent advances in direct open air surface sampling/ionization. *Chem. Rev.* **113**, 2269 (2013).

15. S.-C. Cheng, Y.-S. Lin, M.-Z. Huang, J. Shiea. Applications of electrospray laser desorption ionization mass spectrometry for document examination. *Rapid Commun. Mass Spectrom.* **24**, 203 (2010).

16. C.H. Stephens, B. Shrestha, H.R. Morris, M.E. Bier, P.M. Whitmore, A. Vertes. Minimally invasive monitoring of cellulose degradation by desorption electrospray ionization and laser ablation electrospray ionization mass spectrometry. *Analyst* **135**, 2434 (2010).

17. S. Soparawalla, G.A. Salazar, E. Sokol, R.H. Perry, R.G. Cooks. Trace detection of non-uniformly distributed analytes on surfaces using mass transfer and large-area desorption electrospray ionization (DESI) mass spectrometry. *Analyst* **135**, 1953 (2010).

18. P.M. Flanigan, J.J. Brady, E.J. Judge, R.J. Levis. Determination of inorganic improvised explosive device signatures using laser electrospray mass spectrometry detection with offline classification. *Anal. Chem.* **83**, 7115 (2011).

19. J.J. Brady, E.J. Judge, R.J. Levis. Identification of explosives and explosive formulations using laser electrospray mass spectrometry. *Rapid Commun. Mass Spectrom.* **24**, 1659 (2010).

20. L. Luosujärvi, S. Kanerva, V. Saarela, S. Franssila, R. Kostiainen, T. Kotiaho, T.J. Kauppila. Environmental and food analysis by desorption atmospheric pressure photoionization-mass spectrometry. *Rapid Commun. Mass Spectrom.* **24**, 1343 (2010).

21. S.E. Edison, L.A. Lin, B.M. Gamble, J. Wong, K. Zhang. Surface swabbing technique for the rapid screening for pesticides using ambient pressure desorption ionization with high-resolution mass spectrometry. *Rapid Commun. Mass Spectrom.* **25**, 127 (2011).

22. E.J. Judge, J.J. Brady, D. Dalton, R.J. Levis. Analysis of pharmaceutical compounds from glass, fabric, steel, and wood surfaces at atmospheric pressure

using spatially resolved, nonresonant femtosecond laser vaporization electrospray mass spectrometry. *Anal. Chem.* **82**, 3231 (2010).

23. P.J. Roach, J. Laskin, A. Laskin. Molecular characterization of organic aerosols using nanospray-desorption/electrospray ionization-mass spectrometry *Anal. Chem.* **82**, 7979 (2010).

24. E.J. Judge, J.J. Brady, R.J. Levis. Mass analysis of biological macromolecules at atmospheric pressure using nonresonant femtosecond laser vaporization and electrospray ionization. *Anal. Chem.* **82**, 10203 (2010).

25. M.-Z. Huang, S.-S. Jhang, C.-N. Cheng, S.-C. Cheng, J. Shiea. Effects of matrix, electrospray solution, and laser light on the desorption and ionization mechanisms in electrospray-assisted laser desorption ionization mass spectrometry. *Analyst* **135**, 759 (2010).

26. P. Nemes, A. Vertes. Laser ablation electrospray ionization for atmospheric pressure, in vivo, and imaging mass spectrometry. *Anal. Chem.* **79**, 8098 (2007).

27. J.S. Sampson, K.K. Murray, D.C. Muddiman. Intact and top-down characterization of biomolecules and direct analysis using infrared matrix-assisted laser desorption electrospray ionization coupled to FT-ICR mass spectrometry. *J. Am. Soc. Mass Spectrom.* **20**, 667 (2009).

28. L.S. Eberlin, D.R. Ifa, C. Wu, R.G. Cooks. Three-dimensional vizualization of mouse brain by lipid analysis using ambient ionization mass spectrometry. *Angew. Chem. Int. Ed.* **49**, 873 (2010).

29. Z.-P. Yao. Characterization of proteins by ambient mass spectrometry. *Mass Spectrom. Rev.* **31**, 437 (2012).

30. J.A. Barry, D.C. Muddiman. Global optimization of the infrared matrix-assisted laser desorption electrospray ionization (IR MALDESI) source for mass spectrometry using statistical design of experiments. *Rapid Commun. Mass Spectrom.* **25**, 3527 (2011).

31. S.-C. Cheng, T.-L. Cheng, H.-C. Chang, J. Shiea. Using laser-induced acoustic desorption/electrospray ionization mass spectrometry to characterize small organic and large biological compounds in the solid state and in solution under ambient conditions. *Anal. Chem.* **81**, 868 (2009).

32. J.J. Brady, E.J. Judge, R.J. Levis. Mass spectrometry of intact neutral macromolecules using intense non-resonant femtosecond laser vaporization with electrospray post-ionization. *Rapid Commun. Mass Spectrom.* **23**, 3151 (2009).

33. J.J. Brady, E.J. Judge, R.J. Levis. Analysis of amphiphilic lipids and hydrophobic proteins using nonresonant femtosecond laser vaporization with electrospray post-Ionization. *J. Am. Soc. Mass Spectrom.* **22**, 762 (2011).

34. J.J. Perez, P.M. Flanigan, J.J. Brady, R.J. Levis. Classification of smokeless powders using laser electrospray mass spectrometry and offline multivariate statistical analysis. *Anal. Chem.* **85**, 296 (2013).

35. E.J. Judge, J.J. Brady, P.E. Barbano, R.J. Levis. Nonresonant femtosecond laser vaporization with electrospray postionization for ex vivo plant tissue typing using compressive linear classification. *Anal. Chem.* **83**, 2145 (2011).

36. P.M. Flanigan, L.L. Radell, J.J. Brady, R.J. Levis. Differentiation of eight phenotypes and discovery of potential biomarkers for a single plant organ class using laser electrospray mass spectrometry and multivariate statistical analysis. *Anal. Chem.* **84**, 6225 (2012).

37. P.M. Flanigan, J.J. Perez, S. Karki, R.J. Levis. Quantitative measurements of small molecule mixtures using laser electrospray mass spectrometry. *Anal. Chem.* **85**, 3629 (2013).

38. J.J. Perez, P.M. Flanigan, S. Karki, R.J. Levis. Laser electrospray mass spectrometry minimizes ion suppression facilitating auantitative mass spectral response for multicomponent mixtures of proteins. *Anal. Chem.* **85**, 6667 (2013).

39. D. Strickland, G. Mourou. Compression of amplified chirped optical pulses. *Opt. Commun.* **56**, 219 (1985).

40. M.E. Fermann, I. Hartl. Ultrafast fibre lasers. *Nat. Photon.* **7**, 868 (2013).

41. E. Margoliash. Primary structure and evolution of cytochrome c. *Proc. Natl. Acad. Sci. U.S.A.* **50**, 672 (1963).

42. I.X. Peng, R.R. Ogorzalek Loo, E. Margalith, M.W. Little, J.A. Loo. Electrospray-assisted laser desorption ionization mass spectrometry (ELDI-MS) with an infrared laser for characterizing peptides and proteins. *Analyst* **135**, 767 (2010).

43. H. Zhang, R.M. Caprioli. Capillary electrophoresis combined with matrix-assisted laser desorption/ionization mass spectrometry; continuous sample deposition on a matrix-precoated membrane target. *J. Mass Spectrom.* **31**, 1039 (1996).

44. S. Myung, J.M. Wiseman, S.J. Valentine, Z. Takáts, R.G. Cooks, D.E. Clemmer. Coupling desorption electrospray ionization with ion mobility/mass spectrometry for analysis of protein structure: Evidence for desorption of folded and denatured states. *J. Phys. Chem. B* **110**, 5045 (2006).

45. J.J. Brady, E.J. Judge, R.J. Levis. Nonresonant femtosecond laser vaporization of aqueous protein preserves folded structure. *Proc. Natl. Acad. Sci. U.S.A.* **108**, 12217 (2011).

46. H. Oh, K. Breuker, S.K. Sze, Y. Ge, B.K. Carpenter, F.W. McLafferty. Secondary and tertiary structures of gaseous protein ions characterized by electron capture dissociation mass spectrometry and photofragment spectroscopy. *Proc. Natl. Acad. Sci. U.S.A.* **99**, 15863 (2002).

47. C.A. Cassou, H.J. Sterling, A.C. Susa, E.R. Williams. Electrothermal supercharging in mass spectrometry and tandem mass spectrometry of native proteins. *Anal. Chem.* **85**, 138 (2013).

48. T.A. Fligge, J. Kast, K. Bruns, M. Przybylski. Direct monitoring of protein-chemical reactions utilising nanoelectrospray mass spectrometry. *J. Am. Soc. Mass Spectrom.* **10**, 112 (1999).

49. K. Breuker, O.S. Skinner, F.W. McLafferty. Femtosecond laser vaporization that preserves protein-folded structure: An unproven idea. *Proc. Natl. Acad. Sci. U.S.A.* **109**, E206 (2012).

50. J.J. Brady, E.J. Judge, R.J. Levis. Reply to Breuker et al.: How laser electrospray mass spectrometry (LEMS) measures condensed phase protein structure, not vacuum structure. *Proc. Natl. Acad. Sci. U.S.A.* **109**, E207 (2012).

51. Z. Hall, C.V. Robinson. Do charge state signatures guarantee protein conformations? *J. Am. Soc. Mass Spectrom.* **23**, 1161 (2012).

52. A. Sethuraman, G. Vedantham, T. Imoto, T. Przybycien, G. Belfort. Protein unfolding at interfaces: Slow dynamics of α-helix to β-sheet transition. *Proteins: Struct., Funct., Bioinf.* **56**, 669 (2004).

53. G. Bracco, B. Holst. *Surface science techniques.* Springer, New York, NY (2013).

54. T.S. Chow. Wetting of rough surfaces. *J. Phys.: Condens. Matter* **10**, L445 (1998).

55. R. Digilov. Charge-induced modification of contact angle: The secondary electrocapillary effect. *Langmuir* **16**, 6719 (2000).

56. S. Georgiou, A. Koubenakis. Laser-induced material ejection from model molecular solids and liquids: Mechanisms, implications, and applications. *Chem. Rev.* **103**, 349 (2003).

57. L.V. Zhigilei, E. Leveugle, B.J. Garrison, Y.G. Yingling, M.I. Zeifman. Computer simulations of laser ablation of molecular substrates. *Chem. Rev.* **103**, 321 (2003).

58. P.M. Flanigan, F. Shi, J.J. Perez, S. Karki, C. Pfeiffer, C. Schafmeister, R.J. Levis. Determination of internal energy distributions of laser electrospray mass spectrometry using thermometer ions and other biomolecules. *J. Am. Soc. Mass Spectrom.* **25**, 1572 (2014).

59. P.M. Flanigan, F. Shi, J.J. Archer, R.J. Levis. Internal energy deposition for low energy, femtosecond laser vaporization and nanospray post-ionization mass spectrometry using thermometer ions. *J. Am. Soc. Mass Spectrom.* **26**, 716 (2015).

60. M.-Z. Huang, H.-J. Hsu, L.-Y. Lee, J. Jeng, J. Shiea. Direct protein detection from biological media through electrospray-assisted laser desorption ionization/mass spectrometry. *J. Proteome Res.* **5**, 1107 (2006).

61. Y.H. Rezenom, J. Dong, K.K. Murray. Infrared laser-assisted desorption electrospray ionization mass spectrometry. *Analyst* **133**, 226 (2008).

62. J. Dong. *Merged electrospray ionization mass spectrometry*. Ph.D. Thesis, Louisiana State University, Baton Rouge, LA, (2009).

63. Z. Takáts, J.M. Wiseman, R.G. Cooks. Ambient mass spectrometry using desorption electrospray ionization (DESI): Instrumentation, mechanisms and applications in forensics, chemistry, and biology. *J. Mass Spectrom.* **40**, 1261 (2005).

64. J.T. O'Brien, E.R. Williams, H.-Y.N. Holman. Ambient infrared laser ablation mass spectrometry (AIRLAB-MS) of live plant tissue with plume capture by continuous flow solvent probe. *Anal. Chem.* **87**, 2631 (2015).

65. R.B. Dixon, J.S. Sampson, A.M. Hawkridge, D.C. Muddiman. Ambient aerodynamic ionization source for remote analyte sampling and mass spectrometric analysis. *Anal. Chem.* **80**, 5266 (2008).

66. J.A. Stolee, A. Vertes. Toward single-cell analysis by plume collimation in laser ablation electrospray ionization mass spectrometry. *Anal. Chem.* **85**, 3592 (2013).

CHAPTER 3

AMBIENT MOLECULAR ANALYSIS OF BIOLOGICAL TISSUE USING LOW-ENERGY, FIBER-BASED LASER ELECTROSPRAY MASS SPECTROMETRY

3.1 Overview

In this chapter, direct analysis of plant and animal tissue samples by laser electrospray mass spectrometry (LEMS) was investigated using low-energy, femtosecond duration laser vaporization at wavelengths of 800 and 1042 nm followed by nanospray postionization. Low-energy (<50 μJ), fiber-based 1042 nm LEMS (F-LEMS) allowed interrogation of the molecular species in fresh flower petal and leaf samples using 435 fs, 10 Hz bursts of 20 pulses from a Ytterbium-doped fiber laser and revealed comparable results to high energy (75–1120 μJ), 45 fs, 800 nm Ti:Sapphire-based LEMS (Ti:S-LEMS) measurements. Anthocyanins, sugars and other metabolites were successfully detected and revealed the anticipated metabolite profile for the petal and leaf samples. Phospholipids, especially phosphatidylcholine, were identified from a fresh mouse brain section sample using Ti:S-LEMS without the application of matrix. These lipid features were suppressed in both the fiber-based and Ti:Sapphire-based LEMS measurements when the brain sample was prepared using the optimal cutting temperature compounds that are commonly used in animal tissue cryosectioning.

3.2 Introduction

The ability to detect biomolecules (e.g., small metabolites, lipids and proteins) directly from biological samples remains one of the most important topics in molecular systems biology [1]. Numerous studies have demonstrated that the concentration and distribution of metabolites, such as hydrocarbons, sugars, amino acids, alkaloids, and lipids, are closely associated with biological processes in a living organism [2]. Label-assisted techniques such as fluorophore-tagging microscopy can be used to characterize the biological samples *in vivo* or *ex vivo*, and rely on labeling/staining methods that may perturb the biological system. Label-free techniques such as infrared [3] and Raman [4] spectroscopy can interrogate the sample with submicron lateral resolution in a noninvasive manner. However, such spectroscopy techniques rely upon the vibrational modes of the molecules in question, which require prior knowledge for interpretation, and lack chemical specificity for individual compounds. Mass spectrometry (MS), on the other hand, has seen rapid deployment in biological sample analysis because the requirements of high throughput, sensitivity, and specificity can be simultaneously satisfied in one measurement. In particular, the introduction of ambient ionization mass spectrometry allows analysis with minimal preparation under ambient conditions, thus preserving the native state of the sample [5, 6].

Methods that use laser desorption/electrospray ionization hybrid ambient ionization sources combine the microsampling capability of a laser beam with the high ionization efficiency of an electrospray source [7]. Several such techniques, electrospray-assisted laser desorption ionization (ELDI) [8], laser ablation electrospray ionization (LAESI) [9], infrared matrix-assisted laser desorption electrospray ionization (IR-MALDESI) [10], and

laser electrospray mass spectrometry (LEMS) [11], can provide a lateral resolution of 20−200 μm without the necessity of adding external matrix to the sample. In LEMS, laser pulses as short as 60 fs, usually at 800 nm, interact with the analytes via a nonlinear, multiphoton excitation mechanism [11]. LEMS does not require either the analyte or matrix to be linearly resonant with the laser wavelength and shows little dependence on the types of sample substrate employed [12]. Various biological samples including chicken egg albumen and yolk [13], reduced fat and whole milk [14], whole blood [13, 14], and plant samples [15, 16] have been successfully analyzed by LEMS without the use of external matrix. Investigations of animal tissue samples, a popular target of MS imaging, have not been performed so far by LEMS to examine the feasibility of femtosecond laser vaporization for chemical analysis of animal tissue samples.

The nonresonant, multiphoton excitation process in LEMS occurs when the sample of interest is subjected to a femtosecond laser pulse at an intensity of 10^{13}–10^{14} W/cm^2, which is 6 to 7 orders of magnitude higher than a nanosecond UV or IR laser desorption source under the same laser pulse energy and focusing condition. A solid state Ti:Sapphire amplifier seeded by a Ti:Sapphire oscillator is usually used to create laser pulses at 800 nm with high pulse energy (μJ–mJ) and ultrashort pulse duration (40–60 fs) to fulfill the high intensity requirement. However, the higher cost and lower robustness of the Ti:Sapphire amplified femtosecond laser in comparison with the more common nanosecond UV and IR lasers limit the wide application of Ti:Sapphire laser as a desorption source. In recent studies, we successfully implemented a low-energy, femtosecond fiber laser for vaporization and a nanospray for postionization in the analysis of proteins, whole blood [17], and substituted benzylpyridinium salts [18]. The studies show that the low-energy

fiber laser resulted in comparable internal energy distributions to nanospray [18] and retained intact biological macromolecules after laser radiation [17]. The application of a femtosecond fiber laser rather than a solid state amplifier laser to more complex biological samples is thus of interest for the broad and potential applicability of LEMS as a robust, portable, and affordable analytical tool to non-specialists.

Here, the use of the fiber-based 1042 nm laser vaporization is extended to the analysis of biological tissue samples and compare the results with Ti:Sapphire-based 800 nm laser measurements. A lipid standard sample, 1,2-dihexanoyl-*sn*-glycero-3-phosphocholine PC(6:0/6:0), was analyzed via fiber-based LEMS (F-LEMS) and Ti:Sapphire-based LEMS (Ti:S-LEMS). The vaporization of fresh *Begonia* flower petal and leaf samples using F-LEMS and Ti:S-LEMS was investigated. A mouse brain section was also characterized by the Ti:Sapphire laser without application of any external matrix. Finally, the effect of optimal cutting temperature (OCT) compounds on the analysis of mouse brain sections by F-LEMS and Ti:S-LEMS was investigated.

3.3 Experimental Section

3.3.1 Materials

The lipid standard sample PC(6:0/6:0) was purchased from Avanti Polar Lipids Inc. (Alabaster, AL, USA). HPLC grade methanol and water were purchased from Fisher Scientific (Fair Lawn, NJ, USA) and Burdick & Jackson (Muskegon, MI, USA), respectively. Glacial acetic acid was purchased from EMD Chemicals (Gibbstown, NJ, USA).

3.3.2 Sample Preparation

Stock solution of PC(6:0/6:0) was prepared in 1:1 (v:v) methanol:water solution at a concentration of 250 μM. For laser vaporization experiments, 15 μL aliquot of the lipid solution was deposited on a stainless steel sample slide and allowed to air-dry to a circular spot of ~5 mm in diameter. Fresh *Begonia* flower petal and leaf samples were collected from plants on the Temple University campus. The flowers were harvested from different plants with 3~4 leaves attached and then separated to petal and leaf samples. The petal and leaf samples were affixed to the stainless steel and glass sample slides using double-sided tape prior to analysis. The center regions of the petal or leaf samples were raster scanned and irradiated by laser during analysis. Fresh mouse brain samples were obtained from a healthy mouse and stored in PBS buffer (pH 7.4) with an ice bath. Prior to sectioning, the brain sample was wrapped in a piece of aluminum foil and flash frozen in liquid nitrogen. The frozen brain was then immediately cut into ~200 μm thick transverse sections by a stainless steel blade (X-ACTO #11; Statesville, NC, USA) over the liquid nitrogen under a microscope (Leica Zoom 2000; Buffalo Grove, IL, USA). The sections were thaw-mounted onto microscope slides (Fisher Scientific, Pittsburgh, PA, USA) and stored at −80 °C. OCT-embedded mouse brain tissue cyosections (5 μm thickness) were obtained from Department of Pathology and Laboratory Medicine (Temple University, Philadelphia, PA, USA), mounted on the microscope slides and stored at −80 °C. *All animal procedures followed the Guide for the Care and Use of Laboratory Animals by NIH/NRC.* Fresh and OCT-embedded mouse brain section slides were brought to room temperature under atmospheric pressure in ~15 min prior to analysis. The lipid, plant, and brain sample slides

were then placed on the sample stage and subjected to laser vaporization without further treatment.

3.3.3 Laser Electrospray Mass Spectrometry

The experimental schemes of fiber-based and Ti:Sapphire-based LEMS source are shown in Figure 3.1. Laser vaporization for F-LEMS or Ti:S-LEMS was performed using a fiber-based femtosecond laser (μJewel DE series; IMRA America Inc., Ann Arbor, MI, USA) or a Ti:Sapphire-based femtosecond laser (Legend Elite HE series; Coherent Inc., Santa Clara, CA, USA), respectively. Both lasers were composed of an oscillator and an amplifier to produce amplified, high energy laser pulses (μJ to mJ). The fiber laser employs a Yb-doped fiber as the gain medium in the oscillator and amplifier cavity, employs single-mode fibers for directing the laser beam in and out the cavity, and is air-cooled rather than utilizing a chiller. All of these features provide a femtosecond fiber laser with a compact and robust design in comparison with the solid state Ti:Sapphire laser.

The laser vaporization source was described in detail previously for the Ti:S-LEMS [11] and has been recently modified to couple the fiber laser to the electrospray inlet of a quadrupole time of flight (QTOF) mass spectrometer (micrOTOF-Q II; Bruker Daltonik GmbH, Bremen, Germany) [17, 18]. Briefly, the fiber laser delivers 100 kHz, 435 fs, 1042 nm pulses with maximum pulse energy of 50 μJ. For laser desorption, the pulse repetition rate was stepped down to 10 Hz bursts of 20 pulses by combining a 20 Hz chopper and a 130 Hz chopper. The pulse energy was adjusted by a quarter-wave plate and a beam splitter cube from 20 μJ to 46.5 μJ. The Ti:Sapphire laser was operated at 10 Hz to create 45 fs, 800 nm laser pulses with maximum pulse energy of up to 5 mJ. The pulse energy was

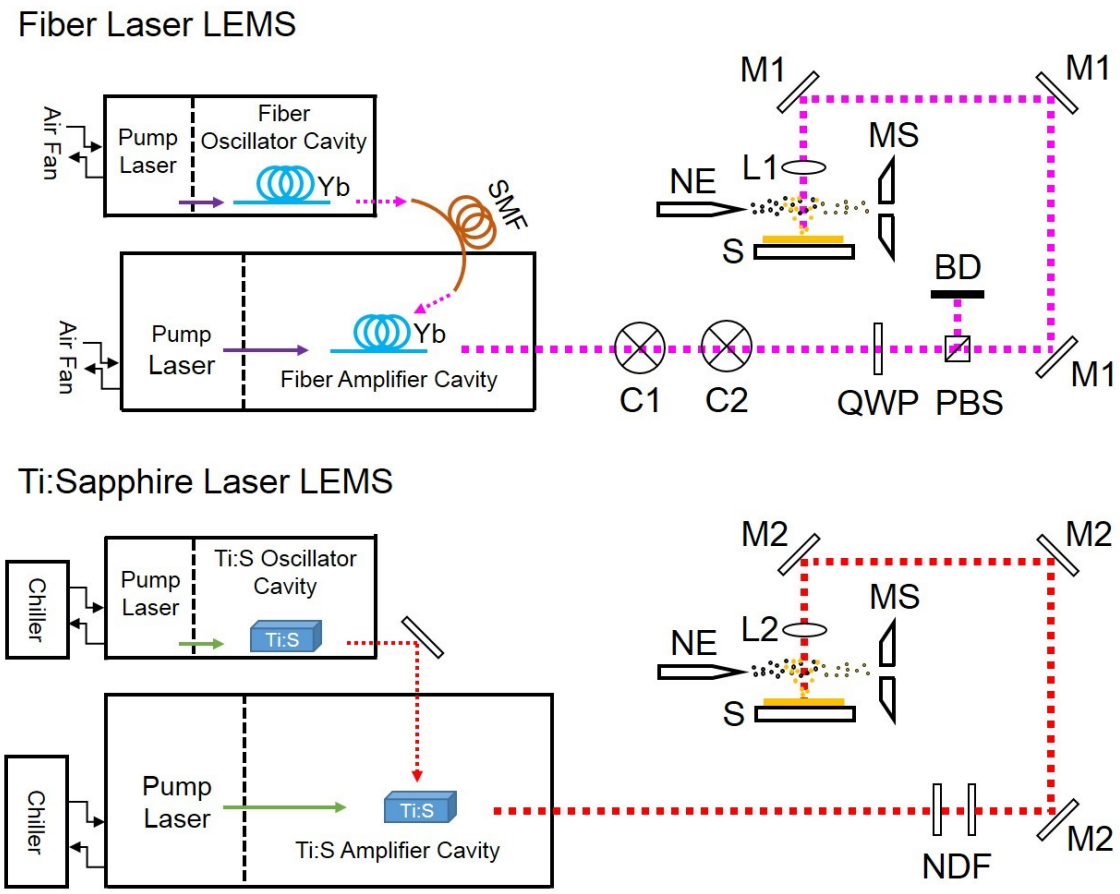

Figure 3.1. Schematic of F-LEMS and Ti:S-LEMS experimental setup. Yb, ytterbium-doped fiber; SMF, single-mode fiber; Ti:S, Ti:Sapphire crystal. M1, M2 are dielectric mirrors coated for 1042 nm and 800 nm wavelength, respectively. L1, L2 are 10 cm focal length lens coated for 1042 nm and 800 nm, respectively. C1, 20 Hz chopper; C2, 130 Hz chopper; QWP, quarter-wave plate; PBS, polarizing beam splitter cube; BD, beam dump; NDF neutral density filter; NE, nanospray emitter; S, metal sample stage; MS, mass spectrometer. Magenta and red dotted lines represent the 1042 nm and 800 nm laser beams whereas dark purple and green solid lines represent the pump laser beams in the corresponding laser systems. Note that the picture is not drawn to scale.

controlled by a pair of neutral density filters to be 75−1120 μJ for the purpose of laser desorption. The samples were placed on a copper sample stage, which was raster scanned by a two-dimensional microscopy stage (MLS203-1; Thorlabs, Newton, NJ, USA) below the nanospray source during laser vaporization. The attenuated laser pulses from the fiber laser or the Ti:Sapphire laser were focused onto the sample surface to a ~75 μm diameter spot with a 10 cm lens at 45° incident angle. The resulting intensities of field were approximately 2.39×10^{12} W/cm^2 and 3.77×10^{13} W/cm^2 when the pulse energy was 46.5 μJ and 75 μJ for the fiber laser and Ti:Sapphire laser, respectively.

The laser vaporized analytes were captured and postionized by a nanospray source. A solution containing 1:1 (v:v) methanol:water with 1% acetic acid was infused to a tapered silica emitter tip (50 μm ID, 20 μm tip ID, New Objective, Woburn, MA, USA) at a flow rate of 250 nL/min using a syringe pump (Model 100; KD Scientific, Holliston, MA, USA). A stable positive mode nanospray mass spectrum was observed when the capillary inlet was biased to −2 kV and the needle was grounded. The sample stage was biased to −1.3 kV during laser vaporization. The spectrometer was calibrated by an ESI calibrant solution (63606; Fluka Analytical/Sigma-Aldrich, Buchs, Switzerland) over a mass range of *m/z* 50−2000. The in-source collision region (ISCID) and collision cell (CID) voltages were set to be 0 and 10 eV, respectively. Raw mass spectra were acquired at a rate of 1 Hz by Bruker Compass micrOTOF control software (ver. 3.0; Bruker Daltonik GmbH, Bremen, Germany). A typical measurement was performed within 40 s per sample. Within this period, 10 blank spectra and 25 to 30 spectra of the sample were acquired. Each measurement was repeated at least two times for a total of 50 to 60 spectra per sample.

3.3.4 Data Analysis

The acquired mass spectra were processed in Bruker Compass DataAnalysis software (ver. 4.0 SP1; Bruker Daltonik GmbH, Bremen, Germany), including signal averaging, blank subtraction, and mass assignment. The processed spectra were exported and plotted in Origin 8.0 (OriginLab, Northampton, MA, USA). Peaks were labeled and confirmed by comparing the blank-subtracted spectra with the nanospray blank spectra. Features identified from plant sample were assigned by searching in the METLIN database [19] (http://metlin.scripps.edu/index.php, last accessed April 23, 2015) and Plant Metabolic Network (http://www.plantcyc.org/, last accessed April 23, 2015) with a maximum mass tolerance of 10 ppm. Identification of lipids from mouse brain sample were enabled by accurate lipids database search in METLIN [19] (http://metlin.scripps.edu/index.php, last accessed April 23, 2015) and LIPID MAPS [20] (http://www.lipidmaps.org/, last accessed April 23, 2015) with a tolerance of 20 ppm. All the assignments were further confirmed by comparing with literature data [15, 21-33].

3.4 Results and Discussion

3.4.1 Direct Analysis of Plant Tissue by F-LEMS and Ti:S-LEMS

To compare the capabilities of the fiber and Ti:Sapphire femtosecond lasers for tissue sample analysis, fresh flower petals were affixed on the stainless steel substrates for analysis. The mass spectra acquired by F-LEMS and Ti:S-LEMS are shown in Figure 3.2. The low-energy F-LEMS (46.5 μJ) mass spectrum displays a broad range of species, including anthocyanidin-associated flavonoid species. The features at *m/z* 581.2 and 727.2,

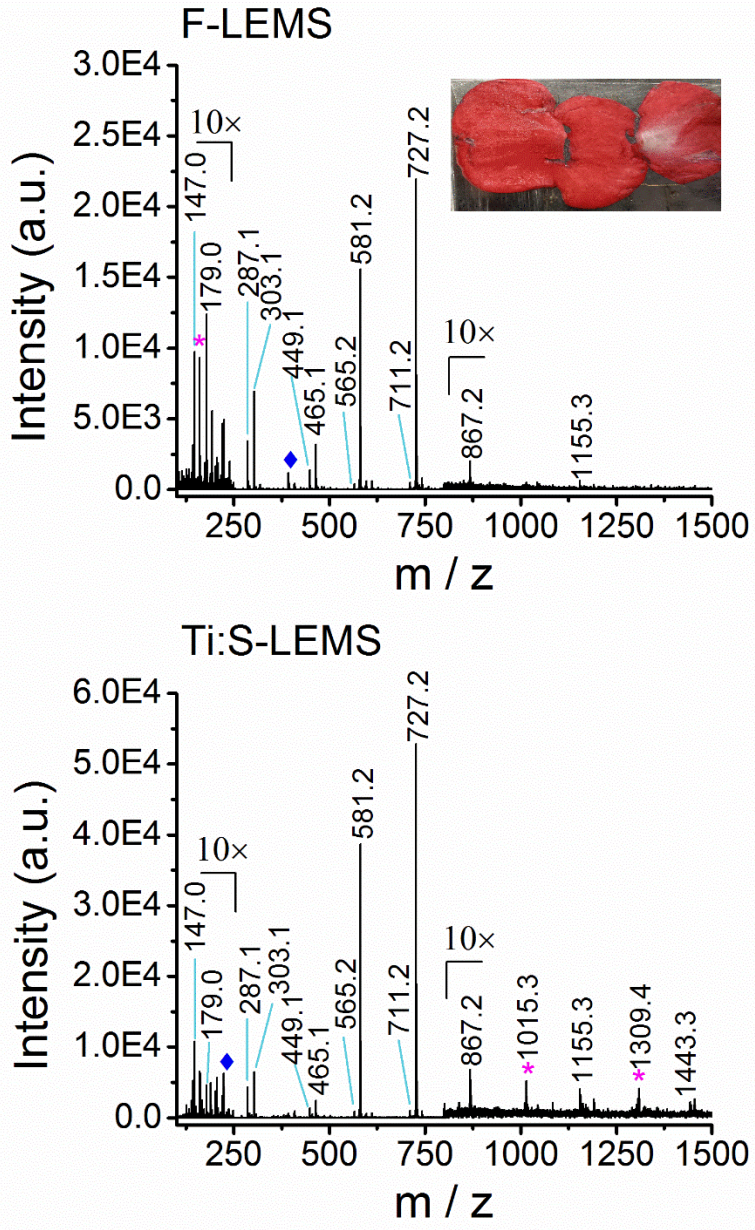

Figure 3.2. Blank-subtracted mass spectra of a flower petal on a stainless steel substrate using F-LEMS with 46.5 µJ pulse energy and Ti:S-LEMS with 280 µJ pulse energy. Inset displays the optical image of the flower petal. Note that peaks labeled with ♦ and * are solvent and unidentified plant features, respectively.

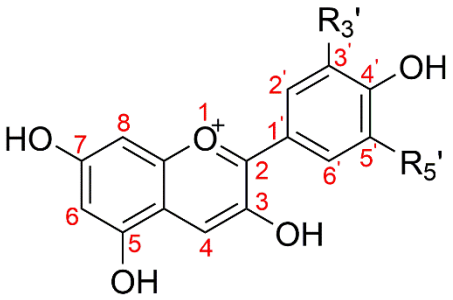

Anthocyanidin	R_3'	R_5'	Color
pelargonidin	H	H	orange
cyanidin	OH	H	reddish-purple
delphinidin	OH	OH	bluish-red

Figure 3.3. Chemical structure of different anthocyanidins specified with their corresponding color and functional groups.

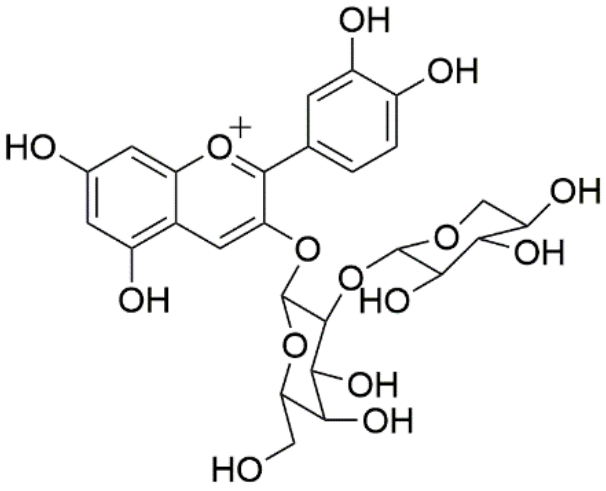

Figure 3.4. Chemical structure of cyanidin-3-*O*-xylosyl-glucoside.

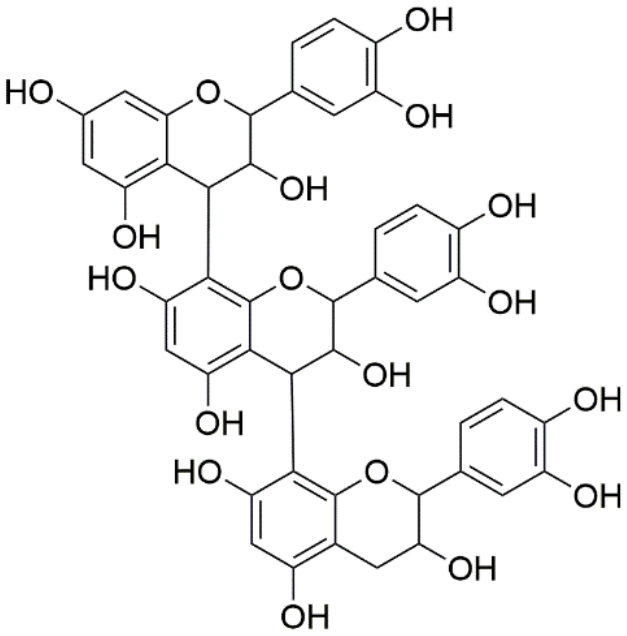

Figure 3.5. Chemical structure of procyanidin trimer.

Table 3.1. Tentative assignments of molecular features in the mass spectra collected from flower petals by F-LEMS and Ti:S-LEMS.

Compounds[a]	Formula	Monoisotopic *m/z*[b]	Measured *m/z*	Petal[c]		Mass Error (ppm)	Ref
				fiber	Ti:S		
coumaric acid-H_2O	$C_9H_6O_2$	147.0446(H)	147.0455	+	+	6.1	[15, 21]
Cy	$C_{15}H_{11}O_6$	287.0550(+)	287.0545	+	+	1.7	[22, 23]
Del	$C_{15}H_{11}O_7$	303.0499(+)	303.0501	+	+	0.7	[23]
Cy-Glu	$C_{21}H_{21}O_{11}$	449.1078(+)	449.1057	+	+	4.7	[15, 22, 23]
Del-Glu	$C_{21}H_{21}O_{12}$	465.1028(+)	465.1022	+	+	1.3	[15, 23]
Pel-xylosyl-Glu	$C_{26}H_{29}O_{14}$	565.1552(+)	565.1548	+	+	0.7	[15, 23]
Cy-xylosyl-Glu	$C_{26}H_{29}O_{15}$	581.1501(+)	581.1505	+	+	0.7	[23]
Del-xylosyl-Glu	$C_{26}H_{29}O_{16}$	597.1450(+)	597.1435	+	+	2.5	[23]
Cy di-Glu	$C_{27}H_{31}O_{16}$	611.1607(+)	611.1576	+	+	5.1	[23]
Pel-xylosyl-Rut	$C_{32}H_{39}O_{18}$	711.2131(+)	711.2131	+	+	0	[23]
Cy-xylosyl-Rut	$C_{32}H_{39}O_{19}$	727.2080(+)	727.2097	+	+	2.3	[23]
Del-xylosyl-Rut	$C_{32}H_{39}O_{20}$	743.2029(+)	743.2035	+	+	0.8	[23]
procyanidin DP3	$C_{45}H_{38}O_{18}$	867.2131(H)	867.2121	+	+	1.2	[24]
procyanidin DP4	$C_{60}H_{50}O_{24}$	1155.2765(H)	1155.2769	+	+	0.3	[24]
procyanidin DP5	$C_{75}H_{62}O_{30}$	1443.3399(H)	1443.3287	–	+	7.8	[24]

[a] Cy denotes cyanidin; Del delphinidin; Pel pelargonidin; Glu glucoside; Rut rutinoside; DP degree of polymerization. [b] Symbols in parentheses indicate protonated (H) and preformed ions (+). [c] + and – indicate presence or absence of the molecular feature in the mass spectra.

corresponding to cyanidin-xylosyl-glucoside (see Figure 3.4) and cyanidin-xylosyl-rutinoside, and other anthocyanin features were observed as the dominant species from the flower petal, as listed in Table 3.1. These anthocyanins were detected as preformed cations (see Figure 3.3) including pelargonidin, cyanidin and delphinidin with modifications including derivatization of mono-glucosides, di-glucosides, acetyl-glucosides, and acetyl-rutinosides. Most of the peaks below *m/z* 200 are likely small organic acids, for example, 147.0 was assigned as coumaric acid with the loss of one water, which are typically found as acyl functional groups for flavonoid species in the plant [15, 23]. Two features at *m/z* 867.2 and 1155.3, corresponding to singly protonated procyanidin oligomers with a degree of polymerization (DP) of 3 (DP3) and 4 (DP4) [24], were observed in the high mass region of the F-LEMS spectrum when magnified by 10. The chemical structure of procyanidin trimer is shown in Figure 3.5. The high energy Ti:S-LEMS (280 μJ) spectrum displays the same molecular features with an additional feature of procyanidin DP5 at *m/z* 1443.3. Anthocyanins, one of the most common class of flavonoids, are naturally abundant pigments that help to protect the plant against excessive UV light radiation [34]. The detection of different anthocyanidins, anthocyanin glycosides and procyanidin oligomers from the flower petals by F-LEMS and Ti:S-LEMS agrees with previous studies indicating that flavonoid species were abundant in plants using LC-ESI-MS [23, 35], atmospheric pressure MALDI-MS [36], as well as ambient ionization methods including DESI-MS [37], ELDI-MS [35], and LAESI-MS [9, 22]. Note that further analysis with collision-induced dissociation (CID) or other complementary fragmentation techniques are required to make definite assignment for the detected flavonoid ion species because of the presence of structural isomers [38].

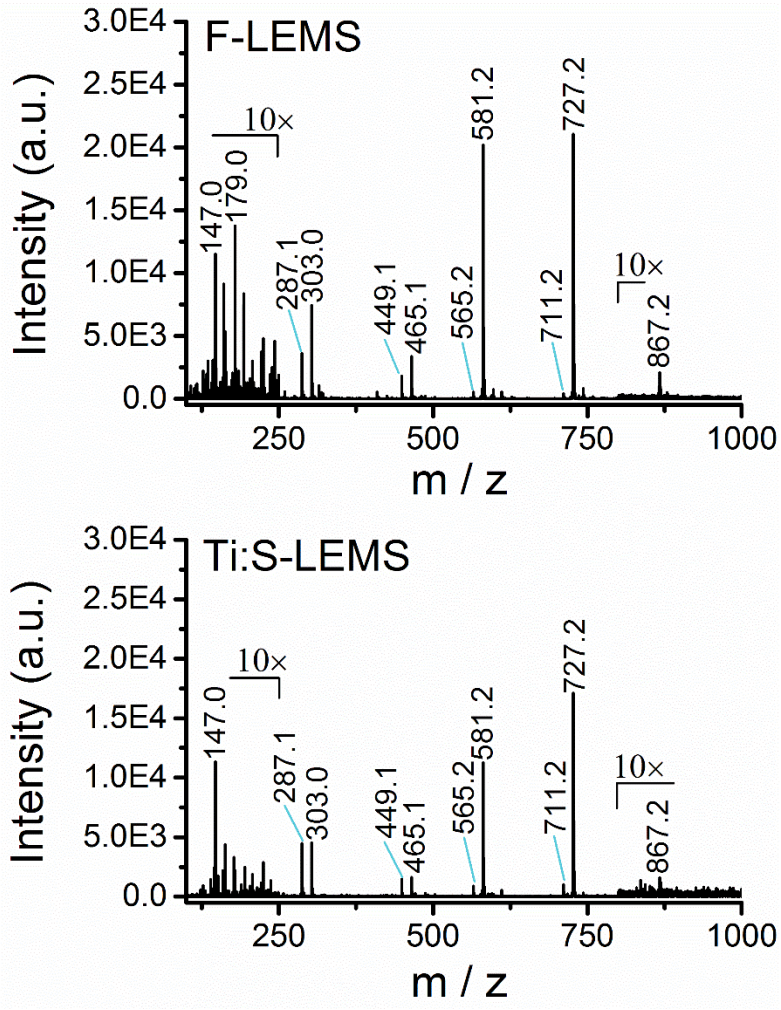

Figure 3.6. Blank-subtracted mass spectra for a flower petal affixed on a glass substrate using F-LEMS with 46.5 μJ pulse energy and Ti:S-LEMS with 160 μJ pulse energy.

To study the role of sample substrate on the laser vaporization of plant tissue by femtosecond laser pulses, flower petals were analyzed on the glass substrates and compared with stainless steel substrates. Glass is a dielectric material that is transparent at the experimental near-IR laser wavelengths and is also a poor thermal conductor, and thus thermal desorption from the substrate was expected to be minimized. The spectra obtained by F-LEMS and Ti:S-LEMS laser vaporization displayed the same ion species, including the small metabolites and procyanidin trimer, and comparable ion intensities to results from stainless steel substrates, as seen in Figure 3.6. This suggests that a femtosecond laser pulse can interact with the plant materials directly via a nonresonant, multiphoton mechanism without sample substrate heating. Near-IR fs-LEMS is different from nanosecond UV and IR laser desorption techniques that require resonant absorption. For instance, direct analysis of secondary metabolites in plant tissues was enabled using matrix-free UV-laser desorption/ionization-MS at single-cell resolution because of a strong absorbance of UV light by the metabolites [39]. However, the results can be biased as many other plant metabolites are not strong UV-absorbers and their UV laser desorption probabilities can be limited. Universal interrogation of diverse metabolites from the plant sample has been illustrated by LAESI with 200 μm or higher spatial resolution because of the resonant absorption of the IR laser radiation by endogenous water matrix [9, 40].

Sample pretreatment (e.g., physical stripping [41], solvent extraction [37], or surface imprinting [42]) is sometimes required to remove the cuticular wax layers from the plant leaf surface for mass analysis when the penetration depth of the desorption probe is limited. Here, flower leaves were directly analyzed by the femtosecond laser pulses in the same manner as the flower petal without any pretreatment. The mass spectrum acquired

using fiber laser vaporization followed by nanospray postionization revealed similar features to the measurements of the high energy Ti:Sapphire laser, as shown in Figure 3.7. A list of the assignments of molecular species from flower leaf by F-LEMS and Ti:S-LEMS analysis is provided in Table 3.2. Peaks at *m/z* 145.0 and 163.1, corresponding to protonated glucose with the loss of two and one water molecules, were observed as the dominant features in the leaf samples by F-LEMS and Ti:S-LEMS. Sucrose-related features at *m/z* 325.1, 365.1, and 381.1, corresponding to $[M–H_2O+H]^+$, $[M+Na]^+$ and $[M+K]^+$, were also found in the leaf samples by LEMS. The observation of these carbohydrates is expected as the leaf is the organ where photosynthesis takes place. The same anthocyanidin-related flavonoid features, namely cyanidin-xylosyl-glucoside (*m/z* 581.2) and cyanidin-xylosyl-rutinoside (*m/z* 727.2), were also observed from the leaf as the petal. The unique profile of metabolites in the plant, including flavonoids, carbohydrates and other metabolites, can serve as signatures for rapid sample screening and classification, e.g., discriminating different varieties of grapes (*Accent, Dunkelfelder, and Dakapo*) [35], phenotypes of *Impatiens* flower petals [15], and color patterns of a *Zebra* plant leaf [16], using laser desorption followed by electrospray postionization MS techniques and multivariate statistical analysis.

The successful vaporization of plant tissue by the fiber laser radiation with <50 μJ pulses was unexpected at such low energy in comparison with the high energy Ti:Sapphire laser vaporization. To probe the effect of pulse energy for femtosecond laser vaporization, flower petals and leaves were analyzed by Ti:S-LEMS using pulse energies over an intensity range of nearly two orders of magnitude (μJ to mJ). Unfortunately, higher pulse energies (~ mJ) are not currently available for the femtosecond fiber laser to perform a

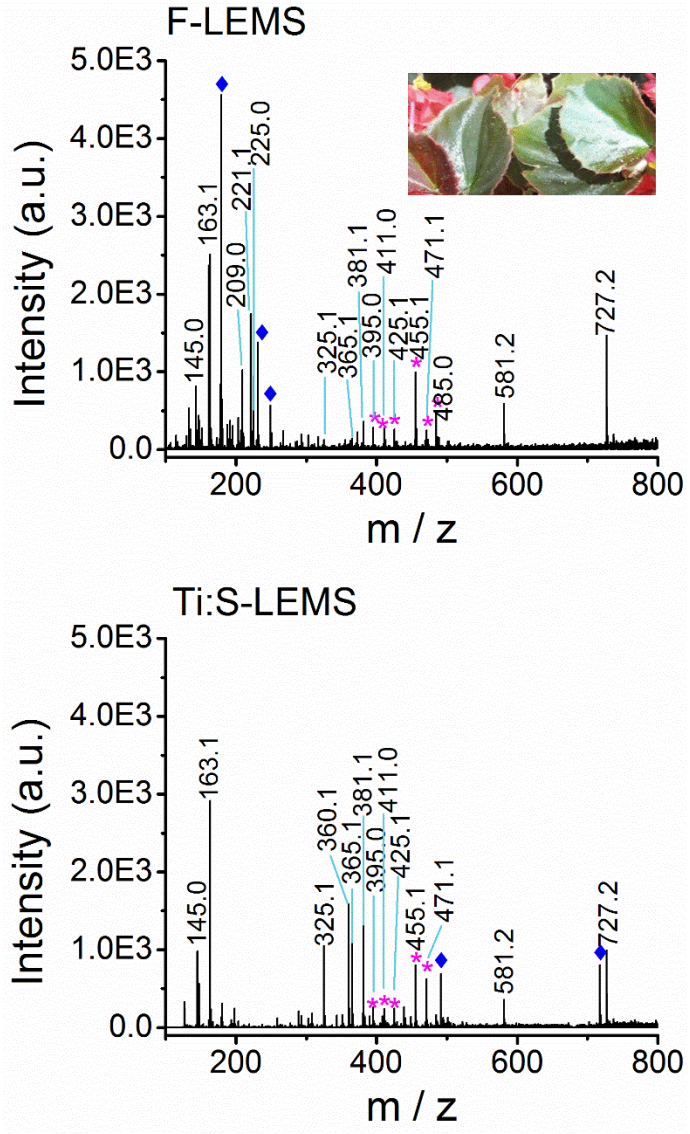

Figure 3.7. Blank-subtracted mass spectra for a flower leaf on a glass substrate using F-LEMS with 46.5 μJ pulse energy and Ti:S-LEMS with 505 μJ pulse energy. Inset displays the optical image of the flower leaf. Note that peaks labeled with ♦ and * are solvent and unidentified plant features, respectively.

Table 3.2. Tentative assignments of molecular features in the mass spectra collected from flower leaves by F-LEMS and Ti:S-LEMS.

Compounds[a]	Formula	Monoisotopic *m/z*[b]	Measured *m/z*	Leaf[c]		Mass Error (ppm)	Ref
				fiber	Ti:S		
glucose–$2H_2O$	$C_6H_8O_4$	145.0506(H)	145.0508	+	+	1.4	[25]
glucose–H_2O	$C_6H_{10}O_5$	163.0607(H)	163.0591	+	+	9.8	[25]
sucrose–H_2O	$C_{12}H_{20}O_{10}$	325.1135(H)	325.1109	+	+	8.0	[25]
sucrose	$C_{12}H_{22}O_{11}$	365.1054(Na)	365.1024	+	+	8.2	[26]
sucrose	$C_{12}H_{22}O_{11}$	381.0794(K)	381.0761	+	+	8.7	[26]
Cy-xylosyl-Glu	$C_{26}H_{29}O_{15}$	581.1501(+)	581.1477	+	+	4.1	[23]
Cy-xylosyl-Rut	$C_{32}H_{39}O_{19}$	727.2080(+)	727.2071	+	+	1.2	[23]

[a] Cy denotes cyanidin; Glu glucoside; Rut rutinoside. [b] Symbols in parentheses indicate protonated (H), sodiated (Na), potassiated (K) species or preformed cations (+). [c] + and – indicate presence or absence of the molecular feature in the mass spectra.

power study at higher energy range for F-LEMS. The mass spectra measured for a flower petal at different laser pulse energies using Ti:S-LEMS are shown in Figure 3.8. The intensity of representative peaks in the spectra of petal are plotted as a function of pulse energy and is displayed in Figure 3.9. Peaks including *m/z* 581.2 and 727.2 increased significantly when the pulse energy was increased from 75 μJ to 505 μJ, and the maximum signal was observed at 280 μJ per pulse. The intensity of procyanidin oligomers also increased at much higher pulse energies (i.e., 280 and 505 μJ). Note that the spectra of flower petals by F-LEMS revealed comparable signal intensities for different glycosylated and polymerized anthocyanidins in comparison with the high energy Ti:Sapphire laser measurements. The comparable signal indicates that a femtosecond fiber laser with lower energy and longer wavelength is viable for laser vaporization in the analysis of plant materials. The mass spectra measured for the flower leaf at different laser pulse energies using Ti:S-LEMS are shown in Figure 3.10 with the intensity of representative peaks in are plotted as a function of pulse energy Figure 3.11. The analysis of leaf samples using Ti:S-LEMS revealed higher ion yields at 505 and 1120 μJ whereas negligible anthocyanin and sugar molecular features were observed at 160 and 280 μJ. This suggests that sufficiently high laser pulse energy is required to detect signal from the plant sample, which is in agreement with previous Ti:S-LEMS and F-LEMS measurements of biological macromolecules [17]. The successful analysis of plant samples using fiber laser vaporization suggests that the low-energy laser vaporization is suitable for the direct analysis of complex biological systems.

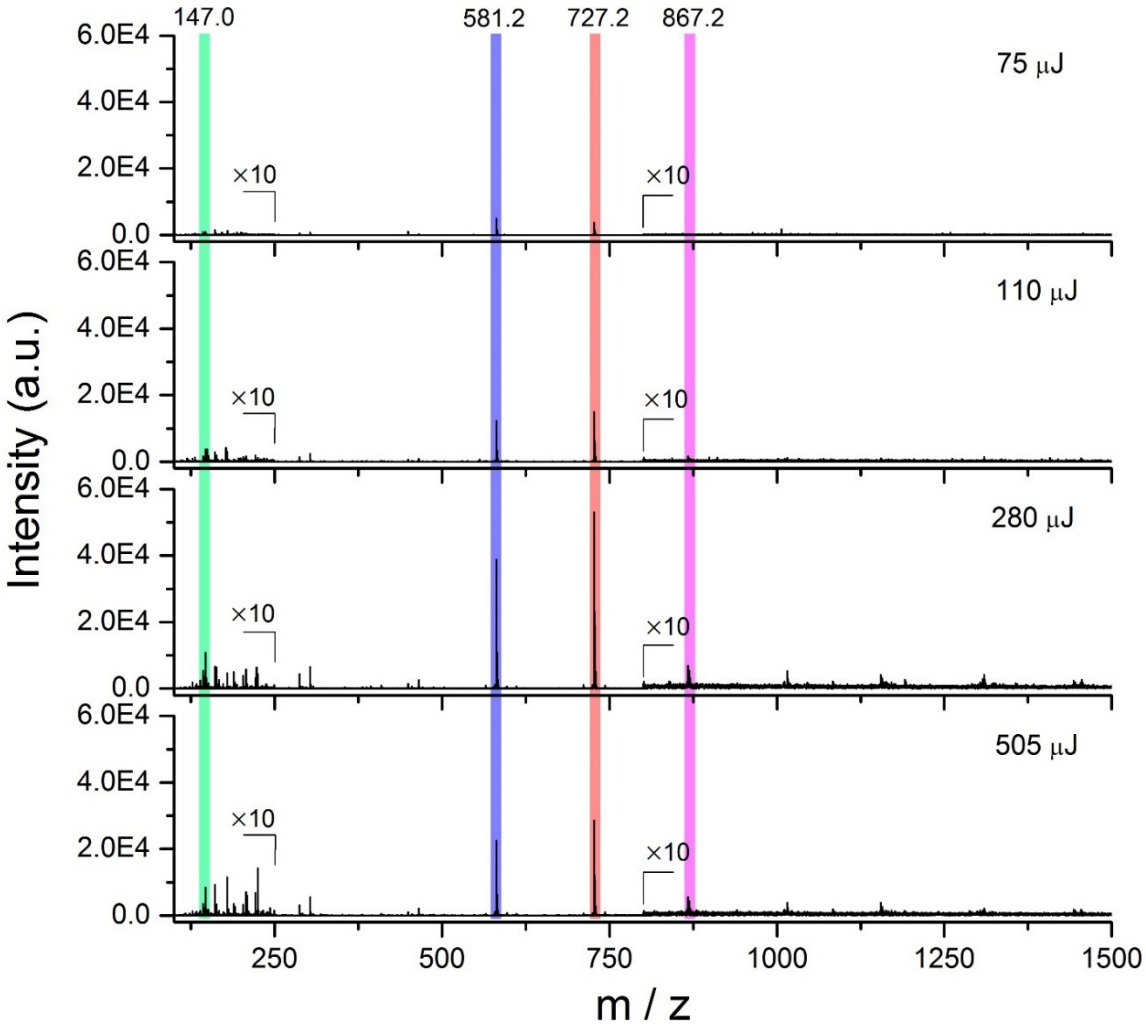

Figure 3.8. Blank-subtracted mass spectra for a flower petal affixed on a stainless steel substrate using Ti:S-LEMS with 75, 110, 280 and 505 μJ pulse energy, respectively.

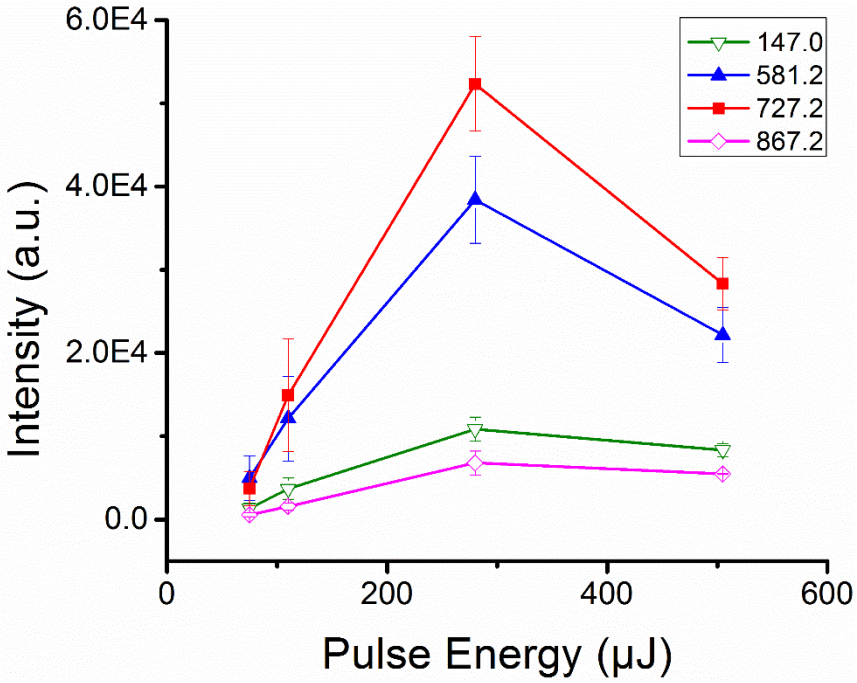

Figure 3.9. Intensity of representative ions (*m/z* 147.0, 581.2, 727.2, and 867.2) of the flower petal plotted as a function of pulse energy (75, 110, 280, and 500 μJ) using Ti:S-LEMS.

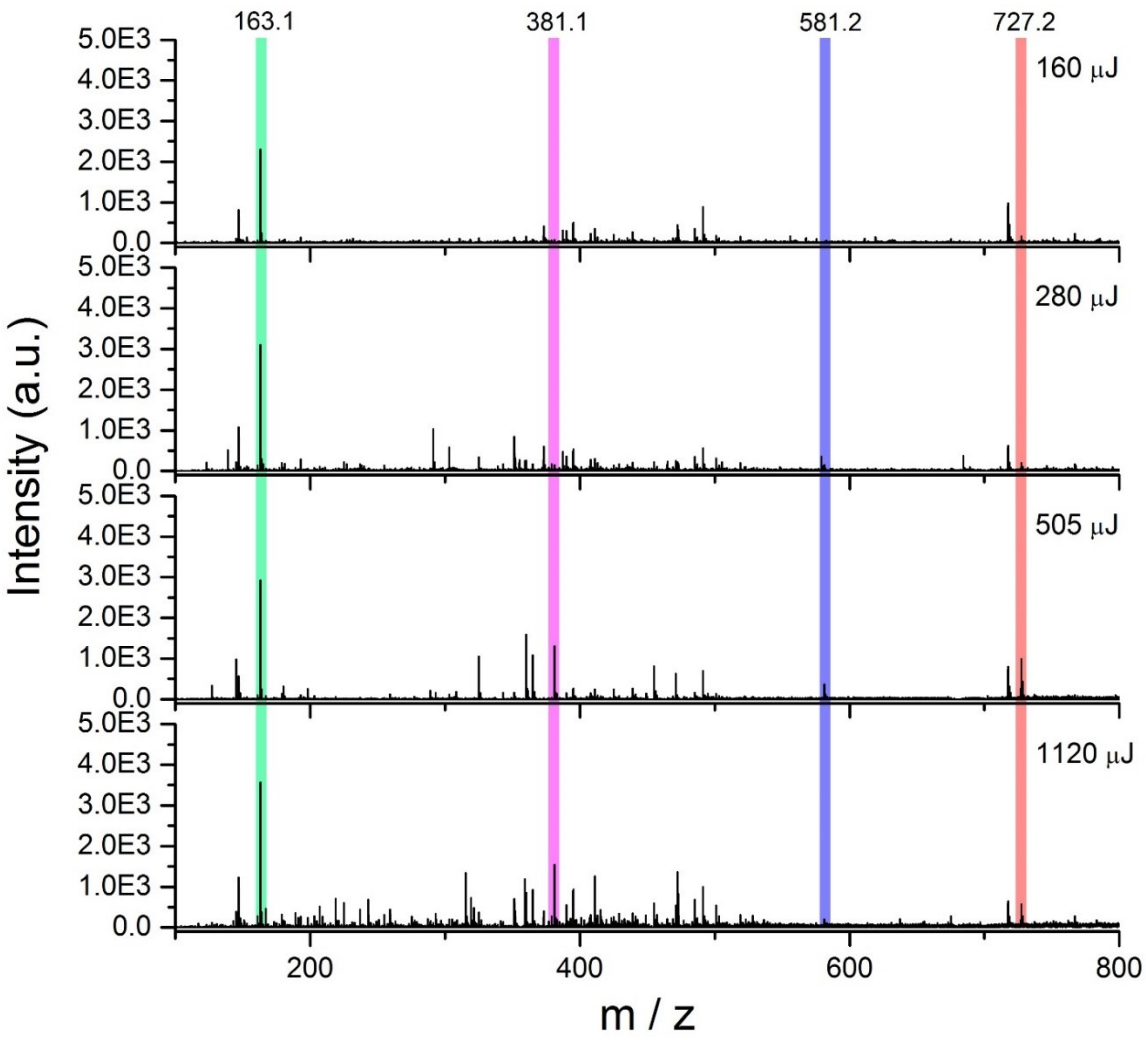

Figure 3.10. Blank-subtracted mass spectra for a flower leaf affixed on a glass substrate using Ti:S-LEMS with 160, 280, 505, and 1120 μJ pulse energy, respectively.

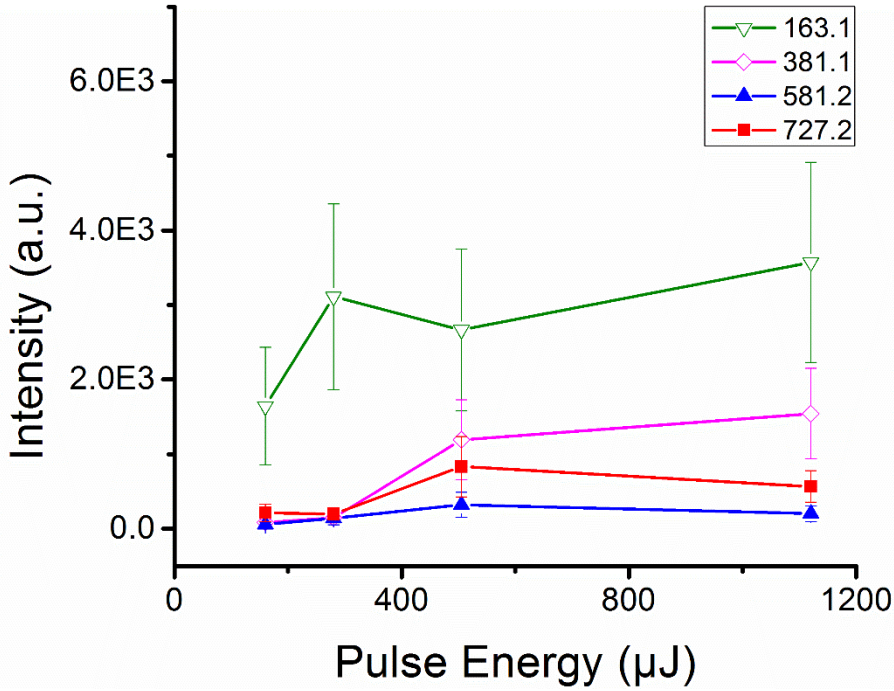

Figure 3.11. Intensity of representative ions (*m/z* 163.1, 381.1, 581.2, and 727.2) of the flower leaf plotted as a function of pulse energy (160, 280, 505, and 1120 μJ) using Ti:S-LEMS.

3.4.2 Identification of a Lipid Standard by F-LEMS and Ti:S-LEMS Coupled with High Resolution Accurate Mass Mass Spectrometer

Lipids play essential roles in cellular and tissue functions including structure, energy storage, and signaling. Studies have shown that many human diseases (e.g., cancer, diabetes, and neurodegenerative diseases) involve the disruption of lipid metabolism or signaling [43]. An ambient ionization MS technique with the capability of rapid, spatially-resolved analysis for lipid detection is therefore of interest. An investigation of analyzing a lipid standard PC(6:0/6:0) was carried out to test the efficiency of femtosecond laser vaporization and nanospray postionization to transfer the lipid samples from the condensed phase to the gas phase for mass analysis. Previous analysis of PC(6:0/6:0) by Ti:S-LEMS using a pulse energy of 2.5 mJ revealed the detection of parent $[M+H]^+$ and fragment $[M–N(CH_3)_3+Na]^+$ ions with the loss of trimethylamine end group [14]. The mass spectra of low-energy F-LEMS and Ti:S-LEMS are shown in Figure 3.12 with a peak at *m/z* 454.3 dominating the spectra, corresponding to protonated PC(6:0/6:0). Low abundance peaks at *m/z* 907.5 and 338.2, corresponding to a dimer ion $[2M+H]^+$ and a fragment ion $[M–C_6H_{12}O_2+H]^+$ with the loss of one of the fatty acid chain, were observed in Ti:S-LEMS and were negligible in F-LEMS spectra. Figure 3.13 shows the analysis of the lipid by Ti:S-LEMS with much higher pulse energies at 280 and 505 μJ. Elevated intensity of fragment ions of *m/z* 338.2, as well as *m/z* 356.2 and 440.2, corresponding to $[M–C_6H_{12}O_2+H_2O+H]^+$ and $[M–CH_2+H]^+$, respectively, were observed. The survival yields, defined as the ratio of the parent ion intensity to the sum of parent and fragment ion intensities, decreased from 0.93 to 0.80 with increasing pulse energy in Figure 3.14, presumably due to the more energetic excitation process under a higher intensity of a laser pulse. In addition, when the

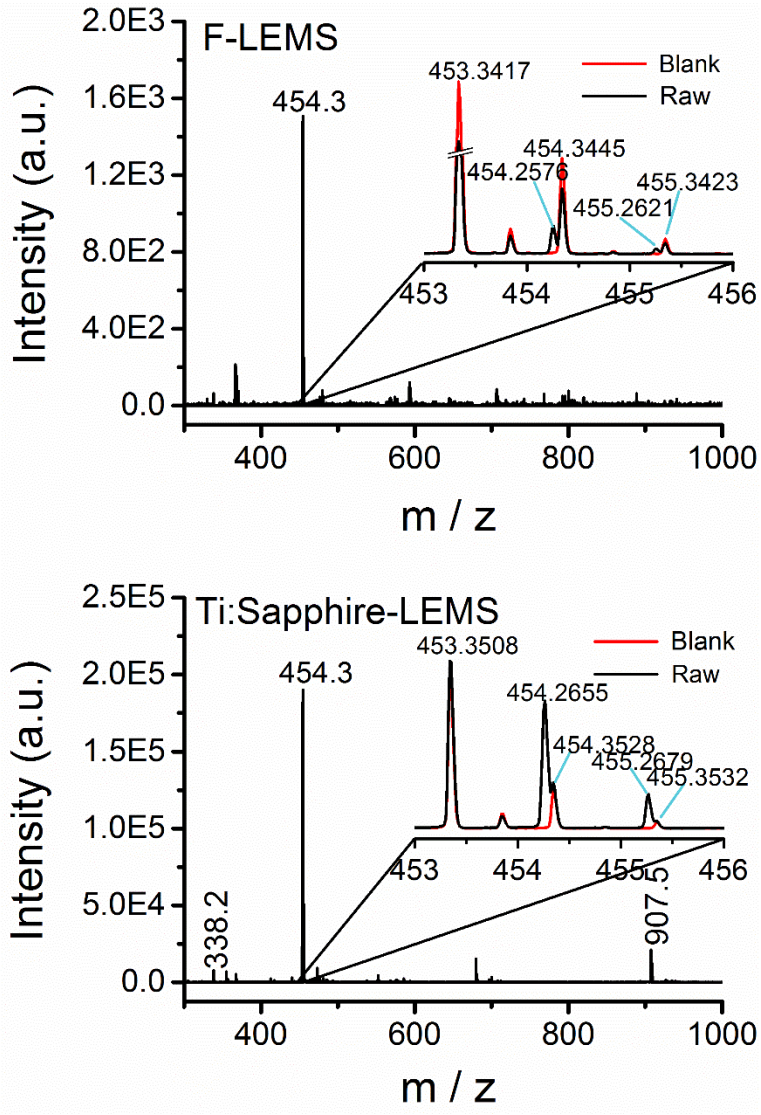

Figure 3.12. Blank-subtracted mass spectra for lipid standard PC(6:0/6:0) on a stainless steel substrate using F-LEMS with 46.5 µJ pulse energy and Ti:S-LEMS with 75 µJ pulse energy. The insets show the expanded view of the PC(6:0/6:0) molecular ion peaks in the raw and blank spectra.

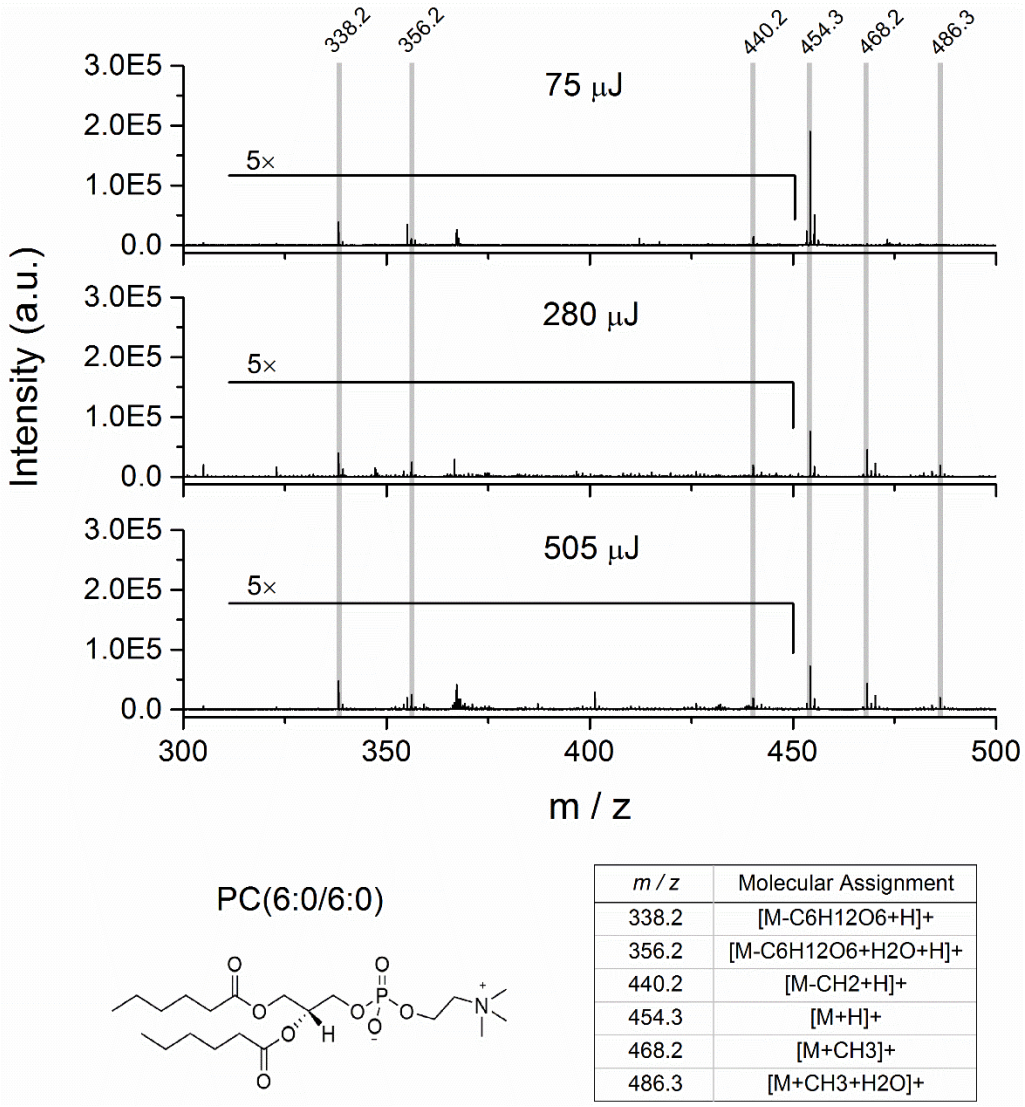

m / z	Molecular Assignment
338.2	[M-C6H12O6+H]+
356.2	[M-C6H12O6+H2O+H]+
440.2	[M-CH2+H]+
454.3	[M+H]+
468.2	[M+CH3]+
486.3	[M+CH3+H2O]+

Figure 3.13. Blank-subtracted mass spectra for lipid standard PC(6:0/6:0) on a stainless steel substrate using Ti:S-LEMS with 75, 280, and 505 μJ pulse energy, respectively. The range of the spectra at *m/z* 300−450 is magnified by 5. Tentative assignments for ion species detected in the spectra.

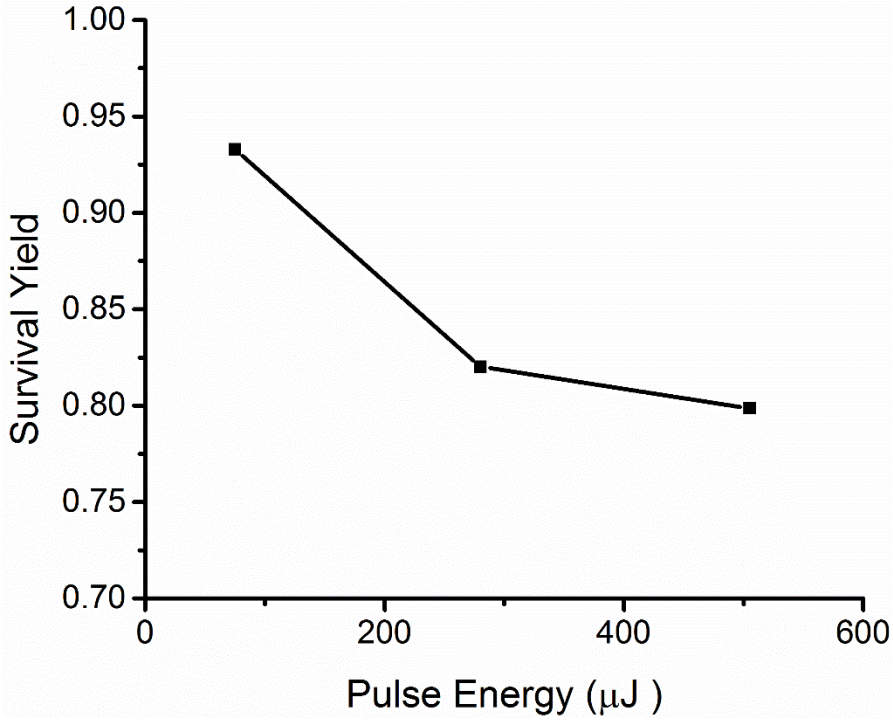

Figure 3.14. Calculated survival yields for PC(6:0/6:0) analyzed by Ti:S-LEMS as a function of pulse energy.

pulse energy was increased from 75 to 280 and 505 μJ, two species formed at *m/z* 468.2 and 486.3 via the intermolecular S_N2 transfer of a methyl group to a parent molecule to form $[M+CH_3]^+$ product and $[M+CH_3+H_2O]^+$ water adduct ions as observed previously when the lipid cluster ions formed by ESI were subjected to collision-induced dissociation [44]. These measurements suggest that lipids can be desorbed intact from the substrates using low-energy femtosecond laser pulses.

High spectral resolution and accuracy-based mass measurements play an important role in unambiguous identification of drugs, lipids, and metabolites species from tissue samples in mass spectrometry [45, 46]. Note that the high mass resolving power and accuracy of our QTOF analyzer enabled the identification of PC(6:0/6:0). The inset of Figure 3.12 demonstrates that the monoisotopic peak of PC(6:0/6:0) at *m/z* 454.2576 is resolved from one of the solvent-related blank features at *m/z* 454.3445 in the raw spectra, which would otherwise interfere with and/or obscure the lipid feature. The measured monoisotopic mass of PC(6:0/6:0) is also only 1.2 mDa difference from its theoretical value 454.2564. The lack of fragmentation for PC(6:0/6:0) using low-energy femtosecond laser pulses is an improvement to high energy Ti:Sapphire laser vaporization, which is beneficial for intact small molecule analysis by mass spectrometry.

3.4.3 Matrix-Free Analysis of a Mouse Brain Section by Ti:S-LEMS

Spatially-resolved ambient ionization MS analysis of animal tissue samples of histologic interest can directly provide chemical information to better understand the biological pathways and processes in the tissue. Molecular profiling of animal tissue samples with minimal sample preparation have been demonstrated by several ambient

ionization MS techniques, including DESI [47-49], nano-DESI [45, 50], IR-MALDESI [51, 52] and LAESI [30, 53]. To investigate the capability of LEMS for the analysis of animal samples, mouse brain was chosen in our analysis. A freshly sectioned mouse brain was analyzed by Ti:S-LEMS without the deposition of matrix, as seen in Figure 3.15. The mass spectrum revealed abundant ion features, especially at *m/z* 700−900. These features were identified as phospholipids, i.e., phosphatidylcholine (PC) and phosphatidylethanolamine (PE), and listed in Table 3.3. The peak detected at *m/z* 760.6 corresponds to PC(34:1) and has been observed previously for the analysis of mouse brain by MALDI [29, 31, 32], SIMS [27], and LAESI [30]. The low abundance features in the mass region *m/z* <700 are likely fragments of lipids or metabolites. For example, the peaks at *m/z* 551.5 and 577.5 have been suggested to arise from diacylglyceride molecules ($[M+H-H_2O]^+$) [54, 55] but could also be fragments of different classes of phospholipids with acyl chains of 32:0 and 34:1, respectively [56]. The ion at *m/z* 184.1 corresponds to either free phosphocholine molecules or phosphocholine fragments of PC lipids, which supports the detection of phosphatidylcholine species from the brain by LEMS. Further analysis by MS/MS or an ion mobility analyzer are required to confirm and elucidate the exact chemical structure of possible isobaric and/or isomeric ions because of the vast structural complexity and diversity of lipids [45, 53].

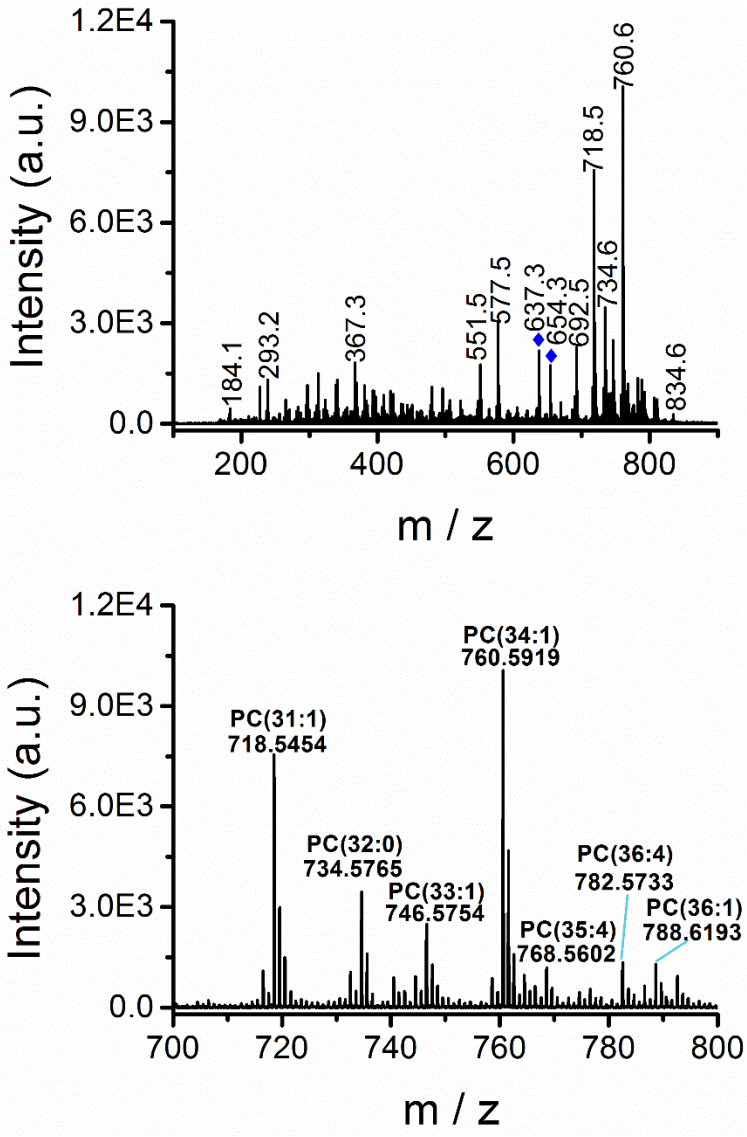

Figure 3.15. Blank-subtracted mass spectrum for a coronal section of mouse brain tissue using Ti:S-LEMS with 280 μJ pulse energy. The *m/z* 700−900 region revealing the presence of various phospholipids is shown in. Note that peaks labeled with ♦ are solvent features.

Table 3.3. Tentative assignments of molecular features in the mass spectra acquired from fresh cut coronal mouse brain section by Ti:S-LEMS.

Compounds[a]	Formula	Monoisotopic *m/z*[b]	Measured *m/z*	Mass Error (ppm)	Ref
Phosphocholine	$C_5H_{14}NO_4P$	184.0733(H)	184.0767	18.5	[27, 28]
PC(29:0)/PE(32:0)	$C_{37}H_{74}NO_8P$	692.5225(H)	692.5287	9.0	N/A
PC(31:1)	$C_{39}H_{76}NO_8P$	718.5381(H)	718.5454	10.2	[29]
PC(32:0)	$C_{40}H_{80}NO_8P$	734.5694(H)	734.5765	9.7	[27, 29-33]
PC(33:1)	$C_{41}H_{80}NO_8P$	746.5694(H)	746.5754	8.0	[30]
PC(34:2)	$C_{42}H_{80}NO_8P$	758.5694(H)	758.5746	6.9	[33]
PC(34:1)	$C_{42}H_{82}NO_8P$	760.5851(H)	760.5919	8.9	[27, 29-33]
PC(35:4)/PE(38:4)	$C_{43}H_{78}NO_8P$	768.5538(H)	768.5602	8.3	[30]
PC(36:4)	$C_{44}H_{80}NO_8P$	782.5694(H)	782.5733	5.0	[29, 30, 32, 33]
PC(36:2)	$C_{44}H_{86}NO_8P$	786.6007(H)	786.6000	0.9	[30, 33]
PC(36:1)	$C_{44}H_{86}NO_8P$	788.6164(H)	788.6193	3.7	[27, 29-33]
PC(37:6)/PE(40:6)	$C_{45}H_{78}NO_8P$	792.5538(H)	792.5617	10.0	[30]
PC(38:6)	$C_{46}H_{80}NO_8P$	806.5694(H)	806.5784	11.2	[29, 30, 32, 33]
PC(38:4)	$C_{46}H_{84}NO_8P$	810.6007(H)	810.6035	3.5	[29, 30, 32, 33]
PC(40:6)	$C_{48}H_{84}NO_8P$	834.6007(H)	834.6049	5.0	[30, 32, 33]

[a] (X:Y) represents the number of carbon atoms and double bonds in the fatty acid chains. PC denotes phosphatidylcholine; PE phosphatidylethanolamine. [b] Symbols in parentheses indicate protonated (H) species.

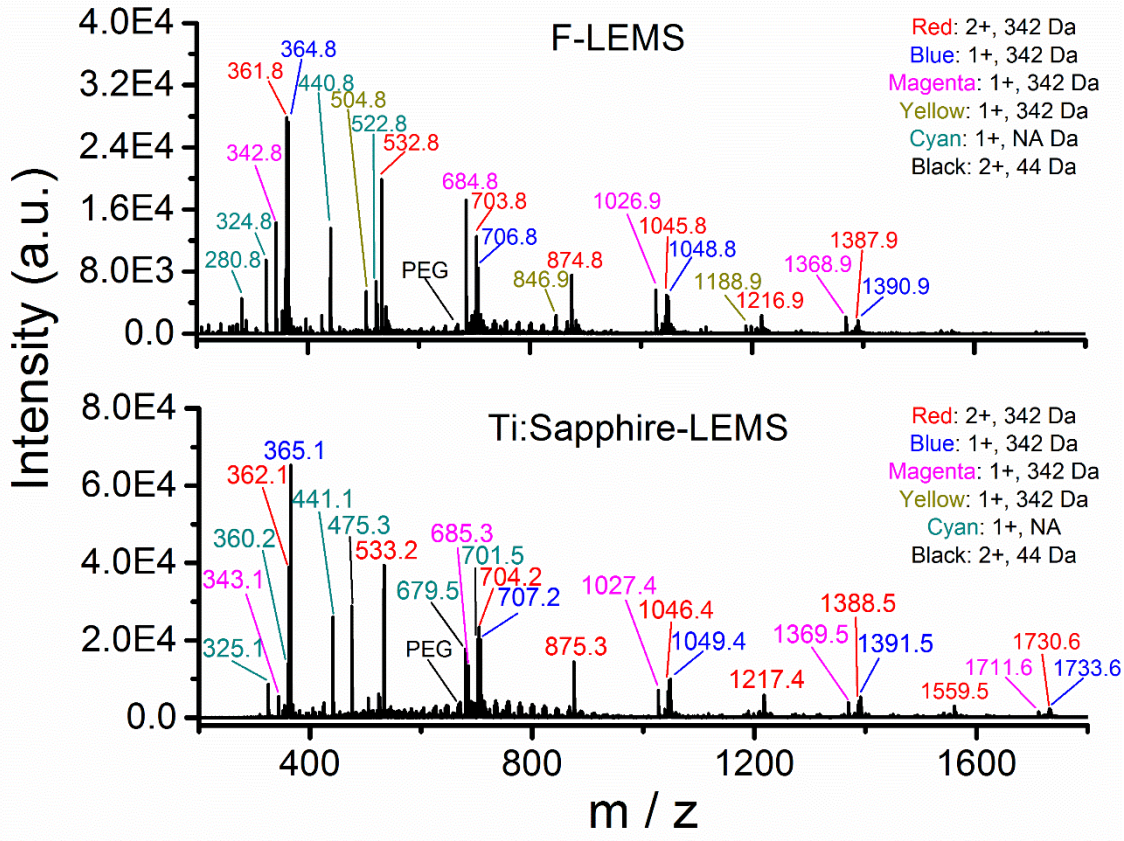

Figure 3.16. Blank-subtracted mass spectra for OCT-embedded mouse brain sections using F-LEMS with 46.5 μJ pulse energy and Ti:S-LEMS with 505 μJ pulse energy. Peaks are categorized into different groups according to their charge states and mass difference with respect to adjacent peaks in the same group.

Section preparation is an important step in the analysis of animal tissue by mass spectrometry to ensure that sample integrity is maintained while avoiding sample contamination [57]. OCT-embedded mouse brain sections were analyzed by F-LEMS and Ti:S-LEMS to investigate the effect of the commonly employed embedding compounds in the process of cryosectioning on LEMS mass analysis. Figure 3.16 shows the spectra acquired from OCT-embedded brain samples using F-LEMS and Ti:S-LEMS. The lipids observed from fresh sectioned brain sample shown in Figure 3.15 were suppressed by species that are more readily ionized from the OCT compounds, including polyethylene glycol (PEG) and a possible polysaccharide with repeat units of 44 and 342 Da, respectively. This suggests that sample preparation is important to avoid ion suppression in the LEMS analysis of animal tissue samples. The OCT compound embedding process should be avoided, rather flash freezing of the tissue block followed by cryosectioning to produce thin slices that are amenable to ambient ionization MS analysis [30, 51].

3.5 Conclusions

The use of a robust, turnkey femtosecond fiber laser to directly analyze tissue samples without the need for external matrix deposition is demonstrated. The results obtained with the low pulse energy (50 μJ) fiber laser source were comparable with analysis using a high energy Ti:Sapphire laser. The similarity of results with two different laser wavelengths suggests that femtosecond laser vaporization involves a nonresonant, multiphoton mechanism to enable universal analysis. Small metabolites, particularly anthocyanins, sugars and their derivatives, were desorbed from plant samples. Various phospholipids were detected from mouse brain samples using femtosecond laser pulses

from the Ti:Sapphire laser. The measurements are of interest for matrix-free mass analysis of tissue samples for the application of molecular imaging and tumor classification. The use of OCT compounds during tissue cryosectioning is detrimental for subsequent LEMS analysis.

The current study lays the groundwork for molecular imaging of plant and animal tissues using low-energy, femtosecond laser vaporization and electrospray postionization with minimal sample pretreatment. The femtosecond fiber laser has the advantage of being a turnkey, robust, and affordable laser that is amenable to non-specialist laboratories. With the rapid advances being make in fiber laser technology, the near-IR femtosecond laser desorption ambient ionization source may benefit from the development of femtosecond fiber lasers with milijoule pulse energy. MS/MS analysis such as collision induced dissociation may also be used in the future to validate the molecular assignments made by high spectral resolution and accuracy based mass measurements.

3.6 References

1. J.K. Nicholson, J.C. Lindon. Systems biology: Metabonomics. *Nature* **455**, 1054 (2008).

2. A. Svatoš. Mass spectrometric imaging of small molecules. *Trends Biotechnol.* **28**, 425 (2010).

3. M.J. Baker, J. Trevisan, P. Bassan, R. Bhargava, H.J. Butler, K.M. Dorling, P.R. Fielden, S.W. Fogarty, N.J. Fullwood, K.A. Heys, C. Hughes, P. Lasch, P.L. Martin-Hirsch, B. Obinaju, G.D. Sockalingum, J. Sulé-Suso, R.J. Strong, M.J. Walsh, B.R. Wood, P. Gardner, F.L. Martin. Using Fourier Transform IR spectroscopy to analyze biological materials. *Nat. Protoc.* **9**, 1771 (2014).

4. L. Opilik, T. Schmid, R. Zenobi. Modern Raman imaging: Vibrational spectroscopy on the micrometer and nanometer scales. *Annu. Rev. Anal. Chem.* **6**, 379 (2013).

5. M.E. Monge, G.A. Harris, P. Dwivedi, F.M. Fernández. Mass spectrometry: Recent advances in direct open air surface sampling/ionization. *Chem. Rev.* **113**, 2269 (2013).

6. P.-K. So, B. Hu, Z.-P. Yao. Mass spectrometry: Towards in vivo analysis of biological systems. *Mol. BioSyst.* **9**, 915 (2013).

7. P.M. Flanigan, R.J. Levis. Ambient femtosecond laser vaporization and nanosecond laser desorption electrospray ionization mass spectrometry. *Annu. Rev. Anal. Chem.* **7**, 229 (2014).

8. J. Shiea, M.-Z. Huang, H.-J. Hsu, C.-Y. Lee, C.-H. Yuan, I. Beech, J. Sunner. Electrospray-assisted laser desorption/ionization mass spectrometry for direct ambient analysis of solids. *Rapid Commun. Mass Spectrom.* **19**, 3701 (2005).

9. P. Nemes, A. Vertes. Laser ablation electrospray ionization for atmospheric pressure, in vivo, and imaging mass spectrometry. *Anal. Chem.* **79**, 8098 (2007).

10. J.S. Sampson, K.K. Murray, D.C. Muddiman. Intact and top-down characterization of biomolecules and direct analysis using infrared matrix-assisted laser desorption electrospray ionization coupled to FT-ICR mass spectrometry. *J. Am. Soc. Mass Spectrom.* **20**, 667 (2009).

11. J.J. Brady, E.J. Judge, R.J. Levis. Mass spectrometry of intact neutral macromolecules using intense non-resonant femtosecond laser vaporization with electrospray post-ionization. *Rapid Commun. Mass Spectrom.* **23**, 3151 (2009).

12. E.J. Judge, J.J. Brady, D. Dalton, R.J. Levis. Analysis of pharmaceutical compounds from glass, fabric, steel, and wood surfaces at atmospheric pressure using spatially resolved, nonresonant femtosecond laser vaporization electrospray mass spectrometry. *Anal. Chem.* **82**, 3231 (2010).

13. E.J. Judge, J.J. Brady, R.J. Levis. Mass analysis of biological macromolecules at atmospheric pressure using nonresonant femtosecond laser vaporization and electrospray ionization. *Anal. Chem.* **82**, 10203 (2010).

14. J.J. Brady, E.J. Judge, R.J. Levis. Analysis of amphiphilic lipids and hydrophobic proteins using nonresonant femtosecond laser vaporization with electrospray post-Ionization. *J. Am. Soc. Mass Spectrom.* **22**, 762 (2011).

15. P.M. Flanigan, L.L. Radell, J.J. Brady, R.J. Levis. Differentiation of eight phenotypes and discovery of potential biomarkers for a single plant organ class using laser electrospray mass spectrometry and multivariate statistical analysis. *Anal. Chem.* **84**, 6225 (2012).

16. E.J. Judge, J.J. Brady, P.E. Barbano, R.J. Levis. Nonresonant femtosecond laser vaporization with electrospray postionization for ex vivo plant tissue typing using compressive linear classification. *Anal. Chem.* **83**, 2145 (2011).

17. F. Shi, P.M. Flanigan, J.J. Archer, R.J. Levis. Direct analysis of intact biological macromolecules by low-energy, fiber-based femtosecond laser vaporization at 1042 nm wavelength with nanospray postionization mass spectrometry. *Anal. Chem.* **87**, 3187 (2015).

18. P.M. Flanigan, F. Shi, J.J. Archer, R.J. Levis. Internal energy deposition for low energy, femtosecond laser vaporization and nanospray post-ionization mass spectrometry using thermometer ions. *J. Am. Soc. Mass Spectrom.* **26**, 716 (2015).

19. C.A. Smith, G. O'Maille, E.J. Want, C. Qin, S.A. Trauger, T.R. Brandon, D.E. Custodio, R. Abagyan, G. Siuzdak. METLIN - A metabolite mass spectral database. *Ther. Drug Monit.* **27**, 747 (2005).

20. D. Cotter, A. Maer, C. Guda, B. Saunders, S. Subramaniam. LMPD: LIPID MAPS proteome database. *Nucleic Acids Res.* **34**, D507 (2006).

21. M. Biesaga, K. Pyrzynska. Liquid chromatography/tandem mass spectrometry studies of the phenolic compounds in honey. *J. Chromatogr. A* **1216**, 6620 (2009).

22. P. Nemes, A.A. Barton, Y. Li, A. Vertes. Ambient molecular imaging and depth profiling of live tissue by infrared laser ablation electrospray ionization mass spectrometry. *Anal. Chem.* **80**, 4575 (2008).

23. M.M. Giusti, L.E. Rodríguez-Saona, D. Griffin, R.E. Wrolstad. Electrospray and tandem mass spectroscopy as tools for anthocyanin characterization. *J. Agric. Food Chem.* **47**, 4657 (1999).

24. M. Ohnishi-Kameyama, A. Yanagida, T. Kanda, T. Nagata. Identification of catechin oligomers from apple (Malus pumila cv. Fuji) in matrix-assisted laser desorption/ionization time-of-flight mass spectrometry and fast-atom bombardment mass spectrometry. *Rapid Commun. Mass Spectrom.* **11**, 31 (1997).

25. Y. Coello, A.D. Jones, T.C. Gunaratne, M. Dantus. Atmospheric pressure femtosecond laser imaging mass spectrometry. *Anal. Chem.* **82**, 2753 (2010).

26. G.-Z. Xin, B. Hu, Z.-Q. Shi, Y.C. Lam, T.T.-X. Dong, P. Li, Z.-P. Yao, K.W.K. Tsim. Rapid identification of plant materials by wooden-tip electrospray ionization mass spectrometry and a strategy to differentiate the bulbs of Fritillaria. *Anal. Chim. Acta* **820**, 84 (2014).

27. M.K. Passarelli, N. Winograd. Lipid imaging with time-of-flight secondary ion mass spectrometry (ToF-SIMS). *Biochim. Biophys. Acta, Mol Cell Biol. Lipids* **1811**, 976 (2011).

28. B. Shrestha, P. Nemes, J. Nazarian, Y. Hathout, E.P. Hoffman, A. Vertes. Direct analysis of lipids and small metabolites in mouse brain tissue by AP IR-MALDI and reactive LAESI mass spectrometry. *Analyst* **135**, 751 (2010).

29. C. Meriaux, J. Franck, M. Wisztorski, M. Salzet, I. Fournier. Liquid ionic matrixes for MALDI mass spectrometry imaging of lipids. *J. Proteomics* **73**, 1204 (2010).

30. P. Nemes, A.S. Woods, A. Vertes. Simultaneous imaging of small metabolites and lipids in rat brain tissues at atmospheric pressure by laser ablation electrospray ionization mass spectrometry. *Anal. Chem.* **82**, 982 (2010).

31. A. Matusch, L.S. Fenn, C. Depboylu, M. Klietz, S. Strohmer, J.A. McLean, J.S. Becker. Combined elemental and biomolecular mass spectrometry imaging for probing the inventory of tissue at a micrometer scale. *Anal. Chem.* **84**, 3170 (2012).

32. A. Thomas, J.L. Charbonneau, E. Fournaise, P. Chaurand. Sublimation of new matrix candidates for high spatial resolution imaging mass spectrometry of lipids: enhanced information in both positive and negative polarities after 1,5-diaminonapthalene deposition. *Anal. Chem.* **84**, 2048 (2012).

33. A.M. Delvolve, B. Colsch, A.S. Woods. Highlighting anatomical sub-structures in rat brain tissue using lipid imaging. *Anal. Methods* **3**, 1729 (2011).

34. A. Castañeda-Ovando, M.d.L. Pacheco-Hernández, M.E. Páez-Hernández, J.A. Rodríguez, C.A. Galán-Vidal. Chemical studies of anthocyanins: A review. *Food Chem.* **113**, 859 (2009).

35. A. Berisha, S. Dold, S. Guenther, N. Desbenoit, Z. Takats, B. Spengler, A. Römpp. A comprehensive high-resolution mass spectrometry approach for characterization of metabolites by combination of ambient ionization, chromatography and imaging methods. *Rapid Commun. Mass Spectrom.* **28**, 1779 (2014).

36. Y. Li, B. Shrestha, A. Vertes. Atmospheric pressure infrared MALDI imaging mass spectrometry for plant metabolomics. *Anal. Chem.* **80**, 407 (2008).

37. B. Li, S.H. Hansen, C. Janfelt. Direct imaging of plant metabolites in leaves and petals by desorption electrospray ionization mass spectrometry. *Int. J. Mass Spectrom.* **348**, 15 (2013).

38. L. Abrankó, B. Szilvássy. Mass spectrometric profiling of flavonoid glycoconjugates possessing isomeric aglycones. *J. Mass Spectrom.* **50**, 71 (2015).

39. D. Hölscher, R. Shroff, K. Knop, M. Gottschaldt, A. Crecelius, B. Schneider, D.G. Heckel, U.S. Schubert, A. Svatoš. Matrix-free UV-laser desorption/ionization (LDI) mass spectrometric imaging at the single-cell level: distribution of secondary metabolites of Arabidopsis thaliana and Hypericum species. *Plant J.* **60**, 907 (2009).

40. B. Shrestha, A. Vertes. In situ metabolic profiling of single cells by laser ablation electrospray ionization mass spectrometry. *Anal. Chem.* **81**, 8265 (2009).

41. B. Li, N. Bjarnholt, S.H. Hansen, C. Janfelt. Characterization of barley leaf tissue using direct and indirect desorption electrospray ionization imaging mass spectrometry. *J. Mass Spectrom.* **46**, 1241 (2011).

42. T. Müller, S. Oradu, D.R. Ifa, R.G. Cooks, B. Kräutler. Direct plant tissue analysis and imprint imaging by desorption electrospray ionization mass spectrometry. *Anal. Chem.* **83**, 5754 (2011).

43. D. Gode, D.A. Volmer. Lipid imaging by mass spectrometry - A review. *Analyst* **138**, 1289 (2013).

44. P.F. James, M.A. Perugini, R.A.J. O'Hair. Sources of artefacts in the electrospray ionization mass spectra of saturated diacylglycerophosphocholines: From condensed phase hydrolysis reactions through to gas phase intercluster reactions. *J. Am. Soc. Mass Spectrom.* **17**, 384 (2006).

45. I. Lanekoff, K. Burnum-Johnson, M. Thomas, J. Short, J.P. Carson, J. Cha, S.K. Dey, P. Yang, M.C. Prieto Conaway, J. Laskin. High-speed tandem mass spectrometric in situ imaging by nanospray desorption electrospray ionization mass spectrometry. *Anal. Chem.* **85**, 9596 (2013).

46. N. Pan, W. Rao, N.R. Kothapalli, R. Liu, A.W.G. Burgett, Z. Yang. The Single-probe: A miniaturized multifunctional device for single cell mass spectrometry analysis. *Anal. Chem.* **86**, 9376 (2014).

47. L.S. Eberlin, X. Liu, C.R. Ferreira, S. Santagata, N.Y.R. Agar, R.G. Cooks. Desorption electrospray ionization then MALDI mass spectrometry imaging of lipid and protein distributions in single tissue sections. *Anal. Chem.* **83**, 8366 (2011).

48. D. Campbell, C. Ferreira, L. Eberlin, R.G. Cooks. Improved spatial resolution in the imaging of biological tissue using desorption electrospray ionization. *Anal. Bioanal. Chem.* **404**, 389 (2012).

49. L.S. Eberlin, M. Gabay, A.C. Fan, A.M. Gouw, R.J. Tibshirani, D.W. Felsher, R.N. Zare. Alteration of the lipid profile in lymphomas induced by MYC overexpression. *Proc. Natl. Acad. Sci. U.S.A.* **111**, 10450 (2014).

50. J. Laskin, B.S. Heath, P.J. Roach, L. Cazares, O.J. Semmes. Tissue imaging using nanospray desorption electrospray ionization mass spectrometry. *Anal. Chem.* **84**, 141 (2012).

51. G. Robichaud, J.A. Barry, K.P. Garrard, D.C. Muddiman. Infrared matrix-assisted laser desorption electrospray ionization (IR-MALDESI) imaging source coupled to a FT-ICR mass spectrometer. *J. Am. Soc. Mass Spectrom.* **24**, 92 (2013).

52. J.A. Barry, M.R. Groseclose, G. Robichaud, S. Castellino, D.C. Muddiman. Assessing drug and metabolite detection in liver tissue by UV-MALDI and IR-MALDESI mass spectrometry imaging coupled to FT-ICR MS. *Int. J. Mass Spectrom.* **377**, 448 (2015).

53. B. Shrestha, A. Vertes. High-throughput cell and tissue analysis with enhanced molecular coverage by laser ablation electrospray ionization mass spectrometry using ion mobility separation. *Anal. Chem.* **86**, 4308 (2014).

54. A.F.M. Altelaar, I. Klinkert, K. Jalink, R.P.J. de Lange, R.A.H. Adan, R.M.A. Heeren, S.R. Piersma. Gold-enhanced biomolecular surface imaging of cells and tissue by SIMS and MALDI mass spectrometry. *Anal. Chem.* **78**, 734 (2005).

55. Y.K. Magnusson, P. Friberg, P. Sjövall, J. Malm, Y. Chen. TOF-SIMS analysis of lipid accumulation in the skeletal muscle of ob/ob mice. *Obesity* **16**, 2745 (2008).

56. M. Pulfer, R.C. Murphy. Electrospray mass spectrometry of phospholipids. *Mass Spectrom. Rev.* **22**, 332 (2003).

57. S.A. Schwartz, M.L. Reyzer, R.M. Caprioli. Direct tissue analysis using matrix-assisted laser desorption/ionization mass spectrometry: Practical aspects of sample preparation. *J. Mass Spectrom.* **38**, 699 (2003).

CHAPTER 4

LASER ELECTROSPRAY MASS SPECTROMETRY IMAGING FOR DYE AND PLANT TISSUE IMAGING

4.1 Overview

This chapter describes an ambient mass spectrometry imaging source that enables measurement of the compositional heterogeneity in a plant sample with both high spatial and mass resolution. The source is based on nonresonant, femtosecond laser electrospray mass spectrometry (LEMS) coupled to a quadrupole time-of-flight (QTOF) mass analyzer. No matrix deposition and minimal sample preparation is necessary for the source. The laser, translation stage, and mass spectrometer are synchronized and controlled using a LabView user interface. Single laser shot is applied to each pixel during the imaging. A scanning rate of 2.0 second per pixel is achieved. Measurement of a patterned ink film indicates the potential of LEMS with a lateral resolution of ~60 μm. Metabolites including sugar, anthocyanins and other small metabolites were successfully mapped from plant samples without oversampling using a spot size of 60 × 70 μm^2. Molecular identification of the detected analytes from the tissue was enabled by accurate mass measurement in conjunction with tandem mass spectrometry. Statistical analysis, nonnegative matrix factorization and principal component analysis, were applied to the imaging data to extract regions with distinct and/or correlated spectral profiles.

4.2 Introduction

Mass spectrometry imaging (MSI) can interrogate a sample in a label-free manner and provide a chemical map in two or three dimensions with excellent molecular specificity [1]. The goal of mapping the chemical composition present in biological samples has been the driving force for the rapid development of MSI in the last few decades [2, 3]. The power of MSI has been demonstrated in many biological applications, such as imaging drugs, lipids, proteins and metabolites in tissues [4, 5], mapping chemical residues in latent fingerprints [6], and discovering clinical biomarker for tumor detection [7]. Ambient ionization sources with imaging capabilities have seen rapid deployment in biological and clinical imaging applications [8]. Among numerous ambient ionization sources to date, laser vaporization has been widely adopted as one of the many desorption methods due to its spatially well-defined energy deposition ability. An additional postionization step (e.g., electrospray ionization (ESI)) may be coupled to the laser desorption source in many laser-based ambient mass spectrometry techniques [9]. The combination of laser desorption with electrospray postionization offers several benefits, including atmospheric pressure analysis, improved analytes sensitivity, enhanced quantitative analysis, and spatially resolved analysis [10].

Ambient laser desorption in conjunction with electrospray postionization was first demonstrated by electrospray-assisted laser desorption/ionization (ELDI) in 2005 [11]. ELDI employs a laser beam at 337 nm wavelength from a nanosecond UV laser to ablate samples and the method has been applied to image slices from two types of fungus, *Ganoderma lucidum* and *Antrodia camphorate,* with a spot size of approximately 100 × 150 μm^2 [12]. Additional examples of laser-electrospray hybrid techniques with imaging

capabilities include matrix-assisted laser desorption electrospray ionization (MALDESI) [13, 14], laser ablation electrospray ionization (LAESI) [15, 16], as well as laser electrospray mass spectrometry (LEMS) [17, 18]. The main difference among these techniques is the laser parameters, in particular pulse duration and wavelength [10, 19]. LAESI and infrared laser MALDESI (IR-MALDESI) use a nanosecond IR laser at 2.94 μm to resonantly excite inherent water in the biological sample to induce desorption, and have been extensively employed to image plant and animal tissue samples recently. Metabolites from plant samples [16, 20, 21] as well as endogenous lipids and small metabolites from a rat brain [21, 22] were imaged by LAESI with a lateral resolution of ~200 μm., though ablation spots of 30 μm size have been demonstrated for single cell analysis (but not imaging) by delivering the mid-IR laser pulses with an etched optical fiber [23, 24]. The distribution of drugs, lipids, and metabolites were also mapped from sections of animal tissue at lateral resolution of 150 to 200 μm in IR-MALDESI [14, 25], and a lateral resolution of 45 μm was reported using oversampling methods where the sampling step size is smaller than the laser spot size [14, 26]. Unlike nanosecond laser pulses where a resonance must occur in a specific matrix, nonresonant, multiphoton laser vaporization occurs in LEMS without the aid of a matrix.

Achieving high resolution analysis in the spatial and spectral domains has been a major focus for mass spectrometry imaging sources including laser-electrospray hybrid ambient ionization methods. Mass spectral imaging using LEMS was previously demonstrated by mapping oxycodone deposited on a metal plate with a lateral resolution of 250 μm on a custom, low resolution orthogonal TOF mass analyzer [18]. Recently, successful analysis was achieved with a laser spot size of ~75 μm [27] and endogenous

metabolites and lipids were directly detected from plant and animal tissue samples in LEMS [28]. However, the ability of LEMS for mass spectrometry imaging of biological samples at <100 μm lateral resolution has not been fully investigated and the capability of performing MS/MS analysis for molecular identification has not been demonstrated by LEMS. Here we explore the application of LEMS imaging for plant tissue samples with a high performance mass spectrometer and a high resolution translation stage. The details of the imaging source including instrument design, software development, and data analysis are presented. Spatially-resolved measurements of patterned ink on a metallic substrate are presented. Mass spectral imaging of a leaf at a lateral resolution of <100 μm is presented. Finally, statistical analysis, nonnegative matrix factorization and principal component analysis, is performed as a means of spectral and spatial features extraction from the large imaging dataset.

4.3 Material and Methods

4.3.1 Sample Preparation

A Rhodamine 6G dye pattern was prepared on a stainless steel plate by a red permanent marker (Sharpie, Downers Grove, IL, USA) for LEMS imaging. The pattern was created by removal of the dye using femtosecond laser ablation (45 fs, 500 μJ) from a Ti:Sapphire laser amplifier (Coherent Inc., Santa Clara, CA, USA) coupled with a two dimensional translation stage (MLS203-1, Thorlabs, Newton, NJ, USA) on a laser ablation platform. The platform controlled by a custom LabVIEW (LabVIEW 2012, National Instruments, Austin, TX, USA) program has the option to set the laser frequency, ablation

range, and a user defined ablation pattern. A single fs laser pulse with a spot size of 50 μm in diameter was used at each ablation site for the ink pattern.

Fresh pink and red *New Guinea Impatiens* flower petal and leaf samples were collected from plants on the Temple University campus. The flower petals and leaves were detached from the flower samples and affixed to the stainless steel sample slides using double-sided tape prior to analysis. The plant samples were then directly placed on the sample stage of the ion source without any other treatment.

4.3.2 LEMS Imaging Source

The imaging source, shown in Figure 4.1, consists of a Ti:Sapphire regenerative amplifier laser (Coherent Inc., Santa Clara, CA, USA), an electrospray emitter coupled to a quadrupole time of flight (QTOF) mass spectrometer (micrOTOF-Q II, Bruker Daltonik GmbH, Bremen, Germany), and a XY translation stage (MLS203-1, Thorlabs, Newton, NJ, USA). The source is computer-controlled by a user interface developed with LabVIEW, which allows user to monitor sampling area, set laser and stage parameters, save stage position information, and initialize/stop imaging acquisition. The QTOF mass analyzer is controlled by the manufacturer's software (micrOTOF controller 3.0, Bruker Daltonik GmbH, Bremen, Germany) and synchronized with the LabVIEW program to enable data storage during imaging acquisition. The source can be operated in either continuous raster mode to acquire a line profile of the sample or in stepped mode to enable step-by-step molecular imaging.

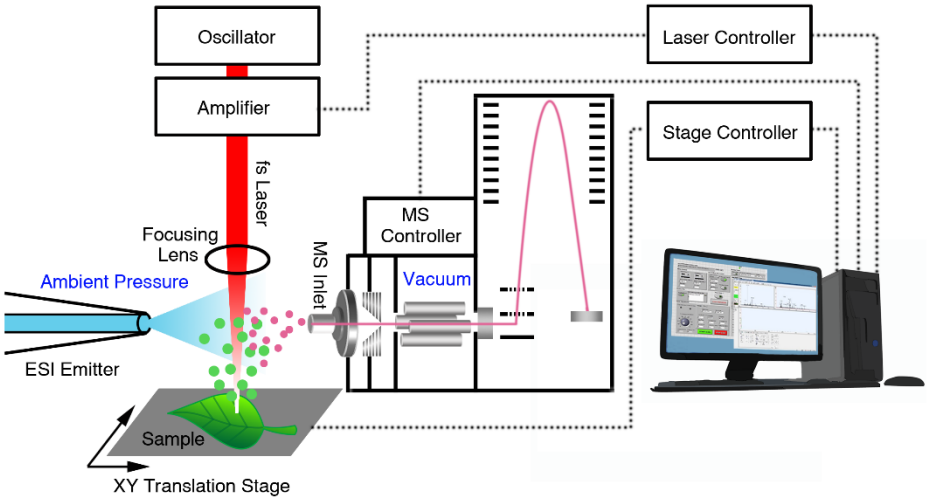

Figure 4.1. Schematic of the femtosecond laser vaporization and electrospray postionization mass spectrometry imaging system. Femtosecond laser pulses from a Ti:Sapphire oscillator were regenatively amplified and focused on the sample by a lens. The sample was placed on an XY translation stage under ambient conditions and raster-scanned step by step during imaging analysis. The laser vaporized analytes were captured and ionized by an ESI source and transferred into a QTOF mass analyzer. The synchronization of translation stage, laser, and mass spectrometer was computer-controlled by a customized user interface.

4.3.2.1 Laser Vaporization

A Ti:Sapphire oscillator (KMLabs Inc., Boulder, CO, USA) seeded the regenerative amplifier to create 60 fs pulses centered at 800 nm. The laser pulse was focused to a spot size of 50 μm in diameter using a 10 cm focal length lens (Thorlabs, Newton, NJ, USA) with an incident angle of 45º with respect to the sample surface. The energy of the pulse was attenuated using a quarter-wave plate and a polarizing beam splitter cube (CVI Laser Optics, Albuquerque, NM, USA) to ~1 mJ for the majority of the imaging experiments, resulting in an intensity of $>10^{14}$ W/cm^2 at the area sampled. For line profiling analysis, the laser was operated at 10 Hz when the sample mounted on the translation stage was continuously raster scanned at 1 mm/s. For imaging analysis, the laser was triggered with the choice of single or multi laser shots at each position when the sample was moved step by step.

4.3.2.2 Electrospray Ionization and Mass Spectrometry

After a laser pulse, the vaporized sample material is captured, ionized, and transferred into the QTOF mass analyzer by the electrospray stream. An acidified solvent, 1:1 (v:v) methanol/water with 1% acetic acid (Fisher Scientific, Fair Lawn, NJ, USA), was continuously pumped through the ESI emitter by a syringe pump (Harvard Apparatus, Holliston, MA, USA) at a flow rate of 3 μL/min. The ESI ion source was operated in positive ion mode employing drying gas at 100 ºC. The ion optics settings of the spectrometer were optimized for best performance and were kept constant during the experiments. The spectrometer was calibrated by an ESI standard sample (Sigma-Aldrich, Buchs, Switzerland) for *m/z* 50–1000. Some of the metabolites were identified by

subjecting parent ions (±0.5 *m/z*) to collision-induced dissociation in nitrogen gas with the collision energy set between 15–30 eV in continuous raster mode. An ESI solvent mass spectrum was acquired before each laser vaporization event to allow background subtraction of solvent-related peaks.

4.3.3 Imaging Operation

Through the LabVIEW user interface, a VGA camera (XVP610, IBM Inc., Armonk, NY, USA) mounted above the ion source can be used to monitor the sample target and select the region of interest. The scanning parameters, such as step size, scanning direction, scanning range, laser frequency, number of shots per pixel, MS scan/ablation delay, and ablation/next MS scan delay are selected for an imaging experiment. A flow chart of the imaging system is shown in Figure 4.2. The LabVIEW program synchronizes the stage movement, laser triggering and mass spectrometer scan to enable step-by-step sampling and simultaneous data storage. The controllers of translation stage and laser are communicated and triggered by LabVIEW using serial communication ports during imaging. The LabVIEW program makes calls to the Windows application programming interface (API) for managing and controlling the mass spectrometer software window to enable data storage. This API scheme bypasses the requirement of component object model (COM) library for the mass spectrometer, which is usually not supplied by the manufacturer, and provides a universal solution to controlling any commercially available mass spectrometer by LabVIEW. A timing diagram of the imaging system is shown in Figure 4.3. In the imaging mode, time-resolved mass spectra were acquired for ~1.4 s at a spectra rate of 10 Hz and recorded as a function of sampling position. The dwell time of

each pixel was ~2.0 s in total, which was primarily limited by the time required to fully sample the vaporized analytes to prevent carry-over between consecutive sampling pixels. As seen in the chromatogram plot of Figure 4.4, the mass spectra response of the ion of interest reaches the maximum immediately after laser ablation and drops to the low percentage range in 0.9 s. The total time to image an organ sample with a step size of 100 μm between pixels for an area of 8.1 × 2.6 mm^2 typically requires approximately 1.5 hour.

4.3.4 Data Processing and Image Visualization

The raw time-resolved mass spectra files (.d) of individual pixels were first converted to standard mass spectrometry format files (.mzML) by MSConvert from ProteoWizard [29] and then processed by a script written in Python 2.7.8 utilizing pyOpenMS library [30], see Figure 4.5. Individual averaged spectrum (.mzML) after blank subtraction was extracted from each time-resolved spectra in the Python script. These pixelated spectra were finally combined with the position information to generate a standard MSI data file (.imzML) by imzML converter [31]. This data processing workflow has the potential to be utilized for any standard MSI RAW data files with multiple MS scans to extract single spectrum for each pixel and incorporate the spatial information afterwards to generate standard MSI file.

The resulted imzML file can be transferred and viewed on any free, publicly available MSI visualization software, such as BioMap [32], DataCube Explorer [33], and MSiReader [34]. Here, MSiReader was chosen to visualize the large MSI dataset with high spatial and mass resolution. The presented MSI images were smoothed with a second order linear interpolation and plotted as heatmap without any contrast enhancement.

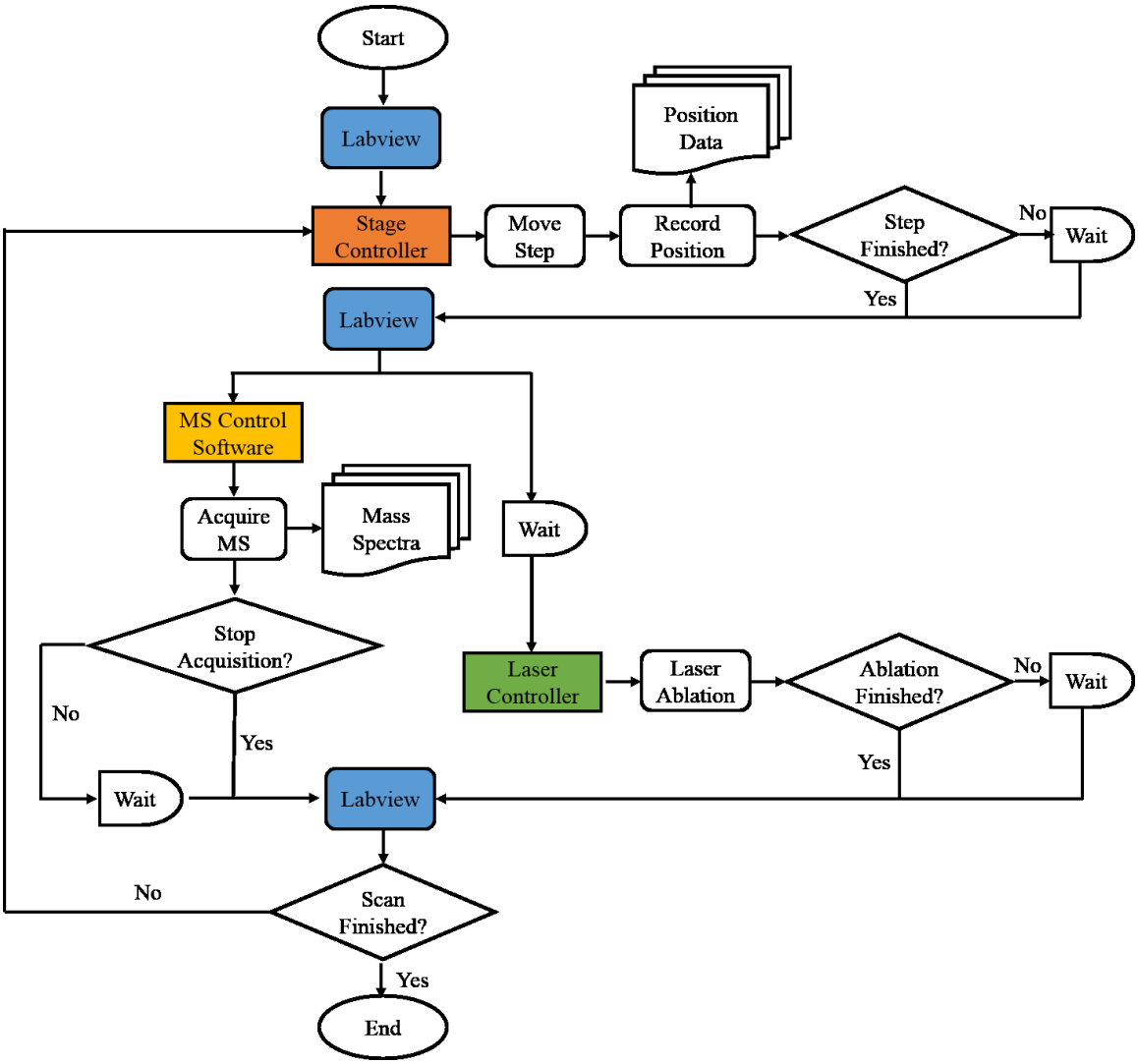

Figure 4.2. Flow chart of pixelated imaging communication sequence of stage, laser, and mass spectrometer.

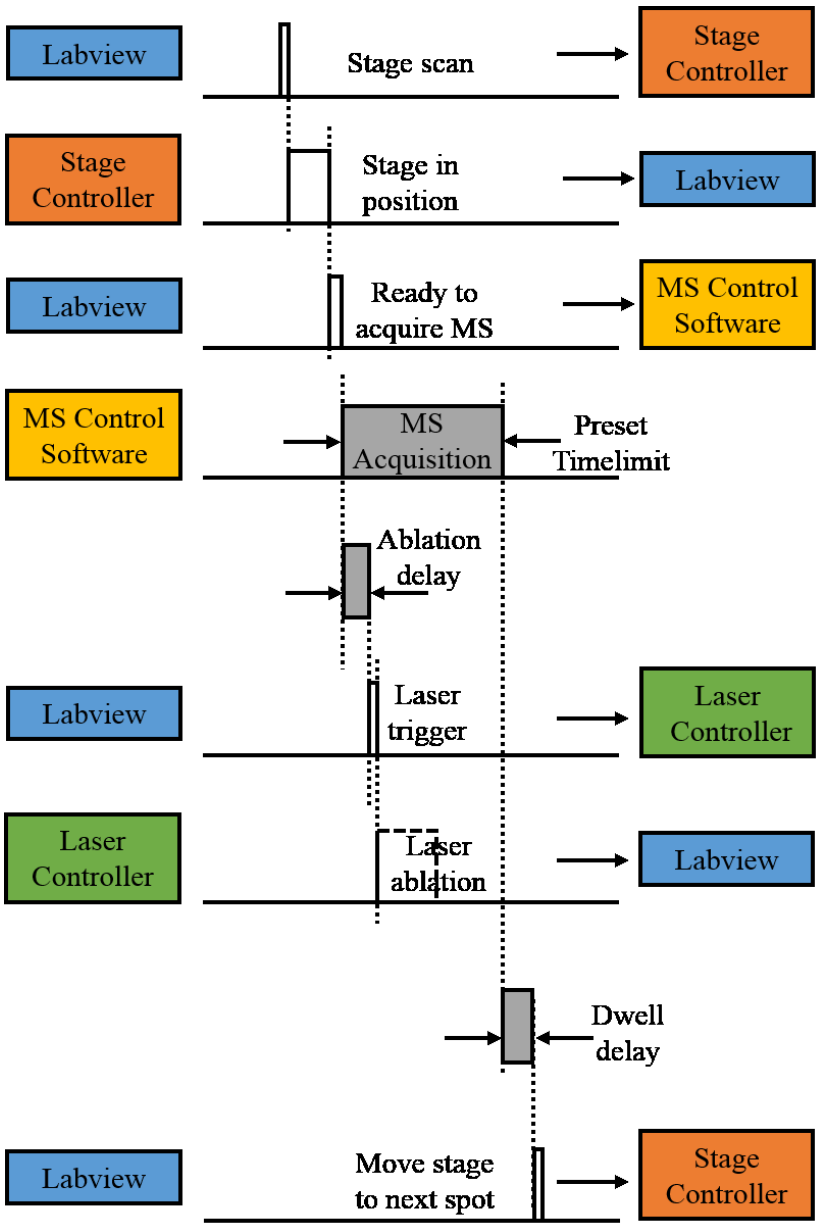

Figure 4.3. Timing diagram of pixelated imaging communication sequence of stage, laser, and mass spectrometer.

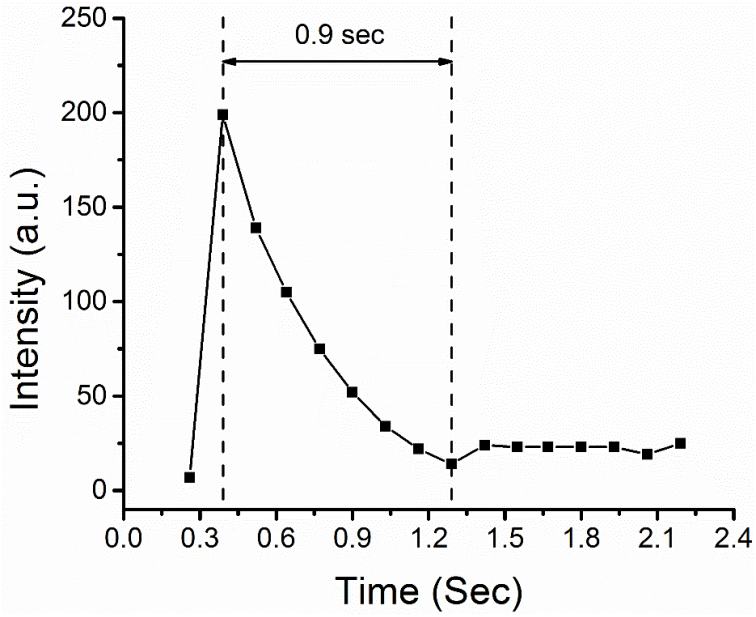

Figure 4.4. Mass spectral response of a dye related ion (*m/z* 442.90 ± 0.01) after a single laser shot ablation of the dye film using a spot size of 50 μm by LEMS.

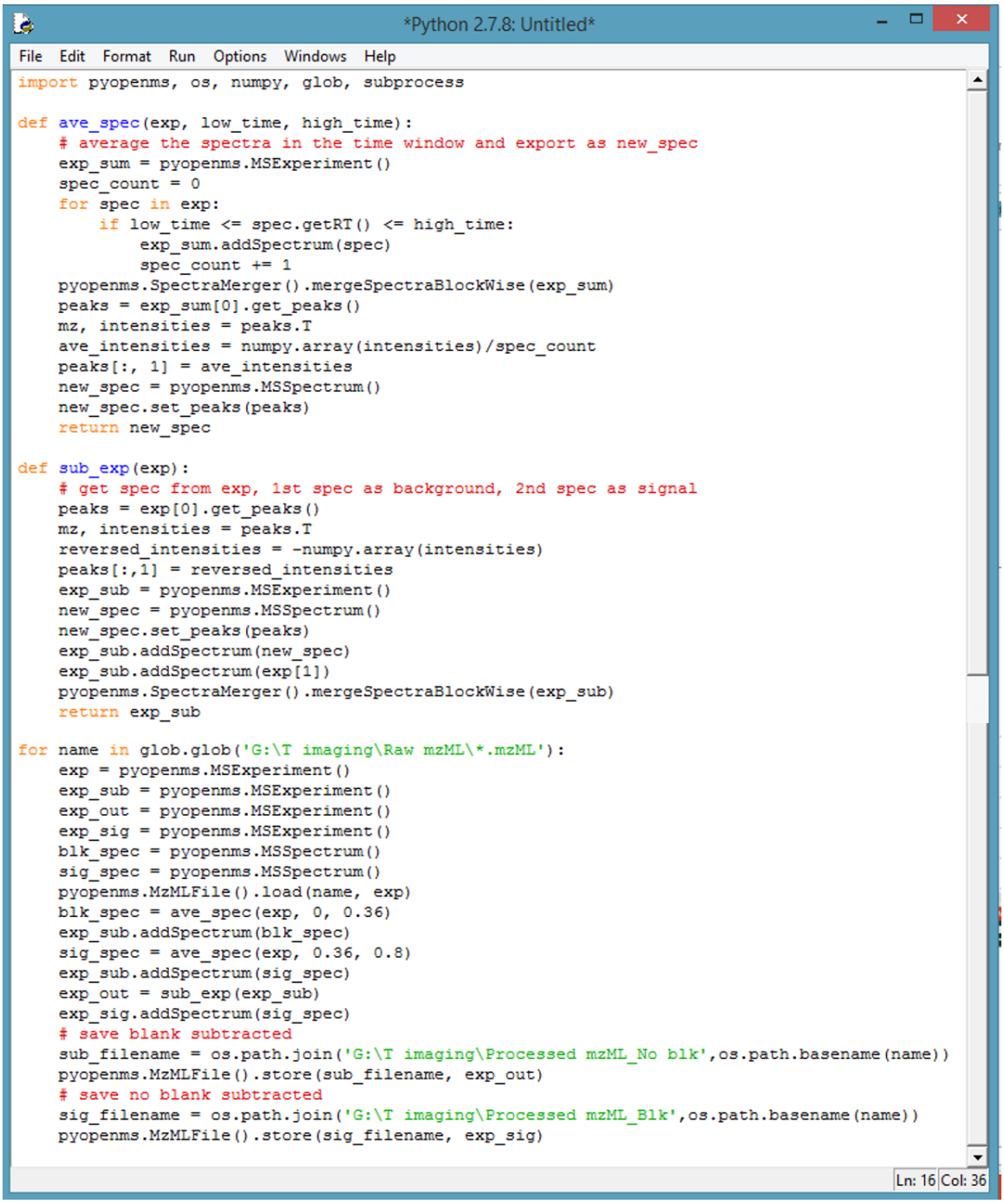

Figure 4.5. Python Script for extracting blank subtracted spectrum from pixelated mass spectra chromatogram.

4.3.5 Statistical Analysis

Nonnegative matrix factorization (NMF) and principal component analysis (PCA) were applied to the MSI data using open source Matlab-based programs OmniSpect [35] and memory efficient PCA [36] for statistical analysis. The program supports input data in the imzML format and explores the entire dataset using NMF and PCA algorithm. The program will load, process, and compute the pixel registered mass spectra to generate statistically important component images and their corresponding component spectra. The NMF and PCA component images were presented as heatmaps without any interpolation or contrast enhancement.

4.3.6 Safety Considerations

Lab personnel were protected from any exposed invisible laser radiation and high voltage supplies by insulating shields. Appropriate laser eye protection was worn by all lab personnel during the experiments.

4.4 Results and Discussion

4.4.1 Imaging An Ink Pattern

To evaluate the imaging capability of LEMS, a red ink pattern on a stainless steel slide was used as the initial sample for study. This pattern was created by removal of the ink using femtosecond laser ablation to form a "T" with the custom laser ablation platform. An optical image of the ink pattern pre- and post-LEMS imaging is shown in Figure 4.6 with dark and bright area corresponding to laser unablated and ablated ink areas, respectively. Figure 4.7 shows the ion image at *m/z* 442.90, corresponding to rhodamine

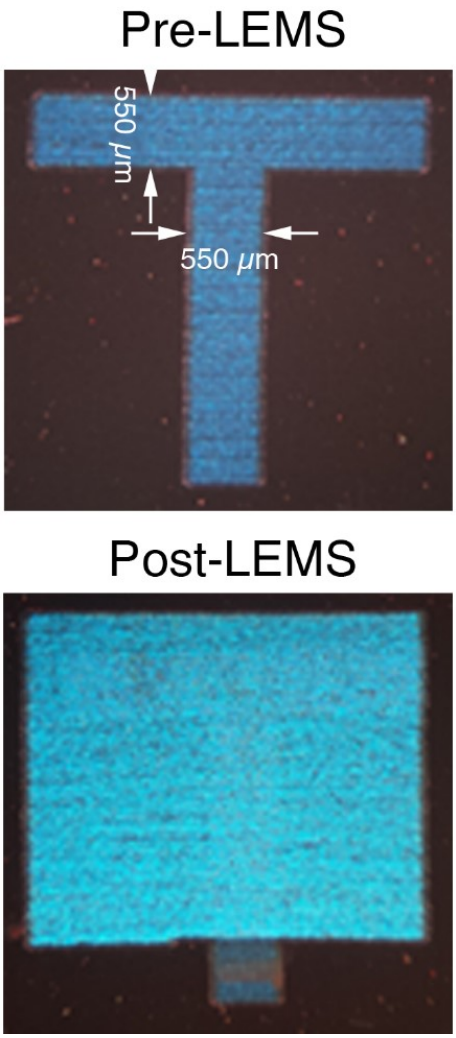

Figure 4.6. Optical image of a laser printed pattern in a thin-film of red ink containing rhodamine 6G dye on a metal slide pre-LEMS and post-LEMS imaging.

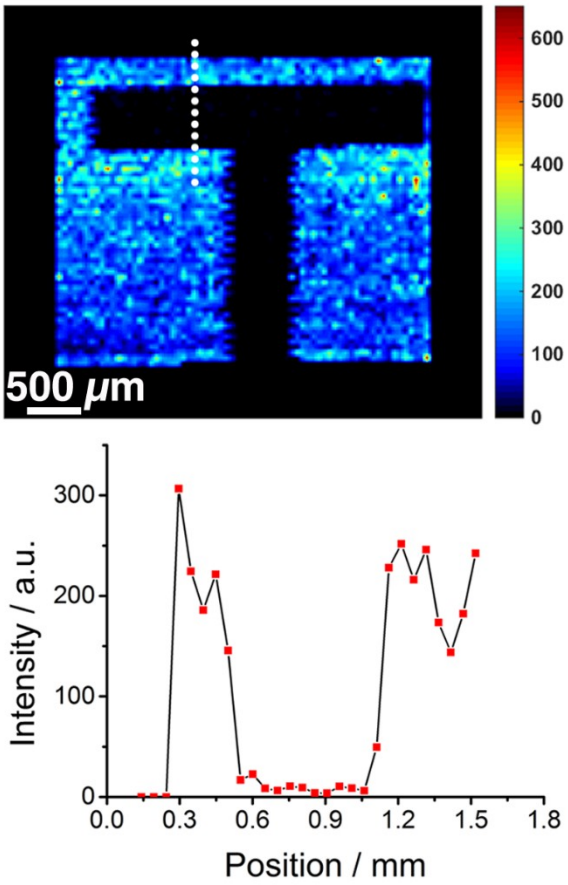

Figure 4.7. Selected ion image (*m/z* 442.90 ± 0.01) acquired with single shot laser per pixel. Intensity plot as a function of positions, as shown by the white dotted line in the ion image.

6G dye with the loss of a chloride ion, obtained by LEMS using a 50 μm laser spot size, which agrees with the optical image of the pattern. The variance of pixel intensity is not due to laser fluctuations, but is due to inhomogeneity inherent in the printed dye film, which has been seen in previous LEMS [37] and MALDI experiments [38]. A plot of the intensity of the dye ion as a function of position from the white dotted line in the ion image is shown in Figure 4.7. The ion intensity of the gap area that is indicated by the white arrow in Figure 4.6, corresponding to the "valley" in the plot, revealed a nearly zero level. The width of the "valley" was determined to be 550 μm, which agrees with the expected distance based on the pre-defined ablation pattern.

To evaluate the degree of sample carry-over between pixels, the background ion signals before firing the laser are extracted from the time-resolved spectra of individual pixels and plotted in Figure 4.8. The background ion image implies little or no sample carry-over between consecutive pixels after the 2.0 s dwell time and the ion image without background subtraction remains the same intensity scale as the background subtracted image. The mean value of the lateral resolution was determined to be 62.9 μm, shown in Figure 4.9, using the distance for which an increase in signal intensity from 20% to 80% of the maximum value as a measure of the lateral resolution [39, 40]. This proof-of-principle experiment of the ink pattern demonstrates that a lateral resolution of ~60 μm can be achieved by the current LEMS imaging system.

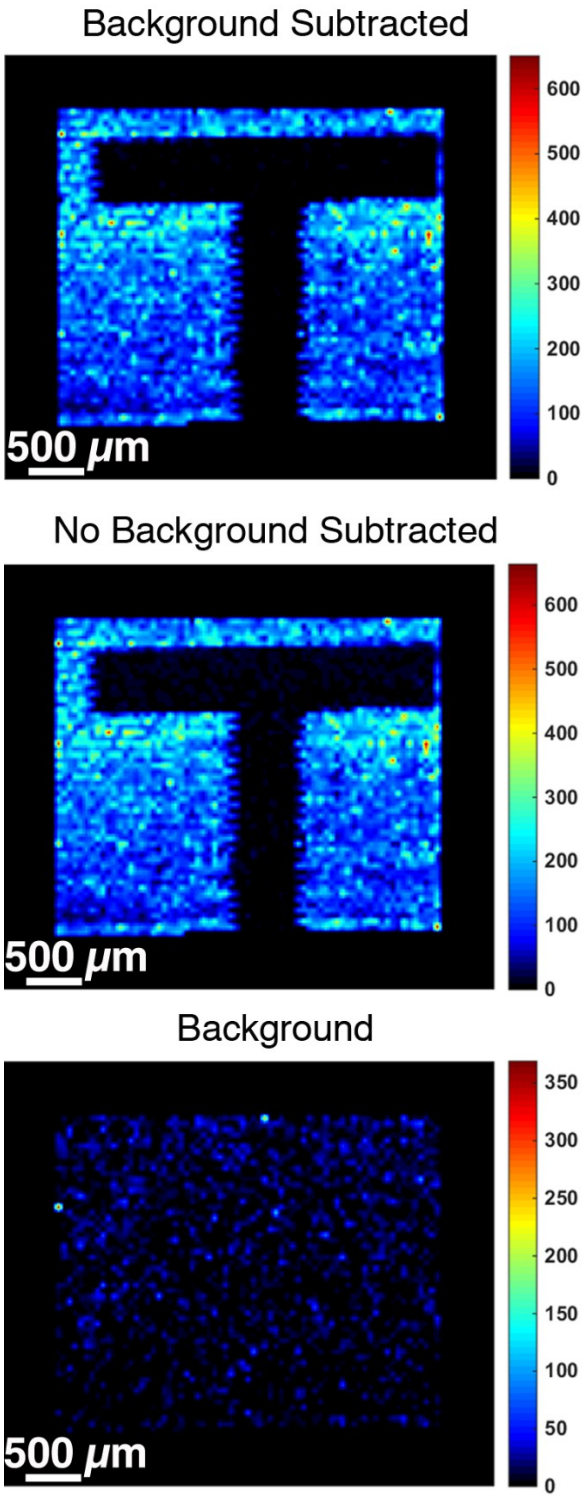

Figure 4.8. Selected ion image (*m/z* 442.90 ± 0.01) with and without background subtraction for individual pixels.

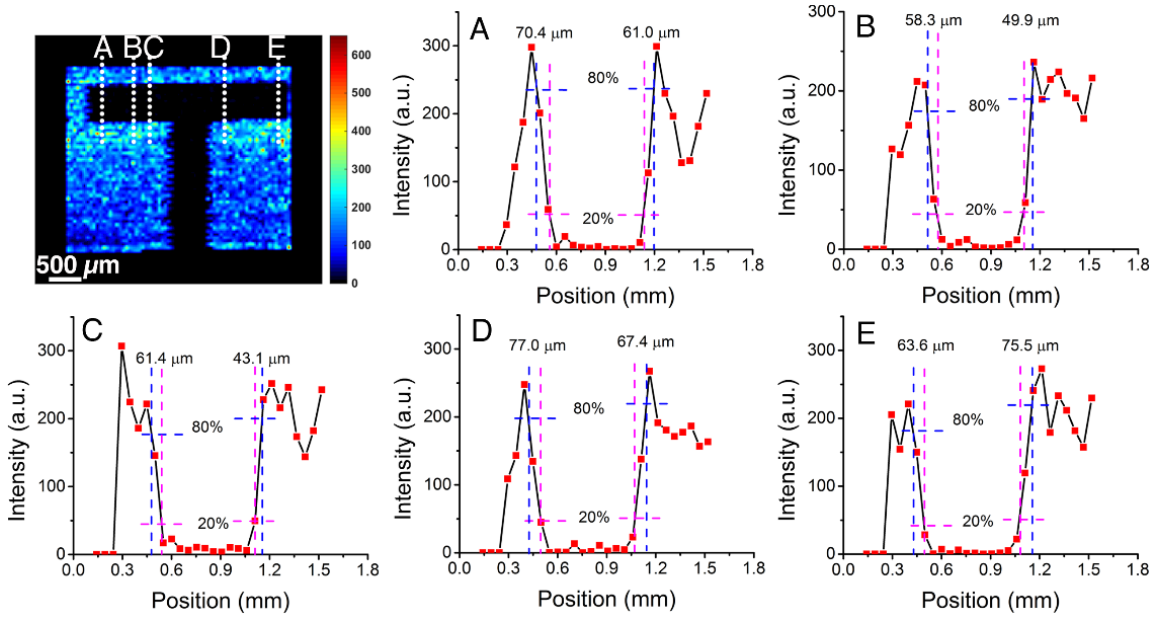

Figure 4.9. Intensity plot as a function of positions, as shown by the white dotted line in the ion image of *m/z* 442.90. The blue and magenta lines indicate 80% and 20% of the maximum peak intensity, respectively.

4.4.2 Direct Analysis of Flower Petal and Leaf by LEMS

To demonstrate the ability of LEMS for characterization of biological samples, a flower petal and leaf sample from a pink *Impatiens* plant were directly analyzed in continuous raster mode with a laser spot size of 60 μm in diameter. The blank subtracted mass spectra of the flower petal and leaf are presented in Figure 4.10 top and bottom, respectively. In the petal spectrum, the *m/z* 741.19 ion was tentatively identified as protonated pelargonidin 3-(p-coumaroyl)glucoside-5-glucoside, a flavonoid pigment associated with pink/red plant tissues [41, 42], by mass searching in METLIN metabolites database [43] (http://metlin.scripps.edu/index.php, last accessed October 7, 2015). This identification was confirmed by the fragmentation pattern using tandem mass spectrometry (MS/MS) analysis with fragments corresponding to the loss of glucose and glucoside coumaroyl group in Figure 4.11. The ions at *m/z* 711.18 and 783.21 were tentatively assigned to delphinidin 3,5-di-acetylglucoside and pelargonidin 3-(p-coumaryl)glucoside-5-acetylglucoside, respectively. Some of the peaks shared between the petal and leaf are *m/z* 287.05 and 471.08, which are protonated cyanidin and sodiated cyanidin glucoside, and an unidentified ion at *m/z* 587.12. Nevertheless, ions that are specific to the leaf were found including *m/z* 179.04 and 161.03, which are likely an unidentified species $[M]^+$ or $[M+H]^+$ and its fragment $[M-H_2O]^+$ or $[M-H_2O+H]^+$. Direct analysis of the plant samples suggest that anthocyanins, sugars and other small metabolites can be detected by LEMS without any sample preparation. Identification of the detected molecular features is possible through exact mass measurement and MS/MS analysis to provide chemical information regarding the sample.

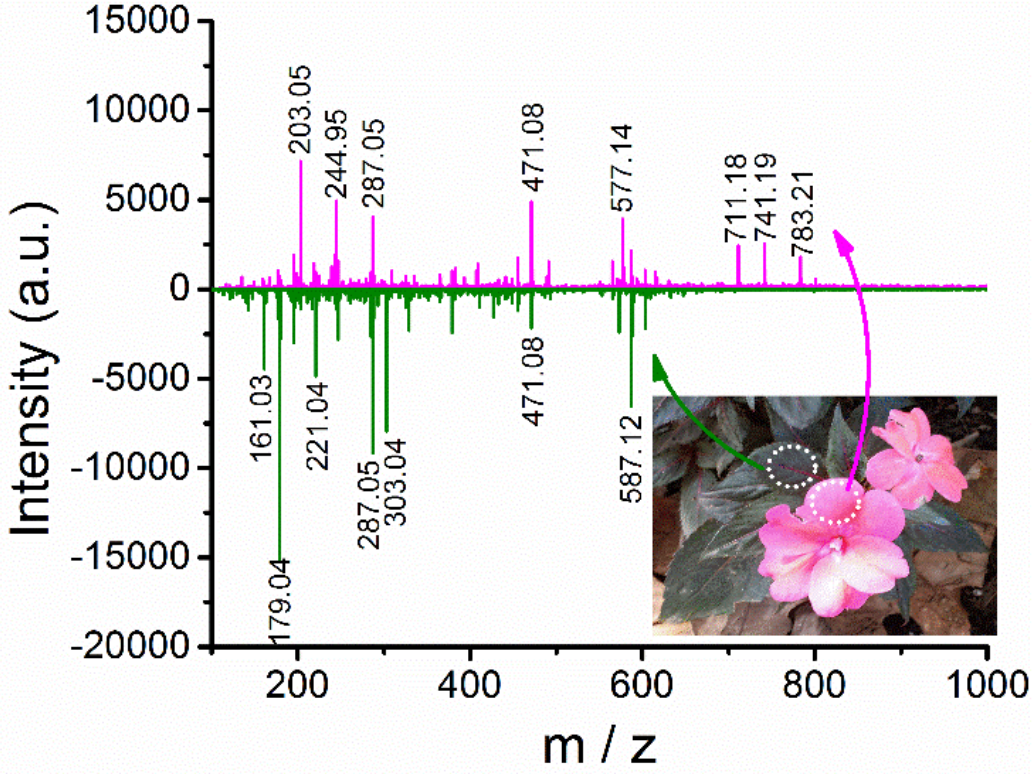

Figure 4.10. Blank-subtracted LEMS mass spectra of a pink *Impatiens* flower petal (top) and leaf (bottom). An optical image of the flower is shown in the inset with the region analyzed circled.

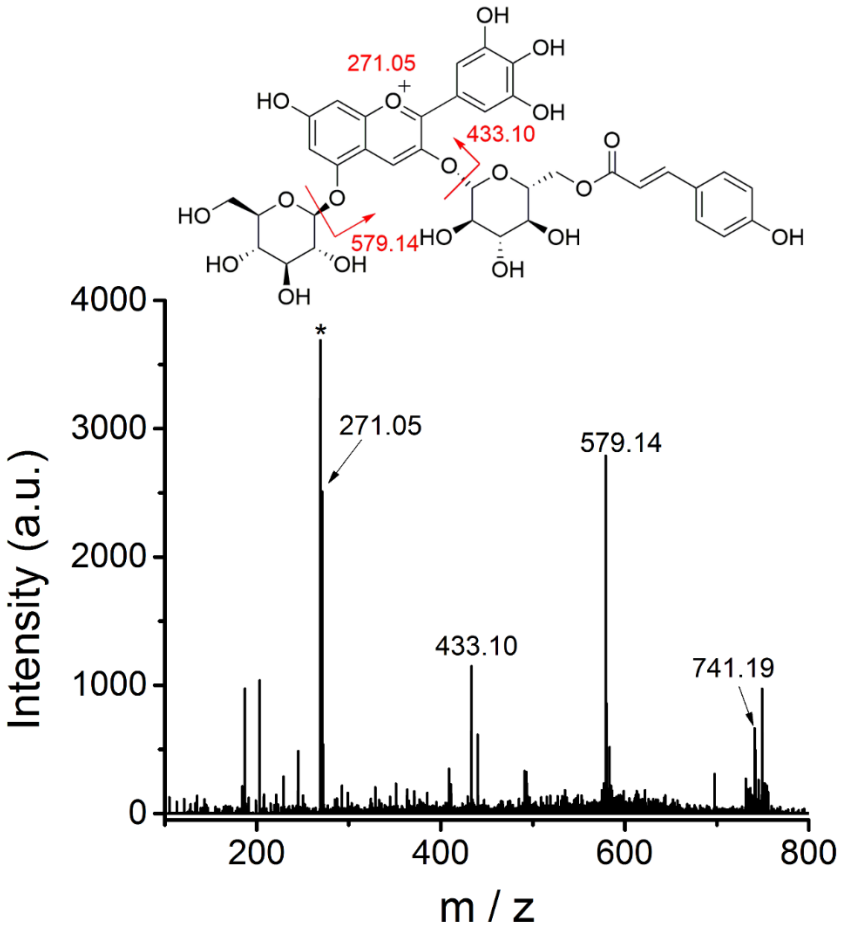

Figure 4.11. Tandem mass spectrum of the ion at *m/z* 741.19 for flower petal. Peak label by symbol (*) is MS/MS background related features.

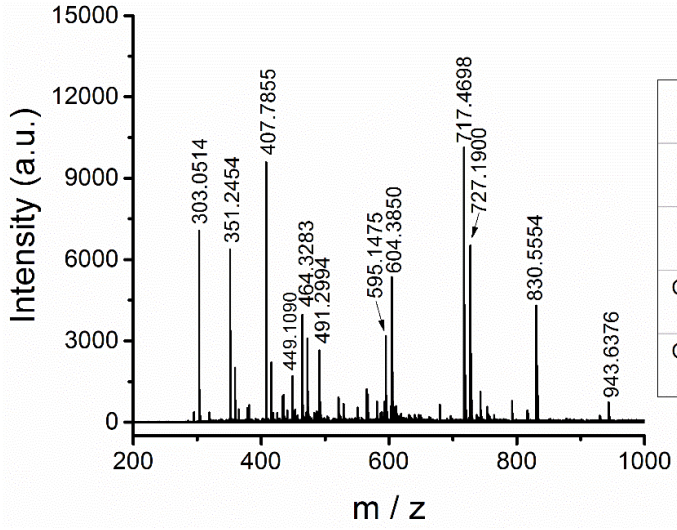

Compounds	Measured *m/z*	Theoretical *m/z*	Mass error (ppm)
Del	303.0514	303.0499	4.9
Cy-Glu	449.1090	449.1078	2.7
Cy-coumaryl-Glu	595.1475	595.1446	4.9
Cy-coumaryl-Sam	727.1900	727.1869	4.3

Figure 4.12. Blank-subtracted LEMS mass spectra of a red *Impatiens* flower leaf. Abbreviations: Del delphinidin; Cy cyanidin; Glu glucoside; Sam sambubioside.

4.4.3 Tissue Imaging of Flower Leaf

To demonstrate the application of LEMS imaging for biological samples, a sample of red *Impatiens* flower leaf was placed in the ion source and directly imaged using a laser spot size of 60 µm and a step size of 100 µm. A continuous raster scan profile of the sample revealed abundant features including *m/z* 303.05, 449.11, 595.15, and 727.19 in Figure 4.12, corresponding to delphinidin, cyanidin 5-glucoside, cyanidin 3-(p-coumaroyl)glucoside, and cyanidin 3-(p-coumaryl)sambubioside, respectively. Other ions at *m/z* 604.38, 717.47, 830.56, and 943.64 are unidentified metabolites.

The same leaf sample was then imaged over an area of 8.1 × 2.6 mm^2 and the optical image of the leaf is shown in Figure 4.13 with the area imaged highlighted by a rectangle. Selected ion images of *m/z* 303.05, 449.11, and 717.47 are also shown in Figure 4.13, respectively. A complete list of the representative ion images is provided in Figure 4.14.

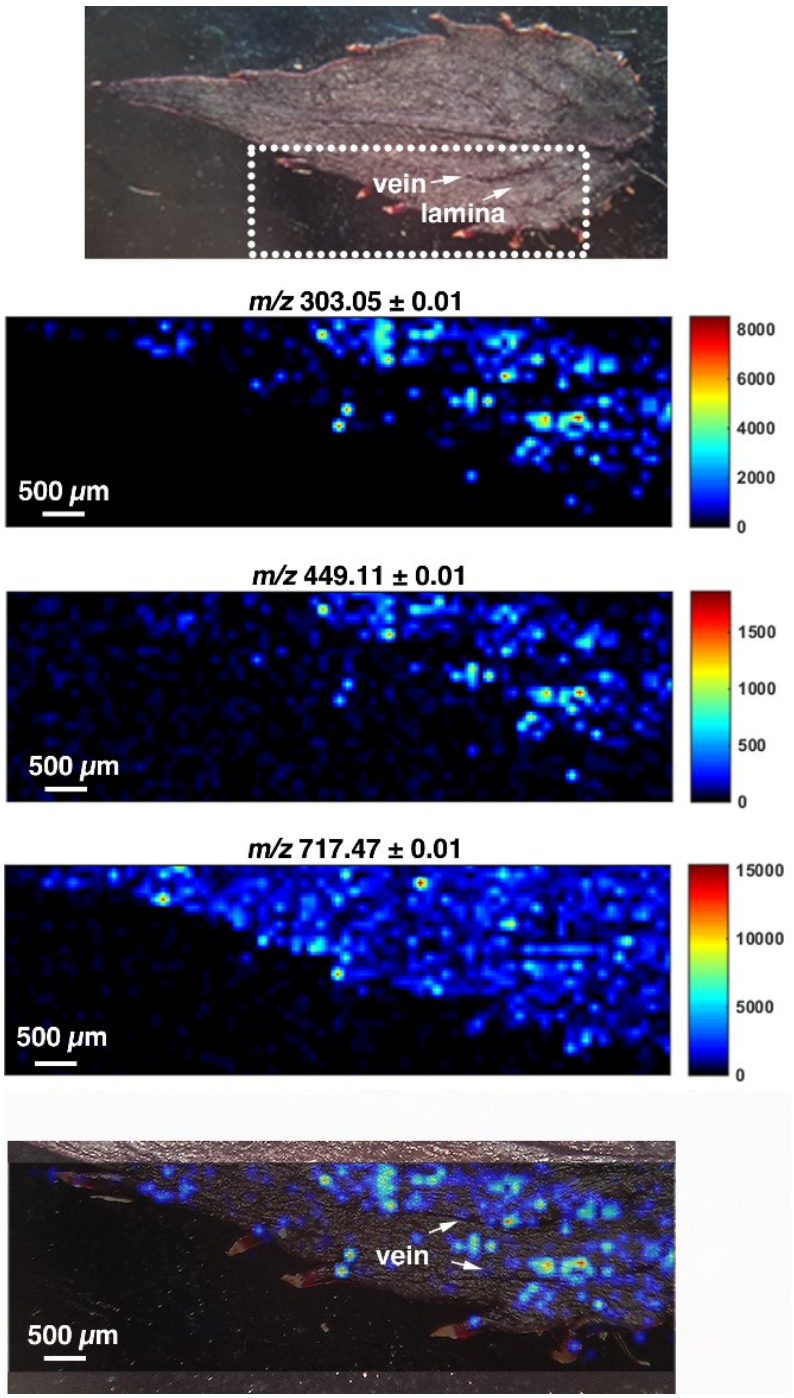

Figure 4.13. Optical image of a red *Impatiens* flower leaf ablated by LEMS using single shot laser per pixel. Mass spectrometry images showing the spatial distributions of ions at *m/z* 303.05, 449.11, and 717.47 with the absolute intensity scale of each isolated ion. Overlay of the *m/z* 303.05 ion image and the leaf sample.

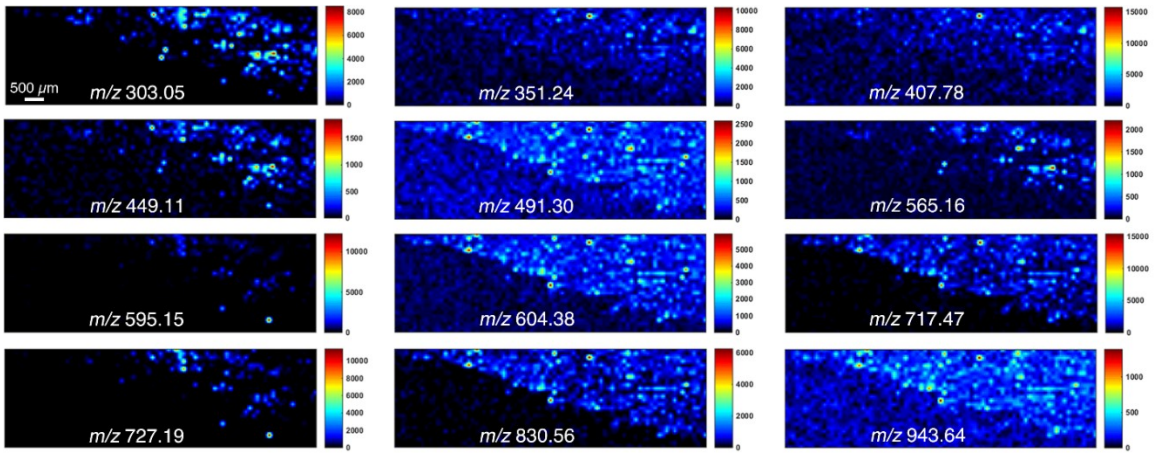

Figure 4.14. Mass spectrometry images of the representative ions for the red *Impatiens* flower leaf sample. The isolation *m/z* width is ± 0.01 for all the ion maps.

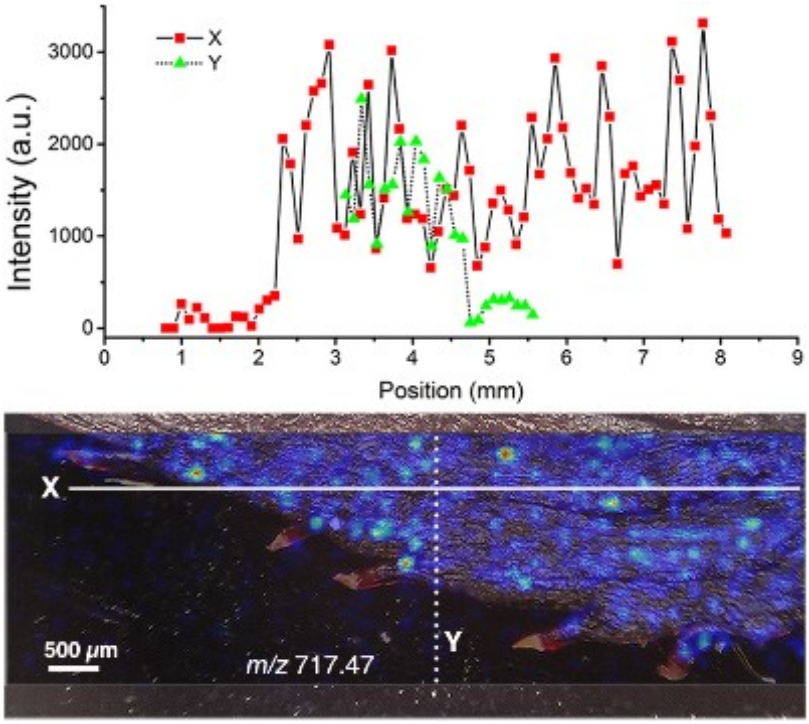

Figure 4.15. The line intensity plot as a function of positions, as shown by the white solid (X) and dashed (Y) line in the ion image of the *m/z* 717.47 ion image overlaid with the leaf sample.

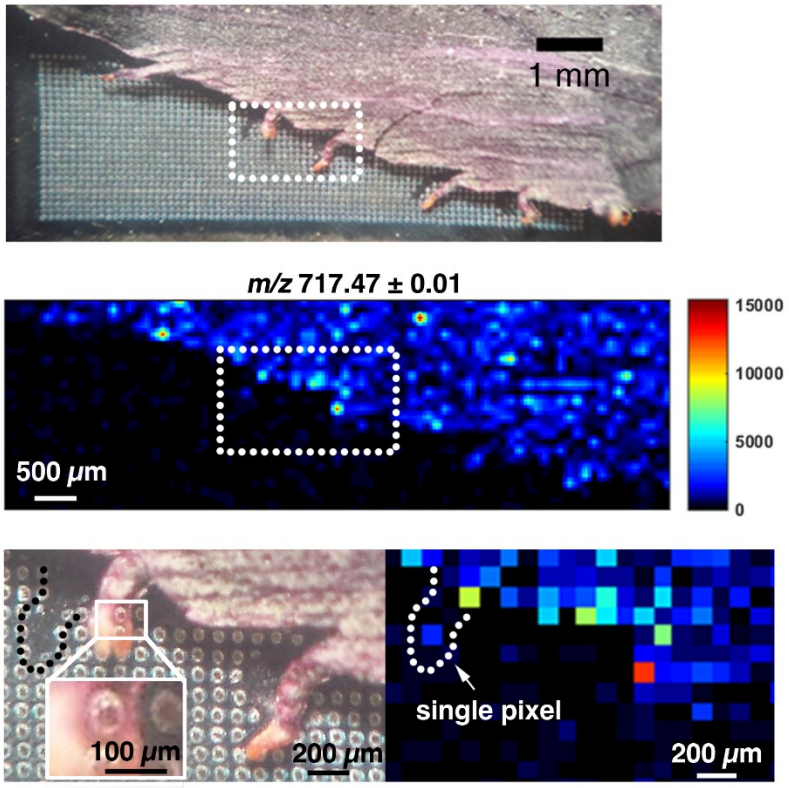

Figure 4.16. Comparison of optical and mass spectrometry image of area indicated by the rectangles in the optical and ion image.

The species at *m/z* 717.47 is distributed evenly throughout the entire leaf area scanned. The ion image also displays a sharp edge that is in good correlation with the margin of the leaf, as seen in the overlay image in Figure 4.15. Representative line intensity plot extracted from the *m/z* 717.47 ion image, shown in Figure 4.15, demonstrates the signal stability within the sample. The variation of the signal could be caused by several factors including the amount of metabolite in the area probed, the changes of surface height from the plant morphology, and the stability of the electrospray, which had been observed in a previous nano-DESI mass spectrometry imaging experiment [44]. In contrast, the ion images of delphinidin (*m/z* 303.05) and cyanidin glucoside (449.11) reveal a distribution that appears to be specific to the vein area of the leaf, as seen in the overlay image of *m/z* 303.05 with the leaf sample in Figure 4.13. The actual laser ablated crater size on tissue was determined to 60 × 70 μm^2, as seen in the microscope image on the left of Figure 4.16. This crater was successfully mapped on the ion image as a single pixel on the ion image, which correspond to the dashed area of the sample. This experiment suggests that tissue imaging of plant samples at a lateral resolution <100 μm is possible for LEMS. Regions that presented distinct spectra profiles can be resolved by LEMS imaging.

4.4.4 Statistical Analysis

The large size and high complexity of the MSI datasets make the manual examination of the selected ion maps impossible when identifying features of interest from hundreds to thousands of detected ions. Instead, statistical analysis (e.g., principal component analysis (PCA) and nonnegative matrix factorization (NMF)) has been utilized in mass spectrometry imaging for high throughput data analysis where the results are

shown not as heatmaps of selected ions but as score plots in the spatial domain [45]. The use of PCA in MSI data analysis is considered to be controversial due to the generation of negative loading and score plots, which are values on the new coordinate system (PCs) and the values have no direct physical meaning, and so other statistical analysis tools such as NMF has been employed to provide more interpretable component images and spectra with non-negative factors [36, 45].

Here, NMF and PCA were applied to the LEMS imaging results of the red *Impatiens* flower leaf sample. The entire dataset is computed and reduced to different components based on the similarities of the spatial distributions. Figure 4.17 displays the major component images and their corresponding component spectra by NMF and PCA analysis. In the first NMF component image (NMF1), solvent features that are suppressed inside the tissue region are classified by the NMF analysis. The second NMF component (NMF2) reveals the same leaf pattern as the selected ion images in Figure 4.13. More importantly, the corresponding component spectrum displays the same ion species as those observed from the line scan spectra in Figure 4.12. The agreement of the component images and corresponding component spectra from NMF analysis with the results from manually selected ion maps and mass spectra indicates that NMF can be applied to the LEMS imaging dataset to extract spatial and spectral features of interest efficiently for high throughput analysis. However, note that NMF generates only one component image that contributes to all biologically relevant ion species in NMF2. In PCA analysis, the PC1 and PC2 component images show similar results as NMF1 and NMF2 that anti-correlated distributions corresponding to plant and solvent species are distinguished. Unlike NMF analysis where plant features are grouped into only one component image, PCA, an

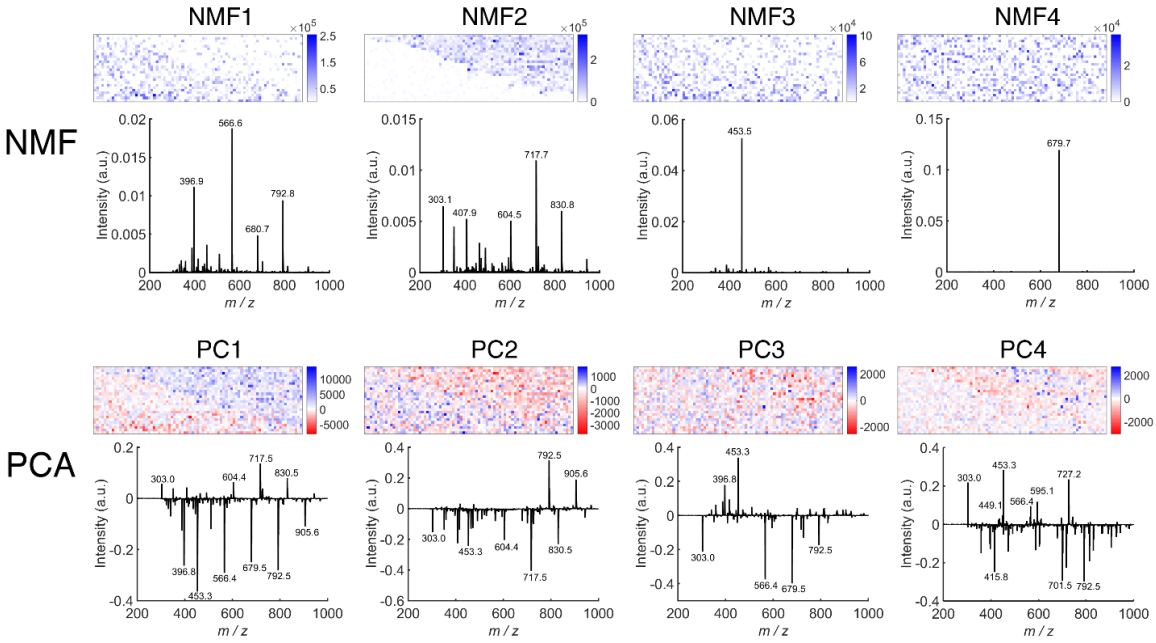

Figure 4.17. Comparison of PCA and NMF outputs of the red *Impatiens* flower leaf sample. The component images (top) and their corresponding component spectra (bottom) are shown for PCA and NMF, respectively.

algorithm based on maximize variance, resolves the unique distribution of *m/z* 303.0, 449.1, 595.1, and 727.2 ions from the remaining plant features in the fourth principal component (PC4) images.

In an effort to optimize the statistical analysis of the test data, we removed pixels corresponding to the non-leaf area from the imaging dataset. This customized dataset was imported to NMF and PCA analysis in Figure 4.18. Leaf species are classified into the first two components NMF1 and NMF2, where NMF2 component image reveals the unique distribution of the vein area. But the NMF2 component spectrum suggests that plant species that are found in the non-vein area also contribute to NMF2 component image. In contrast, these species are classified separately from the vein area species by the PCA analysis in PC3 image. This example demonstrates that statistical analysis can be combined with LEMS imaging to extract features of interest from the large imaging data, and PCA is able to resolve statistically small differences that NMF has difficulty in identifying.

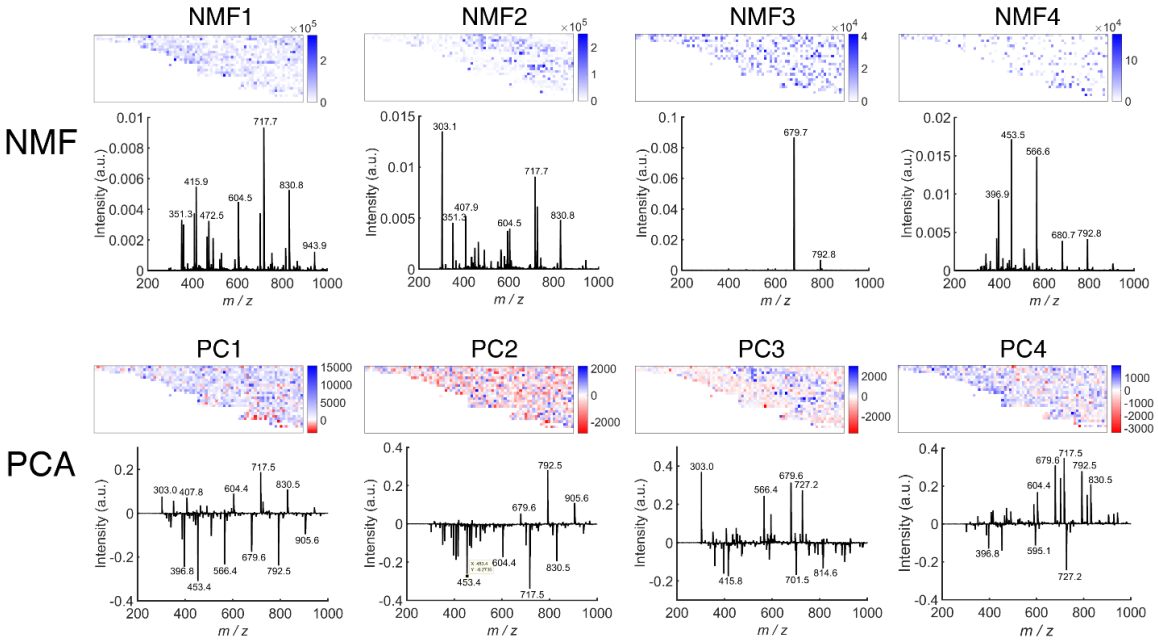

Figure 4.18. Comparison of PCA and NMF outputs using the customized dataset with pixels correspond to non-tissue area removed. The component images (top) and their corresponding component spectra (bottom) are shown for PCA and NMF, respectively.

4.5 Conclusions

The use of nonresonant fs lasers in LEMS imaging overcomes the need for resonant absorption occurring in analyte, matrix or substrate, thus making the vaporization step both universal and sample independent. The design and implementation of the LEMS imaging source on a commercial QTOF mass spectrometer is described. Imaging mass spectrometry can be performed with dwell time as low as 2.0 s/pixel in single or multi-shot ablation with full control over the repetition rate and the delay between the ablation event and the mass spectrometer scan. A lateral resolution of 60 μm was demonstrated without oversampling on an ink pattern by LEMS. Chemically distinct features smaller than 100 μm were successfully mapped by LEMS imaging on tissue samples. Efficient feature extraction from the large amount of LEMS imaging data was achieved by NMF and PCA analysis. Compositional heterogeneity within the sample was successfully distinguished when the imaging data is subjected to PCA analysis.

4.6 References

1. A.D. Palmer, T. Alexandrov. Serial 3D imaging mass spectrometry at its tipping point. *Anal. Chem.* **87**, 4055 (2015).

2. R.M.A. Heeren. Getting the picture: The coming of age of imaging MS. *Int. J. Mass Spectrom.* **377**, 672 (2015).

3. J.L. Norris, R.M. Caprioli. Analysis of tissue specimens by matrix-assisted laser desorption/ionization imaging mass spectrometry in biological and clinical research. *Chem. Rev.* **113**, 2309 (2013).

4. J.M. Wiseman, D.R. Ifa, Y. Zhu, C.B. Kissinger, N.E. Manicke, P.T. Kissinger, R.G. Cooks. Desorption electrospray ionization mass spectrometry: Imaging drugs and metabolites in tissues. *Proc. Natl. Acad. Sci. U.S.A.* **105**, 18120 (2008).

5. E.H. Seeley, R.M. Caprioli. Molecular imaging of proteins in tissues by mass spectrometry. *Proc. Natl. Acad. Sci. U.S.A.* **105**, 18126 (2008).

6. M.J. Bailey, N.J. Bright, R.S. Croxton, S. Francese, L.S. Ferguson, S. Hinder, S. Jickells, B.J. Jones, B.N. Jones, S.G. Kazarian, J.J. Ojeda, R.P. Webb, R. Wolstenholme, S. Bleay. Chemical characterization of latent fingerprints by matrix-assisted laser desorption ionization, time-of-flight secondary ion mass spectrometry, mega electron volt secondary mass spectrometry, gas chromatography/mass spectrometry, X-ray photoelectron spectroscopy, and attenuated total reflection Fourier transform infrared spectroscopic imaging: An intercomparison. *Anal. Chem.* **84**, 8514 (2012).

7. H. Meistermann, J.L. Norris, H.-R. Aerni, D.S. Cornett, A. Friedlein, A.R. Erskine, A. Augustin, M.C. De Vera Mudry, S. Ruepp, L. Suter, H. Langen, R.M. Caprioli, A. Ducret. Biomarker discovery by imaging mass spectrometry: Transthyretin is a biomarker for gentamicin-induced nephrotoxicity in rat. *Mol. Cell. Proteomics* **5**, 1876 (2006).

8. C. Wu, A.L. Dill, L.S. Eberlin, R.G. Cooks, D.R. Ifa. Mass spectrometry imaging under ambient conditions. *Mass Spectrom. Rev.* **32**, 218 (2013).

9. M.E. Monge, G.A. Harris, P. Dwivedi, F.M. Fernández. Mass spectrometry: Recent advances in direct open air surface sampling/ionization. *Chem. Rev.* **113**, 2269 (2013).

10. P.M. Flanigan, R.J. Levis. Ambient femtosecond laser vaporization and nanosecond laser desorption electrospray ionization mass spectrometry. *Annu. Rev. Anal. Chem.* **7**, 229 (2014).

11. J. Shiea, M.-Z. Huang, H.-J. Hsu, C.-Y. Lee, C.-H. Yuan, I. Beech, J. Sunner. Electrospray-assisted laser desorption/ionization mass spectrometry for direct ambient analysis of solids. *Rapid Commun. Mass Spectrom.* **19**, 3701 (2005).

12. M.-Z. Huang, S.-C. Cheng, S.-S. Jhang, C.-C. Chou, C.-N. Cheng, J. Shiea, I.A. Popov, E.N. Nikolaev. Ambient molecular imaging of dry fungus surface by electrospray laser desorption ionization mass spectrometry. *Int. J. Mass Spectrom.* **325–327**, 172 (2012).

13. J.S. Sampson, A.M. Hawkridge, D.C. Muddiman. Generation and detection of multiply-charged peptides and proteins by matrix-assisted laser desorption electrospray ionization (MALDESI) Fourier transform ion cyclotron resonance mass spectrometry. *J. Am. Soc. Mass Spectrom.* **17**, 1712 (2006).

14. G. Robichaud, J.A. Barry, K.P. Garrard, D.C. Muddiman. Infrared matrix-assisted laser desorption electrospray ionization (IR-MALDESI) imaging source coupled to a FT-ICR mass spectrometer. *J. Am. Soc. Mass Spectrom.* **24**, 92 (2013).

15. P. Nemes, A. Vertes. Laser ablation electrospray ionization for atmospheric pressure, in vivo, and imaging mass spectrometry. *Anal. Chem.* **79**, 8098 (2007).

16. P. Nemes, A.A. Barton, Y. Li, A. Vertes. Ambient molecular imaging and depth profiling of live tissue by infrared laser ablation electrospray ionization mass spectrometry. *Anal. Chem.* **80**, 4575 (2008).

17. J.J. Brady, E.J. Judge, R.J. Levis. Mass spectrometry of intact neutral macromolecules using intense non-resonant femtosecond laser vaporization with electrospray post-ionization. *Rapid Commun. Mass Spectrom.* **23**, 3151 (2009).

18. E.J. Judge, J.J. Brady, D. Dalton, R.J. Levis. Analysis of pharmaceutical compounds from glass, fabric, steel, and wood surfaces at atmospheric pressure using spatially resolved, nonresonant femtosecond laser vaporization electrospray mass spectrometry. *Anal. Chem.* **82**, 3231 (2010).

19. G. Robichaud, J.A. Barry, D.C. Muddiman. Atmospheric pressure mass spectrometry imaging, in: *Encyclopedia of Analytical Chemistry*. John Wiley & Sons, Ltd, (2006).

20. P. Nemes, A.A. Barton, A. Vertes. Three-dimensional imaging of metabolites in tissues under ambient conditions by laser ablation electrospray ionization mass spectrometry. *Anal. Chem.* **81**, 6668 (2009).

21. H. Li, B.K. Smith, L. Márk, P. Nemes, J. Nazarian, A. Vertes. Ambient molecular imaging by laser ablation electrospray ionization mass spectrometry with ion mobility separation. *Int. J. Mass Spectrom.* **377**, 681 (2015).

22. P. Nemes, A.S. Woods, A. Vertes. Simultaneous imaging of small metabolites and lipids in rat brain tissues at atmospheric pressure by laser ablation electrospray ionization mass spectrometry. *Anal. Chem.* **82**, 982 (2010).

23. B. Shrestha, A. Vertes. In situ metabolic profiling of single cells by laser ablation electrospray ionization mass spectrometry. *Anal. Chem.* **81**, 8265 (2009).

24. B. Shrestha, J.M. Patt, A. Vertes. In situ cell-by-cell imaging and analysis of small cell populations by mass spectrometry. *Anal. Chem.* **83**, 2947 (2011).

25. J.A. Barry, M.R. Groseclose, G. Robichaud, S. Castellino, D.C. Muddiman. Assessing drug and metabolite detection in liver tissue by UV-MALDI and IR-MALDESI mass spectrometry imaging coupled to FT-ICR MS. *Int. J. Mass Spectrom.* **377**, 448 (2015).

26. G. Robichaud, J. Barry, D. Muddiman. IR-MALDESI mass spectrometry imaging of biological tissue sections using ice as a matrix. *J. Am. Soc. Mass Spectrom.* **25**, 319 (2014).

27. F. Shi, P.M. Flanigan, J.J. Archer, R.J. Levis. Direct analysis of intact biological macromolecules by low-energy, fiber-based femtosecond laser vaporization at

1042 nm wavelength with nanospray postionization mass spectrometry. *Anal. Chem.* **87**, 3187 (2015).

28. F. Shi, P.M. Flanigan, J.J. Archer, R.J. Levis. Ambient molecular analysis of biological tissue using low-energy, femtosecond laser vaporization and nanospray postionization mass spectrometry. *J. Am. Soc. Mass Spectrom.* **27**, 542 (2016).

29. D. Kessner, M. Chambers, R. Burke, D. Agus, P. Mallick. ProteoWizard: Open source software for rapid proteomics tools development. *Bioinformatics* **24**, 2534 (2008).

30. H.L. Röst, U. Schmitt, R. Aebersold, L. Malmström. pyOpenMS: A Python-based interface to the OpenMS mass-spectrometry algorithm library. *Proteomics* **14**, 74 (2014).

31. A.M. Race, I.B. Styles, J. Bunch. Inclusive sharing of mass spectrometry imaging data requires a converter for all. *J. Proteomics* **75**, 5111 (2012).

32. M. Stoeckli, D. Staab, M. Staufenbiel, K.-H. Wiederhold, L. Signor. Molecular imaging of amyloid β peptides in mouse brain sections using mass spectrometry. *Anal. Biochem.* **311**, 33 (2002).

33. I. Klinkert, K. Chughtai, S.R. Ellis, R.M.A. Heeren. Methods for full resolution data exploration and visualization for large 2D and 3D mass spectrometry imaging datasets. *Int. J. Mass Spectrom.* **362**, 40 (2014).

34. G. Robichaud, K.P. Garrard, J.A. Barry, D.C. Muddiman. MSiReader: An open-source interface to view and analyze high resolving power MS imaging files on Matlab platform. *J. Am. Soc. Mass Spectrom.* **24**, 718 (2013).

35. R.M. Parry, A.S. Galhena, C.M. Gamage, R.V. Bennett, M.D. Wang, F.M. Fernández. OmniSpect: An open MATLAB-based tool for visualization and analysis of matrix-assisted laser desorption/ionization and desorption electrospray ionization mass spectrometry images. *J. Am. Soc. Mass Spectrom.* **24**, 646 (2013).

36. A.M. Race, R.T. Steven, A.D. Palmer, I.B. Styles, J. Bunch. Memory efficient principal component analysis for the dimensionality reduction of large mass spectrometry imaging data sets. *Anal. Chem.* **85**, 3071 (2013).

37. J.J. Brady, E.J. Judge, R.J. Levis. Analysis of amphiphilic lipids and hydrophobic proteins using nonresonant femtosecond laser vaporization with electrospray post-Ionization. *J. Am. Soc. Mass Spectrom.* **22**, 762 (2011).

38. R.R. Hensel, R.C. King, K.G. Owens. Electrospray sample preparation for improved quantitation in matrix-assisted laser desorption/ionization time-of-flight mass spectrometry. *Rapid Commun. Mass Spectrom.* **11**, 1785 (1997).

39. T.L. Colliver, C.L. Brummel, M.L. Pacholski, F.D. Swanek, A.G. Ewing, N. Winograd. Atomic and molecular imaging at the single-cell Level with TOF-SIMS. *Anal. Chem.* **69**, 2225 (1997).

40. S.L. Luxembourg, T.H. Mize, L.A. McDonnell, R.M.A. Heeren. High-spatial resolution mass spectrometric imaging of peptide and protein distributions on a surface. *Anal. Chem.* **76**, 5339 (2004).

41. R. Freyre, C. Uzdevenes, L. Gu, K.H. Quesenberry. Genetics and anthocyanin analysis of flower color in Mexican Petunia. *J. Am. Soc. Hortic. Sci.* **140**, 45 (2015).

42. F. He, N.-N. Liang, L. Mu, Q.-H. Pan, J. Wang, M.J. Reeves, C.-Q. Duan. Anthocyanins and their variation in red wines I. Monomeric anthocyanins and their color expression. *Molecules* **17**, 1571 (2012).

43. C.A. Smith, G. O'Maille, E.J. Want, C. Qin, S.A. Trauger, T.R. Brandon, D.E. Custodio, R. Abagyan, G. Siuzdak. METLIN - A metabolite mass spectral database. *Ther. Drug Monit.* **27**, 747 (2005).

44. J. Laskin, B.S. Heath, P.J. Roach, L. Cazares, O.J. Semmes. Tissue imaging using nanospray desorption electrospray ionization mass spectrometry. *Anal. Chem.* **84**, 141 (2012).

45. E.A. Jones, S.-O. Deininger, P.C.W. Hogendoorn, A.M. Deelder, L.A. McDonnell. Imaging mass spectrometry statistical analysis. *J. Proteomics* **75**, 4962 (2012).

CHAPTER 5

SMALL MOLECULE AND LARGE PROTEIN IMAGING FROM ANIMAL TISSUE SAMPLES USING LASER ELECTROSPRAY MASS SPECTROMETRY

5.1 Overview

In this chapter, ambient chemical imaging of animal tissue samples with 100 μm spatial resolution is enabled using nonresonant, femtosecond laser electrospray mass spectrometry (LEMS). Small metabolites, lipids and proteins are simultaneously vaporized directly from the tissue into the gas phase by a single femtosecond laser pulse (800 nm, 1.5 mJ, 50 fs) and ionized by electrospray droplets. Lipids, including glycerophosphocholine (GPC), lysophosphatidylcholine (LysoPC), phosphatidylcholine (PC) and bile acid, are detected from pig liver samples without application of matrix. Pig hemoglobin α subunit (~15 kDa) and its mono- and di-glycosylated derivatives are spatially imaged in the liver sample. Grey and white matter regions of a mouse brain section are spatially resolved in the LEMS imaging measurement. Molecular signatures, including free heme, hemoglobin α, and β subunits, accompanied by LysoPC(16:0), are mapped in the mouse brain with mild traumatic brain injury (TBI), indicating that blood-brain barrier disruption occurred following the injury. Potential biomarkers of TBI are also detected from the brain injury region.

5.2 Introduction

Molecular imaging of small molecules, such as drugs, metabolites, and lipids, has been extensively studied by ambient ionization techniques. Direct imaging of endogenous protein from tissue sample remains challenging for ambient ionization techniques because of the high molecular weight of protein and the high degree of complexity of tissue components. Recently, several groups have shown that by washing tissue sections with organic solvent to remove small analytes or coupling the ion source with the high-field asymmetric ion mobility spectrometry (FAIMS), an ion filtering device, selective detection of intact proteins as large as 15 kDa can be achieved from tissue samples using liquid extraction-based methods, such as LESA [1], LMJ-SSP [2] and nano-DESI [3, 4]. In a recent study where DESI source was coupled with FAIMS, only doubly charged cardiolipins were imaged while large proteins were not observed from tissue samples [2]. LEMS has shown the ability to vaporize neat protein samples such as lysozyme and cytochrome c from condensed phase into the gas phase for mass analysis [5, 6], but direct imaging of protein from native tissue has not been accomplished.

The detection of tissue specific molecules or biomarkers plays a vital role in the early detection of cancer or organ injury [7]. Chemical imaging by mass spectrometry has attracted considerable attention recently for such applications because molecular information and spatial distribution are offered in a single experiment in a label-free manner [8-11]. Here we report the use of LEMS for imaging of tissue heterogeneity and discovery of traumatic brain injury (TBI) biomarkers. TBI is an injury to the brain that temporarily or permanently impairs brain structure and function. Mass spectrometry analysis of TBI tissue is of interest because chemical information can be obtained to better

understand the extensive biological changes that occur in the brain after injury. Molecular imaging of TBI samples has been reported with MALDI-MS and changes of sphingolipids, glycerophospholipids and cholesterol derivatives in rat brain were observed at the injury site [10, 11]. In another study, injured rat spinal cord was imaged by DESI-MS and free arachidonic acid, lysosulfatide, diacylglycerols were found from the injury sample [12].

Here, we report the imaging of endogenous small metabolites, lipids, and proteins from pig liver sample using LEMS without the requirement of sample washing and FAIMS device. Reversed phase HPLC-MS analysis of liver tissue extract was compared with the LEMS imaging results. The analysis of mouse brain tissue 48 hours following a mild controlled cortical impact TBI was also evaluated. The mass spectra results from TBI area of the mouse brain are compared to non-TBI area by LEMS. Principal component analysis (PCA) was applied to the TBI brain imaging dataset to assist feature extraction from the large dataset.

5.3 Experimental

5.3.1 Chemicals and Materials

Acetic acid, formic acid and HPLC grade methanol, acetonitrile and water (Fisher Scientific, Fair Lawn, NJ) were used as supplied from manufacturer. A mixture of acetonitrile/water (v/v, 50/50) with 0.1% acetic acid was used as the nanospray solvent for all the LEMS measurements.

5.3.2 Traumatic Brain Injury

Eight-week-old male C57BL/6J, also known as B6, mouse (Jackson Laboratory, Bar Harbor, ME) was immobilized under anesthesia in a stereotactic frame. The skull was exposed and a 4 mm craniectomy was performed between the superior sagittal suture and bregma and lambda sutures to expose the somatosensory cortex. A mild TBI was delivered to the cortex over the dura using an Impact One Stereotaxic CCI instrument (Leica Microsystems, Buffalo Grove, IL) to deliver an impact with a 2 mm tip at 1.5 m/s, to a depth of 1 mm, and dwell time of 0.5 s. The site of injury was sealed with a glass coverslip and animal safe adhesive to form a "cranial window". After 48 hours, the mouse was euthanized and perfused with phosphate-buffered saline (PBS). The brain tissue was removed and kept in ice-cooled PBS solution. All procedures that required the use of vertebrate animals were approved by The Institutional Animal Care and Use Committee at Temple University (Philadelphia, PA).

5.3.3 Sample Preparation

Pig liver (Pel-Freez Biologicals, 59423-2, Rogers, AR) was sectioned to 50 μm slices at −20 °C using a cryostat (Leica CM3050 S, Buffalo Grove, IL). The mild TBI mouse brain was sectioned fresh using a vibratome (Leica VT1000 S, Buffalo Grove, IL) to create sections approximately 100 μm thick. The liver and brain sections were mounted on glass microscope slides and stored at −80 °C (U410, New Brunswick Scientific, Enfield, CT). The tissue section slides were brought to room temperature in vacuum desiccator for ~15 min and placed on the sample stage prior to imaging.

Pig liver sample was also homogenized and extracted based on a literature protocol [13]. A liver tissue block was flash-frozen and ground to powder in liquid N_2 by mortar and pestle, and aliquots of 50 mg were extracted in 1.5 mL MeOH:H_2O (1:1, v:v). The mixture was sonicated in ice water bath for 2 mins with 1 min break for three times and subjected for centrifugation at 14000 rpm for 10 minutes (Eppendorf 5417C centrifuge, Hauppauge, NY). The supernatant was transferred to LC vials and subjected to LC-MS analysis.

5.3.4 Laser Electrospray Mass Spectrometry (LEMS) Imaging Source

The LEMS imaging source has been described in detail previously [14]. Briefly, a Ti:Sapphire regenerative amplifier seeded by a Ti:Sapphire oscillator (Legend Elite HE series, Coherent Inc., Santa Clara, CA) generates 2.5 mJ, 50 fs pulses centered at 800 nm. The energy of the pulse was reduced to 1.5 mJ by a quaterwave plate and a beam splitter cube. The attenuated laser pulse was focused onto the sample surface to 100 μm diameter spot with a 10 cm lens at 90° incident angle. The resulting intensity of field was approximately 3.82×10^{14} W/cm^2. A peltier cooled sample stage at 10 °C was placed below the axis from the nanospray needle (MT320-50-5-5, New Objective, Woburn, MA) to a capillary extension tube. The stainless steel extension tube (length 85 mm, OD 2 mm and ID 1 mm) was connected to the capillary inlet of a commercial QTOF mass spectrometer (micrOTOF-Q II, Bruker Daltonik GmbH, Bremen, Germany). The sample stage was scanned with a spot-to-spot distance of 100 μm by a XY microscopy stage (MLS203-1, Thorlabs, Newton, NJ) for all imaging experiments. The laser vaporized analytes were captured and ionized by a nanospray source with 1:1 (v:v) acetonitrile:water with 0.1 %

acetic acid at positive mode. A syringe pump (Model 100, KD Scientific, Holliston, MA) infused the nanospray solvent at a flow rate of 200 nL/min.

Typical parameters of the nanospray source are listed as follows. The nanospray needle and extension tube, separated by 6 mm, were kept at a voltage of 0 and −5 kV, respectively. A stable electrospray was obtained with the aid of countercurrent N_2 gas flow (flow rate 4 L/min, temperature 120 ºC) for desolvation. The sample stage was set to a bias of –2 kV. The vertical distance between the sample slides and the nanospray needle was kept at 3 mm and the laser spot was positioned about 1 mm in front of the needle tip. The spectrometer was calibrated with a 95:5 (v:v) acetonitrile:ESI calibrant solution (#63606-10ML, Fluka Analytical/Sigma Aldrich, Buchs, Switzerland) over a mass range of *m/z* 50–3000. The in-source collision region (ISCID) and collision cell (CID) voltages were set to be 0 and 8 eV, respectively.

5.3.5 LC-MS and LC-MS/MS Analysis

LC-MS analysis was performed using an Agilent 1200 series LC system coupled to 6520 QTOF (Agilent Technologies, Santa Clara, CA). Pig liver extracts were analyzed using a Luna C18, 5 µm, 150 × 3.0 mm column (Phenomenex, Torrance, CA). The mobile phase A = 0.1% formic acid in water and B = 0.1 % formic acid in acetonitrile was used. The flow rate was 0.4 mL/min, and sample injection volume was 5 µL. The reversed phase gradient conditions were: 0 min, 0.1% B; 2 min, 0.1% B; 6 min, 25%; 10 min 80% B; 12 min, 90% B; 21 min, 99.9% B; 23 min 99.9% B; 24 min 0.1% B and 26 min 0.1% B. ESI source conditions were set as follows: gas temperature 300 °C, drying gas 12 L/min, nebulizer 45 psi, fragmentor 215 V, skimmer 65 V, and capillary voltage 4000 V. The

instrument was set to acquire over the *m/z* range 100–1000, with the MS acquisition rate of 1 Hz. For the MS/MS of selected precursors the isolation width was set as medium (4 *m/z*). The collision energy was set at 5×(*m/z*)/100+5 eV for different ions. Tissue extracts and solvent blank samples were run in duplicate.

5.3.6 Data Analysis

Spectral features detected by LC-MS and LEMS were tentatively identified by mass searching in the METLIN metabolites database [15] (https://metlin.scripps.edu/) and the Human Metabolome Database [16] (http://www.hmdb.ca/) with a maximum mass tolerance of 30 ppm. The molecular assignment of the abundant features were also confirmed by collision induced dissociation (CID) in LC-MS and LEMS analyses. Protein identification was enabled by intact mass searching in UniPort database (http://www.uniprot.org/) [17]. Mass spectrometry imaging data was processed by custom written Python scripts and converted to imzML file as described previously [14]. Selected ion images (±0.01 *m/z*) were presented with a second order linear interpolation and plotted as heatmap using MSiReader [18]. Statistical analysis, principal component analysis, was applied to the imaging data using an open source Matlab-based program [19]. The principal component images were presented as heatmap with corresponding loading plots.

5.3.7 Safety Considerations

All lab personnel were required to wear laser safety goggles during the experiments. Insulating and opaque shields protected lab personnel from any exposed high voltage supplies and laser irradiation.

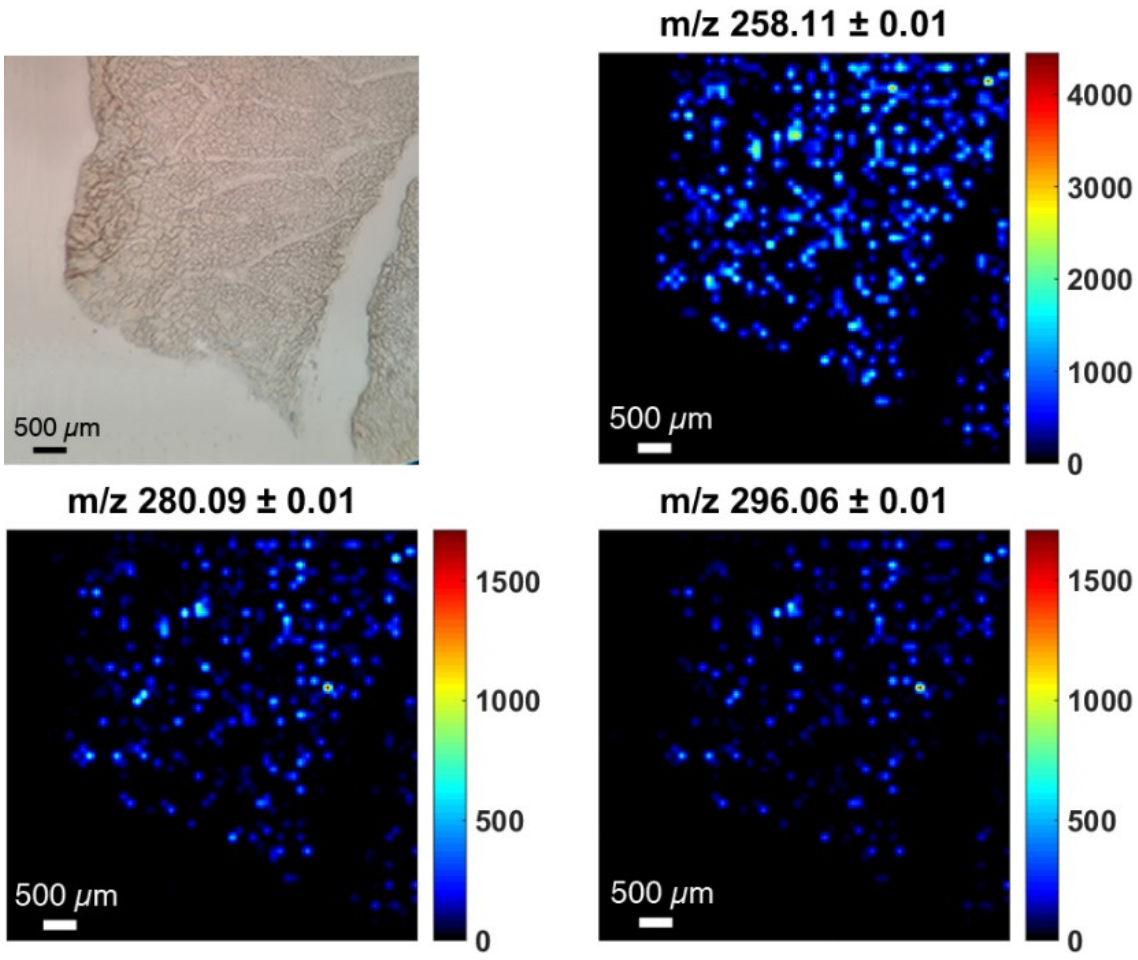

Figure 5.1. Optical image and mass spectrometry images (*m/z* 258.11, 280.09, and 296.06) of a pig liver tissue section on a glass microscope slide.

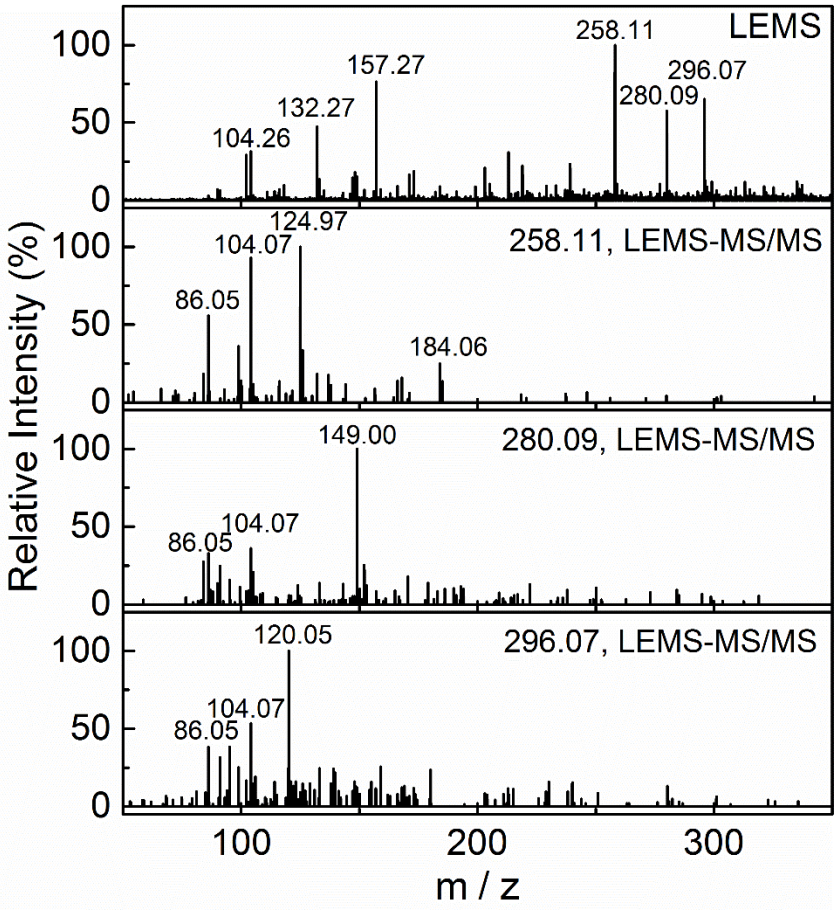

Figure 5.2. Direct MS scan of pig liver tissue by LEMS and MS/MS spectra of *m/z* 258.11, 280.09 and 296.07 ions with a CID energy of 35 eV.

Table 5.1. Tentative assignments of species detected from pig liver by LEMS.

Compounds	Formula	Monoisotopic *m/z*	Measured *m/z*	Mass Error (mDa)
Glycerophosphocholine	$C_8H_{20}NO_6P$	258.1101	258.1076	2.5
Glycerophosphocholine+Na	$C_8H_{20}NO_6PNa$	280.0920	280.0923	0.3
Glycerophosphocholine+K	$C_8H_{20}NO_6PK$	296.0660	296.0629	3.1
Sucrose+Na	$C_{12}H_{22}O_{11}Na$	365.1054	365.1018	3.6
Unidentified			383.1039	
Deoxycholic Acid Glycine Conjugate–H_2O/ Chenodeoxycholic Acid Glycine Conjugate–H_2O	$C_{26}H_{41}O_4$	432.3114	432.3160	4.6
Deoxycholic Acid Glycine Conjugate/ Chenodeoxycholic Acid Glycine Conjugate	$C_{26}H_{43}O_5$	450.3214	450.3176	3.8
LysoPC(16:0)	$C_{24}H_{50}NO_7P$	496.3398	496.3362	3.6
LysoPC(18:2)	$C_{26}H_{50}NO_7P$	520.3398	520.3293	10.5
LysoPC(18:1)	$C_{26}H_{52}NO_7P$	522.3554	522.3448	10.6
LysoPC(18:0)	$C_{26}H_{54}NO_7P$	524.3711	524.3644	6.7
LysoPC(18:0)+Na	$C_{26}H_{54}NO_7PNa$	544.3374	544.3319	5.5
Hemoglobin α subunit 18+			836.5286	
Mono-glycosylated hemoglobin α subunit 18+			845.5440	
Di-glycosylated hemoglobin α subunit 18+			854.4497	
16033.1 Da Protein 18+			891.7149	

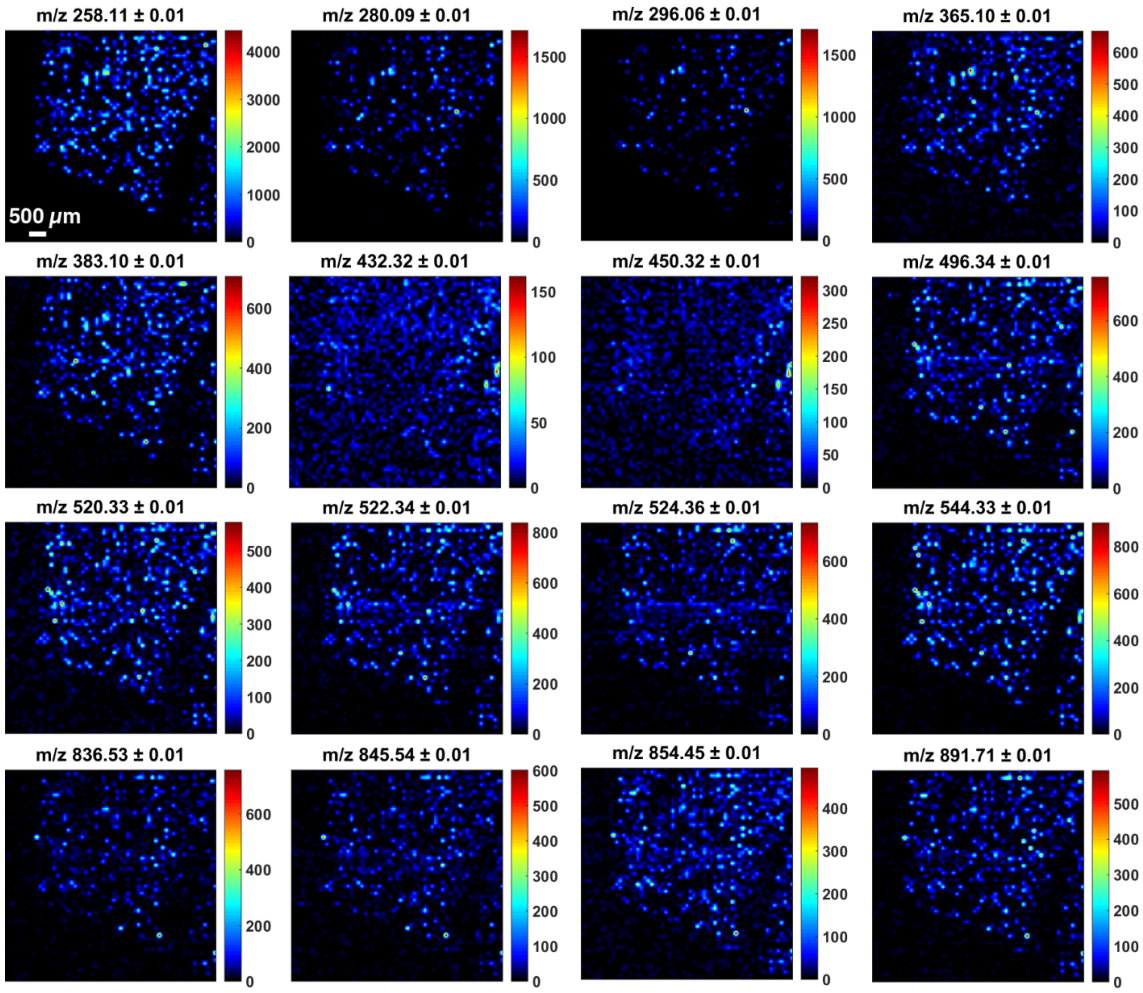

Figure 5.3. Selected ion images of pig liver.

5.4 Results and Discussion

5.4.1 LEMS Imaging of Pig Liver

To test the ability of LEMS to image animal tissue, a pig liver section (an optical image in Figure 5.1) was placed in the ion source and directly analyzed over an area of 6.1 × 6.1 mm^2. The most abundant species was observed at *m/z* 258.11 in Figure 5.1. The ion image of *m/z* 258.11 shows the same tissue pattern as the optical image. The sodium and potassium adducts of the species at *m/z* 258.11 were also observed at *m/z* 280.09 and 296.07, respectively. Exact mass searching in the database suggests the species at *m/z* 258.11 corresponds to glycerophosphocholine (GPC). The identification of GPC and its adducts were further confirmed by the fragmentation pattern using on-tissue tandem mass spectrometry (MS/MS) analysis, as shown in Figure 5.2. A complete list of species detected and identified from the liver is provided in Table 5.1 and corresponding ion images are displayed in Figure 5.2. Ions at *m/z* 450.32 and 432.31 correspond to deoxycholic acid-glycine or chenodeoxycholic acid-glycine conjugate $[M+H]^+$ and the conjugate with the loss of H_2O $[M-H_2O+H]^+$, respectively. Deoxycholic acid or chenodeoxycholic acid is a bile acid that is biosynthesized from cholesterol and will conjugate with glycine [20], and this conjugate has been detected from liver by LC-MS [21]. Several lysophosphatidylcholine (LysoPC) lipids, including LysoPC(16:0), LysoPC(18:2), LysoPC(18:1) and LysoPC(18:0), were also detected and their ion images are shown in Figure 5.3.

Clusters of peaks were observed at the high mass range (*m/z* 600 to 1200) in the single pixel spectrum in Figure 5.4. Deconvoluted results indicate the detection of three multiply charged proteins with a molecular weight of 15038.5, 15200.9, and 15363.3 Da,

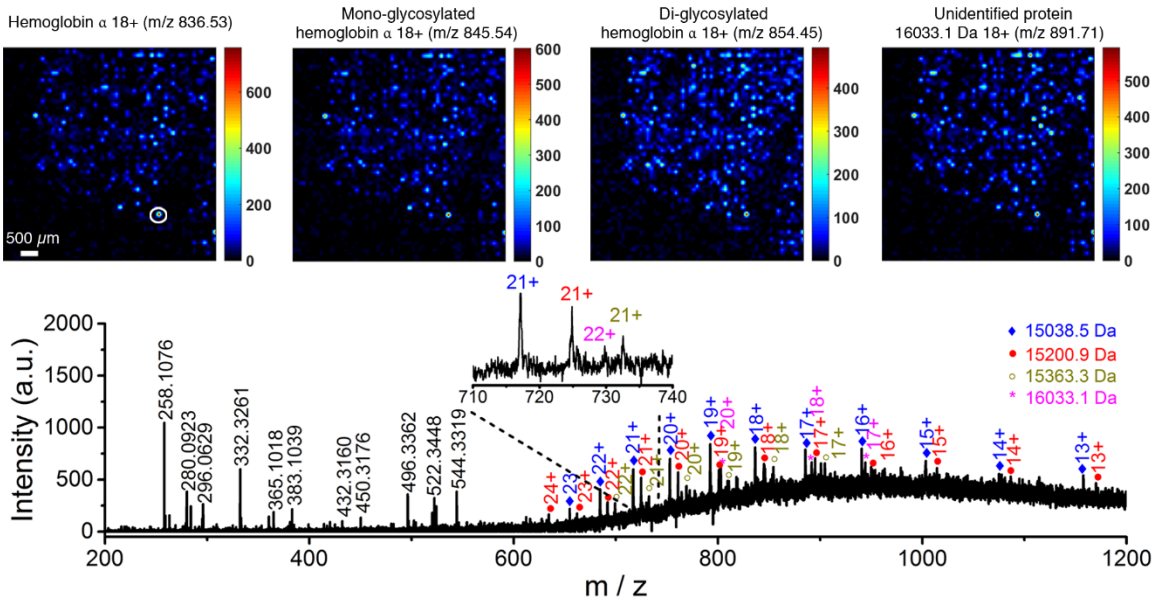

Figure 5.4. Selected ion images of 18+ charge state of hemoglobin α subunit (*m/z* 836.53), mono-glycosylated hemoglobin α subunit (*m/z* 845.54), di-glycosylated hemoglobin α subunit (*m/z* 854.45), and an unidentified protein with a molecular weight of 16033.1 Da (*m/z* 891.71) are shown with the absolute intensity scale. Mass spectrum of selected pixel with circle highlighted in the ion image. Inset shows the enlarged *m/z* 710–740 range.

which correspond to hemoglobin α subunit and the mono-glycosylated and di-glycosylated derivatives. An unidentified protein with a molecular weight of 16033.1 Da is also observed. The broad feature extending from *m/z* 600 to 1000 in the high mass region is likely due to solvent and salt adducts to the proteins, and is consistent with previous examples of the detection of protein from native tissue samples by LESA-MS [1]. In conclusion, small molecules, such as GPC, bile acids and LysoPCs, and large proteins were simultaneously mapped from the liver tissue. This observation shows that LEMS can simultaneously vaporize small metabolites, lipids and proteins into the gas phase for ESI-MS ionization without the use of any matrix or sample pretreatment. All vaporized molecules are detected using a single ESI solvent system regardless of their hydrophobic or hydrophilic nature. The ESI post-ionization process also generates multiply charged proteins with charge states as high as 24+. Protein and glycosylated protein molecules are successfully identified and imaged from pig liver sample by LEMS.

5.4.2 LC-MS and LC-MS/MS Analysis of Pig Liver Extracts

The LEMS imaging of liver provided detailed information about the identity and distribution of a range of liver metabolites, lipids and proteins. LC-MS analysis of the liver extracts was performed to compare with the LEMS measurements. Critical steps in the LC-MS approach include sample preparation and the chromatographic conditions. Typically, different extraction solvents and separation conditions are elucidated for different compound classes, such as small molecules or large proteins. Here, an extraction and LC protocol for small metabolic profiles of tissue extract was adopted [13]. A list of the species found in the pig liver extract by LC-MS is provided on Table 5.2. Figure 5.5 shows the

extracted ion chromatogram of the abundant species. As seen in Figure 5.5, GPC was again detected as the most abundant analyte in the liver extracts, which agrees with the LEMS measurement. The chemical structure of GPC is also confirmed by the corresponding fragment ions in LC-MS/MS analysis shown in Figure 5.6. In addition, small amide molecules, including oleamide, xanthine and hypoxanthine, were detected by LC-MS with their chemical structure confirmed by the fragmentation pattern in LC-MS/MS, as seen in Figure 5.6. The absence of amide species in LEMS measurement might be attributed to the different liver locations sampled by LEMS and LC-MS. Note that, because an extraction and LC protocol for small metabolites was used, the protein species shown by LEMS were not detected by LC-MS.

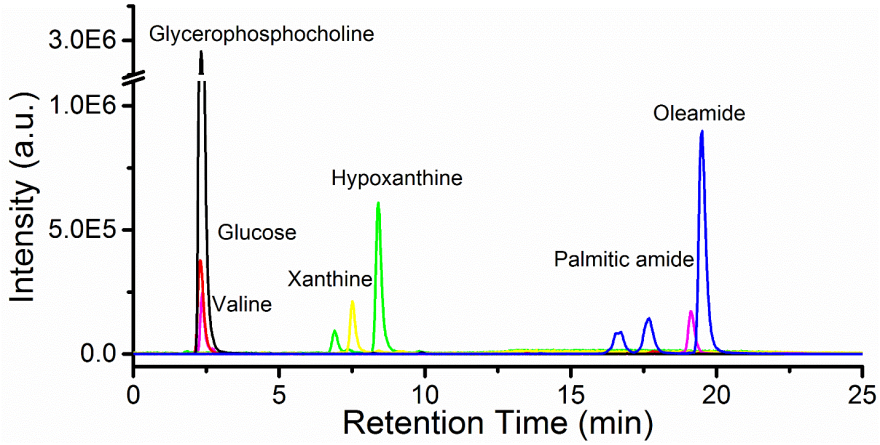

Figure 5.5. Extracted ion chromatogram of representative ions pig liver detected by LC-MS. The isolation width of extracted ion chromatogram is ±0.1.

Table 5.2. Assignments of species detected from pig liver extracts by LC-MS.

Compounds	Retention Time (min)	Formula	Monoisotopic *m/z*	Measured *m/z*
Glycerophosphocholine	2.32	$C_8H_{20}NO_6P$	258.1101	258.1114
Oleamide	19.49	$C_{18}H_{35}NO$	282.2791	282.2818
Hypoxanthine	8.40	$C_5H_4N_4O$	137.0458	137.0463
Phosphocholine	2.29	$C_5H_{14}NO_4P$	184.0733	184.0739
Glucose+Na	2.36	$C_6H_{12}O_6Na$	203.0526	203.0535
Hypoxanthine-H_2O+H	8.43	$C_5H_3N_4$	120.0404	120.0814
PC(4:0/4:0)+Na	2.51	$C_{16}H_{32}NO_8PNa$	420.1758	420.1654
Valine	2.36	$C_5H_{11}NO_2$	118.0863	118.0869
Glycerophosphocholine+Na	2.44	$C_8H_{20}NO_6PNa$	280.0942	280.0935
Xanthine	7.51	$C_5H_4N_4O_2$	153.0407	153.0410
Sucrose+Na	2.63	$C_{12}H_{22}O_{11}Na$	365.1054	365.1074
Palmitic amide	19.12	$C_{16}H_{33}NO$	256.2635	256.2654
Galactosylglycerol+Na	2.76	$C_9H_{18}O_8Na$	277.0894	277.0909
LysoPC(20:4)	17.80	$C_{28}H_{50}NO_7P$	544.3449	544.3441
Phophonoacetaldehyde	2.32	$C_2H_5O_4P$	124.9998	125.0003
Hydroxypinoresinol glucoside	2.41	$C_{26}H_{32}O_{12}$	537.1967	537.1980
Unidentified M-H_2O	14.73			432.3132
Guanine	8.41	$C_5H_5N_5O$	152.0567	152.0570
Unidentified M	14.75			414.3026
Glycerophosphocholine dimer	2.32	$C_{16}H_{40}N_2O_{12}P_2$	515.2176	515.2157
Valine+Na	2.47	$C_5H_{11}NO_2Na$	140.0682	140.0685
Indoleacrylic acid	9.95	$C_{11}H_9NO_2$	188.0706	188.0711
Phosphocholine-H_2O	2.32	$C_5H_{12}NO_3P$	166.0633	166.0630
Halaminol A	17.47	$C_{14}H_{29}NO$	228.2322	228.2335
Glutathione	5.53	$C_{10}H_{17}N_3O_6S$	308.0911	308.0925
Palmitoleamide	17.87	$C_{16}H_{31}NO$	254.2478	254.2494
Folic acid	2.52	$C_{19}H_{19}N_7O_6$	442.1470	442.1472
Glucan+Na	8.41	$C_{18}H_{32}O_{18}Na$	559.1481	559.1539
Xanthine-H_2O+H	7.51	$C_5H_3N_4O$	136.0139	136.0149
Glycerylphosphorylethanolamine	2.22	$C_5H_{14}NO_6P$	216.0632	216.0637
Nicotinuric acid+K	4.48	$C_8H_8N_2O_3K$	219.0167	219.0183
Deoxysepiapterin+Na	2.59	$C_9H_{11}N_5O_2Na$	244.0805	244.0802

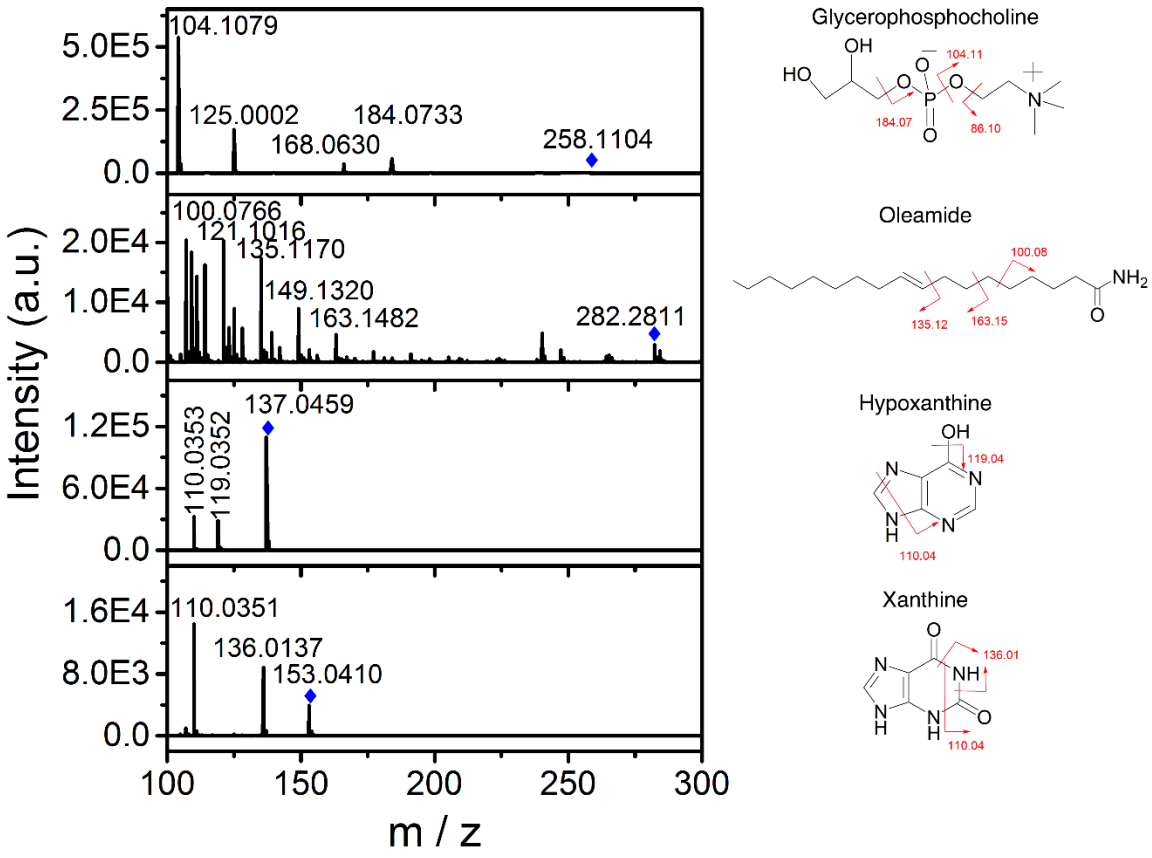

Figure 5.6. LC-MS/MS spectra of selected ions from pig liver extract. The highlighted peaks (♦) correspond to precursor ions selected for MS/MS analysis.

5.4.3 Chemical Imaging of TBI Mouse Brain

To test the capability of LEMS for biomarker discovery, a mild TBI mouse brain section was imaged by LEMS. Figure 5.7 shows the optical image of a TBI mouse brain section with different anatomical structures, including (A) grey matter, (B) white matter, (C) ventricle, and (D) injury site with blood-brain barrier damage. A complete list of the species detected and identified from the brain is provided in Table 5.3 and their distribution is shown in Figure 5.8. A species at *m/z* 268.10, corresponding to adenosine, was observed predominantly in the grey matter region as seen in Figure 5.7. In contrast, several ions, including *m/z* 282.28, 462.32, and 788.61, corresponding to oleamide, an unknown species, and PC(36:1), were exclusively observed in the white matter region in Figure 5.7. The observation of PC(36:1) predominantly at the white matter region agrees with previous studies of mouse brain using MALDI [22] and nano-DESI [23]. On the other hand, species such as PC(32:0) at *m/z* 734.57 (seen in Figure 5.7) distributed on the entire brain region. Note that features corresponding to embedding medium used in the process of vibratome section (seen in Figure 5.7) were observed and their resulting spatial distribution is shown in Figure 5.9. Each of the embedding medium species is observed outside the brain area.

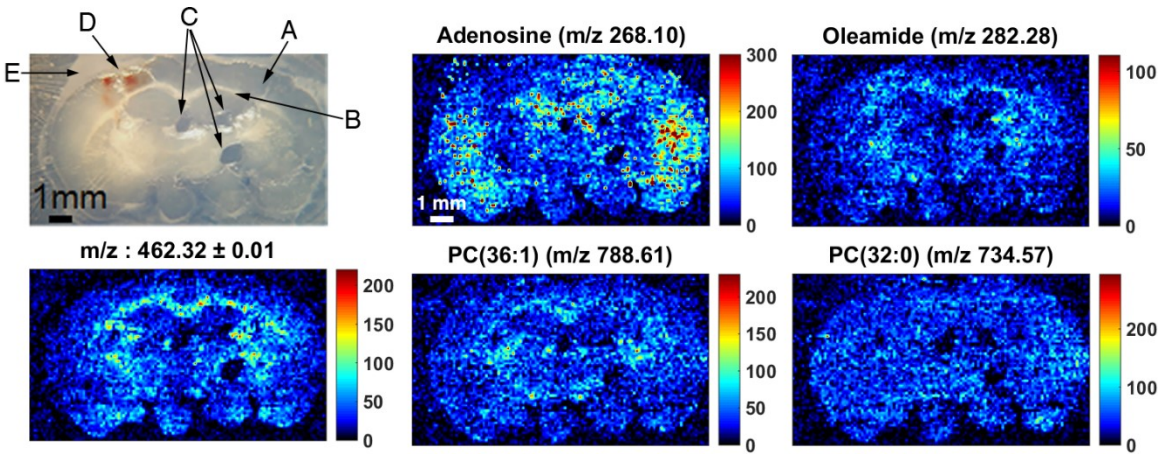

Figure 5.7. Optical image of a mild TBI mouse brain section on a glass microscope slide. A, grey matter; B white matter; C ventricle; D traumatic brain injury; E embedding medium. Selected ion images of *m/z* 268.10, 282.28, 462.32, 788.61, and 734.57, respectively.

Table 5.3. Tentative assignments of species detected from TBI mouse brain by LEMS.

Compounds	Formula	Monoisotopic *m/z*	Measured *m/z*
Adenosine	$C_{10}H_{13}N_5O_4$	268.1040	268.1048
Oleamide	$C_{18}H_{35}NO$	282.2791	282.2797
Unidentified			462.3227
Unidentified			464.3061
LysoPC(16:0)	$C_{24}H_{50}NO_7P$	496.3398	496.3376
CerP(d18:1/8:0)	$C2_6H_{52}NO_6P$	506.3605	506.3529
LysoPC(18:3)	$C_{26}H_{48}NO_7P$	518.3241	518.3249
LysoPC(18:1)	$C_{26}H_{52}NO_7P$	522.3554	522.3499
LysoPC(18:0)	$C_{26}H_{54}NO_7P$	524.3711	524.3563
Heme b	$C_{34}H_{32}O_4N_4Fe$	616.1773	616.1668
Unidentified			630.6144
Unidentified			680.3440
Unidentified			706.3581
PC(32:0)	$C_{40}H_{80}NO_8P$	734.5694	734.5766
PC(32:1)	$C_{41}H_{80}NO_8P$	746.5694	746.5585
PC(34:1)	$C_{42}H_{82}NO_8P$	760.5851	760.5849
PC(36:1)	$C_{44}H_{86}NO_8P$	788.6164	788.6128

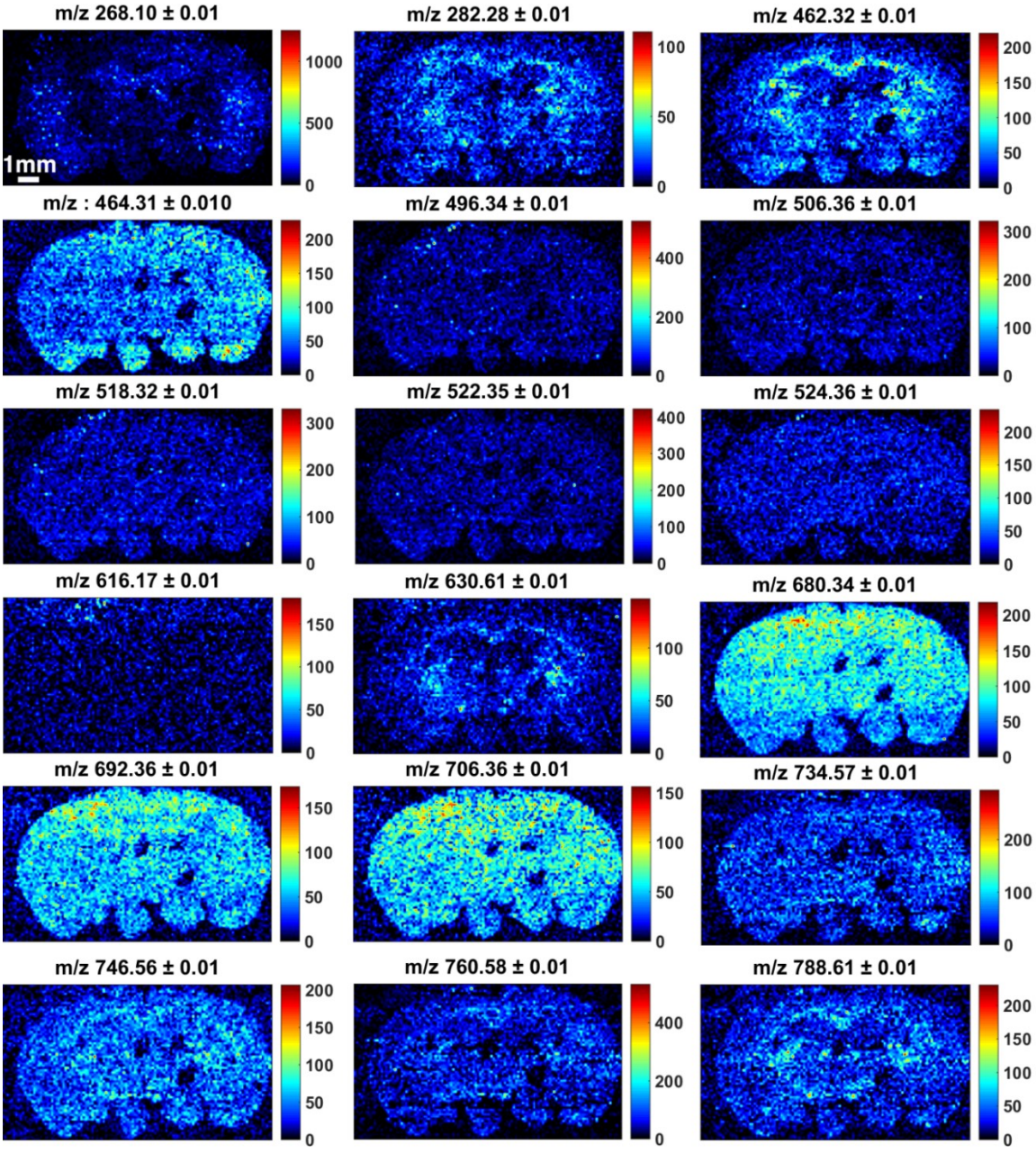

Figure 5.8. Selected ion images of brain species from TBI mouse brain section.

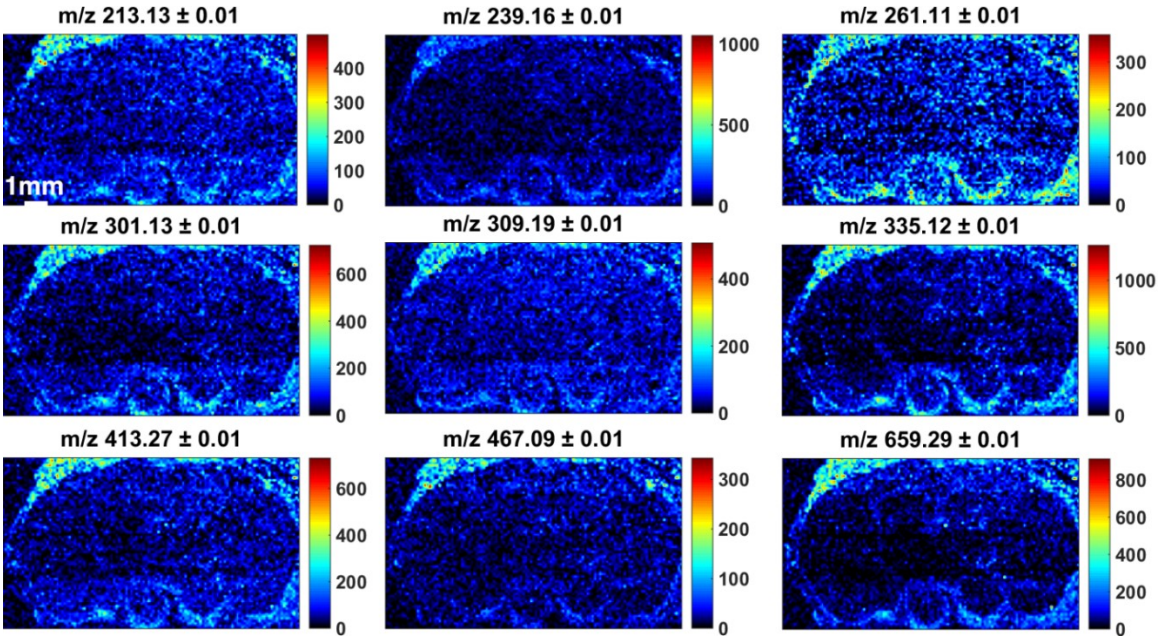

Figure 5.9. Selected ion images, corresponding to embedding medium, in the mouse brain section.

Ion species including singly charged heme b (*m/z* 616.17), 17+ charged hemoglobin α subunit (*m/z* 882.24), and 18+ charged hemoglobin β subunit (*m/z* 868.54) were observed with a localized distribution at the TBI area, seen in Figure 5.10. An overlay of the hemoglobin ion with other brain species were shown in Figure 5.11. As shown in Figure 5.11, peaks corresponding to multiply charged (21+ to 12+) proteins in the mass region (*m/z* 700–1400) were observed from the brain injury area. The deconvoluted molecular mass spectrum suggests the presence of two proteins with molecular masses of 14980.9 and 15616.1 Da, corresponding to mouse hemoglobin α and β subunits, respectively. This is expected after disruption of the blood-brain barrier that is known to occur following brain injury [24]. Hemoglobin in the blood will leak into the brain tissue in the vicinity of the injury site, as also seen in the optical image in Figure 5.7. In a previous high resolution ESI-FTICR-MS measurement, the molecular weight of hemoglobin from two different mouse strains (C3H and B6) was compared, and α chain at 14981 Da and β chain at 15616 Da was detected from B6 black mouse type [25], which is in good agreement with our LEMS imaging measurement of B6 mouse strain type. Interestingly, a lipid, LysoPC(16:0), was observed co-distributed with the hemoglobin ions at the brain injury area as seen in Figure 5.10. Previous studies using MALDI-MS imaging suggested that LysoPC(16:0) will be formed and accumulated in the ischemic injury area as a result of the hydrolysis of PC lipids in the brain upon activation of phospholipase A_2 enzyme [26]. Note that the ion image of adenosine at *m/z* 268.10 in Figure 5.7 indicates that adenosine was absent from TBI area while present abundant at non-TBI area. The loss of adenosine at the TBI area is possibly caused by the interruption of adenosine and adenosine nucleotide metabolism, which was observed in the rat brain following ischemic injury by MALDI-MS imaging

[27]. In addition, two unidentified species at *m/z* 680.34 and 706.35 were observed with elevated intensity at the injury site, as shown in Figure 5.10. These two species accompanied by the adenosine, LysoPC(16:0) and hemoglobin are possible biomarkers that could potentially be used for assessment of TBI.

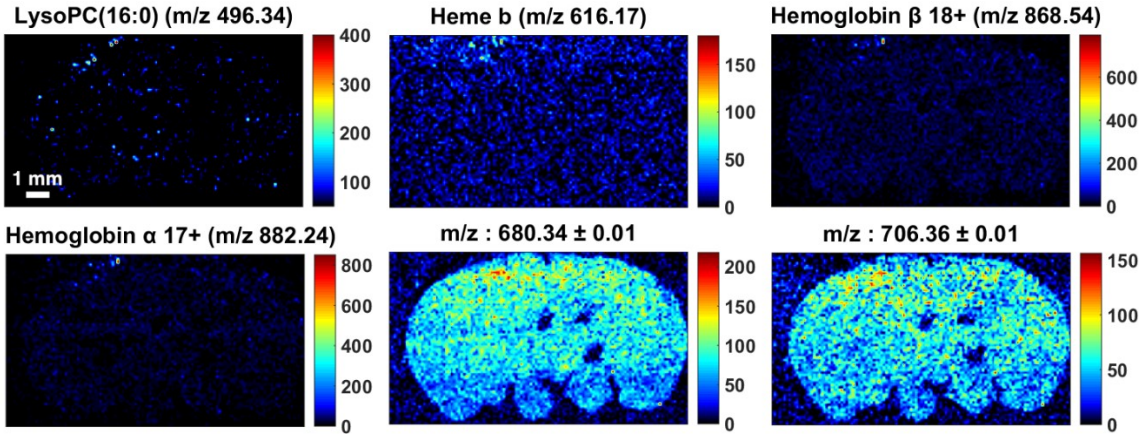

Figure 5.10. Selected ion images of *m/z* 496.34, 616.17, 868.54, 882.24, 680.34, and 706.36, respectively.

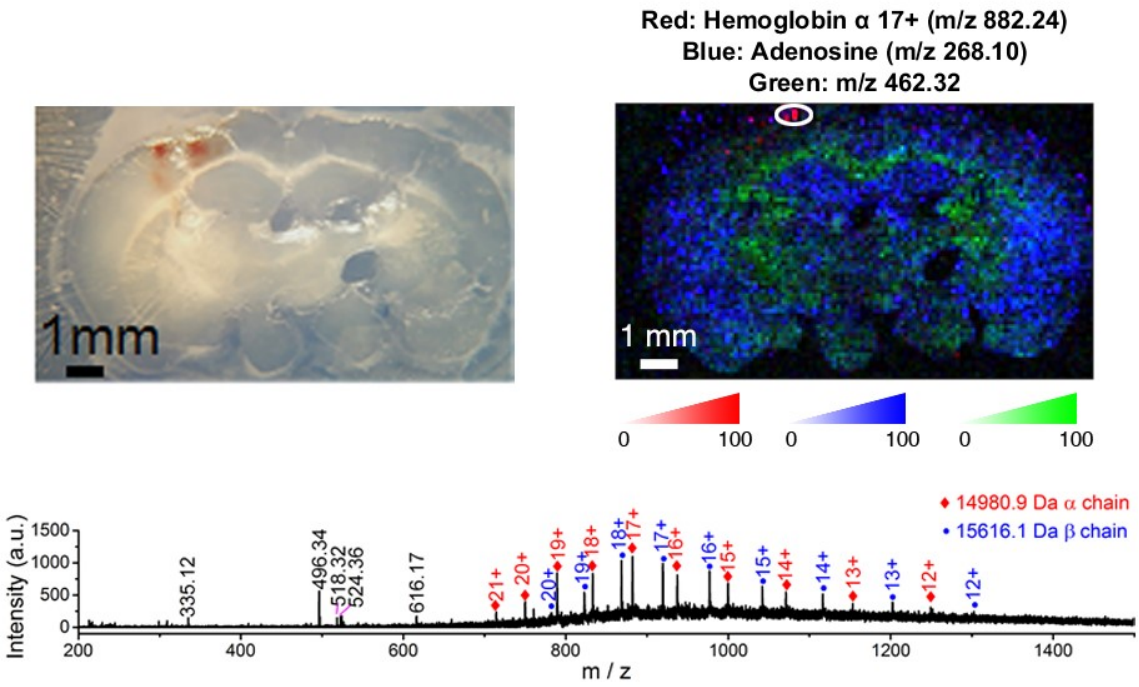

Figure 5.11. Overlay ion images of *m/z* 268.10, 462.32 and 882.24. Extracted mass spectra from the circled area on the ion image.

5.4.4 Principal Component Analysis

The LEMS imaging dataset of TBI mouse brain section is composed of 121 × 70 = 8470 pixels and each pixel has 78000 data points for *m/z* ranging from 50 to 1000, which in theory results in a total number of 78000 MSI images. Although features of interest can be identified by extracting spectra from selected regions as shown in Figure 5.11 and visualizing peaks from the extracted spectra, the large size and high complexity of TBI dataset calls for statistical analysis to assist the evaluation of the large dataset in an efficient and robust way. Here, the imaging dataset is subjected to principal component analysis (PCA), and the component images and spectra are shown in Figure 5.12. Most of the species, including adenosine, LysoPC(16:0) and PC(34:1), are resolved in the brain area in the first principal component image PC1. The distribution of the embedding medium is observed in PC3 with an anti-correlated distribution with respect to brain species in PC1. In the PC7 image, features corresponding to the white matter, as opposed to Figure 5.7, are resolved in the component image. One significant finding by PCA is that the distribution of hemoglobin ion species, representing only <1% of the total pixels, is successfully grouped in PC9 component image with their peaks showing in the loading spectrum. Note that for a homogenous sample like pig liver, tissue related species were grouped only in the first principal component, as seen in Figure 5.13. This example demonstrates that statistical tools such as PCA algorithm can be combined with LEMS to explore the chemical heterogeneity among a complex sample, such as mouse brain, for biomarker detection.

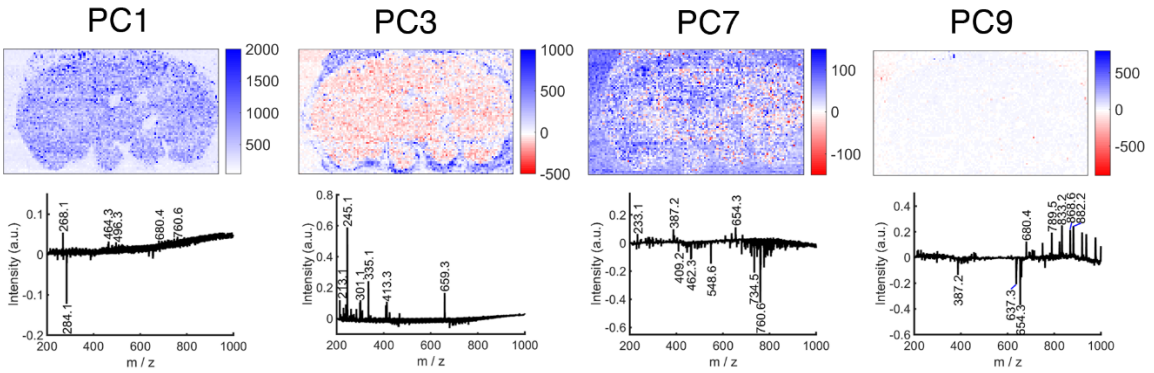

Figure 5.12. Principal component analysis of the TBI mouse brain LEMS imaging data. The principal component images (top) and their corresponding loading plots (bottom) are shown.

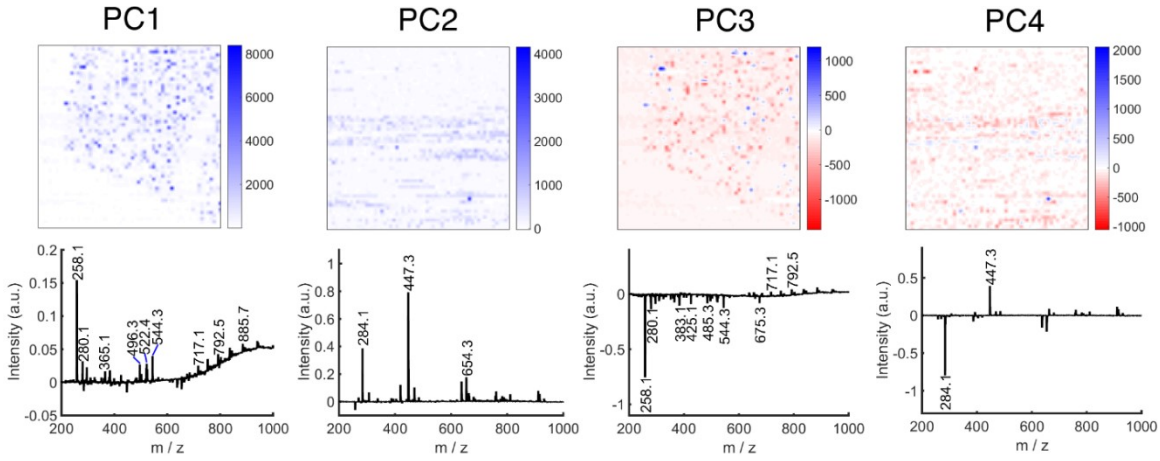

Figure 5.13. Principal component analysis of pig liver LEMS imaging data. The principal component images (top) and their corresponding loading plots (bottom) are shown.

5.5 Conclusions

Mass spectrometry imaging of animal tissue sections were demonstrated by LEMS using single pulse (800 nm, 1.5 mJ, 50 fs) ablation per pixel. Small metabolites, lipids, and large proteins (~15 kDa) were simultaneously measured with the same electrospray solvent system for both pig liver and TBI mouse brain samples without sample pretreatment. Conventional LC-MS analysis of tissue extract was compared with LEMS analysis for pig liver sample, and GPC was observed as the most abundant species in the liver by LEMS and LC-MS. On-tissue MS/MS analysis by LEMS confirms the chemical identification of GPC with the help of fragment ions. In the analysis of the TBI brain injury sample, inner tissue heterogeneity was successfully mapped by species including heme, and hemoglobin as biomarkers for the blood-brain barrier disruption. In addition, the loss of adenosine and increase of LysoPC(16:0) and two other possible biomarkers indicated the chemical changes in the injury area of the brain by LEMS imaging. The heterogeneity of TBI mouse brain sample, including white matter, grey matter and TBI blood-brain barrier damage, was confirmed by principal component analysis.

5.6 References

1. R.L. Griffiths, A.J. Creese, A.M. Race, J. Bunch, H.J. Cooper. LESA FAIMS mass spectrometry for the spatial profiling of proteins from tissue. *Anal. Chem.* **88**, 6758 (2016).

2. C.L. Feider, N. Elizondo, L.S. Eberlin. Ambient ionization and FAIMS mass spectrometry for enhanced imaging of multiply charged molecular ions in biological tissues. *Anal. Chem.* **88**, 11533 (2016).

3. C.-C. Hsu, N.M. White, M. Hayashi, E.C. Lin, T. Poon, I. Banerjee, J. Chen, S.L. Pfaff, E.R. Macagno, P.C. Dorrestein. Microscopy ambient ionization top-down mass spectrometry reveals developmental patterning. *Proc. Natl. Acad. Sci. U.S.A.* **110**, 14855 (2013).

4. C.-C. Hsu, P.-T. Chou, R.N. Zare. Imaging of proteins in tissue samples using nanospray desorption electrospray ionization mass spectrometry. *Anal. Chem.* **87**, 11171 (2015).

5. E.J. Judge, J.J. Brady, D. Dalton, R.J. Levis. Analysis of pharmaceutical compounds from glass, fabric, steel, and wood surfaces at atmospheric pressure using spatially resolved, nonresonant femtosecond laser vaporization electrospray mass spectrometry. *Anal. Chem.* **82**, 3231 (2010).

6. J.J. Brady, E.J. Judge, R.J. Levis. Nonresonant femtosecond laser vaporization of aqueous protein preserves folded structure. *Proc. Natl. Acad. Sci. U.S.A.* **108**, 12217 (2011).

7. K. Strimbu, J.A. Tavel. What are biomarkers? *Curr. Opin. HIV AIDS* **5**, 463 (2010).

8. L.S. Eberlin, I. Norton, A.L. Dill, A.J. Golby, K.L. Ligon, S. Santagata, R.G. Cooks, N.Y.R. Agar. Classifying human brain tumors by lipid imaging with mass spectrometry. *Cancer Res.* **72**, 645 (2012).

9. A.K. Jarmusch, V. Pirro, Z. Baird, E.M. Hattab, A.A. Cohen-Gadol, R.G. Cooks. Lipid and metabolite profiles of human brain tumors by desorption electrospray ionization-MS. *Proc. Natl. Acad. Sci. U.S.A.* **113**, 1486 (2016).

10. J.A. Hankin, S.E. Farias, R.M. Barkley, K. Heidenreich, L.C. Frey, K. Hamazaki, H.-Y. Kim, R.C. Murphy. MALDI mass spectrometric imaging of lipids in rat brain injury models. *J. Am. Soc. Mass Spectrom.* **22**, 1014 (2011).

11. A. Roux, L. Muller, S.N. Jackson, J. Post, K. Baldwin, B. Hoffer, C.D. Balaban, D. Barbacci, J.A. Schultz, S. Gouty, B.M. Cox, A.S. Woods. Mass spectrometry imaging of rat brain lipid profile changes over time following traumatic brain injury. *J. Neurosci. Methods* **272**, 19 (2016).

12. M. Girod, Y. Shi, J.-X. Cheng, R.G. Cooks. Mapping lipid alterations in traumatically injured rat spinal cord by desorption electrospray ionization imaging mass spectrometry. *Anal. Chem.* **83**, 207 (2011).

13. E.J. Want, P. Masson, F. Michopoulos, I.D. Wilson, G. Theodoridis, R.S. Plumb, J. Shockcor, N. Loftus, E. Holmes, J.K. Nicholson. Global metabolic profiling of animal and human tissues via UPLC-MS. *Nat. Protoc.* **8**, 17 (2013).

14. F. Shi, J.J. Archer, R.J. Levis. Nonresonant, femtosecond laser vaporization and electrospray post-ionization mass spectrometry as a tool for biological tissue imaging. *Methods* **104**, 79 (2016).

15. C.A. Smith, G. O'Maille, E.J. Want, C. Qin, S.A. Trauger, T.R. Brandon, D.E. Custodio, R. Abagyan, G. Siuzdak. METLIN - A metabolite mass spectral database. *Ther. Drug Monit.* **27**, 747 (2005).

16. D.S. Wishart, D. Tzur, C. Knox, R. Eisner, A.C. Guo, N. Young, D. Cheng, K. Jewell, D. Arndt, S. Sawhney, C. Fung, L. Nikolai, M. Lewis, M.-A. Coutouly, I. Forsythe, P. Tang, S. Shrivastava, K. Jeroncic, P. Stothard, G. Amegbey, D. Block, D.D. Hau, J. Wagner, J. Miniaci, M. Clements, M. Gebremedhin, N. Guo, Y. Zhang, G.E. Duggan, G.D. MacInnis, A.M. Weljie, R. Dowlatabadi, F. Bamforth, D. Clive, R. Greiner, L. Li, T. Marrie, B.D. Sykes, H.J. Vogel, L. Querengesser. HMDB: the Human Metabolome Database. *Nucleic Acids Res.* **35**, D521 (2007).

17. The UniPort Consortium. UniProt: A hub for protein information. *Nucleic Acids Res.* **43**, D204 (2014).

18. G. Robichaud, K.P. Garrard, J.A. Barry, D.C. Muddiman. MSiReader: An open-source interface to view and analyze high resolving power MS imaging files on Matlab platform. *J. Am. Soc. Mass Spectrom.* **24**, 718 (2013).

19. A.M. Race, R.T. Steven, A.D. Palmer, I.B. Styles, J. Bunch. Memory efficient principal component analysis for the dimensionality reduction of large mass spectrometry imaging data sets. *Anal. Chem.* **85**, 3071 (2013).

20. Sterols: Bile acids and alcohols. http://www.lipidhome.co.uk/lipids/simple/bileacids/index.htm. accessed January 26 2017.

21. Y. Alnouti, I.L. Csanaky, C.D. Klaassen. Quantitative-profiling of bile acids and their conjugates in mouse liver, bile, plasma, and urine using LC–MS/MS. *J. Chromatogr. B* **873**, 209 (2008).

22. H.-Y.J. Wang, S.N.J.J. Post, A.S. Woods. A minimalist approach to MALDI imaging of glycerophospholipids and sphingolipids in rat brain sections. *Int. J. Mass Spectrom.* **278**, 143 (2008).

23. J. Laskin, B.S. Heath, P.J. Roach, L. Cazares, O.J. Semmes. Tissue imaging using nanospray desorption electrospray ionization mass spectrometry. *Anal. Chem.* **84**, 141 (2012).

24. D. Shlosberg, M. Benifla, D. Kaufer, A. Friedman. Blood-brain barrier breakdown as a therapeutic target in traumatic brain injury. *Nat. Rev. Neurol.* **6**, 393 (2010).

25. How does high resolution ES-FTICR-MS under broadband conditions enhance characterization of proteins and peptide mixtures? http://web.ornl.gov/~webworks/cpr/pres/107908_.pdf. accessed December 26 2016.

26. S. Koizumi, S. Yamamoto, T. Hayasaka, Y. Konishi, M. Yamaguchi-Okada, N. Goto-Inoue, Y. Sugiura, M. Setou, H. Namba. Imaging mass spectrometry revealed the production of lyso-phosphatidylcholine in the injured ischemic rat brain. *Neuroscience* **168**, 219 (2010).

27. H. Liu, R. Chen, J. Wang, S. Chen, C. Xiong, J. Wang, J. Hou, Q. He, N. Zhang, Z. Nie, L. Mao. 1,5-Diaminonaphthalene hydrochloride assisted laser desorption/ionization mass spectrometry imaging of small molecules in tissues following focal cerebral ischemia. *Anal. Chem.* **86**, 10114 (2014).

CHAPTER 6

SUMMARY AND OUTLOOK

Combining femtosecond laser vaporization and electrospray ionization in laser electrospray mass spectrometry (LEMS) enables universal surface analysis with minimal or no sample preparation. Previous experiments focused on the direct analysis of a variety of analytes, including synthetic lipids, proteins, pharmaceuticals, explosives, smokeless powders, milk, whole blood, and plant tissues, using a Ti:Sapphire laser amplifier with a low resolution QTOF mass analyzer. In this dissertation, a commercial turn-key, robust femtosecond fiber laser was successfully implemented on a high resolution accurate mass QTOF mass analyzer, and applied for lipids, proteins, and plant and animal tissue sample analysis. The femtosecond fiber laser has longer wavelength, longer pulse duration and lower pulse energy, but was demonstrated with comparable results for the direct surface analysis for small and large molecules in comparison with the Ti:Sapphire laser. The fact that LEMS is viable using the turn-key fiber laser is of interest for the broad and potential applicability of LEMS as a robust, portable, and affordable analytical tool to non-specialists. Future experiments such as the quantitative analysis of complex mixtures and coupling the fiber femtosecond laser with a portable low resolution mass analyzer will be of interest to further assess the potential of LEMS to be a robust ionization source for commercialization.

The imaging capability of LEMS was first shown by scanning oxycodone film deposited on a stainless steel sample slide with 250 μm spatial step size on the low resolution mass analyzer. In this dissertation, molecular imaging by the Ti:Sapphire laser

LEMS was advanced to plant and animal tissue samples. Lateral resolution of 60 μm was obtained by LEMS imaging of a patterned ink film. Metabolites including sugar and anthocyanins were imaged from a leaf sample at a spatial resolution of 100 μm. Small metabolites, lipids and proteins were simultaneously imaged from pig liver and mouse brain samples. Biomarkers corresponding to blood-brain barrier damage and traumatic brain injury (TBI) were detected and imaged from a TBI mouse brain. Statistical analysis tools, such as principal component analysis (PCA), were shown to be useful for automated extraction of features of interest from the large LEMS imaging dataset. These experiments laid the groundwork for the broad application of LEMS for tissue imaging in areas like clinical diagnosis and drug development. For example, imaging of whole-body animal section dosed with a pharmaceutical will be of interest to evaluate the absolute quantification capability of LEMS imaging in comparison with conventional LC-MS analysis.

BIBLIOGRAPHY

Web of Science. www.webofknowledge.com/. accessed Feburay 23 2017.

L. Abrankó, B. Szilvássy. Mass spectrometric profiling of flavonoid glycoconjugates possessing isomeric aglycones. *J. Mass Spectrom.* **50**, 71 (2015).

H.-R. Aerni, D.S. Cornett, R.M. Caprioli. Automated acoustic matrix deposition for MALDI sample preparation. *Anal. Chem.* **78**, 827 (2006).

Y. Alnouti, I.L. Csanaky, C.D. Klaassen. Quantitative-profiling of bile acids and their conjugates in mouse liver, bile, plasma, and urine using LC–MS/MS. *J. Chromatogr. B* **873**, 209 (2008).

A.F.M. Altelaar, I. Klinkert, K. Jalink, R.P.J. de Lange, R.A.H. Adan, R.M.A. Heeren, S.R. Piersma. Gold-enhanced biomolecular surface imaging of cells and tissue by SIMS and MALDI mass spectrometry. *Anal. Chem.* **78**, 734 (2005).

S. Amini-Nik, D. Kraemer, M.L. Cowan, K. Gunaratne, P. Nadesan, B.A. Alman, R.J.D. Miller. Ultrafast mid-IR laser scalpel: Protein signals of the fundamental limits to minimally invasive surgery. *PLoS ONE* **5**, e13053 (2010).

M.J. Bailey, N.J. Bright, R.S. Croxton, S. Francese, L.S. Ferguson, S. Hinder, S. Jickells, B.J. Jones, B.N. Jones, S.G. Kazarian, J.J. Ojeda, R.P. Webb, R. Wolstenholme, S. Bleay. Chemical characterization of latent fingerprints by matrix-assisted laser desorption ionization, time-of-flight secondary ion mass spectrometry, mega electron volt secondary mass spectrometry, gas chromatography/mass spectrometry, X-ray photoelectron spectroscopy, and attenuated total reflection Fourier Transform infrared spectroscopic imaging: An intercomparison. *Anal. Chem.* **84**, 8514 (2012).

M.J. Baker, J. Trevisan, P. Bassan, R. Bhargava, H.J. Butler, K.M. Dorling, P.R. Fielden, S.W. Fogarty, N.J. Fullwood, K.A. Heys, C. Hughes, P. Lasch, P.L. Martin-Hirsch, B. Obinaju, G.D. Sockalingum, J. Sulé-Suso, R.J. Strong, M.J. Walsh, B.R. Wood, P. Gardner, F.L. Martin. Using Fourier Transform IR spectroscopy to analyze biological materials. *Nat. Protoc.* **9**, 1771 (2014).

J.A. Barry, M.R. Groseclose, G. Robichaud, S. Castellino, D.C. Muddiman. Assessing drug and metabolite detection in liver tissue by UV-MALDI and IR-MALDESI mass spectrometry imaging coupled to FT-ICR MS. *Int. J. Mass Spectrom.* **377**, 448 (2015).

J.A. Barry, D.C. Muddiman. Global optimization of the infrared matrix-assisted laser desorption electrospray ionization (IR MALDESI) source for mass spectrometry using statistical design of experiments. *Rapid Commun. Mass Spectrom.* **25**, 3527 (2011).

A. Berisha, S. Dold, S. Guenther, N. Desbenoit, Z. Takats, B. Spengler, A. Römpp. A comprehensive high-resolution mass spectrometry approach for characterization of metabolites by combination of ambient ionization, chromatography and imaging methods. *Rapid Commun. Mass Spectrom.* **28**, 1779 (2014).

S. Berkenkamp, M. Karas, F. Hillenkamp. Ice as a matrix for IR-matrix-assisted laser desorption/ionization: Mass spectra from a protein single crystal. *Proc. Natl. Acad. Sci. U.S.A.* **93**, 7003 (1996).

M. Biesaga, K. Pyrzynska. Liquid chromatography/tandem mass spectrometry studies of the phenolic compounds in honey. *J. Chromatogr. A* **1216**, 6620 (2009).

G. Bracco, B. Holst. *Surface science techniques.* Springer, New York, NY (2013).

J.J. Brady, E.J. Judge, R.J. Levis. Mass spectrometry of intact neutral macromolecules using intense non-resonant femtosecond laser vaporization with electrospray post-ionization. *Rapid Commun. Mass Spectrom.* **23**, 3151 (2009).

J.J. Brady, E.J. Judge, R.J. Levis. Identification of explosives and explosive formulations using laser electrospray mass spectrometry. *Rapid Commun. Mass Spectrom.* **24**, 1659 (2010).

J.J. Brady, E.J. Judge, R.J. Levis. Analysis of amphiphilic lipids and hydrophobic proteins using nonresonant femtosecond laser vaporization with electrospray post-Ionization. *J. Am. Soc. Mass Spectrom.* **22**, 762 (2011).

J.J. Brady, E.J. Judge, R.J. Levis. Nonresonant femtosecond laser vaporization of aqueous protein preserves folded structure. *Proc. Natl. Acad. Sci. U.S.A.* **108**, 12217 (2011).

J.J. Brady, E.J. Judge, R.J. Levis. Reply to Breuker et al.: How laser electrospray mass spectrometry (LEMS) measures condensed phase protein structure, not vacuum structure. *Proc. Natl. Acad. Sci. U.S.A.* **109**, E207 (2012).

K. Breuker, O.S. Skinner, F.W. McLafferty. Femtosecond laser vaporization that preserves protein-folded structure: An unproven idea. *Proc. Natl. Acad. Sci. U.S.A.* **109**, E206 (2012).

J.F. Cahill, V. Kertesz, T.M. Weiskittel, M. Vavrek, C. Freddo, G.J. Van Berkel. Online, absolute quantitation of propranolol from spatially distinct 20- and 40-µm dissections of brain, liver, and kidney thin tissue sections by laser microdissection–liquid vortex capture–mass spectrometry. *Anal. Chem.* **88**, 6026 (2016).

D. Campbell, C. Ferreira, L. Eberlin, R.G. Cooks. Improved spatial resolution in the imaging of biological tissue using desorption electrospray ionization. *Anal. Bioanal. Chem.* **404**, 389 (2012).

C.A. Cassou, H.J. Sterling, A.C. Susa, E.R. Williams. Electrothermal supercharging in mass spectrometry and tandem mass spectrometry of native proteins. *Anal. Chem.* **85**, 138 (2013).

A. Castañeda-Ovando, M.d.L. Pacheco-Hernández, M.E. Páez-Hernández, J.A. Rodríguez, C.A. Galán-Vidal. Chemical studies of anthocyanins: A review. *Food Chem.* **113**, 859 (2009).

P. Chaurand, M. Stoeckli, R.M. Caprioli. Direct profiling of proteins in biological tissue sections by MALDI mass spectrometry. *Anal. Chem.* **71**, 5263 (1999).

H. Chen, A. Venter, R.G. Cooks. Extractive electrospray ionization for direct analysis of undiluted urine, milk and other complex mixtures without sample preparation. *Chem. Commun.* 2042 (2006).

S.-C. Cheng, T.-L. Cheng, H.-C. Chang, J. Shiea. Using laser-induced acoustic desorption/electrospray ionization mass spectrometry to characterize small organic and large biological compounds in the solid state and in solution under ambient conditions. *Anal. Chem.* **81**, 868 (2009).

S.-C. Cheng, Y.-S. Lin, M.-Z. Huang, J. Shiea. Applications of electrospray laser desorption ionization mass spectrometry for document examination. *Rapid Commun. Mass Spectrom.* **24**, 203 (2010).

T.S. Chow. Wetting of rough surfaces. *J. Phys.: Condens. Matter* **10**, L445 (1998).

Sterols: Bile acids and alcohols. http://www.lipidhome.co.uk/lipids/simple/bileacids/index.htm. accessed January 26 2017.

R.B. Cody, J.A. Laramée, H.D. Durst. Versatile new ion source for the analysis of materials in open air under ambient conditions. *Anal. Chem.* **77**, 2297 (2005).

Y. Coello, A.D. Jones, T.C. Gunaratne, M. Dantus. Atmospheric pressure femtosecond laser imaging mass spectrometry. *Anal. Chem.* **82**, 2753 (2010).

T.L. Colliver, C.L. Brummel, M.L. Pacholski, F.D. Swanek, A.G. Ewing, N. Winograd. Atomic and molecular imaging at the single-cell Level with TOF-SIMS. *Anal. Chem.* **69**, 2225 (1997).

J.J. Coon, K.J. McHale, W.W. Harrison. Atmospheric pressure laser desorption/chemical ionization mass spectrometry: A new ionization method based on existing themes. *Rapid Commun. Mass Spectrom.* **16**, 681 (2002).

D. Cotter, A. Maer, C. Guda, B. Saunders, S. Subramaniam. LMPD: LIPID MAPS proteome database. *Nucleic Acids Res.* **34**, D507 (2006).

S.E. Dautel, J.E. Kyle, G. Clair, R.L. Sontag, K.K. Weitz, A.K. Shukla, S.N. Nguyen, Y.-M. Kim, E.M. Zink, T. Luders, C.W. Frevert, S.A. Gharib, J. Laskin, J.P. Carson, T.O. Metz, R.A. Corley, C. Ansong. Lipidomics reveals dramatic lipid compositional changes in the maturing postnatal lung. *Sci. Rep.* **7**, 40555 (2017).

A.M. Delvolve, B. Colsch, A.S. Woods. Highlighting anatomical sub-structures in rat brain tissue using lipid imaging. *Anal. Methods* **3**, 1729 (2011).

R. Digilov. Charge-induced modification of contact angle: The secondary electrocapillary effect. *Langmuir* **16**, 6719 (2000).

A.L. Dill, L.S. Eberlin, C. Zheng, A.B. Costa, D.R. Ifa, L. Cheng, T.A. Masterson, M.O. Koch, O. Vitek, R.G. Cooks. Multivariate statistical differentiation of renal cell carcinomas based on lipidomic analysis by ambient ionization imaging mass spectrometry. *Anal. Bioanal. Chem.* **398**, 2969 (2010).

A.L. Dill, D.R. Ifa, N.E. Manicke, A.B. Costa, J.A. Ramos-Vara, D.W. Knapp, R.G. Cooks. Lipid profiles of canine invasive transitional cell carcinoma of the urinary bladder and adjacent normal tissue by desorption electrospray ionization imaging mass spectrometry. *Anal. Chem.* **81**, 8758 (2009).

R.B. Dixon, J.S. Sampson, A.M. Hawkridge, D.C. Muddiman. Ambient aerodynamic ionization source for remote analyte sampling and mass spectrometric analysis. *Anal. Chem.* **80**, 5266 (2008).

J. Dong. *Merged electrospray ionization mass spectrometry*. Ph.D. Thesis, Louisiana State University, Baton Rouge, LA, (2009).

L.S. Eberlin, A.L. Dill, A.J. Golby, K.L. Ligon, J.M. Wiseman, R.G. Cooks, N.Y.R. Agar. Discrimination of human astrocytoma subtypes by lipid analysis using desorption electrospray ionization imaging mass spectrometry. *Angew. Chem. Int. Ed.* **49**, 5953 (2010).

L.S. Eberlin, M. Gabay, A.C. Fan, A.M. Gouw, R.J. Tibshirani, D.W. Felsher, R.N. Zare. Alteration of the lipid profile in lymphomas induced by MYC overexpression. *Proc. Natl. Acad. Sci. U.S.A.* **111**, 10450 (2014).

L.S. Eberlin, D.R. Ifa, C. Wu, R.G. Cooks. Three-dimensional vizualization of mouse brain by lipid analysis using ambient ionization mass spectrometry. *Angew. Chem. Int. Ed.* **49**, 873 (2010).

L.S. Eberlin, X. Liu, C.R. Ferreira, S. Santagata, N.Y.R. Agar, R.G. Cooks. Desorption electrospray ionization then MALDI mass spectrometry imaging of lipid and protein distributions in single tissue sections. *Anal. Chem.* **83**, 8366 (2011).

L.S. Eberlin, I. Norton, A.L. Dill, A.J. Golby, K.L. Ligon, S. Santagata, R.G. Cooks, N.Y.R. Agar. Classifying human brain tumors by lipid imaging with mass spectrometry. *Cancer Res.* **72**, 645 (2012).

L.S. Eberlin, I. Norton, D. Orringer, I.F. Dunn, X. Liu, J.L. Ide, A.K. Jarmusch, K.L. Ligon, F.A. Jolesz, A.J. Golby, S. Santagata, N.Y.R. Agar, R.G. Cooks. Ambient mass spectrometry for the intraoperative molecular diagnosis of human brain tumors. *Proc. Natl. Acad. Sci. U.S.A.* **110**, 1611 (2013).

S.E. Edison, L.A. Lin, B.M. Gamble, J. Wong, K. Zhang. Surface swabbing technique for the rapid screening for pesticides using ambient pressure desorption ionization with high-resolution mass spectrometry. *Rapid Commun. Mass Spectrom.* **25**, 127 (2011).

M. Ekelöf, E.K. McMurtrie, M. Nazari, S.D. Johanningsmeier, D.C. Muddiman. Direct analysis of triterpenes from high-salt fermented cucumbers using infrared matrix-assisted laser desorption electrospray ionization (IR-MALDESI). *J. Am. Soc. Mass Spectrom.* **28**, 370 (2017).

S.R. Ellis, C. Wu, J.M. Deeley, X. Zhu, R.J.W. Truscott, M.i.h. Panhuis, R.G. Cooks, T.W. Mitchell, S.J. Blanksby. Imaging of human lens lipids by desorption electrospray ionization mass spectrometry. *J. Am. Soc. Mass Spectrom.* **21**, 2095 (2010).

C.L. Feider, N. Elizondo, L.S. Eberlin. Ambient ionization and FAIMS mass spectrometry for enhanced imaging of multiply charged molecular ions in biological tissues. *Anal. Chem.* **88**, 11533 (2016).

J.B. Fenn, M. Mann, C.K. Meng, S.F. Wong, C.M. Whitehouse. Electrospray ionization for mass spectrometry of large biomolecules. *Science* **246**, 64 (1989).

M.E. Fermann, I. Hartl. Ultrafast fibre lasers. *Nat. Photon.* **7**, 868 (2013).

P.M. Flanigan, J.J. Brady, E.J. Judge, R.J. Levis. Determination of inorganic improvised explosive device signatures using laser electrospray mass spectrometry detection with offline classification. *Anal. Chem.* **83**, 7115 (2011).

P.M. Flanigan, R.J. Levis. Ambient femtosecond laser vaporization and nanosecond laser desorption electrospray ionization mass spectrometry. *Annu. Rev. Anal. Chem.* **7**, 229 (2014).

P.M. Flanigan, J.J. Perez, S. Karki, R.J. Levis. Quantitative measurements of small molecule mixtures using laser electrospray mass spectrometry. *Anal. Chem.* **85**, 3629 (2013).

P.M. Flanigan, L.L. Radell, J.J. Brady, R.J. Levis. Differentiation of eight phenotypes and discovery of potential biomarkers for a single plant organ class using laser electrospray mass spectrometry and multivariate statistical analysis. *Anal. Chem.* **84**, 6225 (2012).

P.M. Flanigan, F. Shi, J.J. Archer, R.J. Levis. Internal energy deposition for low energy, femtosecond laser vaporization and nanospray post-ionization mass spectrometry using thermometer ions. *J. Am. Soc. Mass Spectrom.* **26**, 716 (2015).

P.M. Flanigan, F. Shi, J.J. Perez, S. Karki, C. Pfeiffer, C. Schafmeister, R.J. Levis. Determination of internal energy distributions of laser electrospray mass spectrometry using thermometer ions and other biomolecules. *J. Am. Soc. Mass Spectrom.* **25**, 1572 (2014).

T.A. Fligge, J. Kast, K. Bruns, M. Przybylski. Direct monitoring of protein-chemical reactions utilising nanoelectrospray mass spectrometry. *J. Am. Soc. Mass Spectrom.* **10**, 112 (1999).

R. Freyre, C. Uzdevenes, L. Gu, K.H. Quesenberry. Genetics and anthocyanin analysis of flower color in Mexican Petunia. *J. Am. Soc. Hortic. Sci.* **140**, 45 (2015).

S.D. Fuerstenau, W.H. Benner, J.J. Thomas, C. Brugidou, B. Bothner, G. Siuzdak. Mass spectrometry of an intact virus. *Angew. Chem. Int. Ed.* **40**, 541 (2001).

S. Georgiou, A. Koubenakis. Laser-induced material ejection from model molecular solids and liquids: Mechanisms, implications, and applications. *Chem. Rev.* **103**, 349 (2003).

M. Girod, Y. Shi, J.-X. Cheng, R.G. Cooks. Desorption electrospray ionization imaging mass spectrometry of lipids in rat spinal cord. *J. Am. Soc. Mass Spectrom.* **21**, 1177 (2010).

M. Girod, Y. Shi, J.-X. Cheng, R.G. Cooks. Mapping lipid alterations in traumatically injured rat spinal cord by desorption electrospray ionization imaging mass spectrometry. *Anal. Chem.* **83**, 207 (2011).

M.M. Giusti, L.E. Rodríguez-Saona, D. Griffin, R.E. Wrolstad. Electrospray and tandem mass spectroscopy as tools for anthocyanin characterization. *J. Agric. Food Chem.* **47**, 4657 (1999).

D. Gode, D.A. Volmer. Lipid imaging by mass spectrometry - A review. *Analyst* **138**, 1289 (2013).

N.V. Gogichaeva, T. Williams, M.A. Alterman. MALDI TOF/TOF tandem mass spectrometry as a new tool for amino acid analysis. *J. Am. Soc. Mass Spectrom.* **18**, 279 (2007).

F.M. Green, T.L. Salter, I.S. Gilmore, P. Stokes, G. O'Connor. The effect of electrospray solvent composition on desorption electrospray ionisation (DESI) efficiency and spatial resolution. *Analyst* **135**, 731 (2010).

R.L. Griffiths, A.J. Creese, A.M. Race, J. Bunch, H.J. Cooper. LESA FAIMS mass spectrometry for the spatial profiling of proteins from tissue. *Anal. Chem.* **88**, 6758 (2016).

J.H. Gross. *Mass spectrometry: A textbook.* Springer, Berlin Heidelberg (2011).

M. Haapala, J. Pól, V. Saarela, V. Arvola, T. Kotiaho, R.A. Ketola, S. Franssila, T.J. Kauppila, R. Kostiainen. Desorption atmospheric pressure photoionization. *Anal. Chem.* **79**, 7867 (2007).

Z. Hall, C.V. Robinson. Do charge state signatures guarantee protein conformations? *J. Am. Soc. Mass Spectrom.* **23**, 1161 (2012).

J.A. Hankin, R.M. Barkley, R.C. Murphy. Sublimation as a method of matrix application for mass spectrometric imaging. *J. Am. Soc. Mass Spectrom.* **18**, 1646 (2007).

J.A. Hankin, S.E. Farias, R.M. Barkley, K. Heidenreich, L.C. Frey, K. Hamazaki, H.-Y. Kim, R.C. Murphy. MALDI mass spectrometric imaging of lipids in rat brain injury models. *J. Am. Soc. Mass Spectrom.* **22**, 1014 (2011).

J.D. Harper, N.A. Charipar, C.C. Mulligan, X. Zhang, R.G. Cooks, Z. Ouyang. Low-temperature plasma probe for ambient desorption ionization. *Anal. Chem.* **80**, 9097 (2008).

G.A. Harris, A.S. Galhena, F.M. Fernández. Ambient sampling/ionization mass spectrometry: Applications and current trends. *Anal. Chem.* **83**, 4508 (2011).

F. He, N.-N. Liang, L. Mu, Q.-H. Pan, J. Wang, M.J. Reeves, C.-Q. Duan. Anthocyanins and their variation in red wines I. Monomeric anthocyanins and their color expression. *Molecules* **17**, 1571 (2012).

A.J.R. Heck. Native mass spectrometry: A bridge between interactomics and structural biology. *Nat. Methods* **5**, 927 (2008).

R.M.A. Heeren. Getting the picture: The coming of age of imaging MS. *Int. J. Mass Spectrom.* **377**, 672 (2015).

R.R. Hensel, R.C. King, K.G. Owens. Electrospray sample preparation for improved quantitation in matrix-assisted laser desorption/ionization time-of-flight mass spectrometry. *Rapid Commun. Mass Spectrom.* **11**, 1785 (1997).

How does high resolution ES-FTICR-MS under broadband conditions enhance characterization of proteins and peptide mixtures? http://web.ornl.gov/~webworks/cpr/pres/107908_.pdf. accessed December 26 2016.

F. Hillenkamp, E. UnsoLd, R. Kaufmann, R. Nitsche. Laser microprobe mass analysis of organic materials. *Nature* **256**, 119 (1975).

D. Hölscher, R. Shroff, K. Knop, M. Gottschaldt, A. Crecelius, B. Schneider, D.G. Heckel, U.S. Schubert, A. Svatoš. Matrix-free UV-laser desorption/ionization (LDI) mass spectrometric imaging at the single-cell level: distribution of secondary metabolites of Arabidopsis thaliana and Hypericum species. *Plant J.* **60**, 907 (2009).

C.-C. Hsu, P.-T. Chou, R.N. Zare. Imaging of proteins in tissue samples using nanospray desorption electrospray ionization mass spectrometry. *Anal. Chem.* **87**, 11171 (2015).

C.-C. Hsu, N.M. White, M. Hayashi, E.C. Lin, T. Poon, I. Banerjee, J. Chen, S.L. Pfaff, E.R. Macagno, P.C. Dorrestein. Microscopy ambient ionization top-down mass spectrometry reveals developmental patterning. *Proc. Natl. Acad. Sci. U.S.A.* **110**, 14855 (2013).

M.-Z. Huang, S.-C. Cheng, Y.-T. Cho, J. Shiea. Ambient ionization mass spectrometry: A tutorial. *Anal. Chim. Acta* **702**, 1 (2011).

M.-Z. Huang, S.-C. Cheng, S.-S. Jhang, C.-C. Chou, C.-N. Cheng, J. Shiea, I.A. Popov, E.N. Nikolaev. Ambient molecular imaging of dry fungus surface by electrospray laser desorption ionization mass spectrometry. *Int. J. Mass Spectrom.* **325–327**, 172 (2012).

M.-Z. Huang, H.-J. Hsu, L.-Y. Lee, J. Jeng, J. Shiea. Direct protein detection from biological media through electrospray-assisted laser desorption ionization/mass spectrometry. *J. Proteome Res.* **5**, 1107 (2006).

M.-Z. Huang, S.-S. Jhang, C.-N. Cheng, S.-C. Cheng, J. Shiea. Effects of matrix, electrospray solution, and laser light on the desorption and ionization mechanisms in electrospray-assisted laser desorption ionization mass spectrometry. *Analyst* **135**, 759 (2010).

D.R. Ifa, N.E. Manicke, A.L. Dill, R.G. Cooks. Latent fingerprint chemical imaging by mass spectrometry. *Science* **321**, 805 (2008).

P.F. James, M.A. Perugini, R.A.J. O'Hair. Sources of artefacts in the electrospray ionization mass spectra of saturated diacylglycerophosphocholines: From condensed phase hydrolysis reactions through to gas phase intercluster reactions. *J. Am. Soc. Mass Spectrom.* **17**, 384 (2006).

A.K. Jarmusch, V. Pirro, Z. Baird, E.M. Hattab, A.A. Cohen-Gadol, R.G. Cooks. Lipid and metabolite profiles of human brain tumors by desorption electrospray ionization-MS. *Proc. Natl. Acad. Sci. U.S.A.* **113**, 1486 (2016).

E.A. Jones, S.-O. Deininger, P.C.W. Hogendoorn, A.M. Deelder, L.A. McDonnell. Imaging mass spectrometry statistical analysis. *J. Proteomics* **75**, 4962 (2012).

N. Jowett, W. Wöllmer, A.M. Mlynarek, et al. Heat generation during ablation of porcine skin with erbium:yAg laser vs a novel picosecond infrared laser. *JAMA Otolaryngol. Head Neck Surg.* **139**, 828 (2013).

E.J. Judge, J.J. Brady, P.E. Barbano, R.J. Levis. Nonresonant femtosecond laser vaporization with electrospray postionization for ex vivo plant tissue typing using compressive linear classification. *Anal. Chem.* **83**, 2145 (2011).

E.J. Judge, J.J. Brady, D. Dalton, R.J. Levis. Analysis of pharmaceutical compounds from glass, fabric, steel, and wood surfaces at atmospheric pressure using spatially

resolved, nonresonant femtosecond laser vaporization electrospray mass spectrometry. *Anal. Chem.* **82**, 3231 (2010).

E.J. Judge, J.J. Brady, R.J. Levis. Mass analysis of biological macromolecules at atmospheric pressure using nonresonant femtosecond laser vaporization and electrospray ionization. *Anal. Chem.* **82**, 10203 (2010).

R. Juraschek, T. Dülcks, M. Karas. Nanoelectrospray—more than just a minimized-flow electrospray ionization source. *J. Am. Soc. Mass Spectrom.* **10**, 300 (1999).

B.K. Kaletaş, I.M. van der Wiel, J. Stauber, J.D. Lennard, C. Güzel, J.M. Kros, T.M. Luider, R.M.A. Heeren. Sample preparation issues for tissue imaging by imaging MS. *Proteomics* **9**, 2622 (2009).

M. Karas, D. Bachmann, U. Bahr, F. Hillenkamp. Matrix-assisted ultraviolet laser desorption of non-volatile compounds. *Int. J. Mass Spectrom. Ion Processes* **78**, 53 (1987).

M. Karas, F. Hillenkamp. Laser desorption ionization of proteins with molecular masses exceeding 10,000 daltons. *Anal. Chem.* **60**, 2299 (1988).

V. Kertesz, G.J. Van Berkel. Fully automated liquid extraction-based surface sampling and ionization using a chip-based robotic nanoelectrospray platform. *J. Mass Spectrom.* **45**, 252 (2010).

V. Kertesz, G.J. Van Berkel, M. Vavrek, K.A. Koeplinger, B.B. Schneider, T.R. Covey. Comparison of drug distribution images from whole-body thin tissue sections obtained using desorption electrospray ionization tandem mass spectrometry and autoradiography. *Anal. Chem.* **80**, 5168 (2008).

D. Kessner, M. Chambers, R. Burke, D. Agus, P. Mallick. ProteoWizard: Open source software for rapid proteomics tools development. *Bioinformatics* **24**, 2534 (2008).

I. Klinkert, K. Chughtai, S.R. Ellis, R.M.A. Heeren. Methods for full resolution data exploration and visualization for large 2D and 3D mass spectrometry imaging datasets. *Int. J. Mass Spectrom.* **362**, 40 (2014).

S. Koizumi, S. Yamamoto, T. Hayasaka, Y. Konishi, M. Yamaguchi-Okada, N. Goto-Inoue, Y. Sugiura, M. Setou, H. Namba. Imaging mass spectrometry revealed the production of lyso-phosphatidylcholine in the injured ischemic rat brain. *Neuroscience* **168**, 219 (2010).

V.V. Laiko, M.A. Baldwin, A.L. Burlingame. Atmospheric pressure matrix-assisted laser desorption/ionization mass spectrometry. *Anal. Chem.* **72**, 652 (2000).

V.V. Laiko, A.L. Burlingame. *Atmospheric pressure matrix assisted laser desorption.* U.S. Patent 5965884 (1999).

I. Lanekoff, K. Burnum-Johnson, M. Thomas, J. Cha, S.K. Dey, P. Yang, M.C. Prieto Conaway, J. Laskin. Three-dimensional imaging of lipids and metabolites in tissues by nanospray desorption electrospray ionization mass spectrometry. *Anal. Bioanal. Chem.* **407**, 2063 (2015).

I. Lanekoff, K. Burnum-Johnson, M. Thomas, J. Short, J.P. Carson, J. Cha, S.K. Dey, P. Yang, M.C. Prieto Conaway, J. Laskin. High-speed tandem mass spectrometric in situ imaging by nanospray desorption electrospray ionization mass spectrometry. *Anal. Chem.* **85**, 9596 (2013).

I. Lanekoff, O. Geydebrekht, G.E. Pinchuk, A.E. Konopka, J. Laskin. Spatially resolved analysis of glycolipids and metabolites in living Synechococcus sp. PCC 7002 using nanospray desorption electrospray ionization. *Analyst* **138**, 1971 (2013).

I. Lanekoff, B.S. Heath, A. Liyu, M. Thomas, J.P. Carson, J. Laskin. Automated platform for high-resolution tissue imaging using nanospray desorption electrospray ionization mass spectrometry. *Anal. Chem.* **84**, 8351 (2012).

J. Laskin, B.S. Heath, P.J. Roach, L. Cazares, O.J. Semmes. Tissue imaging using nanospray desorption electrospray ionization mass spectrometry. *Anal. Chem.* **84**, 141 (2012).

J. Laskin, I. Lanekoff. Ambient mass spectrometry imaging using direct liquid extraction techniques. *Anal. Chem.* **88**, 52 (2016).

A.C. Leney, A.J.R. Heck. Native mass spectrometry: What is in the name? *J. Am. Soc. Mass Spectrom.* **28**, 5 (2017).

B. Li, N. Bjarnholt, S.H. Hansen, C. Janfelt. Characterization of barley leaf tissue using direct and indirect desorption electrospray ionization imaging mass spectrometry. *J. Mass Spectrom.* **46**, 1241 (2011).

B. Li, S.H. Hansen, C. Janfelt. Direct imaging of plant metabolites in leaves and petals by desorption electrospray ionization mass spectrometry. *Int. J. Mass Spectrom.* **348**, 15 (2013).

H. Li, P. Balan, A. Vertes. Molecular imaging of growth, metabolism, and antibiotic inhibition in bacterial colonies by laser ablation electrospray ionization mass spectrometry. *Angew. Chem. Int. Ed.* **55**, 15035 (2016).

H. Li, B.K. Smith, L. Márk, P. Nemes, J. Nazarian, A. Vertes. Ambient molecular imaging by laser ablation electrospray ionization mass spectrometry with ion mobility separation. *Int. J. Mass Spectrom.* **377**, 681 (2015).

S. Li, Y. Zhang, J.a. Liu, J. Han, M. Guan, H. Yang, Y. Lin, S. Xiong, Z. Zhao. Electrospray deposition device used to precisely control the matrix crystal to improve the performance of MALDI MSI. *Sci. Rep.* **6**, 37903 (2016).

W. Li, J. Zhang, F.L.S. Tse. *Handbook of LC-MS bioanalysis: Best practices, experimental protocols, and regulations.* John Wiley & Sons Inc., Hoboken, NJ (2013).

Y. Li, B. Shrestha, A. Vertes. Atmospheric pressure molecular imaging by infrared MALDI mass spectrometry. *Anal. Chem.* **79**, 523 (2007).

Y. Li, B. Shrestha, A. Vertes. Atmospheric pressure infrared MALDI imaging mass spectrometry for plant metabolomics. *Anal. Chem.* **80**, 407 (2008).

J.W. Lichtman, J.-A. Conchello. Fluorescence microscopy. *Nat. Methods* **2**, 910 (2005).

H. Liu, R. Chen, J. Wang, S. Chen, C. Xiong, J. Wang, J. Hou, Q. He, N. Zhang, Z. Nie, L. Mao. 1,5-Diaminonaphthalene hydrochloride assisted laser desorption/ionization mass spectrometry imaging of small molecules in tissues following focal cerebral ischemia. *Anal. Chem.* **86**, 10114 (2014).

J.A. Loo. Studying noncovalent protein complexes by electrospray ionization mass spectrometry. *Mass Spectrom. Rev.* **16**, 1 (1997).

L. Luosujärvi, S. Kanerva, V. Saarela, S. Franssila, R. Kostiainen, T. Kotiaho, T.J. Kauppila. Environmental and food analysis by desorption atmospheric pressure photoionization-mass spectrometry. *Rapid Commun. Mass Spectrom.* **24**, 1343 (2010).

S.L. Luxembourg, T.H. Mize, L.A. McDonnell, R.M.A. Heeren. High-spatial resolution mass spectrometric imaging of peptide and protein distributions on a surface. *Anal. Chem.* **76**, 5339 (2004).

Y.K. Magnusson, P. Friberg, P. Sjövall, J. Malm, Y. Chen. TOF-SIMS analysis of lipid accumulation in the skeletal muscle of ob/ob mice. *Obesity* **16**, 2745 (2008).

N.E. Manicke, M. Nefliu, C. Wu, J.W. Woods, V. Reiser, R.C. Hendrickson, R.G. Cooks. Imaging of lipids in atheroma by desorption eectrospray ionization mass spectrometry. *Anal. Chem.* **81**, 8702 (2009).

N.E. Manicke, Q. Yang, H. Wang, S. Oradu, Z. Ouyang, R.G. Cooks. Assessment of paper spray ionization for quantitation of pharmaceuticals in blood spots. *Int. J. Mass Spectrom.* **300**, 123 (2011).

E. Margoliash. Primary structure and evolution of cytochrome c. *Proc. Natl. Acad. Sci. U.S.A.* **50**, 672 (1963).

A. Matusch, L.S. Fenn, C. Depboylu, M. Klietz, S. Strohmer, J.A. McLean, J.S. Becker. Combined elemental and biomolecular mass spectrometry imaging for probing the inventory of tissue at a micrometer scale. *Anal. Chem.* **84**, 3170 (2012).

L.A. McDonnell, R.M.A. Heeren. Imaging mass spectrometry. *Mass Spectrom. Rev.* **26**, 606 (2007).

H. Meistermann, J.L. Norris, H.-R. Aerni, D.S. Cornett, A. Friedlein, A.R. Erskine, A. Augustin, M.C. De Vera Mudry, S. Ruepp, L. Suter, H. Langen, R.M. Caprioli, A. Ducret. Biomarker discovery by imaging mass spectrometry: Transthyretin is a biomarker for gentamicin-induced nephrotoxicity in rat. *Mol. Cell. Proteomics* **5**, 1876 (2006).

C. Meriaux, J. Franck, M. Wisztorski, M. Salzet, I. Fournier. Liquid ionic matrixes for MALDI mass spectrometry imaging of lipids. *J. Proteomics* **73**, 1204 (2010).

M.E. Monge, G.A. Harris, P. Dwivedi, F.M. Fernández. Mass spectrometry: Recent advances in direct open air surface sampling/ionization. *Chem. Rev.* **113**, 2269 (2013).

T. Müller, S. Oradu, D.R. Ifa, R.G. Cooks, B. Kräutler. Direct plant tissue analysis and imprint imaging by desorption electrospray ionization mass spectrometry. *Anal. Chem.* **83**, 5754 (2011).

S. Myung, J.M. Wiseman, S.J. Valentine, Z. Takáts, R.G. Cooks, D.E. Clemmer. Coupling desorption electrospray ionization with ion mobility/mass spectrometry for analysis of protein structure: Evidence for desorption of folded and denatured states. *J. Phys. Chem. B* **110**, 5045 (2006).

P. Nemes, A.A. Barton, Y. Li, A. Vertes. Ambient molecular imaging and depth profiling of live tissue by infrared laser ablation electrospray ionization mass spectrometry. *Anal. Chem.* **80**, 4575 (2008).

P. Nemes, A.A. Barton, A. Vertes. Three-dimensional imaging of metabolites in tissues under ambient conditions by laser ablation electrospray ionization mass spectrometry. *Anal. Chem.* **81**, 6668 (2009).

P. Nemes, A. Vertes. Laser ablation electrospray ionization for atmospheric pressure, in vivo, and imaging mass spectrometry. *Anal. Chem.* **79**, 8098 (2007).

P. Nemes, A.S. Woods, A. Vertes. Simultaneous imaging of small metabolites and lipids in rat brain tissues at atmospheric pressure by laser ablation electrospray ionization mass spectrometry. *Anal. Chem.* **82**, 982 (2010).

S.N. Nguyen, A.V. Liyu, R.K. Chu, C.R. Anderton, J. Laskin. Constant-distance mode nanospray desorption electrospray ionization mass spectrometry imaging of biological samples with complex topography. *Anal. Chem.* **89**, 1131 (2017).

J.K. Nicholson, J.C. Lindon. Systems biology: Metabonomics. *Nature* **455**, 1054 (2008).

J.J. Nicklay, G.A. Harris, K.L. Schey, R.M. Caprioli. MALDI imaging and in situ identification of integral membrane proteins from rat brain tissue sections. *Anal. Chem.* **85**, 7191 (2013).

M.W.F. Nielen. Maldi time-of-flight mass spectrometry of synthetic polymers. *Mass Spectrom. Rev.* **18**, 309 (1999).

E. Nordhoff, F. Kirpekar, P. Roepstorff. Mass spectrometry of nucleic acids. *Mass Spectrom. Rev.* **15**, 67 (1996).

J.L. Norris, R.M. Caprioli. Analysis of tissue specimens by matrix-assisted laser desorption/ionization imaging mass spectrometry in biological and clinical research. *Chem. Rev.* **113**, 2309 (2013).

J.T. O'Brien, E.R. Williams, H.-Y.N. Holman. Ambient infrared laser ablation mass spectrometry (AIRLAB-MS) of live plant tissue with plume capture by continuous flow solvent probe. *Anal. Chem.* **87**, 2631 (2015).

H. Oh, K. Breuker, S.K. Sze, Y. Ge, B.K. Carpenter, F.W. McLafferty. Secondary and tertiary structures of gaseous protein ions characterized by electron capture dissociation mass spectrometry and photofragment spectroscopy. *Proc. Natl. Acad. Sci. U.S.A.* **99**, 15863 (2002).

M. Ohnishi-Kameyama, A. Yanagida, T. Kanda, T. Nagata. Identification of catechin oligomers from apple (Malus pumila cv. Fuji) in matrix-assisted laser desorption/ionization time-of-flight mass spectrometry and fast-atom bombardment mass spectrometry. *Rapid Commun. Mass Spectrom.* **11**, 31 (1997).

L. Opilik, T. Schmid, R. Zenobi. Modern Raman imaging: Vibrational spectroscopy on the micrometer and nanometer scales. *Annu. Rev. Anal. Chem.* **6**, 379 (2013).

A.A. Oraevsky, L.B. Da Silva, A.M. Rubenchik, M.D. Feit, M.E. Glinsky, M.D. Perry, B.M. Mammini, W. Small, B.C. Stuart. Plasma mediated ablation of biological tissues with nanosecond-to-femtosecond laser pulses: Relative role of linear and nonlinear absorption. *IEEE J. Sel. Topics Quantum Electron.* **2**, 801 (1996).

O.S. Ovchinnikova, D. Bhandari, M. Lorenz, G.J. Van Berkel. Transmission geometry laser ablation into a non-contact liquid vortex capture probe for mass spectrometry imaging. *Rapid Commun. Mass Spectrom.* **28**, 1665 (2014).

O.S. Ovchinnikova, V. Kertesz, G.J. Van Berkel. Combining transmission geometry laser ablation and a non-contact continuous flow surface sampling probe/electrospray

emitter for mass spectrometry based chemical imaging. *Rapid Commun. Mass Spectrom.* **25**, 3735 (2011).

A.D. Palmer, T. Alexandrov. Serial 3D imaging mass spectrometry at its tipping point. *Anal. Chem.* **87**, 4055 (2015).

N. Pan, W. Rao, N.R. Kothapalli, R. Liu, A.W.G. Burgett, Z. Yang. The Single-probe: A miniaturized multifunctional device for single cell mass spectrometry analysis. *Anal. Chem.* **86**, 9376 (2014).

R.M. Parry, A.S. Galhena, C.M. Gamage, R.V. Bennett, M.D. Wang, F.M. Fernández. OmniSpect: An open MATLAB-based tool for visualization and analysis of matrix-assisted laser desorption/ionization and desorption electrospray ionization mass spectrometry images. *J. Am. Soc. Mass Spectrom.* **24**, 646 (2013).

M.K. Passarelli, N. Winograd. Lipid imaging with time-of-flight secondary ion mass spectrometry (ToF-SIMS). *Biochim. Biophys. Acta, Mol Cell Biol. Lipids* **1811**, 976 (2011).

I.X. Peng, R.R. Ogorzalek Loo, E. Margalith, M.W. Little, J.A. Loo. Electrospray-assisted laser desorption ionization mass spectrometry (ELDI-MS) with an infrared laser for characterizing peptides and proteins. *Analyst* **135**, 767 (2010).

J.J. Perez, P.M. Flanigan, J.J. Brady, R.J. Levis. Classification of smokeless powders using laser electrospray mass spectrometry and offline multivariate statistical analysis. *Anal. Chem.* **85**, 296 (2013).

J.J. Perez, P.M. Flanigan, S. Karki, R.J. Levis. Laser electrospray mass spectrometry minimizes ion suppression facilitating auantitative mass spectral response for multicomponent mixtures of proteins. *Anal. Chem.* **85**, 6667 (2013).

M. Pulfer, R.C. Murphy. Electrospray mass spectrometry of phospholipids. *Mass Spectrom. Rev.* **22**, 332 (2003).

A.M. Race, R.T. Steven, A.D. Palmer, I.B. Styles, J. Bunch. Memory efficient principal component analysis for the dimensionality reduction of large mass spectrometry imaging data sets. *Anal. Chem.* **85**, 3071 (2013).

A.M. Race, I.B. Styles, J. Bunch. Inclusive sharing of mass spectrometry imaging data requires a converter for all. *J. Proteomics* **75**, 5111 (2012).

Y.H. Rezenom, J. Dong, K.K. Murray. Infrared laser-assisted desorption electrospray ionization mass spectrometry. *Analyst* **133**, 226 (2008).

P.J. Roach, J. Laskin, A. Laskin. Molecular characterization of organic aerosols using nanospray-desorption/electrospray ionization-mass spectrometry *Anal. Chem.* **82**, 7979 (2010).

P.J. Roach, J. Laskin, A. Laskin. Nanospray desorption electrospray ionization: An ambient method for liquid-extraction surface sampling in mass spectrometry. *Analyst* **135**, 2233 (2010).

G. Robichaud, J. Barry, D. Muddiman. IR-MALDESI mass spectrometry imaging of biological tissue sections using ice as a matrix. *J. Am. Soc. Mass Spectrom.* **25**, 319 (2014).

G. Robichaud, J.A. Barry, K.P. Garrard, D.C. Muddiman. Infrared matrix-assisted laser desorption electrospray ionization (IR-MALDESI) imaging source coupled to a FT-ICR mass spectrometer. *J. Am. Soc. Mass Spectrom.* **24**, 92 (2013).

G. Robichaud, J.A. Barry, D.C. Muddiman. Atmospheric pressure mass spectrometry imaging, in: *Encyclopedia of Analytical Chemistry*. John Wiley & Sons, Ltd, (2006).

G. Robichaud, K.P. Garrard, J.A. Barry, D.C. Muddiman. MSiReader: An open-source interface to view and analyze high resolving power MS imaging files on Matlab platform. *J. Am. Soc. Mass Spectrom.* **24**, 718 (2013).

E.P. Rosen, M.T. Bokhart, H.T. Ghashghaei, D.C. Muddiman. Influence of desorption conditions on analyte sensitivity and internal energy in discrete tissue or whole body imaging by IR-MALDESI. *J. Am. Soc. Mass Spectrom.* **26**, 899 (2015).

H.L. Röst, U. Schmitt, R. Aebersold, L. Malmström. pyOpenMS: A Python-based interface to the OpenMS mass-spectrometry algorithm library. *Proteomics* **14**, 74 (2014).

A. Roux, L. Muller, S.N. Jackson, J. Post, K. Baldwin, B. Hoffer, C.D. Balaban, D. Barbacci, J.A. Schultz, S. Gouty, B.M. Cox, A.S. Woods. Mass spectrometry imaging of rat brain lipid profile changes over time following traumatic brain injury. *J. Neurosci. Methods* **272**, 19 (2016).

J.S. Sampson, A.M. Hawkridge, D.C. Muddiman. Generation and detection of multiply-charged peptides and proteins by matrix-assisted laser desorption electrospray ionization (MALDESI) Fourier Transform ion cyclotron resonance mass spectrometry. *J. Am. Soc. Mass Spectrom.* **17**, 1712 (2006).

J.S. Sampson, K.K. Murray, D.C. Muddiman. Intact and top-down characterization of biomolecules and direct analysis using infrared matrix-assisted laser desorption electrospray ionization coupled to FT-ICR mass spectrometry. *J. Am. Soc. Mass Spectrom.* **20**, 667 (2009).

S.A. Schwartz, M.L. Reyzer, R.M. Caprioli. Direct tissue analysis using matrix-assisted laser desorption/ionization mass spectrometry: Practical aspects of sample preparation. *J. Mass Spectrom.* **38**, 699 (2003).

E.H. Seeley, R.M. Caprioli. Molecular imaging of proteins in tissues by mass spectrometry. *Proc. Natl. Acad. Sci. U.S.A.* **105**, 18126 (2008).

A. Sethuraman, G. Vedantham, T. Imoto, T. Przybycien, G. Belfort. Protein unfolding at interfaces: Slow dynamics of α-helix to β-sheet transition. *Proteins: Struct., Funct., Bioinf.* **56**, 669 (2004).

F. Shi, J.J. Archer, R.J. Levis. Nonresonant, femtosecond laser vaporization and electrospray post-ionization mass spectrometry as a tool for biological tissue imaging. *Methods* **104**, 79 (2016).

F. Shi, P.M. Flanigan, J.J. Archer, R.J. Levis. Direct analysis of intact biological macromolecules by low-energy, fiber-based femtosecond laser vaporization at 1042 nm wavelength with nanospray postionization mass spectrometry. *Anal. Chem.* **87**, 3187 (2015).

F. Shi, P.M. Flanigan, J.J. Archer, R.J. Levis. Ambient molecular analysis of biological tissue using low-energy, femtosecond laser vaporization and nanospray postionization mass spectrometry. *J. Am. Soc. Mass Spectrom.* **27**, 542 (2016).

J. Shiea, M.-Z. Huang, H.-J. Hsu, C.-Y. Lee, C.-H. Yuan, I. Beech, J. Sunner. Electrospray-assisted laser desorption/ionization mass spectrometry for direct ambient analysis of solids. *Rapid Commun. Mass Spectrom.* **19**, 3701 (2005).

D. Shlosberg, M. Benifla, D. Kaufer, A. Friedman. Blood-brain barrier breakdown as a therapeutic target in traumatic brain injury. *Nat. Rev. Neurol.* **6**, 393 (2010).

B. Shrestha, P. Nemes, J. Nazarian, Y. Hathout, E.P. Hoffman, A. Vertes. Direct analysis of lipids and small metabolites in mouse brain tissue by AP IR-MALDI and reactive LAESI mass spectrometry. *Analyst* **135**, 751 (2010).

B. Shrestha, J.M. Patt, A. Vertes. In situ cell-by-cell imaging and analysis of small cell populations by mass spectrometry. *Anal. Chem.* **83**, 2947 (2011).

B. Shrestha, A. Vertes. In situ metabolic profiling of single cells by laser ablation electrospray ionization mass spectrometry. *Anal. Chem.* **81**, 8265 (2009).

B. Shrestha, A. Vertes. High-throughput cell and tissue analysis with enhanced molecular coverage by laser ablation electrospray ionization mass spectrometry using ion mobility separation. *Anal. Chem.* **86**, 4308 (2014).

C.A. Smith, G. O'Maille, E.J. Want, C. Qin, S.A. Trauger, T.R. Brandon, D.E. Custodio, R. Abagyan, G. Siuzdak. METLIN - A metabolite mass spectral database. *Ther. Drug Monit.* **27**, 747 (2005).

P.-K. So, B. Hu, Z.-P. Yao. Mass spectrometry: Towards in vivo analysis of biological systems. *Mol. BioSyst.* **9**, 915 (2013).

S. Soparawalla, G.A. Salazar, E. Sokol, R.H. Perry, R.G. Cooks. Trace detection of non-uniformly distributed analytes on surfaces using mass transfer and large-area desorption electrospray ionization (DESI) mass spectrometry. *Analyst* **135**, 1953 (2010).

C.H. Stephens, B. Shrestha, H.R. Morris, M.E. Bier, P.M. Whitmore, A. Vertes. Minimally invasive monitoring of cellulose degradation by desorption electrospray ionization and laser ablation electrospray ionization mass spectrometry. *Analyst* **135**, 2434 (2010).

M. Stoeckli, D. Staab, M. Staufenbiel, K.-H. Wiederhold, L. Signor. Molecular imaging of amyloid β peptides in mouse brain sections using mass spectrometry. *Anal. Biochem.* **311**, 33 (2002).

J.A. Stolee, A. Vertes. Toward single-cell analysis by plume collimation in laser ablation electrospray ionization mass spectrometry. *Anal. Chem.* **85**, 3592 (2013).

D. Strickland, G. Mourou. Compression of amplified chirped optical pulses. *Opt. Commun.* **56**, 219 (1985).

K. Strimbu, J.A. Tavel. What are biomarkers? *Curr. Opin. HIV AIDS* **5**, 463 (2010).

A. Svatoš. Mass spectrometric imaging of small molecules. *Trends Biotechnol.* **28**, 425 (2010).

Z. Takáts, J.M. Wiseman, R.G. Cooks. Ambient mass spectrometry using desorption electrospray ionization (DESI): Instrumentation, mechanisms and applications in forensics, chemistry, and biology. *J. Mass Spectrom.* **40**, 1261 (2005).

Z. Takáts, J.M. Wiseman, B. Gologan, R.G. Cooks. Mass spectrometry sampling under ambient conditions with desorption electrospray ionization. *Science* **306**, 471 (2004).

K. Tanaka, H. Waki, Y. Ido, S. Akita, Y. Yoshida, T. Yoshida, T. Matsuo. Protein and polymer analyses up to m/z 100 000 by laser ionization time-of-flight mass spectrometry. *Rapid Commun. Mass Spectrom.* **2**, 151 (1988).

E. Terreno, D.D. Castelli, A. Viale, S. Aime. Challenges for molecular magnetic resonance imaging. *Chem. Rev.* **110**, 3019 (2010).

The UniPort Consortium. UniProt: A hub for protein information. *Nucleic Acids Res.* **43**, D204 (2014).

A. Thomas, J.L. Charbonneau, E. Fournaise, P. Chaurand. Sublimation of new matrix candidates for high spatial resolution imaging mass spectrometry of lipids: enhanced information in both positive and negative polarities after 1,5-diaminonapthalene deposition. *Anal. Chem.* **84**, 2048 (2012).

G.J. Van Berkel, V. Kertesz. Automated sampling and imaging of analytes separated on thin-layer chromatography plates using desorption electrospray ionization mass spectrometry. *Anal. Chem.* **78**, 4938 (2006).

G.J. Van Berkel, V. Kertesz, K.A. Koeplinger, M. Vavrek, A.-N.T. Kong. Liquid microjunction surface sampling probe electrospray mass spectrometry for detection of drugs and metabolites in thin tissue sections. *J. Mass Spectrom.* **43**, 500 (2008).

R.B. Van Breemen, M. Snow, R.J. Cotter. Time-resolved laser desorption mass spectrometry. I. Desorption of preformed ions. *Int. J. Mass Spectrom. Ion Phys* **49**, 35 (1983).

A. Venter, P.E. Sojka, R.G. Cooks. Droplet dynamics and ionization mechanisms in desorption electrospray ionization mass spectrometry. *Anal. Chem.* **78**, 8549 (2006).

A. Vertes, P. Nemes, B. Shrestha, A.A. Barton, Z. Chen, Y. Li. Molecular imaging by Mid-IR laser ablation mass spectrometry. *Appl. Phys. A* **93**, 885 (2008).

H.-Y.J. Wang, S.N.J.J. Post, A.S. Woods. A minimalist approach to MALDI imaging of glycerophospholipids and sphingolipids in rat brain sections. *Int. J. Mass Spectrom.* **278**, 143 (2008).

E.J. Want, P. Masson, F. Michopoulos, I.D. Wilson, G. Theodoridis, R.S. Plumb, J. Shockcor, N. Loftus, E. Holmes, J.K. Nicholson. Global metabolic profiling of animal and human tissues via UPLC-MS. *Nat. Protoc.* **8**, 17 (2013).

M. Wilm, M. Mann. Analytical properties of the nanoelectrospray ion source. *Anal. Chem.* **68**, 1 (1996).

J.M. Wiseman, D.R. Ifa, Q. Song, R.G. Cooks. Tissue imaging at atmospheric pressure using desorption electrospray ionization (DESI) mass spectrometry. *Angew. Chem. Int. Ed.* **45**, 7188 (2006).

J.M. Wiseman, D.R. Ifa, A. Venter, R.G. Cooks. Ambient molecular imaging by desorption electrospray ionization mass spectrometry. *Nat. Protoc.* **3**, 517 (2008).

J.M. Wiseman, D.R. Ifa, Y. Zhu, C.B. Kissinger, N.E. Manicke, P.T. Kissinger, R.G. Cooks. Desorption electrospray ionization mass spectrometry: Imaging drugs and metabolites in tissues. *Proc. Natl. Acad. Sci. U.S.A.* **105**, 18120 (2008).

D.S. Wishart, D. Tzur, C. Knox, R. Eisner, A.C. Guo, N. Young, D. Cheng, K. Jewell, D. Arndt, S. Sawhney, C. Fung, L. Nikolai, M. Lewis, M.-A. Coutouly, I. Forsythe, P. Tang, S. Shrivastava, K. Jeroncic, P. Stothard, G. Amegbey, D. Block, D.D. Hau, J. Wagner, J. Miniaci, M. Clements, M. Gebremedhin, N. Guo, Y. Zhang, G.E. Duggan, G.D. MacInnis, A.M. Weljie, R. Dowlatabadi, F. Bamforth, D. Clive, R. Greiner, L. Li, T. Marrie, B.D. Sykes, H.J. Vogel, L. Querengesser. HMDB: the Human Metabolome Database. *Nucleic Acids Res.* **35**, D521 (2007).

C. Wu, A.L. Dill, L.S. Eberlin, R.G. Cooks, D.R. Ifa. Mass spectrometry imaging under ambient conditions. *Mass Spectrom. Rev.* **32**, 218 (2013).

C. Wu, D.R. Ifa, N.E. Manicke, R.G. Cooks. Molecular imaging of adrenal gland by desorption electrospray ionization mass spectrometry. *Analyst* **135**, 28 (2010).

G.-Z. Xin, B. Hu, Z.-Q. Shi, Y.C. Lam, T.T.-X. Dong, P. Li, Z.-P. Yao, K.W.K. Tsim. Rapid identification of plant materials by wooden-tip electrospray ionization mass spectrometry and a strategy to differentiate the bulbs of Fritillaria. *Anal. Chim. Acta* **820**, 84 (2014).

Z.-P. Yao. Characterization of proteins by ambient mass spectrometry. *Mass Spectrom. Rev.* **31**, 437 (2012).

J.Y. Yew, R.B. Cody, E.A. Kravitz. Cuticular hydrocarbon analysis of an awake behaving fly using direct analysis in real-time time-of-flight mass spectrometry. *Proc. Natl. Acad. Sci. U.S.A.* **105**, 7135 (2008).

A. Zavalin, E.M. Todd, P.D. Rawhouser, J. Yang, J.L. Norris, R.M. Caprioli. Direct imaging of single cells and tissue at sub-cellular spatial resolution using transmission geometry MALDI MS. *J. Mass Spectrom.* **47**, 1473 (2012).

A. Zavalin, J. Yang, K. Hayden, M. Vestal, R.M. Caprioli. Tissue protein imaging at 1 μm laser spot diameter for high spatial resolution and high imaging speed using transmission geometry MALDI TOF MS. *Anal. Bioanal. Chem.* **407**, 2337 (2015).

H. Zhang, R.M. Caprioli. Capillary electrophoresis combined with matrix-assisted laser desorption/ionization mass spectrometry; continuous sample deposition on a matrix-precoated membrane target. *J. Mass Spectrom.* **31**, 1039 (1996).

S.S. Zhao, X. Zhong, C. Tie, D.D.Y. Chen. Capillary electrophoresis-mass spectrometry for analysis of complex samples. *Proteomics* **12**, 2991 (2012).

L.V. Zhigilei, E. Leveugle, B.J. Garrison, Y.G. Yingling, M.I. Zeifman. Computer simulations of laser ablation of molecular substrates. *Chem. Rev.* **103**, 321 (2003).

J. Zou, F. Talbot, A. Tata, L. Ermini, K. Franjic, M. Ventura, J. Zheng, H. Ginsberg, M. Post, D.R. Ifa, D. Jaffray, R.J.D. Miller, A. Zarrine-Afsar. Ambient mass spectrometry imaging with picosecond infrared laser ablation electrospray ionization (PIR-LAESI). *Anal. Chem.* **87**, 12071 (2015).